EFFECTS OF MODIFIED THEORIES ON STELLAR STRUCTURES AND COSMIC EVOLUTION

By

Aisha Siddiqa

A THESIS
SUBMITTED IN PARTIAL FULFILLMENT OF THE
REQUIREMENTS FOR THE DEGREE OF
DOCTOR OF PHILOSOPHY
IN
MATHEMATICS

Supervised By

Prof. Dr. Muhammad Sharif

DEPARTMENT OF MATHEMATICS
UNIVERSITY OF THE PUNJAB
LAHORE-PAKISTAN

SEPTEMBER, 2018

CERTIFICATE

I certify that the research work presented in this thesis is the original work of **Ms. Aisha Siddiqa** D/O **Muhammad Arif** and is carried out under my supervision. I endorse its evaluation for the award of **Ph.D.** degree through the official procedure of **University of the Punjab**.

Prof. Dr. Muhammad Sharif
(**Supervisor**)

<u>Author’s Declaration</u>

I, **Ms Aisha Siddiqa**, hereby state that my PhD thesis entitled “**Effects of Modified Theories on Stellar Structures and Cosmic Evolution**” is my own work and has not been submitted previously by me for taking any degree from **University of the Punjab**, or anywhere else in the country/world.

At any time if my statement is found to be incorrect even after my graduation, the university has the right to withdraw my PhD degree.

Name of Student: **Ms Aisha Siddiqa**

Date: February 15, 2019

DEDICATED

To

My Children Ammar and Moaaz

Table of Contents

List of Figures

Acknowledgements

First and foremost, praises and thanks to **Almighty Allah**, for His uncountable blessings and strengths in achieving this goal successfully. The best prayers and peace be upon the Holy Prophet **Hazrat Muhammad** (PBUH), who is the greatest inspiration for all knowledge seekers.

It is my great pleasure to acknowledge my supervisor **Prof. Dr. Muhammad Sharif** whose guidance, expertise and support enabled me to complete this task. During this period, I would like to acknowledge the valuable inputs and helpful suggestions of my seniors especially **Dr. Ayesha** and fellows **Sobia** and **Arfa**. I would like to thank the Higher Education Commission, Islamabad, Pakistan for its financial support through the *Indigenous Ph.D. 5000 Fellowship Program Phase-II, Batch-III.*

I cannot express in words my heartiest feelings to my parents, their prayers and encouragement enabled me to complete the journey of my studies. I am grateful to my parents in law and whole family who provided a continuous support during my studies and spared me to work hard which means a lot to me. I am also thankful to my siblings for their cooperation and moral support. This acknowledgement will not be completed without special mention of my husband **Dr. Tanveer Hussain** and my sons **Ammar** and **Moaaz** who have always been there for my motivation and encouragement. Without their kind support, the successful completion of my PhD thesis would be a dream for me.

Lahore **Aisha Siddiqa**
September, 2018

Abstract

This thesis is devoted to explore stellar structures as well as evolution, gravitational waves and viscous cosmology in the framework of modified theories of gravity. Firstly, we study physical characteristics of stellar structures in the absence as well as presence of electromagnetic field in the framework of $f(R,T)$ theory. We consider the compact stars whose pressure and density are related through polytropic equation of state and MIT bag model. The energy conditions are satisfied and stellar configurations are found stable for the assumed values of free parameters. Secondly, we discuss anisotropic non-static charged spherical as well as cylindrical sources describing the phenomena of collapse and expansion in $f(R,T)$ theory. We analyze the behavior of density, pressures, anisotropic parameter as well as mass and examine the influence of charge as well as model parameter on these quantities.

Thirdly, we find the polarization modes of gravitational waves for some $f(R)$ dark energy models with the help of Newman-Penrose formalism and find two extra modes than general relativity. We also investigate the propagation of axial gravitational waves in the background of flat FRW universe in $f(R,T)$ theory through axial perturbations. It is found that axial waves can induce velocity memory effect.

Finally, we consider viscous modified Chaplygin gas interacting with $f(R,T)$ gravity in flat FRW universe. We investigate the behavior of total energy density, pressure and equation of state parameter for emergent, intermediate as well as logamediate scenarios of the universe with two interacting models. It is found that bulk viscosity enhances the expansion for the intermediate and logamediate scenarios. We also study the evolution using LRS Bianchi type-I model and discuss the behavior of scale factors as well as deceleration parameter in dark energy dominated era for different bulk viscosity models. We conclude that expansion is faster when bulk viscosity is proportional to the Hubble parameter.

Abbreviations

In this thesis, the signatures of the spacetime will be $(-,+,+,+)$. Also, we shall use the following list of abbreviations.

CG:	Chaplygin Gas
DEC:	Dominant Energy Condition
EH:	Einstein-Hilbert
EoS:	Equation of State
FRW:	Friedmann-Robertson-Walker
GCG:	Generalized Chaplygin Gas
GR:	General Relativity
GWs:	Gravitational Waves
MCG:	Modified Chaplygin Gas
MIT:	Massachusetts Institute of Technology
NEC:	Null Energy Condition
NP:	Newman-Penrose
PMs:	Polarization Modes
SEC:	Strong Energy Condition
WEC:	Weak Energy Condition

Introduction

Human beings have been trying to resolve mysteries of the universe since ancient times and the discovery of accelerated expansion of cosmos is a big achievement in this respect. The observations of high redshift supernova search team [1] as well as supernova cosmology project [2] indicate this expanding phase of the universe. The origin of this expansion is still unknown and a hypothetical term dark energy is introduced to represent its cause. Another mystery refers to gravitationally interacting matter within galaxies which does not have interaction with electromagnetic radiation. Its presence is confirmed by observing the motion of stars and galaxies [3]. According to Planck data, currently our universe is composed of approximately ninety five percent of these dark components, i.e., majority part of the universe is unknown to us. Therefore, it would be interesting to unveil these secrets as well as their consequences on various existing phenomena.

Different theoretical approaches have been introduced to investigate these dark puzzles like modification in matter or geometric part of the EH action leading to modified matter models or modified theories of gravity, respectively. These modified theories mainly involve higher order curvature terms as well as different forms of curvature-matter couplings. The higher order curvature terms have also been introduced in the EH action to deal with the renormalization issue of GR long before the discovery of accelerated expansion. Among the plethora of these modified theories, $f(R)$ theory is the simplest modification of GR. It is obtained by replacing R with its generic function $f(R)$ in the EH action. There exist $f(R)$ gravity models that can explain the early inflation [4], discuss cosmological constraints [5] as well as late-time cosmic expansion [6]. Many astrophysical as well as cosmological aspects have been investigated within the framework of this theory [7].

Harko *et al.* [8] proposed a curvature-matter coupling theory, i.e., $f(R,T)$ gravity where T denotes trace of the energy-momentum tensor. Consideration of curvature-matter coupling in the EH action yields interesting consequences such as covariant derivative of the energy-momentum tensor is no longer zero implying the existence of an extra force as well as non-geodesic path of particles [9]. The theory of GR breaks down near the Planck length $1.6 \times 10^{-35}m$ and this issue can be resolved by considering such coupling [10]. In cosmological scenario, it can explain the problem of galactic flat rotation curves as well as dark matter and dark energy interactions.

Stars or stellar structures are one of the constituents of the universe representing the primary building blocks of galaxies. A star is luminous sphere of plasma bonded with the help of its self-gravitation and this inward gravity is balanced by the outward directed thermal pressure originated by fusion reactions. When this balance is disturbed, the star does not remain stable and under goes collapse when gravity overcomes pressure while faces expansion when gravity is dominated by pressure. Oppenheimer and Snyder [11] were the first to work on gravitational collapse for dust configuration. Misner and Sharp discussed the dynamics of perfect [12] as well as dissipative fluid collapse [13]. Later on, many researchers investigated the collapsing process for different fluid configurations [14]. Glass [15] examined solutions of the field equations which yield collapse and expansion in GR.

The consequence of collapse is a compact object classified as white dwarf, neutron star and black hole. For a compact object having isotropic fluid distribution the mass-radius ratio cannot exceed $\frac{4}{9}$ [16]. The upper bound for the masses of white dwarfs is $1.4M_{\odot}$ [17] while for the masses of neutron stars is $3M_{\odot}$ [18]. For static spherical configurations, the maximum bound for the surface redshift parameter is found as $z_s \leq 2$ with perfect fluid distributions [16] while for anisotropic models it is $z_s \leq 5.211$ [19]. The stability of compact object is an important issue and can be observed by perturbation technique as well as speed of sound. The system remains stable if small perturbations do not change its equilibrium structure or if the sound speed falls between zero and one.

Zubair *et al.* [20] discussed energy conditions, gravitational redshift as well as stability of some observed compact objects in $f(R,T)$ gravity with the help of Krori and Barua solution. Moraes *et al.* [21] worked on the equilibrium states of compact objects using polytropic EoS and MIT bag model in this theory. Carvalho *et al.* [22] analyzed white dwarfs using an EoS describing ionized atoms embedded in a relativistic Fermi gas of electrons in curvature-matter coupling scenario. They observed that white dwarfs have larger radius and mass in $f(R,T)$ gravity than those observed in GR and $f(R)$ theory.

Rosseland and Eddington [23] figured out the presence of electric charge in stars and after that the role of electromagnetic field is extensively observed in literature. Sharif and Abbas [24] investigated charged collapse in modified Gauss-Bonnet gravity showing that charge term does not provide source of gravity. Abbas and his co-authors extended the analysis of [15] for plane symmetric geometry [25], charged spherical configurations [26] and for charged cylindrical source [27] in GR. Bhatti and Yousaf [28] examined charge effects on plane symmetric anisotropic dissipative fluid in the framework of Palatini $f(R)$ gravity. Abbas and Ahmed [29] discussed the collapsing and expanding solutions for charged sphere in $f(R,T)$ theory of gravity.

The compact binary systems and their mergence produce fluctuations in the curvature of spacetime known as GWs. The significance of GWs comes from the fact that they lead to new techniques to explore cosmic issues. After a long history of struggles (from Weber bars to advanced laser interferometers), scientific efforts came true and GWs are finally detected by earth-based detectors. Some of the observed GWs signals by the LIGO scientific collaboration (LIGO stands for laser interferometer gravitational wave observatory) are GW150914 [30], GW170104 [31] and GW170817 [32]. The most recent signal [32] of GWs is consistent with the binary neutron star inspiral. It has an association with gamma ray burst signal GRB170817A detected by gamma-ray burst monitor and provides the first direct evidence of gamma-ray bursts during the mergence of two neutron stars.

Thus being an observable phenomenon GWs has become a topic of central importance. The PMs of a GW provide information regarding geometrical orientation of the source. Generally, these modes are discussed in vacuum via perturbations around Minkowski metric called the linearized theory. To discuss the radiation theory, Newman and Penrose [33] developed the tetrad and spinor formalism. This method is further considered by Eardley *et al.* [34] in linearized gravity concluding that the PMs of plane null waves are represented by six NP parameters as well as they proposed the Lorentz invariant E(2) classification of these waves.

Capozziello *et al.* [35] found a massive longitudinal mode other than GR in $f(R)$

theory and discussed the response function of laser interferometer space antenna for these waves. Alves *et al.* [36] showed that for the quadratic gravity with $\mathcal{L} = R + \alpha R^2 + \gamma R_{\mu\nu}R^{\mu\nu}$ all PMs are non-zero. Kausar *et al.* [37] found two extra modes than GR for $f(R)$ gravity models. Alves *et al.* [38] obtained these modes for curvature-matter coupling theories, i.e., $f(R,T)$ and $f(R,T^{\phi})$ theory. They concluded that in vacuum $f(R,T)$ theory produced the results of $f(R)$ while for $f(R,T^{\phi})$ gravity these modes depend upon the choice of $f(T^{\phi})$. Kausar [39] examined these modes for scalar-tensor theories and found the same result as for $f(R)$ theory.

Malec and Wylężek [40] investigated Huygens principle for cosmological GWs in Regge-Wheeler gauge and found that this principle is satisfied in radiation dominated era while it does not hold in matter dominated universe. Kulczycki and Malec [41] studied perturbations induced by axial and polar GWs in FRW universe. They concluded that Huygens principle has the same status for both types of waves, it is valid for radiation era while it is broken elsewhere. The same authors [42] discussed cosmological rotation of matter induced by axial GWs.

The detection of GWs gives motivation to study the stellar structures with an exterior consisting of GWs. However, according to Bhirkoff's theorem vacuum solution of the Einstein field equations for a sphere does not have gravitational radiation and cylindrical systems are the next option. In case of cylindrical systems, Einstein and Rosen formulated exact solutions of the field equations showing the propagation of cylindrical GWs. Sharif and Bhatti [43] studied cylindrical system with expansion-free condition as well as in the presence of charge. Sharif and Farooq discussed the dynamics of collapse for charged perfect cylindrical system [44] with bulk viscous dissipative fluid [45].

This thesis explores some cosmological and astrophysical issues in the context of $f(R)$ and $f(R,T)$ theories of gravity.

- Chapter **One** comprises the essential preliminaries to understand this thesis.
- In chapter **Two**, we investigate physical characteristics of compact stars in the absence and presence of electromagnetic field.
- Chapter **Three** studies the collapsing and expanding solutions for charged spherical as well as cylindrical configurations.
- In chapter **Four**, we explore PMs of GW for some $f(R)$ models and the propagation of axial GWs in $f(R,T)$ background.
- Chapter **Five** discusses the evolution of isotropic as well as anisotropic universe for bulk viscous fluid.
- Finally, we conclude the results in the last chapter.

Chapter 1

Preliminaries

This chapter covers the basic concepts of all terminologies that will be helpful to understand the research work.

1.1 Modified Theories of Gravity

In the current cosmological and astrophysical research, modified theories of gravity have gained much interest to explain the current accelerated expanding behavior of the universe. Any modification in GR is obtained by modifying its action defined by

$$S = \int \sqrt{-g}\left(\frac{R}{2\kappa^2} + \mathcal{L}_M\right) d^4x,$$

with R as the Ricci scalar, g the determinant of spacetime matrix, $\mathcal{L}_M$ the matter Lagrangian density and $\kappa^2 = 8\pi G$ with $G = 1$. An action basically tells us about the dynamical attribute of a physical system as well as gives its equations of motion. In GR, these equations are $G_{\mu\nu} = 8\pi T_{\mu\nu}$, where $G_{\mu\nu}$ denotes the Einstein tensor and $T_{\mu\nu}$ represents the energy-momentum tensor. Physically, these equations depict how the presence of matter induces curvature in spacetime fabric. Here, we would like to discuss $f(R)$ and $f(R,T)$ theories of gravity and their field equations.

1.1.1 $f(R)$ Gravity

An obvious generalization of GR is the $f(R)$ theory of gravity with the EH action

$$S = \int \sqrt{-g}\left(\frac{f(R)}{2\kappa^2} + \mathcal{L}_M\right) d^4x, \tag{1.1.1}$$

where $f(R)$ is a generic function of R. The corresponding field equations are

$$f_R R_{\mu\nu} - \frac{1}{2} f g_{\mu\nu} - \nabla_\mu \nabla_\nu f_R + g_{\mu\nu} \Box f_R = 8\pi T_{\mu\nu}, \tag{1.1.2}$$

where f_R denotes derivative of f with respect to its argument R, $\Box = \nabla_\mu \nabla^\mu$ is the d' Alembertian operator. These are fourth-order dynamical equations whereas in GR, the field equations are of second-order. These higher-order curvature terms are supposed to mimic the effects of dark energy in order to discuss the expanding universe. Also, any viable $f(R)$ model should avoid the Ostrogradski [7] and Dolgov-Kawasaki instabilities [46] yielding the following constraints

$$f_R > 0, \quad f_{RR} > 0, \quad R \geq R_0,$$

with R_0 denotes current value of the Ricci scalar.

1.1.2 $f(R,T)$ Gravity

A curvature-matter coupling theory helps to study the nature of gravity at quantum level as well as non-geodesic motion of particles. Harko *et al.* [8] introduced $f(R,T)$ gravity which is a generalization of $f(R)$ gravity. The action for $f(R,T)$ gravity is given by

$$S = \int d^4x \sqrt{-g}\left[\frac{1}{2\kappa^2} f(R,T) + \mathcal{L}_m\right]. \tag{1.1.3}$$

It yields the following field equations

$$f_R R_{\mu\nu} - \frac{1}{2} g_{\mu\nu} f + (g_{\mu\nu}\Box - \nabla_\mu \nabla_\nu) f_R = 8\pi T_{\mu\nu} - f_T (T_{\mu\nu} + \Theta_{\mu\nu}), \tag{1.1.4}$$

with $f = f(R,T)$, $f_R = \frac{\partial f}{\partial R}$, $f_T = \frac{\partial f}{\partial T}$ and $\Theta_{\mu\nu}$ is evaluated by

$$\Theta_{\mu\nu} = g^{\gamma\sigma}\frac{\delta T_{\gamma\sigma}}{\delta g^{\mu\nu}}, \quad T_{\mu\nu} = g_{\mu\nu}\mathcal{L}_m - \frac{\partial \mathcal{L}_m}{\partial g^{\mu\nu}}. \tag{1.1.5}$$

The matter Lagrangian density can be defined by pressure or density, i.e., $\mathcal{L}_m = p$ or $\mathcal{L}_m = -\rho$. These two Lagrangian densities are equivalent for a perfect fluid if the curvature-matter coupling is minimal and if this coupling is non-minimal, they give rise to two distinct results of any problem [47]. Harko *et al.* suggested different functional forms of $f(R,T)$ defining minimal/non-minimal coupling between matter and geometry.

- $f(R,T) = R + 2\lambda T$,
- $f(R,T) = f_1(R) + f_2(T)$,
- $f(R,T) = f_1(R) + f_2(R)f_3(T)$,

where $f_1(R)$, $f_2(R)$, $f_3(T)$ are arbitrary functions of their arguments and λ is constant called model parameter. The first two types of models define minimal coupling while the last one has non-minimal coupling. The first model reduces to GR for $\lambda = 0$ and it corresponds to ΛCDM model with time dependent cosmological constant. Following the same arguments as in $f(R)$ case, the constraints on the viability of $f(R,T)$ gravity models are

$$f_R > 0, \quad 1 + \frac{f_T}{8\pi} > 0, \quad f_{RR} > 0, \quad R \geq R_0. \tag{1.1.6}$$

1.2 Electromagnetic Field Theory

The electromagnetic field contains the combine effects of electric and magnetic fields produced by charged objects. The area in the surrounding of a charged particle within which it can exert the electrostatic force on other particles is the electric field. Magnetic field is similar to electric field and describes the effects of nearby magnetized material and electric currents at a point. When charged particles are in motion then magnetic field is also produced such that both fields (electric and magnetic) are orthogonal to each other as well as to the direction of motion. Mathematically, Maxwell field equations describe the evolution of electromagnetic field. The covariant form of Maxwell equations is given as follows

$$\nabla_{[\gamma}F_{\mu\nu]} = 0, \tag{1.2.1}$$

$$\nabla^{\nu}F_{\mu\nu} = 4\pi j_{\mu}, \tag{1.2.2}$$

where j_{μ} gives the source of electromagnetic field and $F_{\mu\nu}$ is the electromagnetic field tensor also called Faraday's tensor. This is a second rank antisymmetric tensor with the following expression in the form of four potential φ_{μ}

$$F_{\mu\nu} = \varphi_{\nu,\mu} - \varphi_{\mu,\nu}. \tag{1.2.3}$$

The four potential is given by

$$\varphi_{\mu} = (\varphi_0, \varphi_i); \quad i = 1, 2, 3, \tag{1.2.4}$$

where φ_0 is the electrostatic potential associated with electric field and φ_i is the magnetic potential related to magnetic field. The four current has the following expression

$$j_{\mu} = \xi(r)V_{\mu}, \tag{1.2.5}$$

with $\xi(r)$ representing charge density. The energy-momentum tensor of electromagnetic field is defined by

$$E_{\mu\nu} = \frac{1}{4\pi}\left(F_{\mu}{}^{\alpha}F_{\nu\alpha} - \frac{1}{4}F^{\alpha\beta}F_{\alpha\beta}g_{\mu\nu}\right). \tag{1.2.6}$$

1.3 Energy Conditions

The energy-momentum tensor of any realistic matter configuration satisfies some constraints, like positivity of energy density and dominance of energy density over pressures, known as energy conditions. The violation of these conditions suggest the presence of exotic fluid. These conditions are derived from the famous Raychaudhuri equation which describes the motion of matter through evolution of expansion scalar ϑ for the congruence of non-spacelike vectors. For non-geodesic motion, the Raychaudhuri equation for timelike congruences has the following form [48]

$$\dot{\vartheta}+\frac{1}{3}\vartheta^{2}-\omega^{\mu\nu}\omega_{\mu\nu}+\sigma^{\mu\nu}\sigma_{\mu\nu}-\nabla_{\mu}(v^{\nu}\nabla_{\nu}v^{\mu})+R_{\mu\nu}v^{\mu}v^{\nu}=0, \tag{1.3.1}$$

where dot represents the derivative with respect to t, v^{μ} is a timelike vector field, $\omega_{\mu\nu}$ and $\sigma_{\mu\nu}$ stand for vorticity and shear tensors of the corresponding congruence, respectively. Similarly, for null congruence the above equation is

$$\dot{\vartheta}+\frac{1}{3}\vartheta^{2}-\omega^{\mu\nu}\omega_{\mu\nu}+\sigma^{\mu\nu}\sigma_{\mu\nu}-\nabla_{\mu}(v^{\nu}\nabla_{\nu}v^{\mu})+R_{\mu\nu}l^{\mu}l^{\nu}=0, \tag{1.3.2}$$

and l^{μ} is a null vector.

Considering gravity to be attractive, i.e., $\vartheta<0$ as well as neglecting the quadratic terms with the assumptions of rotation-free motion ($\omega^{2}=0$) and negligible distortions ($\sigma^{2}=0$), we have from Eqs.(1.3.1) and (1.3.2)

$$R_{\mu\nu}v^{\mu}v^{\nu}-A_{t}\geq 0,\quad R_{\mu\nu}l^{\mu}l^{\nu}-A_{t}\geq 0,$$

where $A_{t}=\nabla_{\mu}(v^{\nu}\nabla_{\nu}v^{\mu})$ is the acceleration term. The above constraints are further transformed in terms of the energy-momentum tensor through the field equations as

$$(T_{\mu\nu}-\frac{1}{2}g_{\mu\nu}T)v^{\mu}v^{\nu}-A_{t}\geq 0,\quad T_{\mu\nu}l^{\mu}l^{\nu}-A_{t}\geq 0.$$

These inequalities provide the following constraints on the energy-momentum tensor

- **WEC:** This condition states that the energy density measured by an observer having timelike tangent vector v^μ should be positive, given by

$$T_{\mu\nu}v^\mu v^\nu - A_t \geq 0. \tag{1.3.3}$$

- **NEC:** The above condition for a null vector instead of timelike gives the NEC

$$T_{\mu\nu}l^\mu l^\nu - A_t \geq 0, \tag{1.3.4}$$

  which is the second expression obtained from Raychaudhuri equation.

- **SEC:** According to this condition, gravity should be attractive as derived by Raychaudhuri equation

$$(T_{\mu\nu} - \frac{1}{2}g_{\mu\nu}T)v^\mu v^\nu - A_t \geq 0. \tag{1.3.5}$$

- **DEC:** This condition states that the speed of energy flow in a matter distribution satisfies the causality condition

$$T_{\mu\nu}v^\mu v^\nu - A_t \geq 0, \quad T_{\mu\nu}T^\nu_\delta l^\mu l^\delta - A_t \geq 0. \tag{1.3.6}$$

Now we consider the anisotropic energy-momentum tensor, timelike and null vectors in the following form [49]

$$\begin{aligned}
T^{\mu\nu} &= \rho e^\mu_0 e^\nu_0 + p_1 e^\mu_1 e^\nu_1 + p_2 e^\mu_2 e^\nu_2 + p_3 e^\mu_3 e^\nu_3, \\
v^\mu &= \frac{1}{\sqrt{-1+a^2+b^2+c^2}}(e^\nu_0 + a e^\nu_1 + b e^\nu_2 + c e^\nu_3), \\
l^\mu &= e^\nu_0 + \hat{a} e^\nu_1 + \hat{b} e^\nu_2 + \hat{c} e^\nu_3,
\end{aligned}$$

where ρ is the energy density, p_i denote pressures and a, b, c, $\hat{a}$, $\hat{b}$, $\hat{c}$ are arbitrary functions of coordinates. The vectors e^ν_α form an orthonormal basis and satisfy the relation

$$g_{\mu\nu}e^{\mu}_{\alpha}e^{\nu}_{\beta} = \eta_{\alpha\beta}. \tag{1.3.7}$$

Using the above expressions of $T_{\mu\nu}$, v^{μ} and l^{μ}, we have the following energy conditions for perfect fluid matter distribution

- WEC: $\rho - A_t \geq 0, \quad \rho + p - A_t \geq 0,$
- NEC: $\rho + p - A_t \geq 0,$
- SEC: $\rho + 3p - A_t \geq 0, \quad \rho + p - A_t \geq 0,$
- DEC: $\rho - A_t \geq 0, \quad \rho \pm p - A_t \geq 0.$

In the presence of electromagnetic field, $T_{\mu\nu}$ is replaced by $T_{\mu\nu} + E_{\mu\nu}$.

1.4 Compact Objects

The end of nuclear fusion processes in a star leads to the stellar death whose remnants are referred to compact objects depending upon the original mass of the star. A compact object will be a white dwarf if initial mass of the star is less than eight times the solar mass while it will be a neutron star or black hole for more massive stars. White dwarfs and neutron stars have been observed in the universe while the existence of black holes is supported by some ground-based observations. Compact objects have their own physical features including density, pressure, mass, radius, compactness, surface redshift and luminosity. The surface gravitational redshift is defined as the decrease in frequency and increase in wavelength of the electromagnetic radiation as they travel from high to low gravity regime, compactness means denseness and luminosity gives the emitted amount of energy per unit time.

1.4.1 Degeneracy Pressure

Here, we discuss degeneracy pressure which halts the collapse in these compact objects except black holes. In particle physics, a particle which has no further substructure is called an elementary particle. Elementary fermions and bosons are considered as the fundamental particles. Fermions can further be classified into six quarks named as up (u), down (d), strange (s), charm (c), top (t), bottom (b) and leptons consisting of Electron, Positron, Muon, Tau and Neutrinos. Similarly, bosons are further classified into gauge and scalar bosons.

For both types of particles (fermions and bosons), the governing way of particle distribution over various energy levels is different. One of these ways is the Fermi-Dirac statistics for spin half particles and the other one is the Bose-Einstein statistics for integer spin particles. Fermions are distributed according to Fermi-Dirac statistics and obey the Pauli exclusion principle, i.e., no two identical fermions can occupy the same energy state while bosons are dispersed via Bose-Einstein statistics and do not obey the Pauli exclusion principle. Degenerate matter is a type of very dense matter whose particles follow the Pauli exclusion principle and pressure exerted by such kind of matter is the degeneracy pressure, e.g., electron and neutron degeneracy pressures.

1.4.2 White Dwarfs

The term dwarf is generally used for a star of smaller mass while its color indicates its surface temperature like hot star emits blue-white light and cooler ones red light. White dwarfs have masses comparable with the solar mass while radius with that of the Earth making it dense [17]. Alven Clark in 1862 discovered the first white dwarf named as Sirius B. In a normal star, the fusion reaction converting hydrogen into helium produces pressure against gravity but in white dwarfs, no fusion processes exist instead gravity is opposed by electron degeneracy pressure.

1.4.3 Neutron Stars

These are one of the outcomes of stellar collapse and are more massive as well as smaller in size than white dwarfs. Their constituents are neutrons (a combination of two down and one up quark) whose degeneracy pressure stops further collapse by balancing gravitational pull. A neutron star can also collapse to form a black hole if it is dense enough. If it is not much dense to form a black hole there is a possibility to turn into a quark star.

1.4.4 Quark stars

Six quarks and their antiparticles make up composite particles like protons and neutrons. Quarks themselves have fractional charges and combine to form electrically charged particles with integer charge. Quark stars are hypothetical compact objects composed of up, down and strange quarks. It is supposed that due to extreme temperature and pressure nuclear matter dissolves into quarks. The transition of neutron stars into quark stars has been discussed in the literature [50].

1.4.5 Black Holes

Black holes are totally collapsed objects in which a huge amount of matter is packed in a very small region making the gravitational field so strong that nothing even light cannot escape from it and hence we have no information about interior of a black hole. Black holes are characterized by their mass, charge and angular momentum.

The famous black hole solutions are Schwarzschild, Reissner-Nordström, Kerr and Kerr-Newman.

1.4.6 Equation of State for Degenerate Matter

The temperature of a white dwarf or neutron star drops to zero. With the passage of time, the only pressure supporting the inward force of attraction is the pressure produced by degenerate matter composed of electrons and neutrons. Consider an ideal situation of a single non-interacting fermions specie at zero temperature, the resulting EoS is of the polytropic form, i.e., $p = \sigma_1 \rho^{\sigma_2}$, where σ_1 and σ_2 represent polytropic constant and index, respectively [17]. In general, the polytropic EoS for $\sigma_2 = \frac{5}{3}$ can well describe the non-relativistic neutron stars and white dwarfs while $p = \sigma_1 \rho^2$ can be used to describe the Bose-Einstein condensate stars or properties of dark matter. At low temperature, particles form quantum degenerate condensate in a dilute Bose gas by occupying the same quantum state. In neutron stars and white dwarfs, the Bose-Einstein condensed core can be formed as a result of dark matter accretion [51].

1.4.7 Equation of State for Quark Matter

A satisfactory EoS for quark matter should predict the nature of a color charge, i.e., enhancement of a color charge with increasing distance while its ineffectiveness on other color charges within a smaller range. To obtain such an EoS is a difficult task, not obtained yet. However, several searches indicate that some confinement mechanism for quarks is required for this purpose and the term bag is referred to the region where quarks are supposed to be confined. In this respect, Bogoliubov

[52] in 1967 formulated the first bag model for the quarks confined in a spherical cavity giving some accurate predictions but suffer some flaws. After that in 1974, five scientists from MIT proposed another bag model known as the MIT bag model [53]. This model is an extension of Bogoliubov bag model and simulate the quark matter kinematics within the nucleon as well as it covers most of Bogoliubov's drawbacks by introducing bag constant $\mathcal{B}$ which gives the confining pressure. The EoS representing MIT bag model is $p = \tilde{a}(\rho - 4\mathcal{B})$, with $\tilde{a}$ and $\mathcal{B}$ as constants.

1.5 Gravitational Waves and Polarization Modes

General relativity predicts the existence of a massless spin-2 field called graviton that mediates force of gravity and this further implies the existence of GWs. Gravitational wave is a ripple in the curvature of spacetime produced by a moving object. These waves are invisible, travel with nearly speed of light and stretch as well as squeeze an object as they travel. Any object having mass and moving with some acceleration produces GWs but the GWs produced by objects on earth are too hard to detect due to their small masses. However, binary systems of compact objects are important source to observe GWs. These waves help to understand outer space phenomena and can provide information of different cosmic events which cannot be conveyed by electromagnetic radiation, e.g., electromagnetic radiation cannot provide information about black holes but GWs emitted by black holes are source of information about them.

Polarization of a wave is an expression showing the orientation of the wave, it may be constant or can rotate with wave cycle. To find PMs of GWs faraway from their sources or in vacuum, a negligible self-gravity matter is considered such that the relative tidal acceleration between any two points is only observable and measurable field. Considering a coordinate system with observer P as origin, the acceleration is defined in terms of Riemann tensor as [34]

$$a_i^{Grav} = -R_{i0j0}x^j,$$

where R_{i0j0} are components of the Riemann tensor showing external gravitational effects. To deal with the issue of gravitational radiation, Newman and Penrose [33] introduced tetrad formalism for the decomposition of Riemann tensor. They defined the following relations between the Cartesian basis (t, x, y, z) and complex null-tetrad $(k, l, n, \tilde{n})$

$$k = \frac{1}{\sqrt{2}}(t+z), \quad l = \frac{1}{\sqrt{2}}(t-z), \tag{1.5.1}$$

$$n = \frac{1}{\sqrt{2}}(x+iy), \quad \tilde{n} = \frac{1}{\sqrt{2}}(x-iy), \tag{1.5.2}$$

satisfying the relations

$$-k.l = n.\tilde{n} = 1, \quad k.n = k.\tilde{n} = l.n = l.\tilde{n} = 0. \tag{1.5.3}$$

Following formula is used to transform any tensor from Cartesian to null basis

$$S_{abc...} = S_{\alpha\beta\gamma...}a^\alpha b^\beta c^{\gamma...}, \tag{1.5.4}$$

where $(a, b, c, ...)$ vary over the set $\{k, l, n, \tilde{n}\}$ and $(\alpha, \beta, \gamma, ...)$ vary over $\{t, x, y, z\}$.

For plane null waves, independent components of the Riemann tensor defining PMs have the following form in terms of null-tetrad [34]

$$\Psi_2 = -\frac{1}{6}R_{lklk}, \quad \Psi_3 = -\frac{1}{2}R_{lkl\tilde{n}}, \quad \Psi_4 = -R_{l\tilde{n}l\tilde{n}}, \quad \Phi_{22} = -R_{lnl\tilde{n}}. \tag{1.5.5}$$

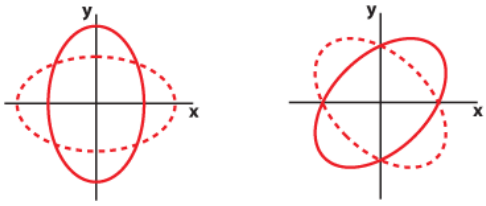

Figure 1.1: Ψ_4 represents plus and cross tensorial modes.

These are some helpful relations of null-tetrad components of the Riemann and Ricci tensors

$$R_{lk} = R_{lklk}, \quad R_{ll} = 2R_{lnl\tilde{n}}, \quad R_{ln} = R_{lkln}, \; R_{l\tilde{n}} = R_{lkl\tilde{n}}, \; R = -2R_{lk}. \qquad (1.5.6)$$

The classification of weak plane null waves defined by Eardley *et al.* [34] is given in Table **1**. The expressions of Ψ_3 and Ψ_4 are complex and each one corresponds to two independent modes associated with real and imaginary parts as well as the change induced by these modes on a sphere of test particles is shown in Figures **1.1-1.3**, respectively.

Table**1**: The E(2) Classes of Weak Plane Null Waves

Classes	Condition for NP Parameters
II_6	$\Psi_2 \neq 0$
III_5	$\Psi_2 = 0$ and $\Psi_3 \neq 0$
N_3	$\Psi_2 = 0 = \Psi_3$, $\Psi_4 \neq 0$ and $\Phi_{22} \neq 0$
N_2	$\Psi_2 = 0 = \Psi_3 = \Phi_{22}$ and $\Psi_4 \neq 0$
O_1	$\Psi_2 = 0 = \Psi_3 = \Psi_4$ and $\Phi_{22} \neq 0$
O_0	$\Psi_2 = 0 = \Psi_3 = \Phi_{22} = \Psi_4$

1.6 Regge-Wheeler Perturbations

The study of GWs for perturbed Schwarzschild background is significant because the emission of GWs from black holes carry information about their mass, spin as well as

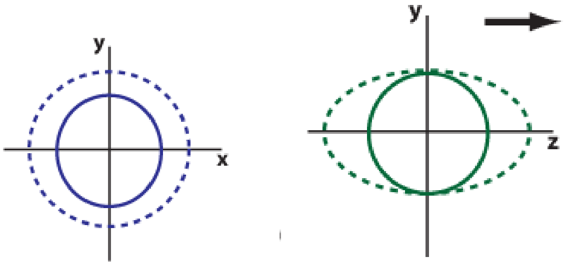

Figure 1.2: Left figure represents Φ_{22} the breathing scalar mode and right one represents Ψ_2 the purely longitudinal mode.

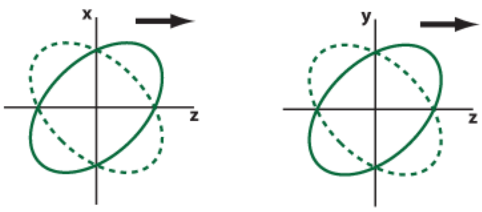

Figure 1.3: Ψ_3 represents the mixed mode.

charge and the analysis of perturbations tells about the stability of the object. Regge and Wheeler [54] explored this phenomenon by perturbing the metric coefficients of Schwarzschild metric as $g_{\mu\nu} + h_{\mu\nu}$ and then proceeded to have an explicit solution of $h_{\mu\nu}$ in four coordinates (t, r, θ, ϕ). For this purpose, they consider $h_{\mu\nu}$ in terms of spherical harmonics Y_l^m in which the subscript l denotes the angular momentum and superscript m is its projection on z-axis. Spherical harmonics are defined by

$$Y_l^m(\theta,\phi) = (-1)^m\sqrt{\frac{2l+1}{4\pi}\frac{(l-m)!}{(l+m)!}}P_l^m(\cos\theta)e^{im\phi}; \qquad l = 0, 1, 2, ... \ ,$$
$$m = -l, -l+1, -l+2, ..., l,$$

where $P_l^m(\cos\theta)$ stand for Legendre polynomials (with the superscript showing the order not power) and are defined by

$$P_l^m(x) = \frac{(-1)^m}{2^l l!}(1-x^2)^{\frac{m}{2}}\frac{d^{l+m}}{dx^{l+m}}(x^2-1)^l.$$

Spherical harmonics are introduced in obtaining the solution of Laplace equation in spherical coordinates and have different parities with respect to an inversion of the system about origin. If the sign of wave function remains the same under the reflection of spacial coordinates, it is of even parity, otherwise odd parity wave. Hence, this decomposition of $h_{\mu\nu}$ in spherical harmonics leads to even as well as odd parity solutions. Here we consider only odd parity waves (due to simplicity as compared to even parity waves) for which the perturbation matrix is given by

$$h_{\mu\nu} = \begin{pmatrix} 0 & 0 & -k_0\frac{\partial}{\sin\theta\partial\theta}Y_l^m & k_0\frac{\sin\theta\partial}{\partial\theta}Y_l^m \\ 0 & 0 & -k_1\frac{\partial}{\sin\theta\partial\phi}Y_l^m & k_1\frac{\sin\theta\partial}{\partial\theta}Y_l^m \\ sym & sym & k_2\left(\frac{\partial^2}{\sin\theta\partial\theta\partial\phi} - \frac{\cos\theta\partial}{\sin^2\theta\partial\phi}\right)Y_l^m & sym \\ sym & sym & \frac{1}{2}k_2\left(\frac{\partial^2}{\sin\theta\partial\theta\partial\phi} + \frac{\cos\theta\partial}{\partial\theta - \frac{\sin\theta\partial^2}{\partial\theta\partial\theta}}\right) & -k_2\left(\frac{\sin\theta\partial^2}{\partial\theta\partial\phi} - \frac{\cos\theta\partial}{\partial\phi}\right)Y_l^m \end{pmatrix},$$

where $k_0,\ k_1$ and k_2 are functions of t and r while *sym* means that the entry comes from symmetric property of the tensor $h_{\mu\nu}$. Considering the special case of $m=0$ such that ϕ disappears from calculations and assuming the function $k_2=0$ simplifies the odd-parity perturbation matrix as

$$h_{\mu\nu}=e^{-im\phi}\sin\theta\frac{\partial}{\partial\theta}P_l(\cos\theta)\begin{pmatrix}0 & 0 & 0 & k_0\\ 0 & 0 & 0 & k_1\\ 0 & 0 & 0 & 0\\ k_0 & k_1 & 0 & 0\end{pmatrix}, \tag{1.6.1}$$

known as odd-parity perturbations in the Regge and Wheeler gauge where $P_l(\cos\theta)$ is the l^{th} order Legendre polynomial.

1.7 Cosmological Models and Parameters

A cosmological model provides mathematical interpretation of the universe and helps to understand cosmic evolution as well as other cosmic phenomena. Our universe is homogeneous and isotropic on large scales according to the cosmological principle and this concept is mathematically encoded as standard cosmic model. Firstly, Alexander Friedmann in 1922 proposed this model while Howard Percy Robertson and Arthur Geoffrey Walker made some improvements and the modified model is known as FRW universe model whose mathematical form is given as

$$ds^2=dt^2-\frac{a(t)^2}{1-\mathcal{K}r^2}(dx^2+dy^2+dz^2), \tag{1.7.1}$$

where $a(t)$ denotes the scale factor and $\mathcal{K}$ is the spatial curvature such that $\mathcal{K}=-1,0,1$ correspond to open, flat and closed universe. The FRW spacetime can well describe cosmic dynamics on large scales but on small scales where inhomogeneities are inevitable, FRW model is not a suitable choice [55]. In this regard, the simplest generalization of flat FRW universe is the Bianchi type-I model having different scale factors in each spatial direction. Its line element is given by

$$ds^2 = -dt^2 + a_1^2dx^2 + a_2^2dy^2 + a_3^2dz^2, \tag{1.7.2}$$

where a_i are the scale factors. Bianchi type-I metric becomes locally rotationally symmetric (LRS) when the scale factors in any two directions are considered to be equal, i.e, the expansion in two directions is same.

In the following, we briefly explain some parameters that help to explore evolution of the universe.

- First one is the scale factor which indicates expansion. For the standard cosmological model, it is same in all the three directions.

- The next is Hubble parameter defined by the quotient of temporal derivative of a scale factor by itself, i.e., $H_i = \frac{\dot{a}_i}{a_i}$ or $H = \frac{\sum_{i=0}^{3} H_i}{3}$, the mean Hubble parameter and $H = \frac{\dot{a}}{a}$ for FRW model. It gives expansion rate of the universe and is equivalent to Hubble law that the velocity with which two galaxies are moving apart from each other is directly proportional to the distance between them with the Hubble parameter as constant of proportionality.

- A quantity providing information about increase and decrease in the expansion of the universe is the deceleration parameter denoted by $\tilde{q}$ and is defined by

  $$\tilde{q} = -\frac{a\ddot{a}}{a^2}.$$

  Its positive value shows deceleration while negative one indicates acceleration in expansion rate of the universe.

- The parameter which describes different evolutionary phases of the universe is known as EoS parameter defined by $\omega = \frac{p}{\rho}$. It shows existence of stiff fluid, dust and radiation for $\omega = 1,\ 0,\ \frac{1}{3}$, respectively while its negative values correspond to dark energy dominated phase which is subdivided into phantom and non-phantom phases according to $\omega < -1$ and $\omega > -1$.

1.8 Chaplygin Gas Model

The Russian Mathematician Sergey Alexeyevich Chaplygin proposed the following EoS [56]

$$p = \frac{-b_2}{\rho}; \quad b_2 > 0, \tag{1.8.1}$$

to describe the force on a wing of airplane. Kamenshchik *et al.* [57] considered this EoS in cosmology to discuss accelerated expansion of the universe. Further, a GCG model with the EoS

$$p = \frac{-b_2}{\rho^\delta}; \quad b_2 > 0,\ 0 < \delta \leq 1, \tag{1.8.2}$$

is considered as a unified model of dark energy and dark matter [58]. In fact, the GCG model could replace both the dark matter a pressureless fluid and dark energy having huge negative pressure. From this EoS, pressure becomes negligible as compared to density at the epoch when energy density is very very large (early epoch during evolution of the universe) such that GCG EoS corresponds to dark matter while if energy density is very small, its negative power gives a huge negative pressure and the EoS represents dark energy dominated era. Benaoum [59] proposed another extended model of CG EoS known as MCG defined by

$$p = b_1\rho - \frac{b_2}{\rho^\delta}. \tag{1.8.3}$$

Here b_1, b_2 are positive constants and $0 < \delta \leq 1$. The MCG is compatible with accelerated expansion of the universe. For $b_2 = 0$, this model reduces to barotropic EoS and for $b_1 = 0$, it reduces to GCG model.

Chapter 2

Stellar Structures in $f(R, T)$ Gravity

This chapter is devoted to study physical features of perfect fluid stellar configurations in the absence and presence of electromagnetic field. We discuss the behavior of pressure, density, mass function as well as gravitational redshift of stellar objects and investigate their stability through speed of sound. The chapter has following format. Section **2.1** contains the field equations and physical features of compact objects obeying polytropic EoS as well as MIT bag model. In section **2.2**, we discuss physical characteristics of charged stellar objects via polytropic EoS. This work has been published in the form of two research papers [60, 61].

2.1 Physical Features of Compact Objects

We consider spherically symmetric compact object whose geometry is described by the metric

$$ds^2 = -B(r)dt^2 + A(r)dr^2 + r^2(d\theta^2 + \sin^2\theta d\phi^2). \tag{2.1.1}$$

The energy-momentum tensor of perfect fluid in comoving coordinates is

$$T_{\mu\nu} = (\rho + p)V_\mu V_\nu + p g_{\mu\nu}, \tag{2.1.2}$$

where V_μ is the four velocity satisfying $V_\mu V^\mu = -1$ and $T = 3p - \rho$. We take $\mathcal{L}_m = p$ and consequently $\Theta_{\mu\nu} = -2T_{\mu\nu} + p g_{\mu\nu}$. Here we consider the model $f(R,T) = f_1(R) + f_2(T) = R + \alpha R^2 + \lambda T$ [62]. The $f(R,T)$ theory is reduced to $f(R)$ gravity for $T = 0$ which happens in the radiation dominated era. Thus discussion of this era in the evolution of universe within $f(R,T)$ scenario is an issue. This model solves the issue and describes the radiation dominated era. This model is reduced to GR when α and λ approach to zero and to $f(R)$ Starobinsky model [4] when only $\lambda = 0$. It simplifies the field equations (1.1.4) as

$$(1 + 2\alpha R)G_{\mu\nu} + 2\alpha(g_{\mu\nu}\Box R - \nabla_\mu\nabla_\nu R) + \frac{\alpha}{2}R^2 g_{\mu\nu} = 8\pi T_{\mu\nu} + \lambda T_{\mu\nu} - \lambda p g_{\mu\nu} + \frac{\lambda}{2}T g_{\mu\nu}, \tag{2.1.3}$$

and the trace equation is

$$6\alpha\Box R - R = 8\pi T + 3\lambda T - 4\lambda p, \tag{2.1.4}$$

which indicates the propagation of a new degree of freedom, i.e., R. Thus we consider R as an independent dynamical variable [63].

Equation (2.1.3) leads to the following field equations

$$\frac{A'}{rA^2} + \frac{1}{r^2} - \frac{1}{r^2 A} - \frac{R(3\alpha R + 2)}{6(1 + 2\alpha R)} + \frac{\alpha R' B'}{AB(1 + 2\alpha R)} = \frac{1}{1 + 2\alpha R} \left[\frac{16}{3}\pi\rho + 8\pi p + \frac{11}{6}\lambda\rho + \frac{7}{6}\lambda p\right], \tag{2.1.5}$$

$$\frac{B'}{rAB} - \frac{1}{r^2} + \frac{1}{r^2 A} + \frac{2\alpha R'}{(1 + 2\alpha R)}\left(\frac{B'}{2AB} - \frac{2}{rA}\right) + \frac{\alpha R^2}{2(1 + 2\alpha R)} = \frac{1}{(1 + 2\alpha R)}\left[8\pi p + \frac{\lambda}{2}(3p - \rho)\right], \tag{2.1.6}$$

$$\frac{r^2}{2A}\left(\frac{B'}{B}\right)' - \frac{r^2A'}{A^2}\left(\frac{2}{r}+\frac{B'}{4B}\right) + \frac{r^2B'}{2AB}\left(\frac{1}{r}+\frac{B'}{2B}\right) + \frac{2\alpha r^2}{(1+2\alpha R)}$$
$$\left[\frac{A^2}{4}+\frac{R}{6\alpha}-\frac{A'}{Ar}\right] = \frac{r^2}{(1+2\alpha R)}\left[\frac{-2}{3}\lambda p+\frac{1}{2}\lambda\rho+\frac{8}{3}\pi\rho\right], \tag{2.1.7}$$

where prime denotes differentiation with respect to r. In further calculations, we substitute $\tilde{B} = \frac{B'}{B}$. Adding Eqs.(2.1.5) and (2.1.6), we obtain

$$\begin{aligned} A' &= \frac{2rA^2}{3(1+2\alpha R)}\left[8\pi(\rho+3p)+2\lambda(\rho+2p)+R\left(\frac{1}{2}-\frac{3\alpha\tilde{B}}{rA}\right)\right. \\ &- \left.\frac{3\tilde{B}}{2rA}-\frac{3\alpha R'}{A}\left(\tilde{B}-\frac{2}{r}\right)\right]. \end{aligned} \tag{2.1.8}$$

Similarly, Eq.(2.1.7) can be rewritten as

$$\begin{aligned} \tilde{B}' &= \frac{2A'}{A}\left(\frac{2}{r}+\frac{\tilde{B}}{4}\right)-\tilde{B}\left(\frac{1}{r}+\frac{\tilde{B}}{2}\right)-\frac{4\alpha A}{(1+2\alpha R)}\left[\frac{A^2}{2}-\frac{A'}{Ar}+\frac{R}{6\alpha}\right] \\ &+ \frac{2A}{(1+2\alpha R)}\left[\frac{8}{3}\pi\rho+\lambda\left(\frac{\rho}{2}-\frac{2p}{3}\right)\right], \end{aligned} \tag{2.1.9}$$

while the trace equation gives

$$R'' = \left(\frac{A'}{2A}-\frac{\tilde{B}}{2}-\frac{2}{r}\right)R' + \frac{A}{6\alpha}\left(R+2(4\pi+\lambda)(3p-\rho)-(\rho+p)\lambda\right). \tag{2.1.10}$$

The covariant divergence of the field equations yields [64]

$$\nabla^\mu T_{\mu\nu} = \frac{f_T}{8\pi-f_T}\left[(T_{\mu\nu}+\Theta_{\mu\nu})\nabla^\mu \ln f_T + \nabla^\mu\Theta_{\mu\nu} - \frac{1}{2}g_{\mu\nu}\nabla^\mu T\right].$$

For the model $f(R,T) = R+\alpha R^2+\lambda T$, this gives

$$\nabla^\mu T_{\mu\nu} = \frac{\lambda}{8\pi-\lambda}\left[\nabla^\mu\Theta_{\mu\nu}-\frac{1}{2}g_{\mu\nu}\nabla^\mu T\right],$$

which yields the hydrostatic equilibrium equation as

$$p' + (\rho+p)\frac{\tilde{B}}{2} = \frac{\lambda}{2(8\pi-\lambda)}(\rho'-p').$$

This can also be written as

$$p' = -\frac{(\rho+p)\tilde{B}}{2\left[1-\frac{\lambda}{2(8\pi-\lambda)}\left(\frac{d\rho}{dp}-1\right)\right]}. \tag{2.1.11}$$

To study the compact objects in the framework of $f(R,T)$ gravity, we consider polytropic EoS and MIT bag model.

2.1.1 Equilibrium Configuration of Polytropic Stars

Here we discuss polytropic star having EoS $p=\sigma_1\rho^{\frac{5}{3}}$ and the constant σ_1 is assigned the value $\sigma_1 = 1.475\times 10^{-3}(fm^3/MeV)^{2/3}$ [21]. Equations (2.1.8)-(2.1.11) for $\rho = \left(\frac{p}{\sigma_1}\right)^{\frac{3}{5}}$ become

$$\begin{aligned}
A' &= \frac{2rA^2}{3(1+2\alpha R)}\left[8\pi\left(\left(\frac{p}{\sigma_1}\right)^{\frac{3}{5}}+3p\right)+2\lambda\left(\left(\frac{p}{\sigma_1}\right)^{\frac{3}{5}}+2p\right)\right.\\
&+ \left. R\left(\frac{1}{2}-\frac{3\alpha\tilde{B}}{rA}\right)-\frac{3\tilde{B}}{2rA}-\frac{3\alpha R'}{A}\left(\tilde{B}-\frac{2}{r}\right)\right], \qquad (2.1.12)\\
\tilde{B}' &= \frac{2A'}{A}\left(\frac{2}{r}+\frac{\tilde{B}}{4}\right)-\tilde{B}\left(\frac{1}{r}+\frac{\tilde{B}}{2}\right)-\frac{4\alpha A}{(1+2\alpha R)}\left[\frac{A^2}{2}-\frac{A'}{Ar}+\frac{R}{6\alpha}\right]\\
&+ \frac{2A}{(1+2\alpha R)}\left[\frac{8}{3}\pi\left(\frac{p}{\sigma_1}\right)^{\frac{3}{5}}+\lambda\left(\frac{1}{2}\left(\frac{p}{\sigma_1}\right)^{\frac{3}{5}}-\frac{2p}{3}\right)\right], \qquad (2.1.13)\\
R'' &= \left(\frac{A'}{2A}-\frac{\tilde{B}}{2}-\frac{2}{r}\right)R'+\frac{A}{6\alpha}\left(R+2(4\pi+\lambda)\left(3p-\left(\frac{p}{\sigma_1}\right)^{\frac{3}{5}}\right)\right.\\
&- \left.\left(\left(\frac{p}{\sigma_1}\right)^{\frac{3}{5}}+p\right)\lambda\right), \qquad (2.1.14)\\
p' &= \frac{-\left(\left(\frac{p}{\sigma_1}\right)^{\frac{3}{5}}+p\right)\tilde{B}}{2\left[1-\frac{\lambda}{2(8\pi+\lambda)}\left(\frac{3}{5\sigma_1}\left(\frac{p}{\sigma_1}\right)^{\frac{-2}{5}}-1\right)\right]}. \qquad (2.1.15)
\end{aligned}$$

Now we discuss the initial conditions required to integrate the above system of differential equations. The pressure and density of a compact object are regular and finite at all points. Imposing this condition at the center $r = 0$, we have from the field equations $A(0) = 1$, $A'(0) = 0$, $\tilde{B}(0) = 0$ and $R'(0) = 0$ [63]. Also, $\rho(0) = \rho_i$ and $p(0) = p_i$, where ρ_i and p_i are some initial values at the center which we fix for numerical analysis. To solve the system, we also require the value of Ricci scalar at the center, i.e., $R(0)$. Thus we have three free initial conditions, $\rho(0)$, $p(0)$ and $R(0)$. The EoS reduces one condition such that we require only the values of $p(0)$ and $R(0)$. For both cases, we use the following initial conditions

$$A(0) = 1, \quad \tilde{B}(0) = 0, \quad P(0) = 100, \quad R(0) = 10^4, \quad R'(0) = 0. \qquad (2.1.16)$$

Here, we are taking the units of radius as km, mass as $M_\odot$ and density (pressure, Ricci scalar) as MeV/fm^3 [21]. We solve Eqs.(2.1.12)-(2.1.15) numerically using the above mentioned initial conditions and investigate the effects of model parameters α and λ. The plots of the metric functions, Ricci scalar, energy density, pressure, energy condition, mass function, redshift parameter and speed of sound for this EoS are shown in Figures **2.1-2.5**.

In the left columns of these figures, $\lambda = -10$ and α is varied whereas in the right columns, $\alpha = 10$ and λ is varied. The initial conditions and the values of constants are chosen such that we have positive values of density, pressure and mass as well as maximum values of density, pressure and curvature scalar at the center of the star. The viability condition for our model yields $\lambda > -4\pi$, hence for graphical analysis we consider this range. The plots of the metric functions A, B and Ricci scalar are shown in Figure **2.1**. From the first row, we observe that B decreases as α increases while increase in λ yields larger values of B but as the radial coordinate increases, B attains smaller values for larger λ. Similarly, the second row shows that A decreases with increase in α and increases with increase in λ. The Ricci scalar decreases with

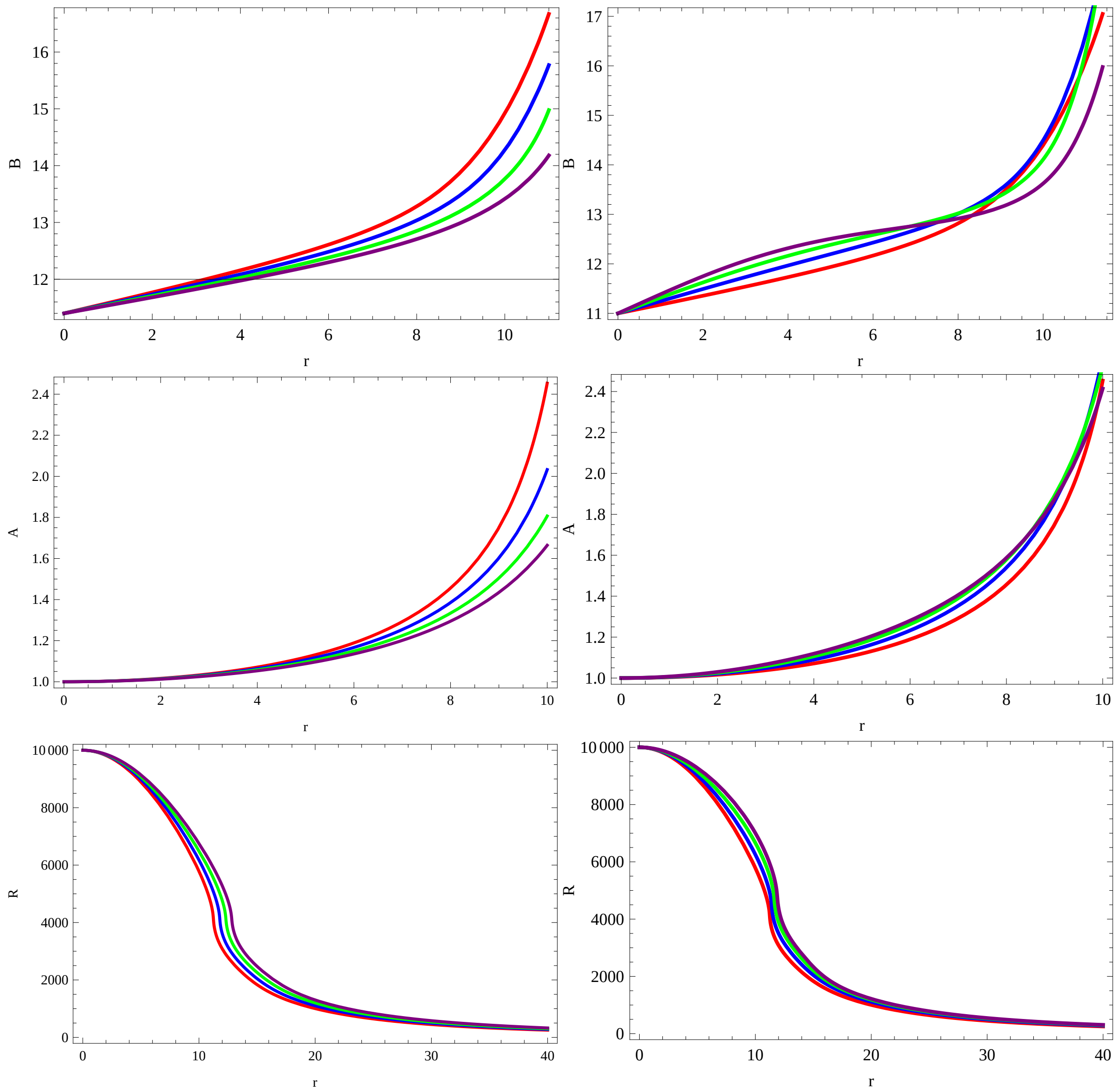

Figure 2.1: Plots of B, A and R versus r for $p = \sigma_1 \rho^{\frac{5}{3}}$, $\sigma_1 = 1.475 \times 10^{-3}$. In the left column $\lambda = -10$, $\alpha = 10$ (red), $\alpha = 11$ (blue), $\alpha = 12$ (green) and $\alpha = 13$ (purple) while in the right column $\alpha = 10$, $\lambda = -10$ (red), $\lambda = -9$ (blue), $\lambda = -8$ (green) and $\lambda = -7$ (purple).

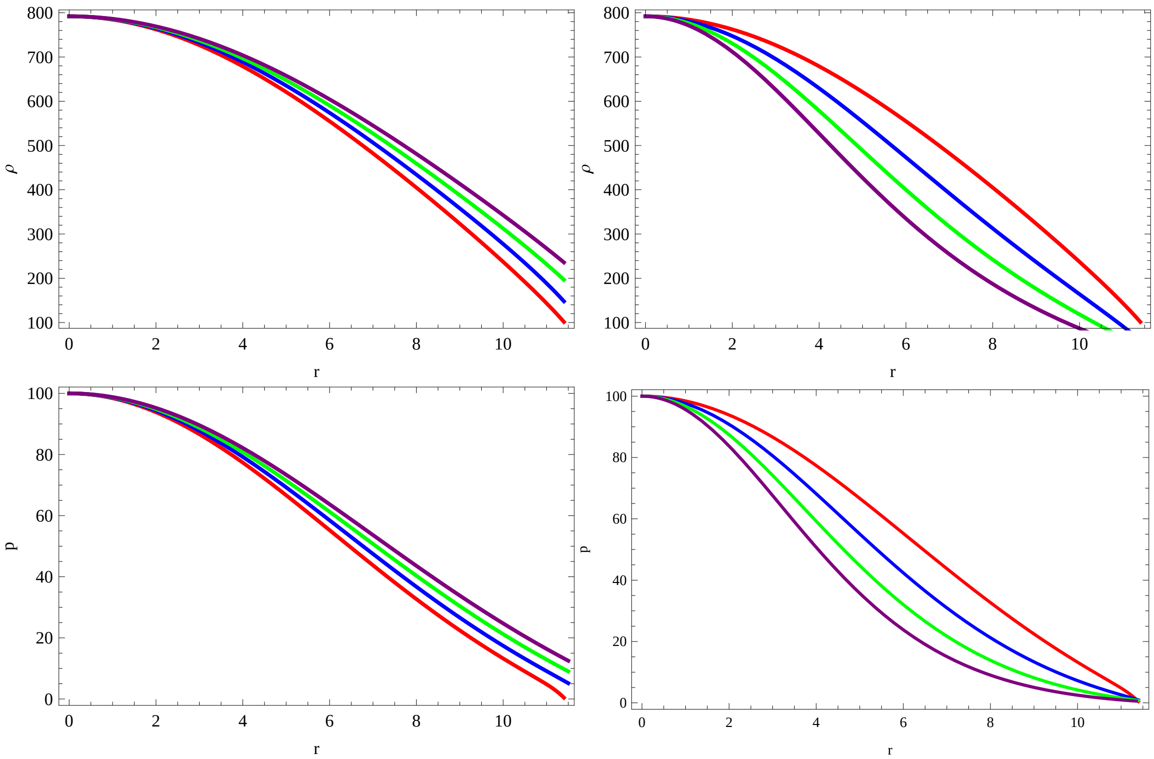

Figure 2.2: Plots of ρ and p versus r for $p = \sigma_1 \rho^{\frac{5}{3}}$, $\sigma_1 = 1.475 \times 10^{-3}$. In the left column $\lambda = -10$, $\alpha = 10$ (red), $\alpha = 11$ (blue), $\alpha = 12$ (green) and $\alpha = 13$ (purple) while in the right column $\alpha = 10$, $\lambda = -10$ (red), $\lambda = -9$ (blue), $\lambda = -8$ (green) and $\lambda = -7$ (purple).

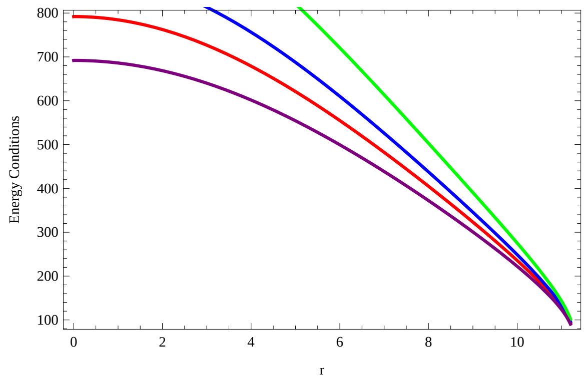

Figure 2.3: Plots of $\rho - A_t$ (red), $\rho + p - A_t$ (blue), $\rho + 3p - A_t$ (green) and $\rho - p - A_t$ (purple) for $p = \sigma_1 \rho^{\frac{5}{3}}$, $\sigma_1 = 1.475 \times 10^{-3}$, $\lambda = -10$, $\alpha = 10$.

the increase in radius of the star but it decreases rapidly till the boundary of the star as compared to its exterior. Also, it increases for the increase in α as well as λ.

The first row of Figure **2.2** shows that energy density increases with the increase in α while it decreases with increase in λ. The plots in the second row shows that $p = 0$ for $\alpha = 10$ and $\lambda = -10$ at $r \approx 11.4km$. Thus the polytropic star with $\alpha = 10$ and $\lambda = -10$ has the radius approximately $11.4km$. The authors [21] showed that the star has the radius approximately $r \approx 12km$ for the same EoS and model $f(R, T) = R + 2\lambda T$ with different values of λ. For our model, pressure increases with increase in α and decreases with increase in λ. However, the radius of the star remains the same for different values of λ and vary as α varies. For curvature-matter coupled gravity, particles follow non-geodesic trajectories for which the energy conditions are given in section **1.3**. Here we use these conditions and the term A_t (which is the covariant derivative of acceleration) is obtained as

$$A_t = \frac{1}{2AB}\left[B'' - \frac{B'^2}{2B} - \frac{A'B'}{2A} + \frac{B'}{r}\right]. \tag{2.1.17}$$

Figure **2.3** shows that all the energy conditions are satisfied for the considered values of parameters in this case.

The first row of Figure **2.4** indicates the behavior of mass function

$$m(r) = \frac{r}{2}\left(1 - \frac{1}{A(r)}\right), \tag{2.1.18}$$

which increases with radius of the star. Also, mass of the star decreases with increase in α while for increase in λ, it first shows an increase but for larger values of r, it shows an opposite behavior. The compactness factor and surface gravitational redshift are defined as

$$u(r) = \frac{m(r)}{r}, \tag{2.1.19}$$

$$z_s = (1 - 2u(R_b))^{-\frac{1}{2}} - 1, \tag{2.1.20}$$

here R_b is the total radius of the star. The second and third rows of this figure give the behavior of compactness $u(r)$ and surface gravitational redshift z_s, respectively. Both increase with radial coordinate and λ while decrease with α. The speed of sound ($v_s^2 = \frac{dp}{d\rho}$) for this EoS lies within the range $0 \leq v_s^2 \leq 1$ as shown in Figure **2.5** implying that the polytropic stars are stable (for the chosen initial conditions and model parameters) in $f(R,T)$ gravity.

2.1.2 Equilibrium Configuration of Quark Stars

This section deals with the physical properties of quark stars governed by EoS $p = \tilde{a}(\rho - 4\mathcal{B})$ with constants $\tilde{a} = 0.28$ and $\mathcal{B} = 60MeV/fm^3$ [21]. Substituting $\rho = \left(\frac{p}{\tilde{a}} + 4\mathcal{B}\right)$, Eqs.(2.1.8)-(2.1.11) give

$$\begin{aligned} A' &= \frac{2rA^2}{3(1+2\alpha R)}\left[8\pi\left(\left(\frac{p}{\tilde{a}} + 4\mathcal{B}\right) + 3p\right) + 2\lambda\left(\left(\frac{p}{\tilde{a}} + 4\mathcal{B}\right) + 2p\right)\right. \\ &+ \left. R\left(\frac{1}{2} - \frac{3\alpha\tilde{B}}{rA}\right) - \frac{3\tilde{B}}{2rA} - \frac{3\alpha R'}{A}\left(\tilde{B} - \frac{2}{r}\right)\right], \end{aligned} \tag{2.1.21}$$

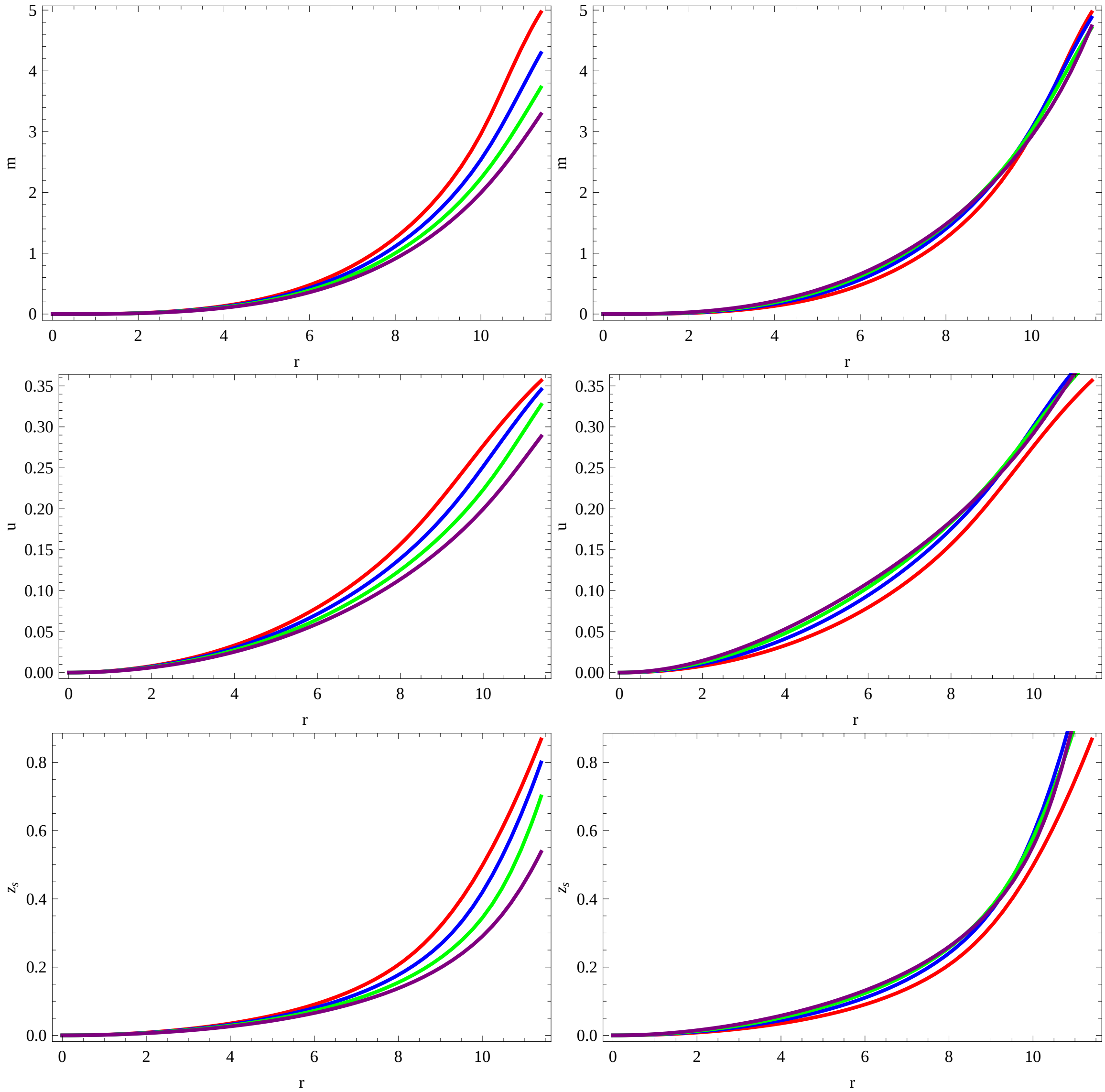

Figure 2.4: Plots of m, u and z_s versus r for $p = \sigma_1 \rho^{\frac{5}{3}}$, $\sigma_1 = 1.475 \times 10^{-3}$. In the left column $\lambda = -10$, $\alpha = 10$ (red), $\alpha = 11$ (blue), $\alpha = 12$ (green) and $\alpha = 13$ (purple) while in the right column $\alpha = 10$, $\lambda = -10$ (red), $\lambda = -9$ (blue), $\lambda = -8$ (green) and $\lambda = -7$ (purple).

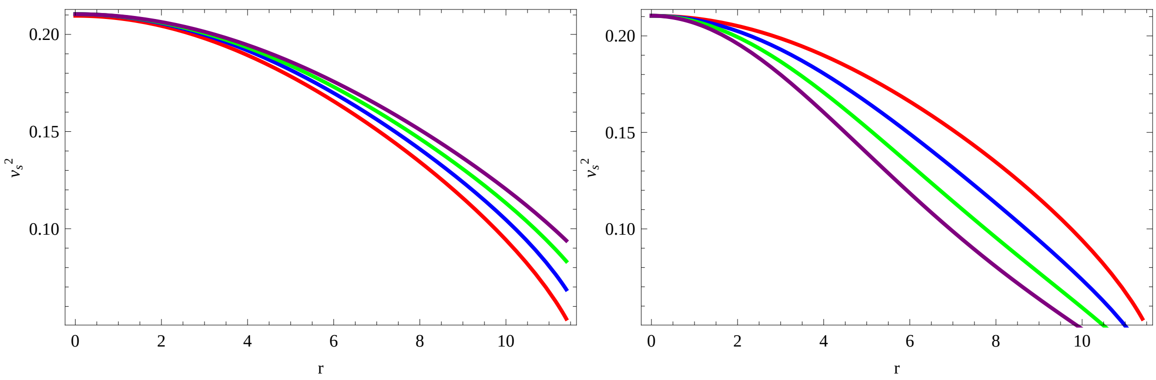

Figure 2.5: Plots of v_s^2 versus r for $p = \sigma_1 \rho^{\frac{5}{3}}$, $\sigma_1 = 1.475 \times 10^{-3}$. In the left graph $\lambda = -10$, $\alpha = 10$ (red), $\alpha = 11$ (blue), $\alpha = 12$ (green) and $\alpha = 13$ (purple) while in the right graph $\alpha = 10$, $\lambda = -10$ (red), $\lambda = -9$ (blue), $\lambda = -8$ (green) and $\lambda = -7$ (purple).

$$\begin{aligned}
\tilde{B}' &= \frac{2A'}{A}\left(\frac{2}{r}+\frac{\tilde{B}}{4}\right) - \tilde{B}\left(\frac{1}{r}+\frac{\tilde{B}}{2}\right) - \frac{4\alpha A}{(1+2\alpha R)}\left[\frac{A^2}{2} - \frac{A'}{Ar} + \frac{R}{6\alpha}\right] \\
&+ \frac{2A}{(1+2\alpha R)}\left[\frac{8}{3}\pi\left(\frac{p}{\tilde{a}}+4\mathcal{B}\right) + \lambda\left(\frac{1}{2}\left(\frac{p}{\tilde{a}}+4\mathcal{B}\right) - \frac{2p}{3}\right)\right], \qquad (2.1.22) \\
R'' &= \left(\frac{A'}{2A} - \frac{\tilde{B}}{2} - \frac{2}{r}\right)R' + \frac{A}{6\alpha}\left(R + 2(4\pi+\lambda)\left(3p - \left(\frac{p}{\tilde{a}}+4\mathcal{B}\right)\right)\right. \\
&- \left.\left(\left(\frac{p}{\tilde{a}}+4\mathcal{B}\right)+p\right)\lambda\right), \qquad (2.1.23) \\
p' &= \frac{-\left(\left(\frac{p}{\tilde{a}}+4\mathcal{B}\right)+p\right)\tilde{B}}{2\left[1 - \frac{\lambda}{2(8\pi+\lambda)}\left(\frac{1}{\tilde{a}}-1\right)\right]}. \qquad (2.1.24)
\end{aligned}$$

Imposing the same initial conditions, we obtain numerical solution of the above system of differential equations. The values of model parameter α remain the same while the values of λ are taken different from the previous case so that we have viable pressure, density and curvature scalar. The effect of model parameters (α, λ) on A, B and R is similar to the previous case as shown in Figure **2.6**. The pressure is zero at $r \approx 10.2km$ as observed from the first row of Figure **2.7** for $\alpha = 10$ and $\lambda = -10$. This indicates that increase in α increases density and pressure while increase in

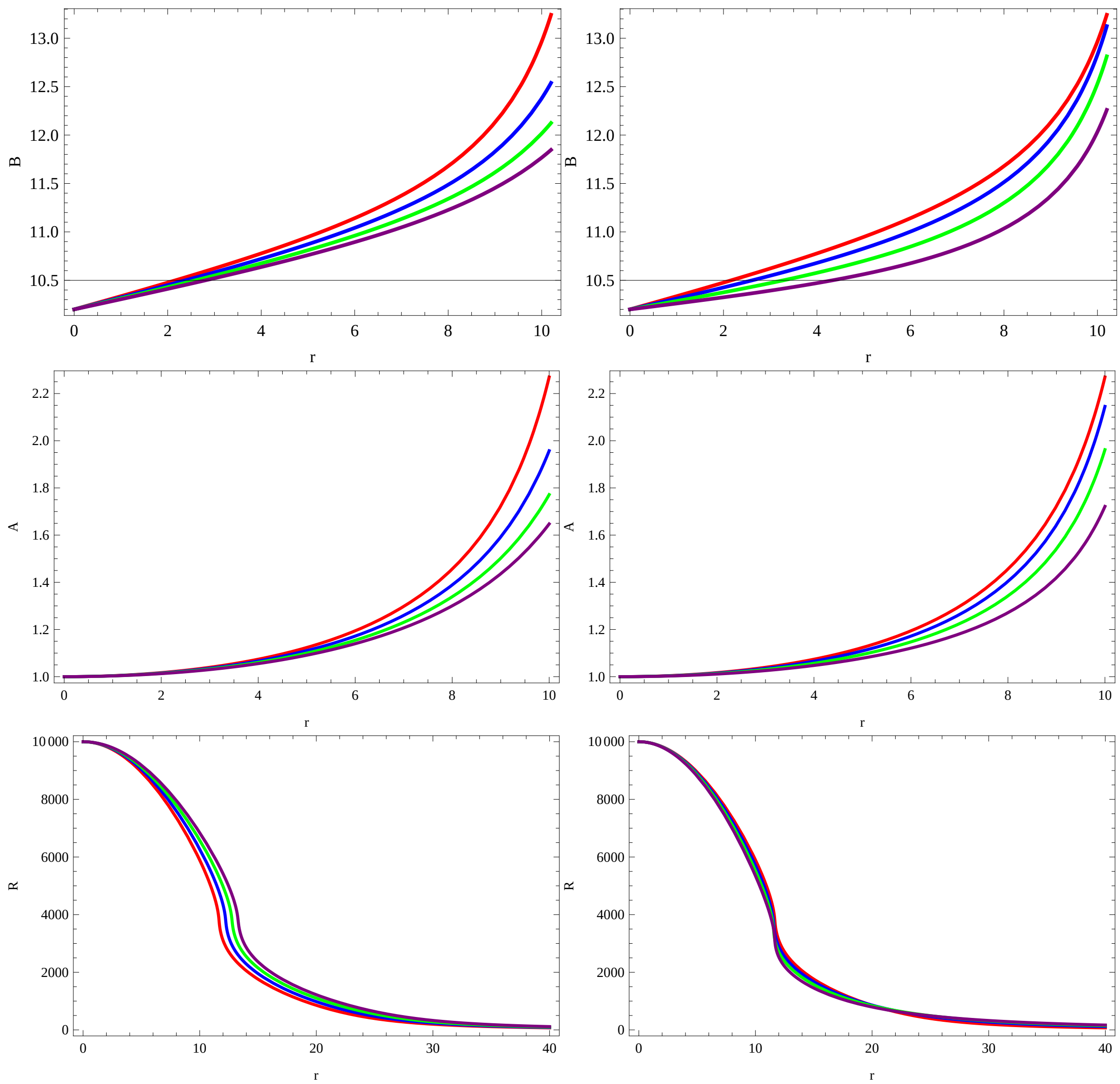

Figure 2.6: Plots of B, A and R versus r for $p = \tilde{a}(\rho - 4\mathcal{B})$, $\tilde{a} = 0.28$, $\mathcal{B} = 60$. In left column $\lambda = -10$, $\alpha = 10$ (red), $\alpha = 11$ (blue), $\alpha = 12$ (green) and $\alpha = 13$ (purple) while in right column $\alpha = 10$, $\lambda = -10$ (red), $\lambda = -10.5$ (blue), $\lambda = -11$ (green) and $\lambda = -11.5$ (purple).

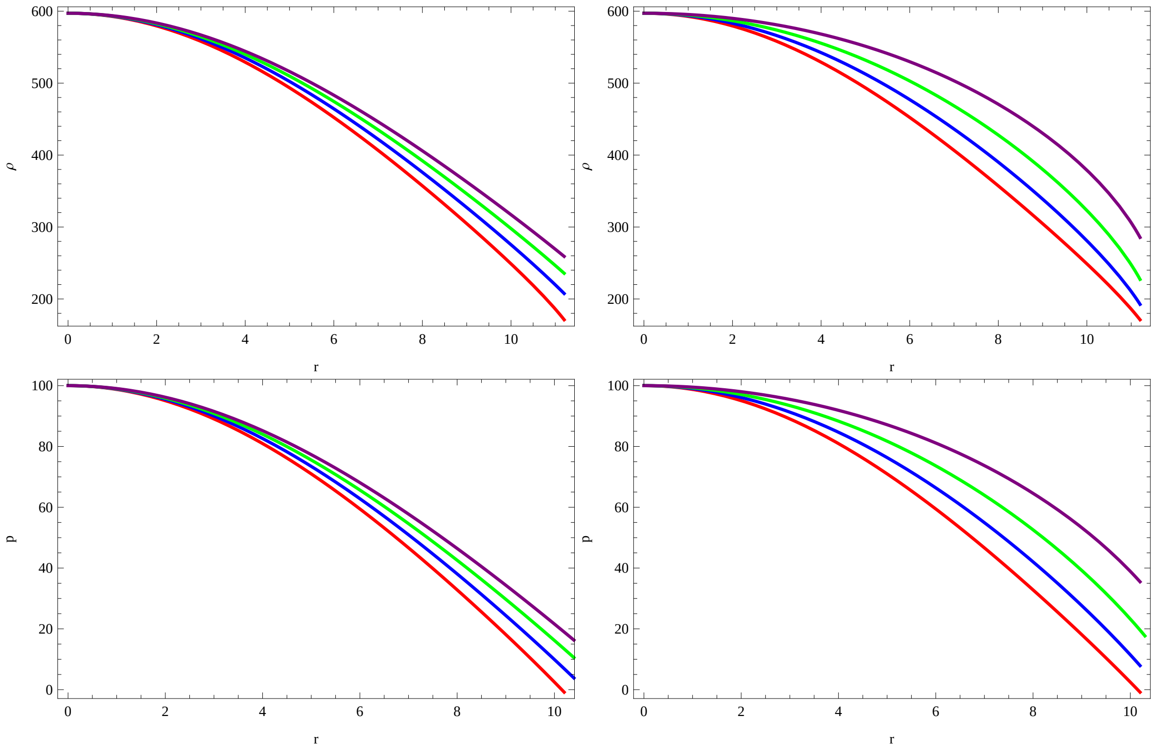

Figure 2.7: Plots of ρ and p versus r for $p = \tilde{a}(\rho - 4\mathcal{B})$, $\tilde{a} = 0.28$, $\mathcal{B} = 60$. In left column $\lambda = -10$, $\alpha = 10$ (red), $\alpha = 11$ (blue), $\alpha = 12$ (green) and $\alpha = 13$ (purple) while in right column $\alpha = 10$, $\lambda = -10$ (red), $\lambda = -10.5$ (blue), $\lambda = -11$ (green) and $\lambda = -11.5$ (purple).

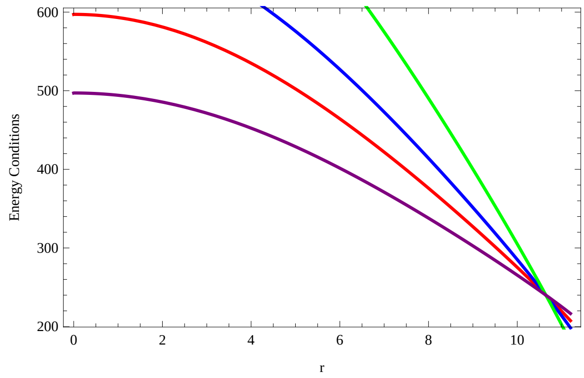

Figure 2.8: Plots of $\rho - A_t$ (red), $\rho + p - A_t$ (blue), $\rho + 3p - A_t$ (green) and $\rho - p - A_t$ (purple) for $p = \tilde{a}(\rho - 4\mathcal{B})$, $\tilde{a} = 0.28$, $\mathcal{B} = 60$, $\lambda = -10$, $\alpha = 10$.

λ produces opposite effects by decreasing pressure and density. Figure **2.8** shows that energy conditions are satisfied for quark star EoS with the considered model. The behavior of mass function, compactness and gravitational redshift are shown in Figure **2.9** where the model parameters affect in the same way as in the previous case. However, the speed of sound remains constant ($v_s^2 \approx 0.28$) with respect to radius for $\alpha = 10$ as well as $\lambda = -10$ and increase or decrease in these parameters does not affect v_s^2.

2.2 Physical Features of Charged Compact Objects

The action for $f(R,T)$ theory in the presence of electromagnetic field is defined as

$$S = \int d^4x\sqrt{-g}\left[\frac{1}{16\pi}f(R,T) + \mathcal{L}_m + \mathcal{L}_e\right]. \tag{2.2.1}$$

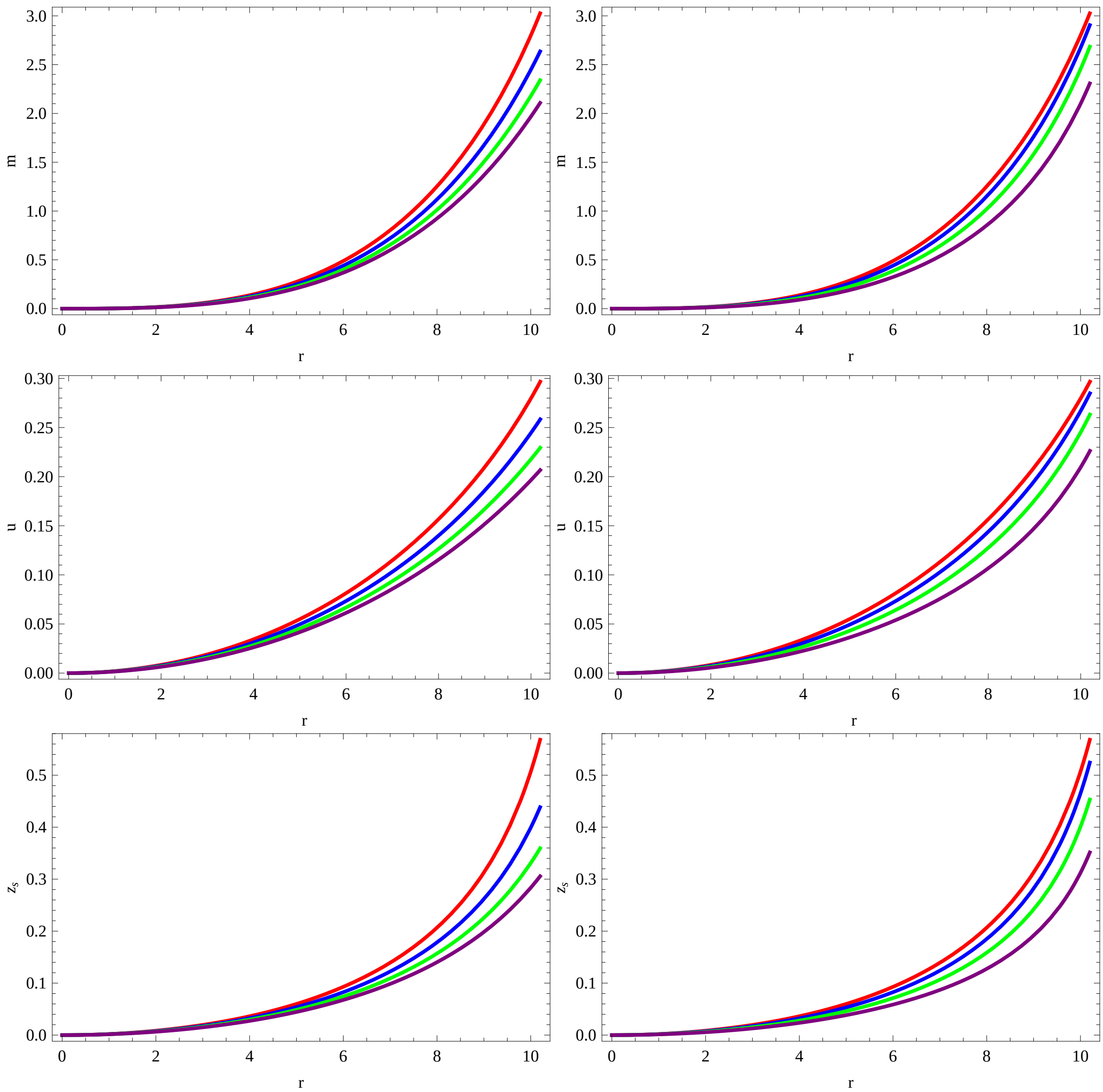

Figure 2.9: Plots of m, u and z_s versus r for $p = \tilde{a}(\rho - 4\mathcal{B})$, $\tilde{a} = 0.28$, $\mathcal{B} = 60$. In left column $\lambda = -10$, $\alpha = 10$ (red), $\alpha = 11$ (blue), $\alpha = 12$ (green) and $\alpha = 13$ (purple) while in right column $\alpha = 10$, $\lambda = -10$ (red), $\lambda = -10.5$ (blue), $\lambda = -11$ (green) and $\lambda = -11.5$ (purple).

Here $\mathcal{L}_e = lF_{\mu\nu}F^{\mu\nu}$, l is an arbitrary constant. The corresponding field equations are

$$f_R R_{\mu\nu} - \frac{1}{2}g_{\mu\nu}f + (g_{\mu\nu}\Box - \nabla_\mu\nabla_\nu)f_R = 8\pi T_{\mu\nu} - f_T(T_{\mu\nu} + \Theta_{\mu\nu}) + 8\pi E_{\mu\nu}. \quad (2.2.2)$$

In this section, we consider the same spherical symmetric spacetime as well as the energy-momentum tensor as taken in section **2.1**. We are considering comoving frame in which charges are at rest and hence no magnetic field is produced. The four potential and four current in comoving coordinates are defined as

$$\varphi_\mu = \varphi(r)\delta^0_\mu, \quad j_\mu = \xi(r)V_\mu, \quad (2.2.3)$$

φ stands for electric scalar potential and ξ represents charge density. For the metric (2.1.1), the Maxwell field equations give

$$\varphi^{''} + \varphi^{'}\left(\frac{2}{r} - \frac{A'}{2A} - \frac{B'}{2B}\right) = 4\pi\xi(r)A\sqrt{B}, \quad (2.2.4)$$

whose integration yields

$$\varphi^{'} = \frac{\sqrt{AB}q}{r^2}; \quad q = 4\pi\int_0^r \xi(r)\sqrt{A}r^2 dr, \quad (2.2.5)$$

q denotes the total charge on the sphere with $\varphi'(0) = 0$ [65]. We consider the model $R + 2\lambda T$ which simplifies the field equations as

$$G_{\mu\nu} = 8\pi T_{\mu\nu} + 2\lambda T_{\mu\nu} - 2\lambda p g_{\mu\nu} + T g_{\mu\nu} + 8\pi E_{\mu\nu}, \quad (2.2.6)$$

leading to the following set of field equations

$$\frac{A'}{rA^2} + \frac{1}{r^2} - \frac{1}{r^2 A} = 8\pi\rho + \frac{\varphi'^2}{AB} + \lambda(3\rho - p), \quad (2.2.7)$$

$$\frac{B'}{rAB} - \frac{1}{r^2} + \frac{1}{r^2 A} = 8\pi p - \frac{\varphi'^2}{AB} + \lambda(3p - \rho), \quad (2.2.8)$$

$$\frac{-1}{4rA^2B^2}\left(2A'B^2 - 2B'AB - 2rB''BA + rB'^2A + rB'A'B\right)$$

$$= 8\pi p + \frac{\varphi'^2}{AB} + \lambda(3p - \rho). \tag{2.2.9}$$

The first two field equations can be written as

$$A' = rA^2 \left[\frac{1}{r^2 A} - \frac{1}{r^2} + 8\pi\rho + \lambda(3\rho - p) + \frac{\varphi'^2}{AB}\right], \tag{2.2.10}$$

$$B' = rAB \left[-\frac{1}{r^2 A} + \frac{1}{r^2} + 8\pi p + \lambda(3p - \rho) - \frac{\varphi'^2}{AB}\right]. \tag{2.2.11}$$

For the model $f(R,T) = R+2\lambda T$, the equation of hydrostatic equilibrium becomes

$$p' + (\rho + p)\frac{B'}{2B} = \frac{\lambda}{(8\pi + 2\lambda)} \left[\rho' - p' + \frac{2\varphi'}{r^2\sqrt{AB}} \left(\frac{r^2\varphi'}{\sqrt{AB}}\right)'\right].$$

This can also be written as

$$p' = \frac{-(\rho + p)\frac{B'}{2B} + \frac{2\lambda}{(8\pi+2\lambda)} \frac{\varphi'}{r^2\sqrt{AB}} \left(\frac{r^2\varphi'}{\sqrt{AB}}\right)'}{\left[1 - \frac{\lambda}{(8\pi+2\lambda)} \left(\frac{d\rho}{dp} - 1\right)\right]}. \tag{2.2.12}$$

We have four equations (2.2.4), (2.2.10), (2.2.11) and (2.2.12) in six unknowns A, B, ρ, p, φ' and ξ. The charge density in terms of energy density can be expressed as [66]

$$\xi = \gamma\rho, \tag{2.2.13}$$

where γ is a constant. Further, the energy density is written in terms of pressure via EoS so that we have four differential equations in four unknowns (A, B, p and φ'). Now we discuss the initial conditions required to solve this system of equations ((2.2.4), (2.2.10), (2.2.11) and (2.2.12)). Imposing the condition of finiteness of pressure and density at the center $r = 0$, we have from the field equations $A(0) = 1$, $A'(0) = 0$ and $B'(0) = 0$. We have already defined the initial condition for φ' i.e., $\varphi'(0) = 0$. Thus we have two initial conditions $A(0) = 1$ and $\varphi'(0) = 0$ while $B(0)$ and $p(0)$ are free to choose. For both cases, we use the following initial conditions

$$A(0) = 1, \quad B(0) = 5, \quad p(0) = 100, \quad \varphi'(0) = 0. \tag{2.2.14}$$

In the following, we consider the polytropic EoS for $\sigma_2 = \frac{5}{3}$ and 2, to investigate the evolution of charged spherically symmetric configurations.

2.2.1 Polytropic Star for $\sigma_2 = \frac{5}{3}$

Equations (2.2.4), (2.2.10), (2.2.11) and (2.2.12) for $\rho = \left(\frac{p}{\sigma_1}\right)^{\frac{3}{5}}$ become

$$\varphi^{''} + \varphi^{'}\left(\frac{2}{r} - \frac{A'}{2A} - \frac{B'}{2B}\right) = 4\pi\gamma\left(\frac{p}{\sigma_1}\right)^{\frac{3}{5}} A\sqrt{B}, \tag{2.2.15}$$

$$A' = rA^2\left[\frac{1}{r^2A} - \frac{1}{r^2} + 8\pi\left(\frac{p}{\sigma_1}\right)^{\frac{3}{5}} + \lambda(3\left(\frac{p}{\sigma_1}\right)^{\frac{3}{5}} - p) + \frac{\varphi'^2}{AB}\right], \tag{2.2.16}$$

$$B' = rAB\left[-\frac{1}{r^2A} + \frac{1}{r^2} + 8\pi p + \lambda(3p - \left(\frac{p}{\sigma_1}\right)^{\frac{3}{5}}) - \frac{\varphi'^2}{AB}\right], \tag{2.2.17}$$

$$p' = \frac{-(\left(\frac{p}{\sigma_1}\right)^{\frac{3}{5}} + p)\frac{B'}{2B} + \frac{2\lambda}{(8\pi+2\lambda)}\frac{\varphi'}{r^2\sqrt{AB}}\left(\frac{r^2\varphi'}{\sqrt{AB}}\right)'}{\left[1 - \frac{\lambda}{(8\pi+2\lambda)}\left(\frac{3}{5\sigma_1}\left(\frac{p}{\sigma_1}\right)^{\frac{-2}{5}} - 1\right)\right]}. \tag{2.2.18}$$

We solve Eqs.(2.2.15)-(2.2.18) numerically using the above mentioned initial conditions and investigate the effects of model parameter λ. The plots of the metric functions, energy density, pressure, speed of sound, mass function, redshift parameter, charge, electric field intensity and energy conditions are shown in Figures **2.10-2.13**. The plots of the metric functions B, A, ρ, p and v_s^2 are shown in Figure **2.10**. The first graph shows that B increases with increase in radial coordinate and decrease in λ. The scale in the plot of A is greater than 1 but $A(0) = 1$ so, it first increases and then starts decreasing with the radius. Also, as λ decreases, A increases. The pressure is zero at $r \approx 1.5km$ suggesting that this is the radius of charged polytropic star in this case. The speed of sound for this EoS lies within the range $0 \leq v_s^2 \leq 1$ implying that the polytropic star with $\sigma_2 = \frac{5}{3}$ is stable (for the chosen initial conditions and model

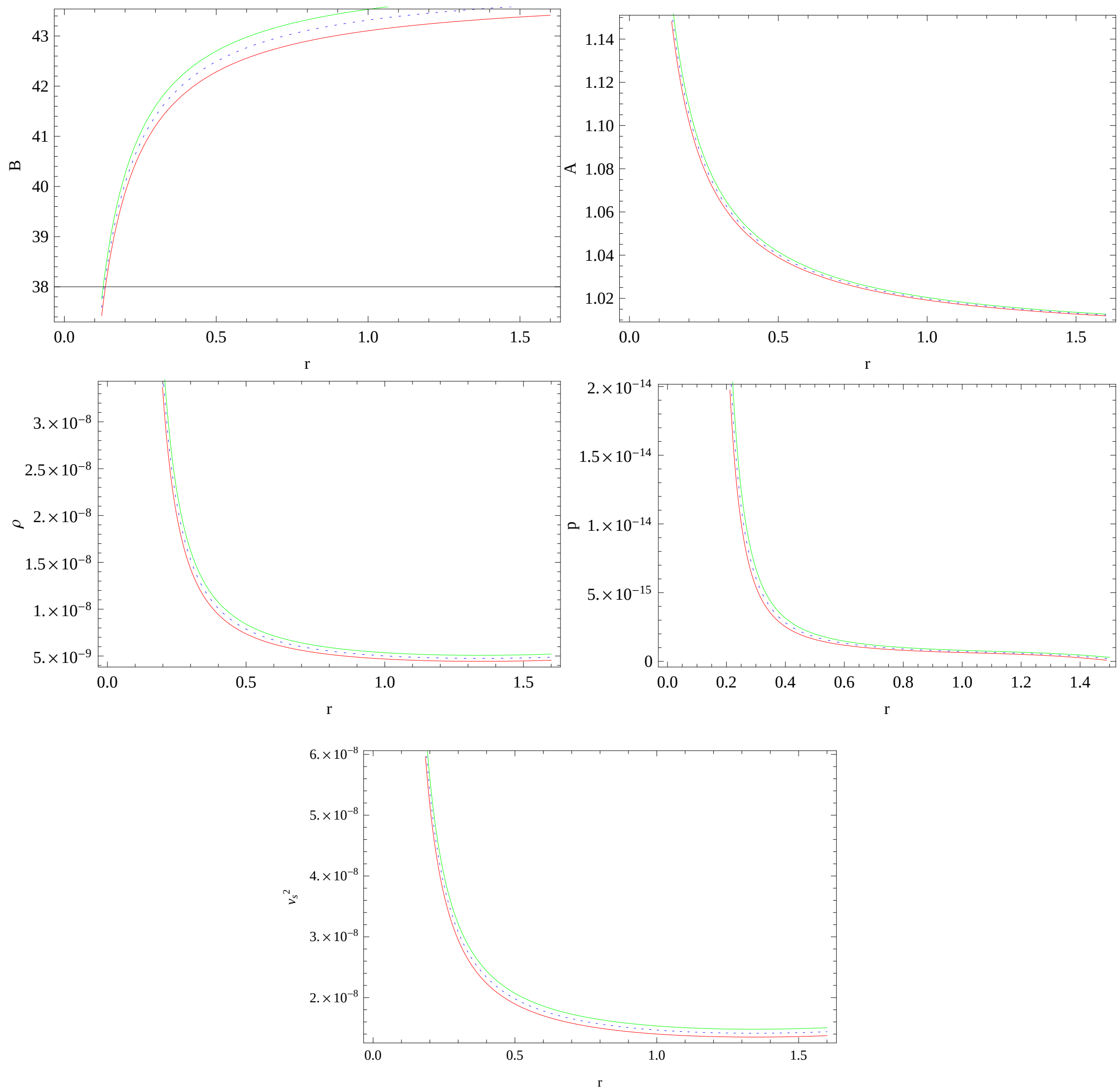

Figure 2.10: Plots of B, A, ρ, p and v_s^2 versus r for $p = \sigma_1 \rho^{\frac{5}{3}}$, $\sigma_1 = 0.003$, $\gamma = 1$, $\lambda = -0.3$ (red), $\lambda = -0.301$ (blue) and $\lambda = -0.302$ (green).

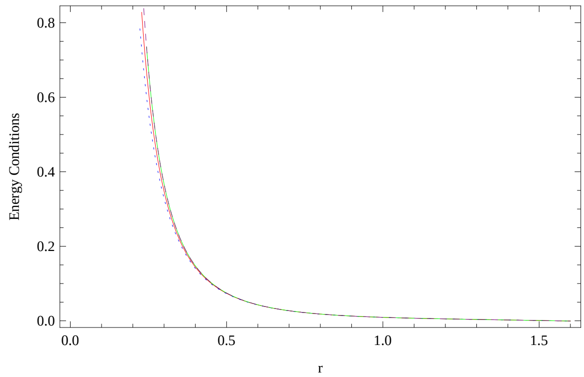

Figure 2.11: Plots of $\rho+\frac{\varphi'^2}{8\pi AB}-A_t$ (red), $\rho+p-A_t$ (blue), $\rho-p+\frac{\varphi'^2}{4\pi AB}-A_t$ (green) and $\rho+3p-\frac{\varphi'^2}{4\pi AB}-A_t$ (purple) for $p=\sigma_1\rho^{\frac{5}{3}}$, $\sigma_1=0.003$, $\gamma=1$, $\lambda=-0.3$,.

parameters) for our model. The decrease in model parameter increases the quantities ρ, p and v_s^2. In the presence of charge, the energy conditions become

- WEC: $\rho+\frac{\varphi'^2}{8\pi AB}-A_t\geq 0, \quad \rho+p-A_t\geq 0,$
- NEC: $\rho+p-A_t\geq 0,$
- SEC: $\rho+3p-\frac{\varphi'^2}{4\pi AB}-A_t\geq 0, \quad \rho+p-A_t\geq 0,$
- DEC: $\rho+\frac{\varphi'^2}{8\pi AB}-A_t\geq 0, \quad \rho\pm p+\frac{\varphi'^2}{4\pi AB}-A_t\geq 0.$

All energy conditions are satisfied as shown in Figure **2.11**.

The second graph in the first row of Figure **2.12** indicates the behavior of mass function obtained by

$$m(r)=\frac{r}{2}\left(1-\frac{1}{A}\right)+\frac{r^3\varphi'^2}{2AB}, \tag{2.2.19}$$

which increases with the radius of star as well as with the decrease in λ. The surface gravitational redshift

$$z_s=\left(1-\frac{2m(R_b)}{R_b}\right)^{-\frac{1}{2}}-1, \tag{2.2.20}$$

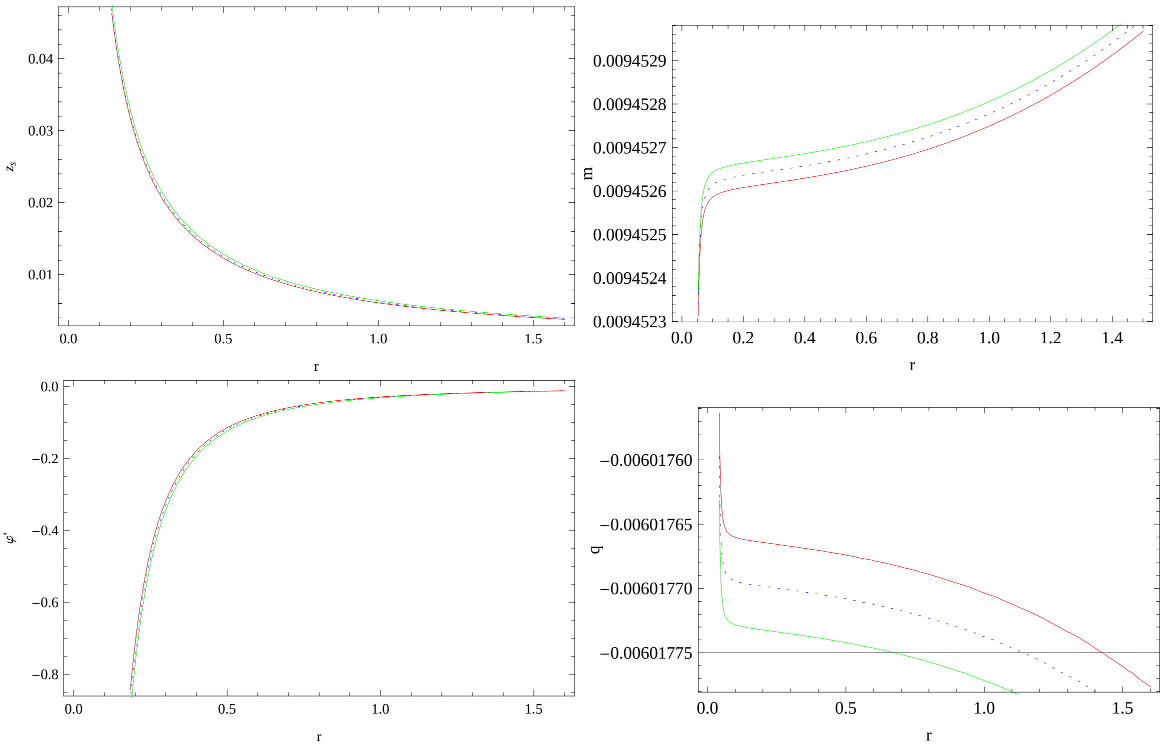

Figure 2.12: Plots of z_s, m, φ' and q versus r for $p = \sigma_1 \rho^{\frac{5}{3}}$, $\sigma_1 = 0.003$ and $\gamma = 1$. In the left column $\lambda = -0.3$ (red), $\lambda = -0.35$ (blue), $\lambda = -0.4$ (green) while in the right column $\lambda = -0.3$ (red), $\lambda = -0.30001$ (blue), $\lambda = -0.30002$ (green).

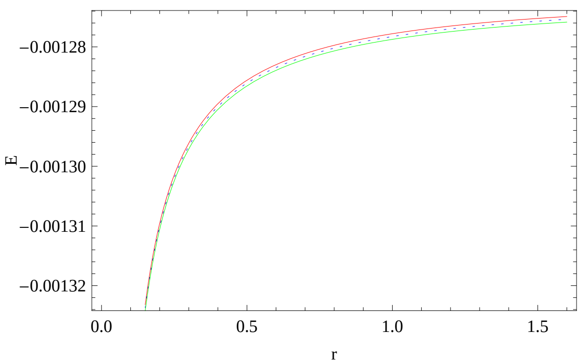

Figure 2.13: Plot of electric field intensity versus r for $p = \sigma_1 \rho^{\frac{5}{3}}$, $\sigma_1 = 0.003$, $\gamma = 1$, $\lambda = -0.3$ (red), $\lambda = -0.301$ (blue) and $\lambda = -0.302$ (green).

($m(R_b)$ is the total mass of the star) increases with increase in radial coordinate and decrease in λ as shown in the first graph of Figure **2.12**. The left graph in the second row of Figure **2.12** indicates that the derivative of electric scalar potential is negative and increasing while the right graph shows that the total charge of polytropic star is also negative but decreasing. The relation between electric field intensity E_α and electromagnetic field tensor is defined as

$$E_\alpha = F_{\alpha\beta} V^\beta. \tag{2.2.21}$$

We have only one non-zero component of $F_{\alpha\beta}$ i.e., $F_{10} = \varphi'$ yielding only one component of electric field intensity $E_1 = \frac{\varphi'}{\sqrt{B}}$ or we can simply write $E = \frac{\varphi'}{\sqrt{B}}$. Figure **2.13** shows that E has negative values. Since the electric field (E) and gravitational field are analogous, it can be interpreted that negative E is opposite to the gravitational pull and can resist or slow down the collapse. Moreover, the negative charge shows a dominance of electrons. Thus cumulatively we can say that the star is stable because electron degeneracy pressure balances gravity. The charge density has the same behavior as energy density (using Eq.(2.2.13)) as we take $\gamma = 1$ for graphical analysis.

2.2.2 Polytropic Star for $\sigma_2 = 2$

In this case, the density takes the form $\rho = \left(\frac{p}{\sigma_1}\right)^{\frac{1}{2}}$ and Eqs.(2.2.4), (2.2.10), (2.2.11) and (2.2.12) become

$$\varphi'' + \varphi'\left(\frac{2}{r} - \frac{A'}{2A} - \frac{B'}{2B}\right) = 4\pi\gamma\left(\frac{p}{\sigma_1}\right)^{\frac{1}{2}} A\sqrt{B}, \tag{2.2.22}$$

$$A' = rA^2\left[\frac{1}{r^2 A} - \frac{1}{r^2} + 8\pi\left(\frac{p}{\sigma_1}\right)^{\frac{3}{5}} + \lambda(3\left(\frac{p}{\sigma_1}\right)^{\frac{1}{2}} - p) + \frac{\varphi'^2}{AB}\right], \tag{2.2.23}$$

$$B' = rAB\left[-\frac{1}{r^2A} + \frac{1}{r^2} + 8\pi p + \lambda(3p - \left(\frac{p}{\sigma_1}\right)^{\frac{1}{2}}) - \frac{\varphi'^2}{AB}\right], \tag{2.2.24}$$

$$p' = \frac{-(\left(\frac{p}{\sigma_1}\right)^{\frac{1}{2}} + p)\frac{B'}{2B} + \frac{2\lambda}{(8\pi+2\lambda)}\frac{\varphi'}{r^2\sqrt{AB}}\left(\frac{r^2\varphi'}{\sqrt{AB}}\right)'}{\left[1 - \frac{\lambda}{(8\pi+2\lambda)}\left(\frac{1}{2\sigma_1}\left(\frac{p}{\sigma_1}\right)^{\frac{-1}{2}} - 1\right)\right]}. \tag{2.2.25}$$

Imposing the same initial conditions, the numerical solution of the above system of equations is obtained. The first row of Figure **2.14** shows similar change in the metric functions with radius and model parameter λ as in the previous case. The second row of this figure represents decreasing energy density and pressure. The zoomed graph of pressure indicates that it is zero at $r \approx 0.06km$. Also, the speed of sound lies between zero and one showing stability of the stellar structure.

Figure **2.15** represents how redshift parameter, mass function, derivative of electric scalar potential, charge and electric field intensity grow with radius and exhibit change with parameter λ. Mass and redshift parameter are inversely related with λ while φ', q as well as E have a direct relation with λ. These behavior are in agreement with the previous case. Here again φ' yields negative electric field to counteract gravitational pull and charge is negative showing that the origin of this force is electron degeneracy pressure. The plots of four energy conditions are combined in Figure **2.16**.

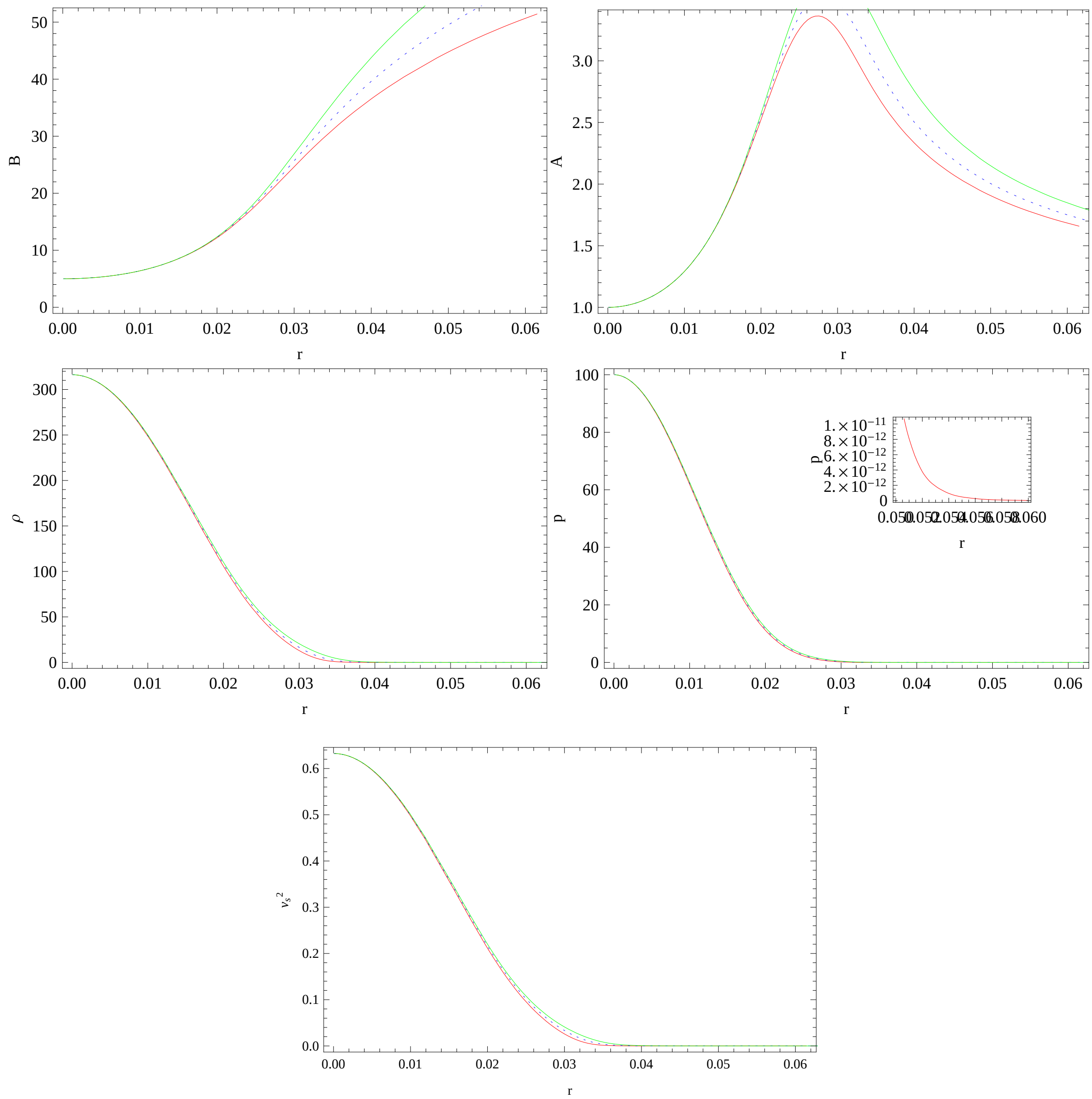

Figure 2.14: Plots of B, A, ρ, p and v_s^2 versus r for $p = \sigma_1 \rho^2$, $\sigma_1 = 0.001$, $\gamma = 1$, $\lambda = -0.3$ (red), $\lambda = -0.32$ (blue) and $\lambda = -0.34$ (green).

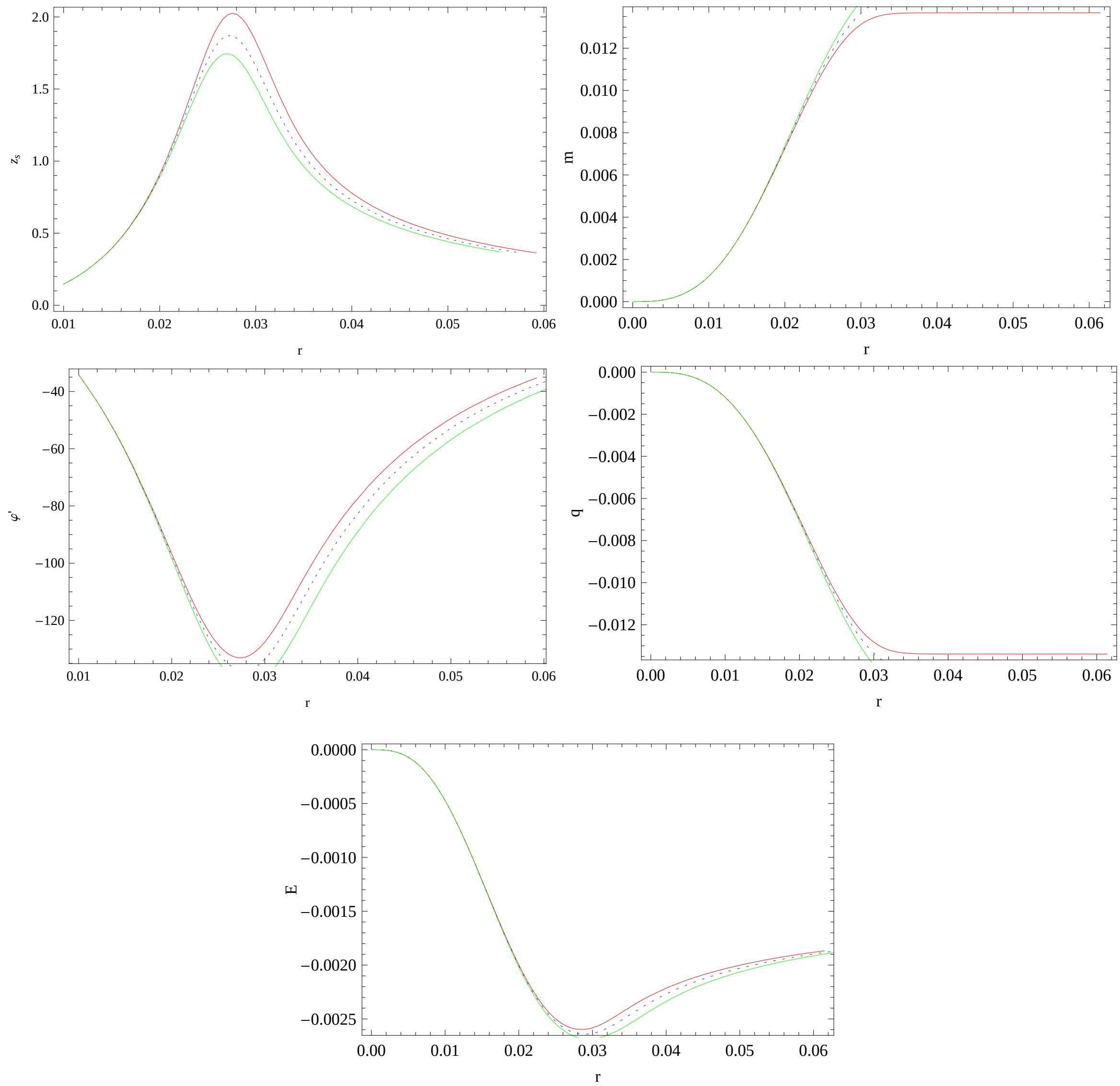

Figure 2.15: Plots of z_s, m, φ', q and E versus r for $p = \sigma_1\rho^2$, $\sigma_1 = 0.001$, $\gamma = 1$. In first graph $\lambda = -0.3$ (red), $\lambda = -0.29$ (blue) and $\lambda = -0.28$ (green) while in remaining three $\lambda = -0.3$ (red), $\lambda = -0.32$ (blue) and $\lambda = -0.34$ (green)

.

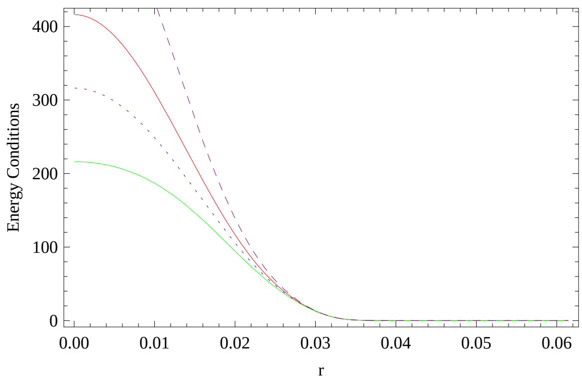

Figure 2.16: Plots of $\rho + \frac{\varphi'^2}{8\pi AB} - A_t$ (red), $\rho + p - A_t$ (blue), $\rho - p + \frac{\varphi'^2}{4\pi AB} - A_t$ (green) and $\rho + 3p - \frac{\varphi'^2}{4\pi AB} - A_t$ (purple) for $p = \sigma_1 \rho^2$, $\sigma_1 = 0.001$, $\gamma = 1$ and $\lambda = -0.3$.

Chapter 3

Collapsing and Expanding Models of Charged Configurations

In this chapter, we generate collapsing and expanding solutions for anisotropic non-static charged stellar objects in $f(R,T)$ gravity. We formulate the Einstein-Maxwell field equations and consider an auxiliary solution of these equations. Further, we evaluate expansion scalar whose negative values lead to collapse and positive values give expansion. In both cases, we explore the influence of charge as well as model parameter on density, pressures, anisotropic parameter and mass through graphs. We also check the energy conditions for both type of solutions. The chapter is organized in two sections. In section **3.1**, we formulate Einstein-Maxwell equations for spherical symmetric configurations and discuss the cases of collapse and expansion . Section **3.2** investigates the same phenomenon for cylindrically symmetric sources. The results of section **3.1**, have been published [67] and that of section **3.2** are submitted for publication [68].

3.1 Spherical Symmetric Models

The non-static spherically symmetric spacetime is taken as

$$ds^2 = -W^2(t,r)dt^2 + X^2(t,r)dr^2 + Y^2(t,r)(d\theta^2 + \sin^2\theta d\phi^2). \tag{3.1.1}$$

The energy-momentum tensor of anisotropic source (with no thermal conduction) is given by

$$T_{\mu\nu} = (\rho + p_t)V_\mu V_\nu + p_\perp g_{\mu\nu} + (p_r - p_t)X_\mu X_\nu, \tag{3.1.2}$$

where X_μ, p_r and p_t stand for four-vector, radial and tangential pressures, respectively. For the above metric, the four-vectors V_μ and X_μ have the expressions

$$V^\mu = (W^{-1}, 0, 0, 0), \quad X^\mu = (0, X^{-1}, 0, 0), \tag{3.1.3}$$

satisfying the relation $X^\mu X_\nu = 1$. Using Eqs.(1.2.1)-(1.2.3) and (2.2.3), we have following Maxwell equations

$$\varphi^{''} + \varphi^{'}\left(\frac{2Y'}{Y} - \frac{X'}{X} - \frac{W'}{W}\right) = 4\pi\xi W X^2, \tag{3.1.4}$$

$$\dot{\varphi}^{'} + \varphi^{'}\left(\frac{2\dot{Y}}{Y} - \frac{\dot{X}}{X} - \frac{\dot{W}}{W}\right) = 0. \tag{3.1.5}$$

Integration of Eq.(3.1.4) gives

$$\varphi^{'} = \frac{\sqrt{XW}q}{Y^2}, \quad q = 4\pi\int_0^r \xi X Y^2 dr, \tag{3.1.6}$$

q denotes the total charge on the sphere with $\varphi'(0) = 0$.

We consider the model $f(R,T) = R + 2\lambda T$ to study the effects of curvature-matter coupling on stellar evolution. This model and the assumption $\mathcal{L}_m = -\rho$ simplify the field equations defined in Eq.(2.2.2) as

$$G_{\mu\nu} = (8\pi + 2\lambda)T_{\mu\nu} + 2\lambda\rho g_{\mu\nu} + \lambda T g_{\mu\nu} + 8\pi E_{\mu\nu}, \tag{3.1.7}$$

which leads to the following set of field equations

$$\frac{1}{Y^2}-\frac{1}{X^2}\left[\frac{2Y''}{Y}-\frac{2X'Y'}{XY}+\frac{Y'^2}{Y^2}\right]+\frac{1}{W^2}\left[\frac{\dot{X}\dot{Y}}{XY}+\frac{\dot{Y}^2}{Y^2}\right]$$
$$=(8\pi+\lambda)\rho-\lambda p_r-2\lambda p_t+\frac{q^2}{Y^4}, \tag{3.1.8}$$
$$\frac{\dot{Y}'}{Y}-\frac{\dot{Y}}{Y}\frac{W'}{W}-\frac{\dot{X}}{X}\frac{Y'}{Y}=0, \tag{3.1.9}$$
$$\frac{1}{X^2}\left[\frac{2Y'W'}{YW}+\frac{Y'^2}{Y^2}\right]-\frac{1}{Y^2}+\frac{1}{W^2}\left[\frac{2\dot{Y}\dot{W}}{YW}-\frac{\dot{Y}^2}{Y^2}-\frac{2\ddot{Y}}{Y}\right]$$
$$=(8\pi+3\lambda)p_r+\lambda\rho+2\lambda p_t-\frac{q^2}{Y^4}, \tag{3.1.10}$$
$$\frac{1}{X^2}\left[\frac{W''}{W}+\frac{Y''}{Y}+\frac{Y'W'}{YW}-\frac{X'Y'}{XY}-\frac{X'W'}{XW}\right]+\frac{1}{W^2}\left[\frac{\dot{X}\dot{W}}{XW}+\frac{\dot{Y}\dot{W}}{YW}\right.$$
$$\left.-\frac{\dot{X}\dot{Y}}{XY}-\frac{\ddot{X}}{X}-\frac{\ddot{Y}}{Y}\right]=(8\pi+4\lambda)p_t+\lambda\rho+\lambda p_r+\frac{q^2}{Y^4}. \tag{3.1.11}$$

Solving the field equations simultaneously, we obtain the following explicit expressions of density, radial and tangential pressures

$$\begin{aligned}
\rho &= \frac{1}{8(2\pi+\lambda)(4\pi+\lambda)W^3X^3Y^4}\left[2\lambda X^2Y^3\dot{W}(Y\dot{X}+2X\dot{Y})+WX^2Y^2\right.\\
&\times \left\{4(2\pi+\lambda)X\dot{Y}^2-2\lambda Y^2\ddot{X}+Y(8\pi+3\lambda)\dot{x}\dot{y}-4\lambda X\ddot{Y}\right\}+2\lambda W^2Y^3\\
&\times \left\{2XW'Y'+Y(XW''-W'X')\right\}-2W^3\left\{X^3\left\{q^2(4\pi+3\lambda)-2(2\pi+\right.\right.\\
&\times \left.\left.\left.\lambda)Y^2\right\}-4(2\pi+\lambda)Y^3X'Y'+2(2\pi+\lambda)XY^2(Y'^2+2YY'')\right\}\right], \qquad (3.1.12)\\
p_r &= \frac{1}{8(2\pi+\lambda)(4\pi+\lambda)W^3X^3Y^4}\left[2X^2Y^3\dot{W}(2(4\pi+\lambda)X\dot{Y}-\lambda Y\dot{X})\right.\\
&+ WX^2Y^2\left\{-4(2\pi+\lambda)X\dot{Y}^2+2\lambda Y^2\ddot{X}+Y(\lambda\dot{X}\dot{Y}-4(4\pi+\lambda)X\ddot{Y})\right\}\\
&+ 2W^3X\left\{X^2(q^2(4\pi+3\lambda)-2(2\pi+\lambda)Y^2)+2(2\pi+\lambda)Y^2Y'^2\right\}\\
&+ \left.2W^2Y^3\left\{2(4\pi+\lambda)XW'Y'+\lambda Y(W'X'-XW'')\right\}\right], \qquad (3.1.13)\\
p_t &= \frac{1}{8(2\pi+\lambda)(4\pi+\lambda)W^3X^3Y^4}\left[2X^2Y^3\dot{W}\left\{(4\pi+\lambda)Y\dot{X}+4\pi X\dot{Y}\right\}\right.
\end{aligned}$$

$$- \quad WX^2Y^3\left\{(8\pi+3\lambda)\dot{X}\dot{Y}+2(4\pi+\lambda)Y\ddot{X}+8\pi X\ddot{Y}\right\}$$
$$+ \quad 2W^2Y^3\left\{4\pi X\dot{W}\dot{Y}-(4\pi+\lambda)Y(W'X'-XW'')\right\}$$
$$- \quad 2W^3\left\{q^2(4\pi+\lambda)X^3+2(2\pi+\lambda)Y^3X'Y'-2(2\pi+\lambda)XY^3Y''\right\}\Big]. \quad (3.1.14)$$

The anisotropic parameter is defined as

$$\triangle = p_r - p_t. \quad (3.1.15)$$

To discuss the phenomena of collapse and expansion, we evaluate the expansion scalar given by

$$\vartheta = \frac{1}{WXY}\left(\dot{X}Y + 2X\dot{Y}\right). \quad (3.1.16)$$

We take an auxiliary solution of Eq.(3.1.9) as

$$W = \frac{\dot{Y}}{\alpha_1 Y^{\gamma_1}}, \quad X = \alpha_1 Y^{\gamma_1}, \quad (3.1.17)$$

where γ_1 and $\alpha_1 > 0$ are arbitrary constants, which leads to

$$\vartheta = \alpha_1(2+\gamma_1)Y^{\gamma_1-1}. \quad (3.1.18)$$

When ϑ is positive we have an expanding solution otherwise a collapsing one. The value of ϑ depends on α_1, γ_1 and Y in which α_1 and Y are always positive implying that we have collapse for $\gamma_1 < -2$ and expansion for $\gamma_1 > -2$. We discuss these cases in the following subsections.

3.1.1 Collapse for $\gamma_1 < -2$

If the collapse of a self-gravitating object results into a black hole, trapped surfaces (horizons) are formed. We assume that collapse of spherically symmetric charged source results into a charged black hole. This concept is further used to find the unknown metric coefficient Y. The mass function for the considered source is given by [12]

$$m(t,r) = \frac{Y}{2X^2W}\left(X^2W^2 + X^2\dot{Y}^2 - W^2Y'^2\right) + \frac{q^2}{2Y}. \qquad (3.1.19)$$

The solution (3.1.17) simplifies the mass expression as

$$m(t,r) = \frac{Y}{2}\left(1 + \alpha_1^2 Y^{2\gamma_1} - \frac{Y'^2}{\alpha_1^2 Y^{2\gamma_1}} + \frac{q^2}{Y^2}\right). \qquad (3.1.20)$$

When $Y' = \alpha_1^2 Y^{2\gamma_1}$, this implies that we have inner and outer horizons $Y^- = m - \sqrt{m^2 - q^2}$, $Y^+ = m + \sqrt{m^2 - q^2}$, respectively which are consistent with the horizons of regular Reissner-Nordström and Vaidya-Reissner-Nordström spacetimes, also known as marginally trapped tubes [69]. The expression $Y' = \alpha_1^2 Y^{2\gamma_1}$ yields

$$Y_{trap} = \left(\alpha_1^2(1-2\gamma_1)r + H_1(t)\right)^{\frac{1}{1-2\gamma_1}}, \qquad (3.1.21)$$

where $H_1(t)$ is an integration function. Hence the collapsing solution has the form

$$W = \frac{1}{\alpha_1(1-2\gamma_1)}\dot{H}_1\left(\alpha_1^2(1-2\gamma_1)r + H_1(t)\right)^{\frac{\gamma_1}{1-2\gamma_1}}, \qquad (3.1.22)$$

$$X = \alpha_1\left(\alpha_1^2(1-2\gamma_1)r + H_1(t)\right)^{\frac{1}{1-2\gamma_1}}, \qquad (3.1.23)$$

$$Y_{trap} = \left(\alpha_1^2(1-2\gamma_1)r + H_1(t)\right)^{\frac{1}{1-2\gamma_1}}. \qquad (3.1.24)$$

We take $H_1(t) = \frac{t}{\alpha_1^2}$ and obtain the following values of ρ, p_r and p_t for the collapse solution

$$\begin{aligned}
\rho &= \frac{-\left(\frac{t}{\alpha_1^2} + r(1-2\gamma_1)\alpha_1^2\right)^{\frac{2(2+\gamma_1)}{2\gamma_1-1}}}{8(2\pi+\lambda)(4\pi+\lambda)(t + r(1-2\gamma_1)\alpha_1^4)^2}\left[8\pi\left\{-\left(\frac{t + r(1-2\gamma_1)\alpha_1^4}{\alpha_1^2}\right)^{\frac{2\gamma_1}{1-2\gamma_1}}\right.\right.\\
&\times \left(-q^2 + \left(\frac{t + r(1-2\gamma_1)\alpha_1^4}{\alpha_1^2}\right)^{\frac{2}{1-2\gamma_1}}\right)(4\gamma_1^2\alpha_1^8 r^2 + (t + r\alpha_1^4)^2)\\
&+ \gamma_1\alpha_1^4\left\{\alpha_1^2\left(\frac{t + r(1-2\gamma_1)\alpha_1^4}{\alpha_1^2}\right)^{\frac{4}{1-2\gamma_1}} + \left(\frac{t + r(1-2\gamma_1)\alpha_1^4}{\alpha_1^2}\right)^{\frac{2\gamma_1}{1-2\gamma_1}}\right.
\end{aligned}$$

$$
\begin{aligned}
&\times && \left(-q^2+\left(\frac{t+r(1-2\gamma_1)\alpha_1^4}{\alpha_1^2}\right)^{\frac{2}{1-2\gamma_1}}\right)(4rt+4r^2\alpha_1^4)\Bigg\}\Bigg\}+\lambda \\
&\times && \Bigg\{-\left(\frac{t+r(1-2\gamma_1)\alpha_1^4}{\alpha_1^2}\right)^{\frac{2\gamma_1}{1-2\gamma_1}}\left(-q^2+\left(\frac{t+r(1-2\gamma_1)\alpha_1^4}{\alpha_1^2}\right)^{\frac{2}{1-2\gamma_1}}\right) \\
&\times && (8\gamma_1^2\alpha_1^8r^2+2(t+r\alpha_1^4)^2)+r\alpha_1^4\Bigg\{5\alpha_1^2\left(\frac{t+r(1-2\gamma_1)\alpha_1^4}{\alpha_1^2}\right)^{\frac{4}{1-2\gamma_1}} \\
&+ && \left(\frac{t+r(1-2\gamma_1)\alpha_1^4}{\alpha_1^2}\right)^{\frac{2\gamma_1}{1-2\gamma_1}}\left(-q^2+\left(\frac{t+r(1-2\gamma_1)\alpha_1^4}{\alpha_1^2}\right)^{\frac{2}{1-2\gamma_1}}\right) \\
&\times && (8rt+8r^2\alpha_1^4)\}\}\Big], \qquad (3.1.25)
\end{aligned}
$$

$$
\begin{aligned}
p_r &= && \frac{-\left(\frac{t}{\alpha_1^2}+r(1-2\gamma_1)\alpha_1^2\right)^{\frac{2(2+\gamma_1)}{2\gamma_1-1}}}{8(2\pi+\lambda)(4\pi+\lambda)(t+r(1-2\gamma_1)\alpha_1^4)^2}\Big[-(8\gamma_1^2\alpha_1^8r^2+2(t+r\alpha_1^4)^2) \\
&\times && \Bigg\{-4\pi q^2-3\lambda q^2+(4\pi+2\lambda)\left(\frac{t+r(1-2\gamma_1)\alpha_1^4}{\alpha_1^2}\right)^{\frac{2}{1-2\gamma_1}}\Bigg\}+\gamma_1\alpha_1^4 \\
&\times && \Bigg\{32\pi r\left(\frac{t+r(1-2\gamma_1)\alpha_1^4}{\alpha_1^2}\right)^{\frac{2\gamma_1}{1-2\gamma_1}}\left(-q^2+\left(\frac{t+r(1-2\gamma_1)\alpha_1^4}{\alpha_1^2}\right)^{\frac{2}{1-2\gamma_1}}\right) \\
&\times && (t+r\alpha_1^4)+\lambda\Bigg\{\alpha_1^2\left(\frac{t+r(1-2\gamma_1)\alpha_1^4}{\alpha_1^2}\right)^{\frac{4}{1-2\gamma_1}}+\left(\frac{t+r(1-2\gamma_1)\alpha_1^4}{\alpha_1^2}\right)^{\frac{2\gamma_1}{1-2\gamma_1}} \\
&\times && \left(-3q^2+\left(\frac{t+r(1-2\gamma_1)\alpha_1^4}{\alpha_1^2}\right)^{\frac{2}{1-2\gamma_1}}\right)(8rt+8r^2\alpha_1^4)\Bigg\}\Bigg\}\Bigg], \qquad (3.1.26)
\end{aligned}
$$

$$
\begin{aligned}
p_t &= && \frac{-\left(\frac{t}{\alpha_1^2}+r(1-2\gamma_1)\alpha_1^2\right)^{\frac{2(2+\gamma_1)}{2\gamma_1-1}}}{8(2\pi+\lambda)(4\pi+\lambda)(t+r(1-2\gamma_1)\alpha_1^4)^2}\Bigg[-2q^2\left(\frac{t+r(1-2\gamma_1)\alpha_1^4}{\alpha_1^2}\right)^{\frac{2\gamma_1}{1-2\gamma_1}} \\
&\times && (4\pi+\lambda)(4r^2\gamma_1^2\alpha_1^8+(t+r\alpha_1^4)^2)+\gamma_1\alpha_1^4\left\{32\pi rq^2(t+r\alpha_1^4)\right. \\
&\times && \left(\frac{t+r(1-2\gamma_1)\alpha_1^4}{\alpha_1^2}\right)^{\frac{2\gamma_1}{1-2\gamma_1}}+\lambda\Bigg\{\alpha_1^2\left(\frac{t+r(1-2\gamma_1)\alpha_1^4}{\alpha_1^2}\right)^{\frac{4}{1-2\gamma_1}} \\
&+ && 8rq^2\left(\frac{t+r(1-2\gamma_1)\alpha_1^4}{\alpha_1^2}\right)^{\frac{2\gamma_1}{1-2\gamma_1}}(t+r\alpha_1^4)\Bigg\}\Bigg\}\Bigg]. \qquad (3.1.27)
\end{aligned}
$$

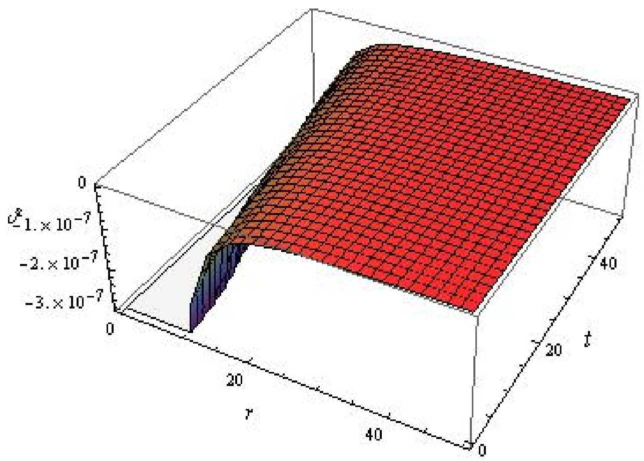

Figure 3.1: Plot of ϑ versus r and t for $\gamma_1 = -2.5$, $\alpha_1 = 1$.

For the collapse solution, the anisotropic parameter and mass function take the form

$$\triangle = -\left(\frac{\left(\frac{t+r(1-2\gamma_1)\alpha_1^4}{\alpha_1^2}\right)^{\frac{2}{1-2\gamma_1}}(-1+2q^2\left(\frac{t+r(1-2\gamma_1)\alpha_1^4}{\alpha_1^2}\right)^{\frac{2}{1-2\gamma_1}})}{2(4\pi+\lambda)}\right), \quad (3.1.28)$$

$$m = \frac{1}{2}\left(\frac{t+r(1-2\gamma_1)\alpha_1^4}{\alpha_1^2}\right)^{\frac{1}{1-2\gamma_1}} + \frac{q^2}{\left(\frac{t+r(1-2\gamma_1)\alpha_1^4}{\alpha_1^2}\right)^{\frac{1}{1-2\gamma_1}}}. \quad (3.1.29)$$

Here we discuss the graphical behavior of different physical quantities for this collapse solution. The graph of expansion scalar (Figure **3.1**) shows increasing behavior with radius but no change with time. Figures **3.2-3.5** show the graphs of density, radial/tangential pressure and anisotropy. We observe that density is decreasing while radial and tangential pressures as well as anisotropy are increasing with r but remain unchanged with time. The mass function is increasing with radial coordinate as shown in Figure **3.6**. The effects of charge and model parameter λ are summarized in Table **2**.

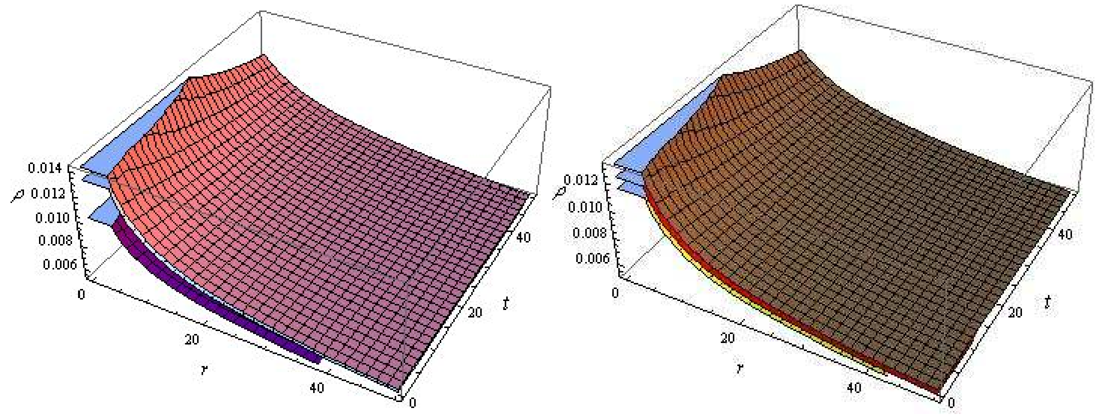

Figure 3.2: Plots of ρ versus r and t for $\gamma_1 = -2.5$, $\alpha_1 = 1$. The left graph is for $q = 0$ (pink), $q = 0.5$ (blue), $q = 1$ (purple) with $\lambda = 1$ and the right graph is for $\lambda = 1$ (brown), $\lambda = 2$ (red), $\lambda = 3$ (yellow) with $q = 0.5$.

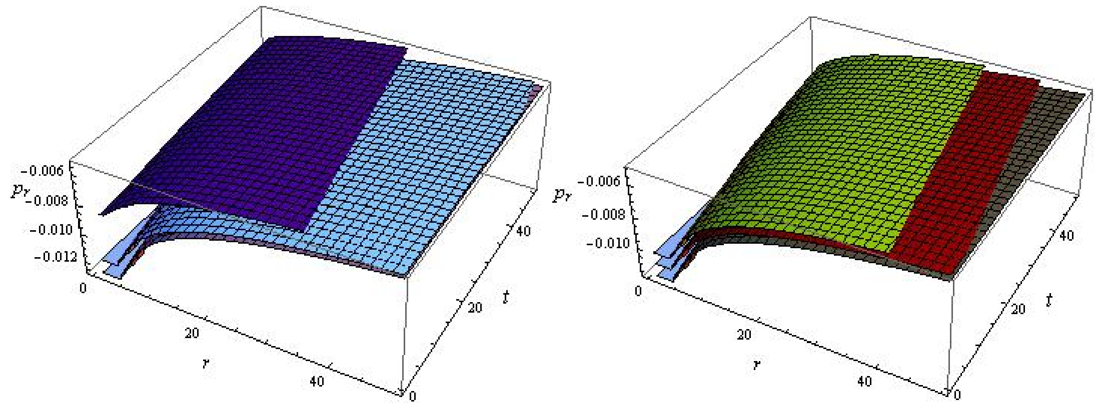

Figure 3.3: Plots of p_r versus r and t for $\gamma_1 = -2.5$, $\alpha_1 = 1$. The left graph is for $q = 0$ (pink), $q = 0.5$ (blue), $q = 1$ (purple) with $\lambda = 1$ while the right graph is for $\lambda = 1$ (brown), $\lambda = 2$ (red), $\lambda = 3$ (yellow) with $q = 0.5$.

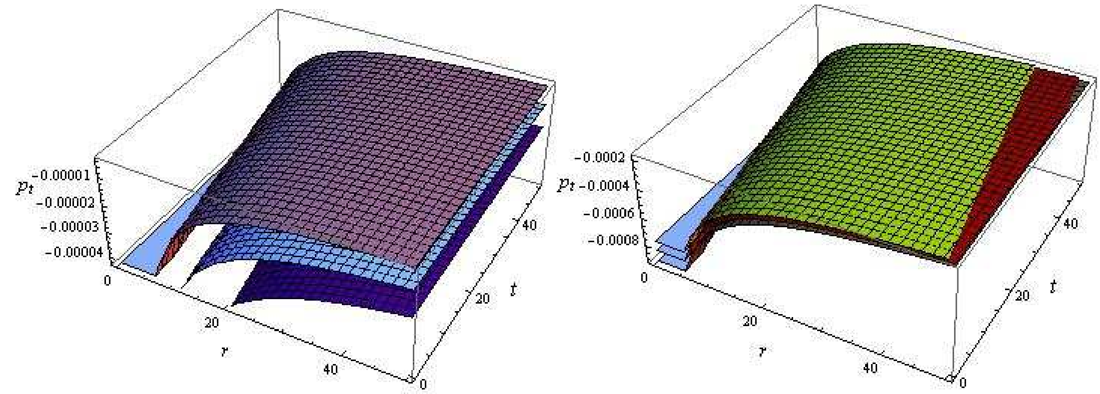

Figure 3.4: Plots of p_t versus r and t for $\gamma_1 = -2.5$, $\alpha_1 = 1$. The left graph is for $q = 0$ (pink), $q = 0.1$ (blue), $q = 0.15$ (purple) with $\lambda = 1$ and the right graph is for $\lambda = 1$ (brown), $\lambda = 2$ (red), $\lambda = 3$ (yellow) with $q = 0.5$.

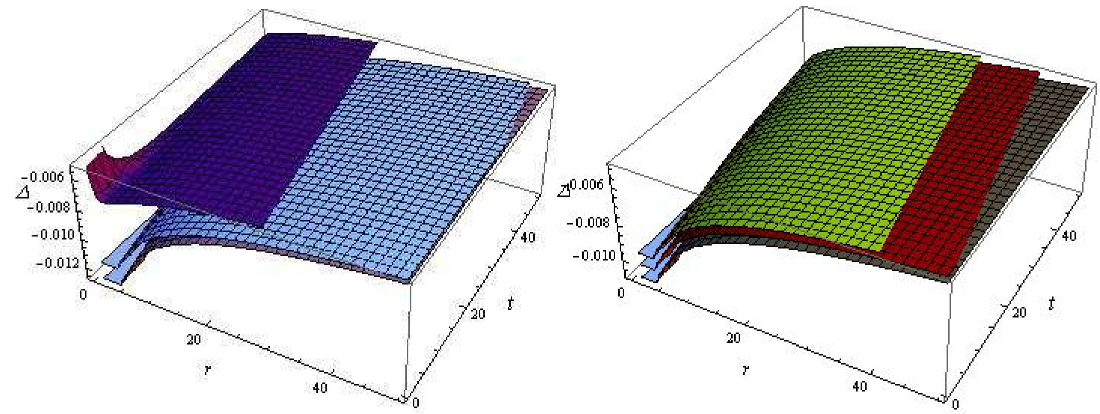

Figure 3.5: Plots of $\triangle$ versus r and t for $\gamma_1 = -2.5$, $\alpha_1 = 1$. The left graph is for $q = 0$ (pink), $q = 0.4$ (blue), $q = 0.8$ (purple) with $\lambda = 1$ while the right graph is for $\lambda = 1$ (brown), $\lambda = 2$ (red), $\lambda = 3$ (yellow) with $q = 0.5$.

Table **2**: Effects of increasing q and λ for collapsing solution

Physical Parameter	ρ	p_r	p_t	$\triangle$	m
As q Increases	decreases	increases	decreases	increases	increases
As λ Increases	decreases	increases	increases	increases	no change

The energy conditions are

- NEC: $\rho + p_r - A_t \geq 0,\ \rho + p_t + \frac{q^2}{4\pi Y^4} - A_t \geq 0,$
- WEC: $\rho + \frac{q^2}{8\pi Y^4} - A_t \geq 0,\ \rho + p_r - A_t \geq 0,\ \rho + p_t + \frac{q^2}{4\pi Y^4} - A_t \geq 0,$
- DEC: $\rho - p_r + \frac{q^2}{4\pi Y^4} - A_t \geq 0,\ \rho - p_t - A_t \geq 0,$
- SEC: $\rho + p_r + 2p_t + \frac{q^2}{4\pi Y^4} - A_t \geq 0.$

The term A_t is found as

$$A_t = \frac{1}{X^2}\left[\frac{W''}{W} + \frac{W'^2}{W^2} - \frac{W'}{W}\left(\frac{X'}{X} - \frac{2Y'}{Y}\right)\right] + \frac{\dot{W}^2}{W^4}. \tag{3.1.30}$$

The collapsing solution yields

$$A_t = \frac{\gamma_1(1+4\gamma_1)\alpha_1^6\left(\frac{t}{\alpha_1^2 + r(1-2\gamma_1)\alpha_1^2}\right)^{\frac{2\gamma_1}{2\gamma_1 - 1}}}{(t + r(1-2\gamma_1)\alpha_1^4)^2}. \tag{3.1.31}$$

All the expressions of energy conditions defined above are plotted in Figure **3.7**. These plots show that all the energy conditions are satisfied for the collapse solution as well as considered values of the free parameters.

3.1.2 Expansion for $\gamma_1 > -2$

To discuss the evolution of density and pressures in the expanding case, the value of metric function Y is needed. For non-static spherical symmetric metric, Y can either

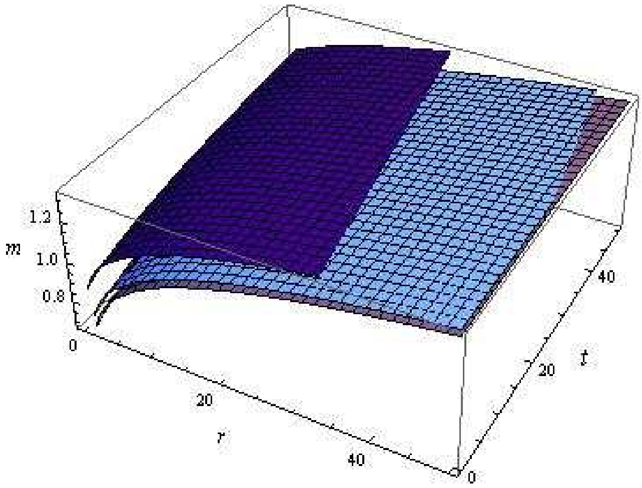

Figure 3.6: Plot of m versus r and t for $\gamma_1 = -2.5$, $\alpha_1 = 1$, $q = 0$ (pink), $q = 0.4$ (blue), $q = 0.8$ (purple).

be a function of $r + t$ or $r - t$ [70]. We consider $Y = r + t$ and check the values of ϑ through graph (Figure **3.8**) which are positive (i.e., the solution is expanding). Thus the expanding solution is given by

$$W = \frac{1}{\alpha_1 (r+t)^{\gamma_1}}, \quad X = \alpha_1 (r+t)^{\gamma_1}, \quad Y = r + t. \tag{3.1.32}$$

Consequently, the expressions of ρ, p_r and p_t take the form

$$\begin{aligned}
\rho &= \frac{1}{8(r+t)^4(2\pi+\lambda)(4\pi+\lambda)}\left[(r+t)^2(8\pi+4\lambda) - q^2(8\pi+6\lambda)\right. \\
&+ \frac{(r+t)^{2-2\gamma_1}}{\alpha_1^2}(16\pi\gamma_1 - 8\pi - 4\lambda + 6\gamma_1\lambda + 4\gamma_1^2\lambda) + \alpha_1^2(r+t)^{2+2\gamma_1} \\
&\times \left.(8\pi + 8\pi\gamma_1 + 4\lambda + \gamma_1\lambda - 4\gamma_1^2\lambda)\right], \qquad (3.1.33) \\
p_r &= \frac{1}{8(r+t)^4(2\pi+\lambda)(4\pi+\lambda)}\left[(r+t)^2(8\pi+4\lambda) - q^2(8\pi+6\lambda)\right. \\
&+ \frac{(r+t)^{2-2\gamma_1}}{\alpha_1^2}(16\pi\gamma_1 - 8\pi - 4\lambda + 6\gamma_1\lambda + 4\gamma_1^2\lambda) + \alpha_1^2(r+t)^{2+2\gamma_1} \\
&\times \left.(8\pi + 16\pi\gamma_1 + 4\lambda + 5\gamma_1\lambda - 4\gamma_1^2\lambda)\right], \qquad (3.1.34) \\
p_t &= \frac{(r+t)^{-2(2+\gamma_1)}}{8(\alpha_1)^2(2\pi+\lambda)(4\pi+\lambda)}\left[-8\pi\left\{q^2(r+t)^{2\gamma_1}\alpha_1^2 + \gamma_1 t^2\left\{1 - 2\gamma_1\right.\right.\right.
\end{aligned}$$

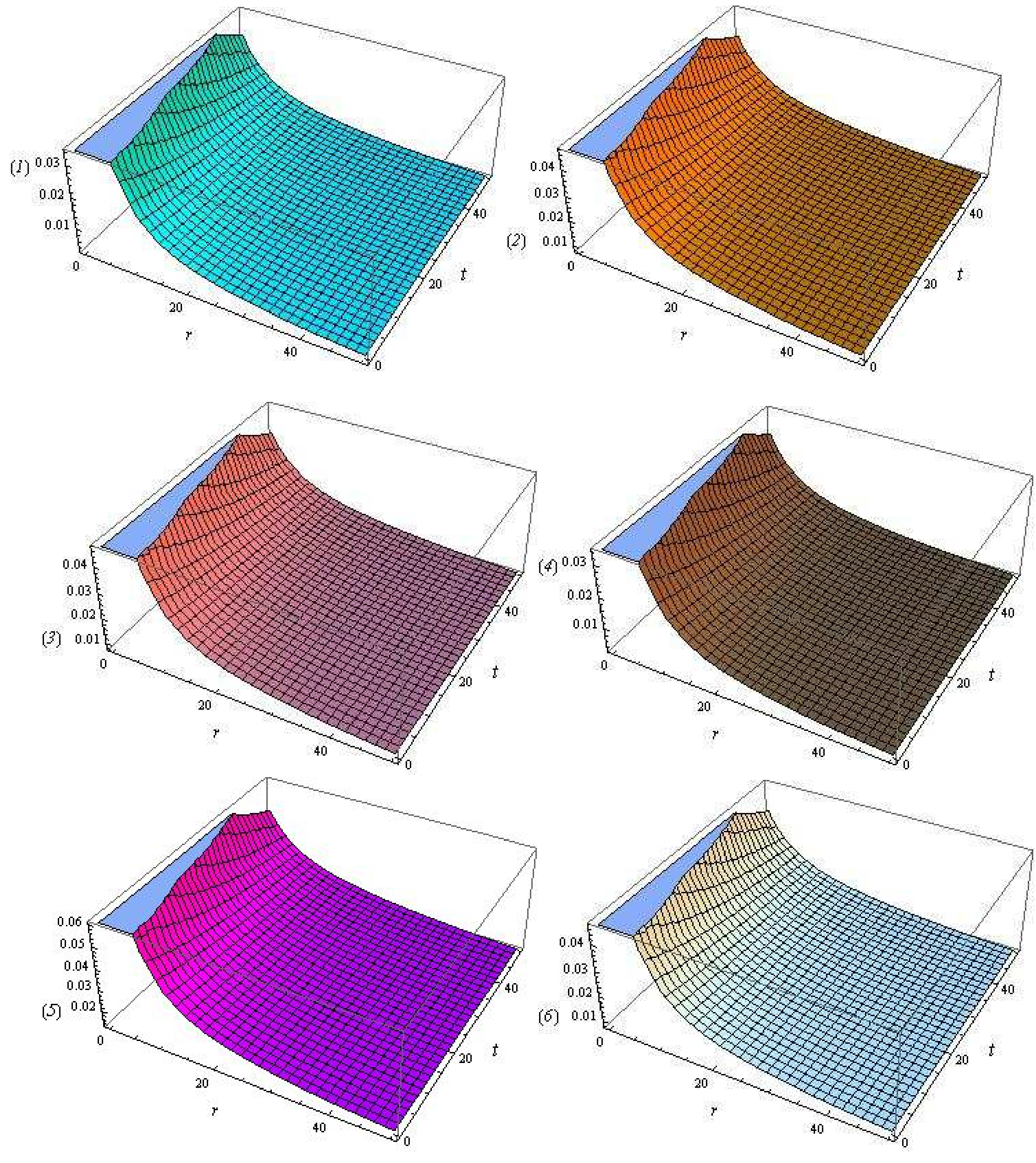

Figure 3.7: Plots of (1) $\rho + p_r - A_t$, (2) $\rho + p_t + \frac{q^2}{4\pi Y^4} - A_t$, (3) $\rho + \frac{q^2}{8\pi Y^4} - A_t$, (4) $\rho + p_r + 2p_t + \frac{q^2}{4\pi Y^4} - A_t$, (5) $\rho - p_r + \frac{q^2}{4\pi Y^4} - A_t$, (6) $\rho - p_t - A_t$ for $\gamma_1 = -2.5$, $\alpha_1 = 1$, $q = 0.5$ and $\lambda = 1$.

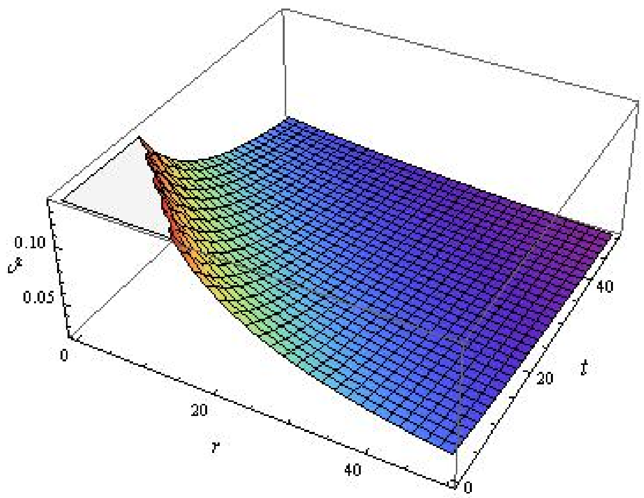

Figure 3.8: Plot of ϑ versus r and t for $\gamma_1 = 0.05$, $\alpha_1 = 1$.

$$
\begin{aligned}
&+ \quad (r+t)^{4\gamma_1}\alpha_1^4(1+2\gamma_1)\big\} + r^2\gamma_1(1+2\gamma_1 rt)\left\{1+(r+t)^{4\gamma_1}\alpha_1^4\right. \\
&+ \quad 2\gamma_1(-1+(r+t)^{4\gamma_1}\alpha_1^4)\big\}\big\}\left\{2q^2(r+t)^{2\gamma_1}\alpha_1^2+\gamma_1 t^2\left\{2-4\gamma_1\right.\right. \\
&+ \quad (r+t)^{4\gamma_1}\alpha_1^4(1+4\gamma_1)\big\} + r^2\gamma_1(1+2\gamma_1 rt)\left\{2+(r+t)^{4\gamma_1}\alpha_1^4\right. \\
&+ \quad 4\gamma_1(-1+(r+t)^{4\gamma_1}\alpha_1^4)\big\}\big\}\big]. \qquad (3.1.35)
\end{aligned}
$$

The anisotropic parameter and mass function for expanding solution are evaluated as

$$
\begin{aligned}
\triangle &= \frac{(r+t)^{-2(2+\gamma_1)}}{2(4\pi+\lambda)\alpha_1^2}\left[-2q^2(r+t)^{2\gamma_1}\alpha_1^2+(r^2+t^2)\left\{-1+\gamma_1\right.\right. \\
&+ \quad (r+t)^{2\gamma_1}\alpha_1^2+(r+t)^{4\gamma_1}\alpha_1^4(1+\gamma_1)+\gamma_1^2(2-2(r+t)^{4\gamma_1}\alpha_1^4)\big\}-2\gamma_1 t \\
&\times \quad \left\{1-2\gamma_1^2-\gamma_1-(r+t)^{2\gamma_1}\alpha_1^2+(r+t)^{4\gamma_1}\alpha_1^4(2\gamma_1^2-\gamma_1-1)\right\}\big], \qquad (3.1.36) \\
m &= \frac{1}{2}\left[(r+t)+\frac{q^2}{r+t}\right]. \qquad (3.1.37)
\end{aligned}
$$

The evolution of physical parameters during expansion is represented through graphs. Figures **3.9-3.13** show the plots of density, radial as well as tangential pressure, anisotropic parameter and mass function, respectively. It is found that in contrast to the collapsing case, here the quantities vary with time coordinate. The

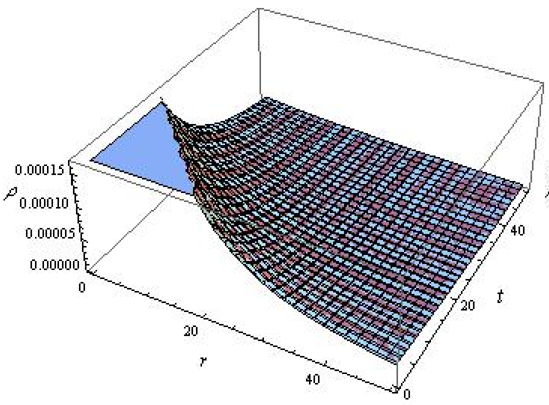

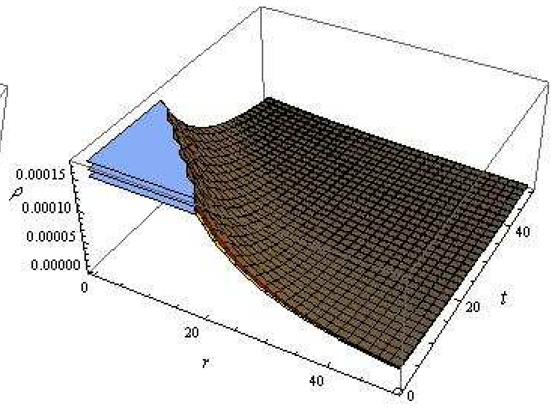

Figure 3.9: Plots of ρ versus r and t for $\gamma_1 = 0.05$, $\alpha_1 = 1$. The left graph is for $q = 0$ (pink), $q = 0.5$ (blue), $q = 1$ (purple) with $\lambda = 1$ and the right graph is for $\lambda = 1$ (brown), $\lambda = 2$ (red), $\lambda = 3$ (yellow) with $q = 0.5$.

increase (or decrease) in charge does not induce a measurable fluctuations in physical quantities. The graphical analysis is summarized in Tables **3** and **4**. The solution (3.1.32) yields the value of A_t as

$$A_t = \frac{(r+t)^{-2(1+\gamma_1)}\gamma_1}{\alpha_1^2}(-1 + \gamma_1(3 + (r+t)^{4\gamma_1}\alpha_1^4)). \tag{3.1.38}$$

The energy conditions for this case are also satisfied as shown in Figure **3.14**.

Table **3**: Change in physical parameters with respect to r and t for the expanding solution

Coordinate	ϑ	ρ	p_r	p_t	$\triangle$	m
r	decreases	decreases	increases	increases	increases	increases
t	decreases	decreases	increases	increases	increases	increases

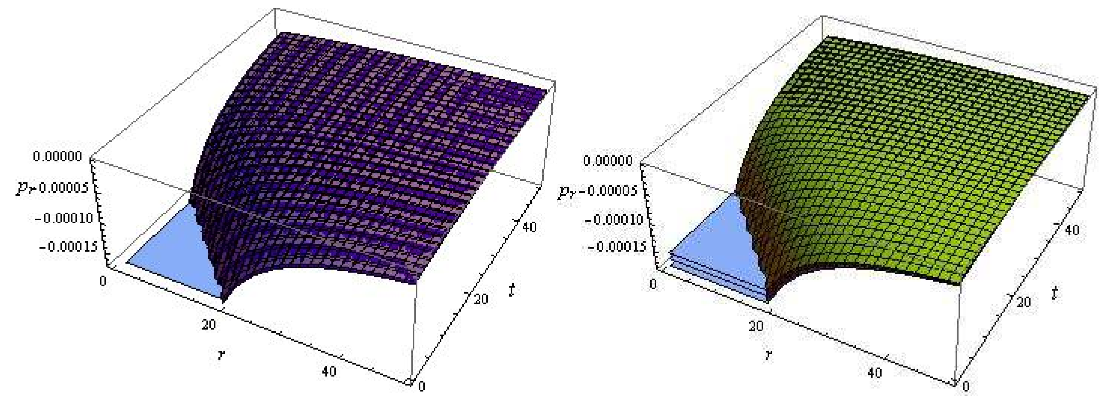

Figure 3.10: Plots of p_r versus r and t for $\gamma_1 = 0.05$, $\alpha_1 = 1$. The left graph is for $q = 0$ (pink), $q = 0.5$ (blue), $q = 1$ (purple) with $\lambda = 1$ while the right graph is for $\lambda = 1$ (brown), $\lambda = 2$ (red), $\lambda = 3$ (yellow) with $q = 0.5$.

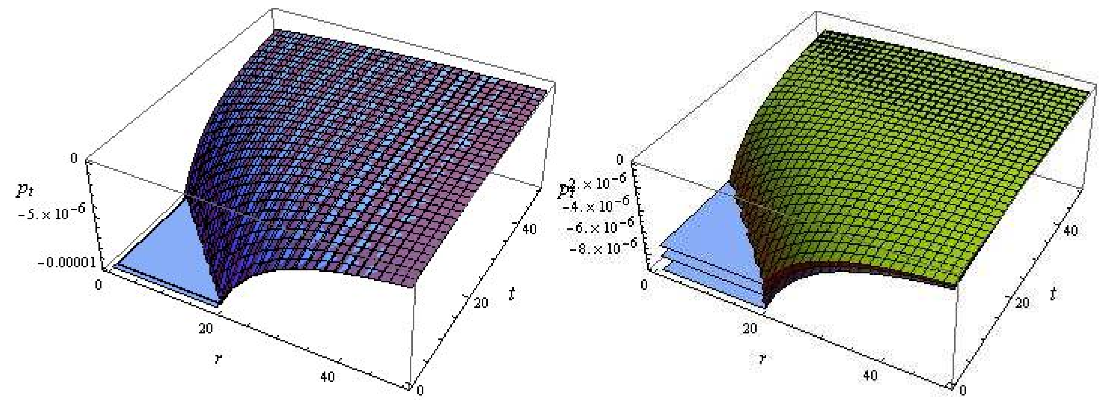

Figure 3.11: Plots of p_t versus r and t for $\gamma_1 = 0.05$, $\alpha_1 = 1$. The left graph is for $q = 0$ (pink), $q = 0.5$ (blue), $q = 1$ (purple) with $\lambda = 1$ and the right graph is for $\lambda = 1$ (brown), $\lambda = 2$ (red), $\lambda = 3$ (yellow) with $q = 0.5$.

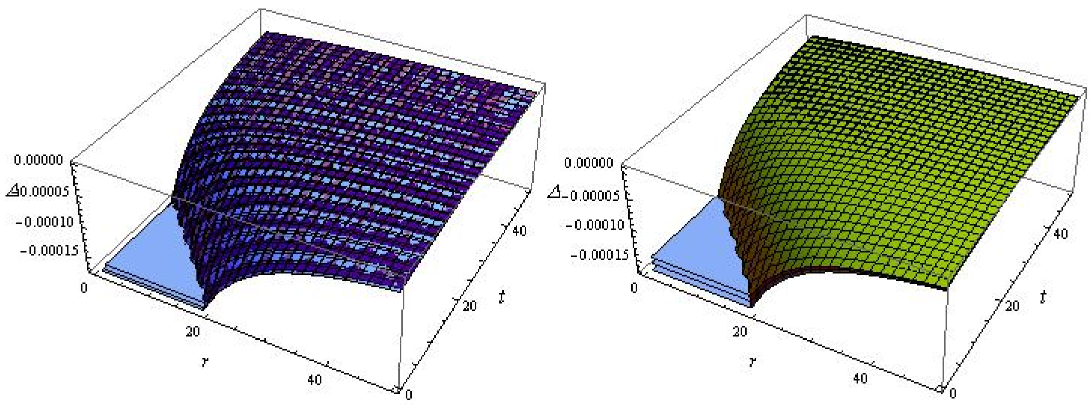

Figure 3.12: Plots of $\triangle$ versus r and t for $\gamma_1 = 0.05$, $\alpha_1 = 1$. The left graph is for $q = 0$ (pink), $q = 0.5$ (blue), $q = 1$ (purple) with $\lambda = 1$ while the right graph is for $\lambda = 1$ (brown), $\lambda = 2$ (red), $\lambda = 3$ (yellow) with $q = 0.5$.

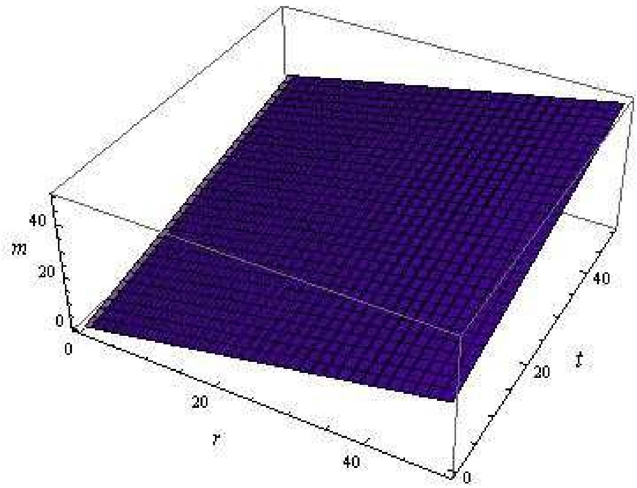

Figure 3.13: Plot of m versus r and t for $\gamma_1 = 0.05$, $\alpha_1 = 1$, $q = 0$ (pink), $q = 0.5$ (blue), $q = 1$ (purple).

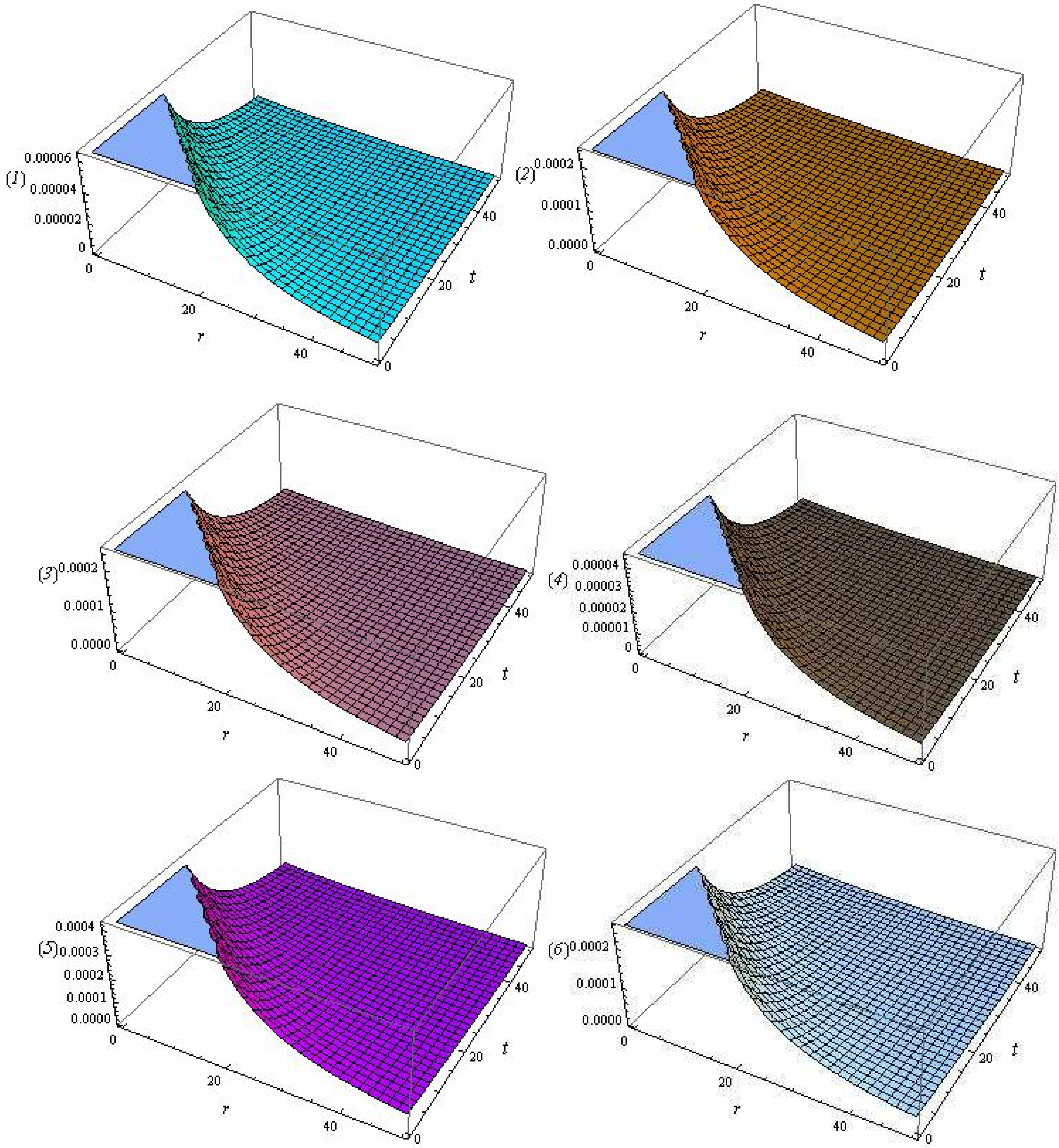

Figure 3.14: Plots of (1) $\rho + p_r - A_t$, (2) $\rho + p_t + \frac{q^2}{4\pi Y^4} - A_t$, (3) $\rho + \frac{q^2}{8\pi Y^4} - A_t$, (4) $\rho + p_r + 2p_t + \frac{q^2}{4\pi Y^4} - A_t$, (5) $\rho - p_r + \frac{q^2}{4\pi Y^4} - A_t$, (6) $\rho - p_t - A_t$ for $\gamma_1 = 0.05$, $\alpha_1 = 1$, $q = 0.5$ and $\lambda = 1$.

Table **4**: Effects of increasing λ for the expanding solution

Physical Parameter	ρ	p_r	p_t	$\triangle$
As λ Increases	decreases	increases	increases	decreases

3.2 Cylindrical Symmetric Models

The non-static cylindrically symmetric spacetime is taken as

$$ds^2 = -A^2(t,r)dt^2 + B^2(t,r)dr^2 + C^2(t,r)d\theta^2 + dz^2. \tag{3.2.1}$$

The energy-momentum tensor for anisotropic fluid is given by

$$T_{\mu\nu} = (\rho + p_r)V_\mu V_\nu + p_r g_{\mu\nu} - (p_r - p_z)S_\mu S_\nu - (p_r - p_\theta)K_\mu K_\nu, \tag{3.2.2}$$

where S_μ, K_μ are unit four-vectors, p_r, p_θ, p_z are the pressures in r, θ and z directions, respectively. The four-vectors V_μ, S_μ and K_μ have the expressions

$$V^\mu = (A^{-1}, 0, 0, 0), \quad K^\mu = (0, 0, C^{-1}, 0), \quad S^\mu = (0, 0, 0, 1), \tag{3.2.3}$$

which satisfy the following relations

$$V^\mu V_\nu = -1,\ K^\mu K_\nu = S^\mu S_\nu = 1,\ S^\mu K_\nu = V^\mu K_\nu = V^\mu S_\nu = 0.$$

The Maxwell equations for the metric (3.2.1) yields

$$\varphi'' + \varphi'\left(\frac{C'}{C} - \frac{A'}{A} - \frac{B'}{B}\right) = 4\pi\xi AB^2, \tag{3.2.4}$$

$$\dot{\varphi}' + \varphi'\left(\frac{\dot{C}}{C} - \frac{\dot{A}}{A} - \frac{\dot{B}}{B}\right) = 0. \tag{3.2.5}$$

Integration of Eq.(3.2.4) gives

$$\varphi' = \frac{AB}{C}q, \quad q = 4\pi\int_0^r \xi BC dr, \tag{3.2.6}$$

where q is the total charge of the cylinder. The corresponding field equations for $f(R,T)=R+2\lambda T$ and $\mathcal{L}_m=-\rho$ are

$$\frac{1}{B^2}\left[\frac{B'C'}{BC}-\frac{C''}{C}\right]+\frac{1}{A^2}\frac{\dot{B}\dot{C}}{BC}+\frac{A^2q^2}{C^2}=8\pi\rho-\lambda(-\rho+p_r+p_\theta+p_z), \tag{3.2.7}$$

$$\frac{\dot{C}'}{C}-\frac{\dot{C}}{C}\frac{A'}{A}-\frac{\dot{B}}{B}\frac{C'}{C}=0, \tag{3.2.8}$$

$$\frac{1}{A^2}\left[\frac{\dot{A}C'}{AC}-\frac{\ddot{C}}{C}\right]+\frac{1}{B^2}\frac{A'C'}{AC}+\frac{B^2q^2}{C^2}=8\pi p_r+\lambda(\rho+3p_r+p_\theta+p_z), \tag{3.2.9}$$

$$\frac{1}{A^2}\left[\frac{\dot{A}\dot{B}}{AB}-\frac{\ddot{B}}{B}\right]+\frac{1}{C^2}\left(\frac{\dot{C}}{B}\right)^2\left[\frac{A''}{A}-\frac{A'B'}{AB}\right]-\frac{q^2}{C^2}=8\pi p_\theta$$
$$+\lambda(\rho+p_r+3p_\theta+p_z), \tag{3.2.10}$$

$$\frac{1}{A^2}\left[-\frac{\ddot{B}}{B}-\frac{\ddot{C}}{C}-\frac{\dot{B}\dot{C}}{BC}+\frac{\dot{A}}{A}\left(\frac{\dot{B}}{B}+\frac{\dot{C}}{C}\right)\right]+\frac{1}{B^2}\left[\frac{A''}{A}+\frac{C''}{C}-\frac{A'B'}{AB}\right.$$
$$\left.-\frac{C'}{C}\left(\frac{B'}{B}+\frac{A'}{A}\right)\right]-\frac{q^2}{C^2}=8\pi p_z+\lambda(\rho+p_r+p_\theta+3p_z), \tag{3.2.11}$$

A simultaneous solution of the field equations give the following explicit expressions of density and pressure components

$$\begin{aligned}
\rho &= \frac{1}{8(8\pi^2+6\pi\lambda+\lambda^2)A^3B^3C^2}\left[q^2(8\pi+5\lambda)A^5B^3-2AB^2C(-2(2\pi\right.\\
&+ \lambda)\dot{B}\dot{C}+\lambda(C\ddot{B}+B\ddot{C}))+\lambda B^2C\dot{A}(2C\dot{B}+B(\dot{C}+2C'))-\lambda A^2\\
&\times (C^2+\dot{C}^2)(A'B'-BA'')+A^3(-2q^2\lambda B^3+q^2\lambda B^5+4(2\pi+\lambda)\\
&\times \left. CB'C'-4(2\pi+\lambda)BCC'')\right], \qquad (3.2.12)\\
p_r &= \frac{1}{8(2\pi+\lambda)(4\pi+\lambda)A^3B^3C^2}\left[-q^2\lambda A^5B^3+q^2A^3B^3(2\lambda+(8\pi\right.\\
&+ 3\lambda)B^2)-2AB^2C(-\lambda C\ddot{B}+(4\pi+\lambda)B\ddot{C})+B^2C\dot{A}(-2\lambda C\dot{B}\\
&+ B(-\lambda\dot{C}+2(8\pi+3\lambda)C'))+A^2(4(2\pi+\lambda)BCA'C'+\lambda(C^2\\
&+ \left.\dot{C}^2)(A'B'-BA''))\right], \qquad (3.2.13)\\
p_\theta &= \frac{1}{8(2\pi+\lambda)(4\pi+\lambda)A^3B^3q^2}\left[-q^2\lambda A^5B^3-q^2A^3B^3(8\pi+2\lambda\right.
\end{aligned}$$

$$
\begin{aligned}
&+ \quad \lambda B^2) - 2AB^2C((4\pi+\lambda)C\ddot{B} - \lambda B\ddot{C}) + B^2C\dot{A}(2(4\pi+\lambda)C\dot{B} \\
&- \quad \lambda B(\dot{C} + 2C')) + A^2(\lambda C^2 - (8\pi+3\lambda)\dot{C}^2)(A'B' - BA'')\Big], \qquad (3.2.14) \\
p_z \quad &= \quad \frac{-1}{8(2\pi+\lambda)(4\pi+\lambda)A^3B^3C^2}\Big[q^2\lambda A^5B^3 + 2AB^2C(2(2\pi+\lambda)\dot{B}\dot{C} \\
&+ \quad (4\pi+\lambda)(C\ddot{B} + B\ddot{C})) - B^2C\dot{A}(2(4\pi+\lambda)C\dot{B} + B((8\pi+3\lambda) \\
&\times \quad \dot{C} - 2\lambda C')) + A^2(4(2\pi+\lambda)BCA'C' + (8\pi+3\lambda)C^2(A'B' \\
&- \quad BA'') + \lambda\dot{C}^2(-A'B' + BA'')) + A^3(2q^2(4\pi+\lambda)B^3 + q^2\lambda B^5 \\
&+ \quad 4(2\pi+\lambda)CB'C' - 4(2\pi+\lambda)BCC'')]. \qquad (3.2.15)
\end{aligned}
$$

The anisotropic parameter is $\triangle = p_r - p_\theta$. The expansion scalar is evaluated as

$$\vartheta = \frac{1}{A}\left(\frac{\dot{B}}{B} + \frac{\dot{C}}{C}\right), \qquad (3.2.16)$$

and an auxiliary solution of Eq.(3.2.8) is

$$A = \frac{\dot{C}}{\alpha_2 C^{\gamma_2}}, \quad B = \alpha_2 C^{\gamma_2}, \qquad (3.2.17)$$

where γ_2 and $\alpha_2 > 0$ are arbitrary constants. The above solution leads to

$$\vartheta = \alpha_2(1+\gamma_2)C^{\gamma_2 - 1}. \qquad (3.2.18)$$

The value of ϑ depends on α_2, γ_2 and C in which α_2 and C are always positive implying that we have collapse for $\gamma_2 < -1$ and expansion for $\gamma_2 > -1$. We explore these cases one by one in the following subsections.

3.2.1 Collapse for $\gamma_2 < -1$

For collapsing solution, we find the unknown metric function C in the solution (3.2.17) such that the collapse leads to the formation of trapped surfaces. The mass function for the cylindrically symmetric charged source is obtained as

$$m(t,r)=\frac{1}{8}\left[1-\left(\frac{C'}{B}\right)^2+\left(\frac{\dot{C}}{A}\right)^2\right]+qC. \tag{3.2.19}$$

Equation (3.2.17) simplifies the mass expression as

$$m(t,r)=\frac{1}{8}\left(1+\alpha_2^2C^{2\gamma_2}-\frac{C'^2}{\alpha_2^2C^{2\gamma_2}}\right)+qC. \tag{3.2.20}$$

For trapped surface formation $m=\frac{1}{8}+qC$ [27], which yields

$$C_{trap}=\left[\alpha_2^2(1-2\gamma_2)r+H_2(t)\right]^{\frac{1}{1-2\gamma_2}}, \tag{3.2.21}$$

where $H_2(t)$ is an integration function and the collapsing solution becomes

$$\begin{aligned} A &= \frac{1}{\alpha_2(1-2\gamma_2)}\dot{H}_2\left(\alpha_2^2(1-2\gamma_2)r+H_2(t)\right)^{\frac{\gamma_2}{1-2\gamma_2}}, & (3.2.22)\\ B &= \alpha_2\left(\alpha_2^2(1-2\gamma_2)r+H_2(t)\right)^{\frac{\gamma_2}{1-2\gamma_2}}, & (3.2.23)\\ C_{trap} &= \left(\alpha_2^2(1-2\gamma_2)r+H_2(t)\right)^{\frac{1}{1-2\gamma_2}}. & (3.2.24)\end{aligned}$$

For the sake of simplicity, we consider $H_2(t)$ as a linear function of t, i.e., $H_2(t)=\frac{t}{\alpha_2^2}$ and obtain the following expressions of density and pressures

$$\begin{aligned}\rho &= \frac{\left(\frac{t}{\alpha_2^2}+r(1-2\gamma_2)\alpha_2^2\right)^{\frac{2+4\gamma_2}{2\gamma_2-1}}}{8(1-2\gamma_2)^2(8\pi^2+6\pi\lambda+\lambda^2)\alpha_2^6)}\left[q^2(8\pi+5\lambda)\left(\frac{t}{\alpha_2^2}+r(1-2\gamma_2)\alpha_2^2\right)^{\frac{6\gamma_2}{1-2\gamma_2}}\right.\\ &- \frac{1}{(t+r(1-2\gamma_2)\alpha_2^4)^2}\left(2(1-2\gamma_2)^2\gamma_2(-4\pi+(-1+3\gamma_2)\lambda)\alpha_2^{12}\right.\\ &\times \left.\left(\frac{t}{\alpha_2^2}+r(1-2\gamma_2)\alpha_2^2\right)^{\frac{2+2\gamma_2}{1-2\gamma_2}}\right)+\frac{\gamma_2(-1+2\gamma_2)\lambda\alpha_2^{12}\left(\frac{t}{\alpha_2^2}+r(1-2\gamma_2)\alpha_2^2\right)^{\frac{2+2\gamma_2}{1-2\gamma_2}}}{(t+r(1-2\gamma_2)\alpha_2^4)^4}\\ &\times (1+t^2(1-2\gamma_2)^2-2rt(-1+2\gamma_2)^3\alpha_2^4+r^2(1-2\gamma_2)^4\alpha_2^8)-\frac{1}{(t+r(1-2\gamma_2)\alpha_2^4)^2}\\ &\times \left((1-2\gamma_2)^2\gamma_2\lambda\alpha_2^{12}\left(\frac{t}{\alpha_2^2}+r(1-2\gamma_2)\alpha_2^2\right)^{\frac{2+2\gamma_2}{1-2\gamma_2}}(-1-2\alpha_2^4+\gamma_2(-2+4\alpha_2^4))\right)\end{aligned}$$

$$
\begin{aligned}
&+ \quad (1-2\gamma_2)^2\alpha_2^3\left(\frac{t}{\alpha_2^2}+r(1-2\gamma_2)\alpha_2^2\right)^{\frac{\gamma_2}{1-2\gamma_2}}\left\{-2q^2\lambda\alpha_2^3\left(\frac{t}{\alpha_2^2}+r(1-2\gamma_2)\alpha_2^2\right)^{\frac{3\gamma_2}{1-2\gamma_2}}\right.\\
&+ \quad q^2\lambda\alpha_2^5\left(\frac{t}{\alpha_2^2}+r(1-2\gamma_2)\alpha_2^2\right)^{\frac{5\gamma_2}{1-2\gamma_2}}+4\gamma_2(2\pi+\lambda)\alpha_2^5\left(\frac{t}{\alpha_2^2}+r(1-2\gamma_2)\alpha_2^2\right)^{\frac{5\gamma_2}{1-2\gamma_2}}\\
&- \quad \left.\left.\frac{1}{(t+r(1-2\gamma_2)\alpha_2^4)^2}8\gamma_2(2\pi+\lambda)\alpha_2^9\left(\frac{t}{\alpha_2^2}+r(1-2\gamma_2)\alpha_2^2\right)^{\frac{2+\gamma_2}{1-2\gamma_2}}\right\}\right], \qquad (3.2.25)
\end{aligned}
$$

$$
\begin{aligned}
p_r &= \frac{\left(\frac{t}{\alpha_2^2}+r(1-2\gamma_2)\alpha_2^2\right)^{\frac{2+4\gamma_2}{2\gamma_2-1}}}{8(1-2\gamma_2)^2(2\pi^2+\lambda)(4\pi^2+\lambda)\alpha_2^6)}\left[-q^2\lambda\left(\frac{t}{\alpha_2^2}+r(1-2\gamma_2)\alpha_2^2\right)^{\frac{6\gamma_2}{1-2\gamma_2}}\right.\\
&+ \frac{1}{(t+r(1-2\gamma_2)\alpha_2^4)^2}\left(2(1-2\gamma_2)^2\gamma_2(-8\pi+3(-1+\gamma_2)\lambda)\alpha_2^{12}\right.\\
&\times \left.\left(\frac{t}{\alpha_2^2}+r(1-2\gamma_2)\alpha_2^2\right)^{\frac{2+2\gamma_2}{1-2\gamma_2}}\right)+(q-2q\gamma_2)^2\alpha_2^6\left(\frac{t}{\alpha_2^2}+r(1-2\gamma_2)\alpha_2^2\right)^{\frac{4\gamma_2}{1-2\gamma_2}}\\
&\times (2\lambda+(8\pi+3\lambda)\alpha_2^2\left(\frac{t}{\alpha_2^2}+r(1-2\gamma_2)\alpha_2^2\right)^{\frac{2\gamma_2}{1-2\gamma_2}})-(-8\pi(-1+2\gamma_2)\\
&\times (t+r(1-2\gamma_2)\alpha_2^4)^2+\lambda(1+t^2(5-12\gamma_2+4\gamma_2^2)-2rt(1-2\gamma_2)^2(-5+2\gamma_2)\alpha_2^4\\
&+ r^2(-5+2\gamma_2)(-1+2\gamma_2)^3\alpha_2^3))((t+r(1-2\gamma_2)\alpha_2^4)^4\gamma_2(-1+2\gamma_2)\alpha_2^{12}\\
&\times \left(\frac{t}{\alpha_2^2}+r(1-2\gamma_2)\alpha_2^2\right)^{\frac{2+2\gamma_2}{1-2\gamma_2}})-\frac{1}{(t+r(1-2\gamma_2)\alpha_2^4)^2}(1-2\gamma_2)^2\gamma_2\alpha_2^{12}\\
&\times \left(\frac{t}{\alpha_2^2}+r(1-2\gamma_2)\alpha_2^2\right)^{\frac{2+2\gamma_2}{1-2\gamma_2}}(16\pi(-1+2\gamma_2)\alpha_2^4\\
&+ \left.\lambda(1-6\alpha_2^4+2\gamma_2(1+6\alpha_2^4)))\right], \qquad (3.2.26)
\end{aligned}
$$

$$
\begin{aligned}
p_\theta &= \frac{\left(\frac{t}{\alpha_2^2}+r(1-2\gamma_2)\alpha_2^2\right)^{\frac{2+4\gamma_2}{-1+2\gamma_2}}}{8(1-2\gamma_2)^2(2\pi+\lambda)(4\pi+\lambda)\alpha_2^6}\left[-q^2\lambda\left(\frac{t}{\alpha_2^2}+r(1-2\gamma_2)\alpha_2^2\right)^{\frac{6\gamma_2}{1-2\gamma_2}}\right.\\
&- \frac{2(1-2\gamma_2)^2\gamma_2(4\pi(-1+3\gamma_2)+3(-1+\gamma_2)\lambda)\alpha_2^{12}\left(\frac{t}{\alpha_2^2}+r(1-2\gamma_2)\alpha_2^2\right)^{\frac{2+2\gamma_2}{1-2\gamma_2}}}{(t+r(1-2\gamma_2)\alpha_2^4)^2}\\
&+ \frac{(1-2\gamma_2)^2\gamma_2\alpha_2^{12}\left(\frac{t}{\alpha_2^2}+r(1-2\gamma_2)\alpha_2^2\right)^{\frac{2+2\gamma_2}{1-2\gamma_2}}}{(t+r(1-2\gamma_2)\alpha_2^4)^2}(8\pi\gamma_2+(-1+2\gamma_2)\lambda(1+2\alpha_2^4))
\end{aligned}
$$

$$
\begin{aligned}
&+ \quad \frac{(1-2\gamma_2)^3\gamma_2\alpha_2^{12}\left(\frac{t}{\alpha_2^2}+r(1-2\gamma_2)\alpha_2^2\right)^{\frac{2+2\gamma_2}{1-2\gamma_2}}}{(t+r(1-2\gamma_2)\alpha_2^4)^2}\left(\lambda-\frac{8\pi+3\lambda}{(1-2\gamma_2)^2(t+r(1-2\gamma_2)\alpha_2^4)^2}\right.\\
&- \quad q^2(1-2\gamma_2)^2\alpha_2^6)\left(\frac{t}{\alpha_2^2}+r(1-2\gamma_2)\alpha_2^2\right)^{\frac{4\gamma_2}{1-2\gamma_2}}\left(8\pi+\lambda\left(2+\alpha_2^2\right.\right.\\
&\times \quad \left.\left.\left.\left(\frac{t}{\alpha_2^2}+r(1-2\gamma_2)\alpha_2^2\right)^{\frac{2\gamma_2}{1-2\gamma_2}}\right)\right)\right], \qquad (3.2.27)
\end{aligned}
$$

$$
\begin{aligned}
p_z \quad &= \quad \frac{\alpha_2^6\left(\frac{t}{\alpha_2^2}+r(1-2\gamma_2)\alpha_2^2\right)^{\frac{2+2\gamma_2}{-1+2\gamma_2}}}{8(1-2\gamma_2)^2(2\pi+\lambda)(4\pi+\lambda)}\left[8\pi(1-2\gamma_2)^2\left(\frac{-2\gamma_2\left(\frac{t}{\alpha_2^2}+r(1-2\gamma_2)\alpha_2^2\right)^{\frac{2}{1-2\gamma_2}}}{(t+r(1-2\gamma_2)\alpha_2^4)^2}\right.\right.\\
&- \quad \left.\frac{q^2\left(\frac{t}{\alpha_2^2}+r(1-2\gamma_2)\alpha_2^2\right)^{\frac{2\gamma_2}{1-2\gamma_2}}}{\alpha_2^6}\right)+\lambda\left(\frac{-q^2\left(\frac{t}{\alpha_2^2}+r(1-2\gamma_2)\alpha_2^2\right)^{\frac{2\gamma_2}{1-2\gamma_2}}}{\alpha_2^{12}}\right.\\
&\times \quad \left(2(1-2\gamma_2)^2\alpha_2^6+\left(\frac{t}{\alpha_2^2}+r(1-2\gamma_2)\alpha_2^2\right)^{\frac{2\gamma_2}{1-2\gamma_2}}+(1-2\gamma_2)^2\alpha_2^6\right.\\
&\times \quad \left.\left(\frac{t}{\alpha_2^2}+r(1-2\gamma_2)\alpha_2^2\right)^{\frac{2\gamma_2}{1-2\gamma_2}}\right)+(-1+(4rt(1-2\gamma_2)^2\alpha_2^4+2r^2(-1+2\gamma_2)^3\alpha_2^8)\\
&\times \quad (-3+\gamma_2-\alpha_2^4+2\gamma_2\alpha_2^4+2t^2(3+\alpha_2^4+\gamma_2^2(2+4\alpha_2^4)-\gamma_2(7+4\alpha_2^4))))\\
&\times \quad \left.\left.\left((t+r(1-2\gamma_2)\alpha_2^4)^4\gamma_2(-1+2\gamma_2)\left(\frac{t}{\alpha_2^2}+r(1-2\gamma_2)\alpha_2^2\right)^{\frac{2}{1-2\gamma_2}}\right)^{-1}\right)\right]. \qquad (3.2.28)
\end{aligned}
$$

For the solution (3.2.22)-(3.2.24), the anisotropic parameter and mass function become

$$
\begin{aligned}
\triangle \quad &= \quad \frac{\alpha_2^6\left(\frac{t}{\alpha_2^2}+r(1-2\gamma_2)\alpha_2^2\right)^{\frac{2+2\gamma_2}{-1+2\gamma_2}}}{8(1-2\gamma_2)(4\pi+\lambda)}\left[-q^2(-1+\gamma_2)\alpha_2^{-6}\left(\frac{t}{\alpha_2^2}+r(1-2\gamma_2)\alpha_2^2\right)^{\frac{2\gamma_2}{1-2\gamma_2}}\right.\\
&\times \quad \left(1+\alpha_2^2\left(\frac{t}{\alpha_2^2}+r(1-2\gamma_2)\alpha_2^2\right)^{\frac{2\gamma_2}{-1+2\gamma_2}}\right)+\left(1-4rt(1-2\gamma_2)^2\alpha_2^4(1-\alpha_2^4\right.\\
&- \quad \gamma_2(-1+2\alpha_2^4))+2r^2(-1+2\gamma_2)^3\alpha_2^8(1-\alpha_2^8-\gamma_2(-1+2\alpha_2^4))
\end{aligned}
$$

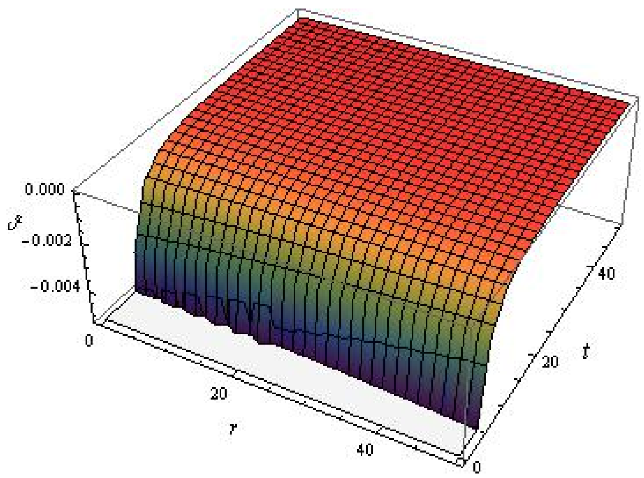

Figure 3.15: Plot of ϑ versus r and t for $\gamma_2 = -1.5$, $\alpha_2 = 0.1$.

$$+ \quad \frac{2t^2(-1+\alpha_2^4+\gamma_2(3-4\alpha_2^4)+\gamma_2^2(-2+4\alpha_2^4))}{(t+r(1-2\gamma_2)\alpha_2^4)^4\gamma_2\left(\frac{t}{\alpha_2^2}+r(1-2\gamma_2)\alpha_2^2\right)^{\frac{2}{-1+2\gamma_2}}}\Bigg)\Bigg], \tag{3.2.29}$$

$$m = \frac{1}{8}+q\left(\frac{t}{\alpha_2^2}+r(1-2\gamma_2)\alpha_2^2\right)^{\frac{1}{1-2\gamma_2}}. \tag{3.2.30}$$

For the collapsing case, the graphical representation of different parameters is given in Figures **3.15-3.21**. We observe that the quantities are changing with respect to temporal coordinate while no change is observed with respect to radial coordinate. The change in different quantities with respect to time is given in Table **5** while the effects of charge as well as model parameter λ are summarized in Table **6**.

Table **5**: Change in parameters with respect to t for the collapse solution

Parameter	ρ	p_r	p_θ	p_z	$\triangle$	m
As t increases	decreases	decreases	increases	decreases	decreases	increases

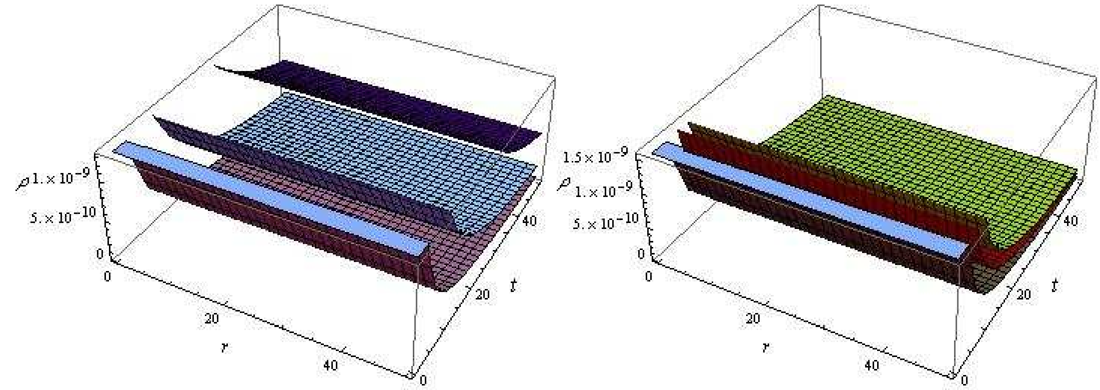

Figure 3.16: Plots of ρ versus r and t for $\gamma_2 = -1.5$, $\alpha_2 = 0.1$. The left graph is for $q = 0$ (pink), $q = 0.00005$ (blue), $q = 0.0001$ (purple) with $\lambda = -0.1$ and the right graph is for $\lambda = -0.1$ (brown), $\lambda = -0.2$ (red), $\lambda = -0.3$ (yellow) with $q = 0.0001$.

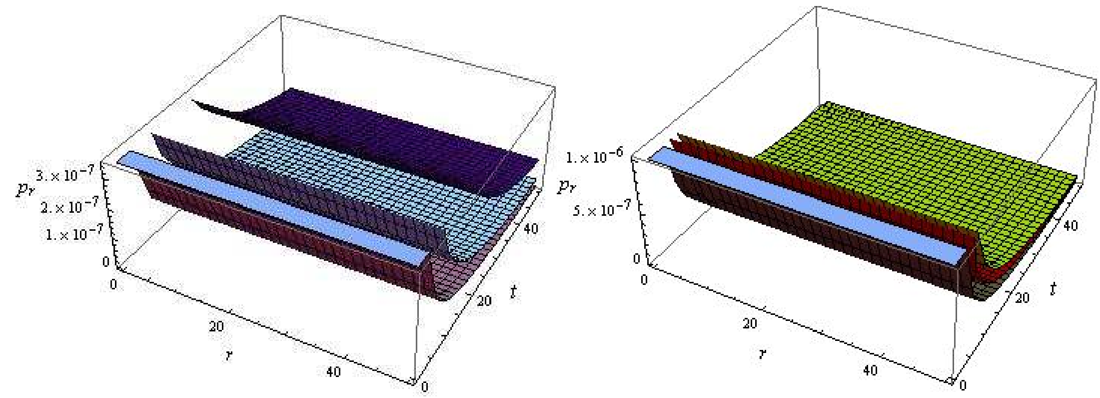

Figure 3.17: Plots of p_r versus r and t for $\gamma_2 = -1.5$, $\alpha_2 = 0.1$. The left graph is for $q = 0$ (pink), $q = 0.01$ (blue), $q = 0.02$ (purple) with $\lambda = -0.1$ while the right graph is for $\lambda = -0.1$ (brown), $\lambda = -0.2$ (red), $\lambda = -0.3$ (yellow) with $q = 0.01$.

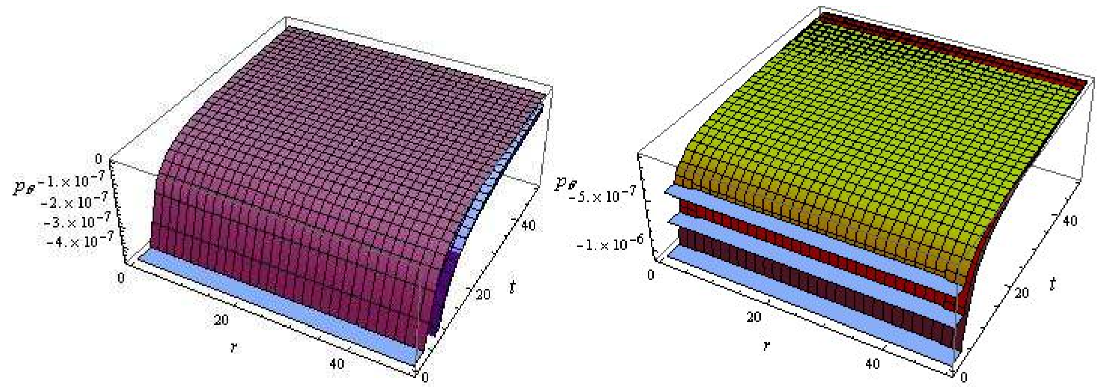

Figure 3.18: Plots of p_θ versus r and t for $\gamma_2 = -1.5$, $\alpha_2 = 0.1$. The left graph is for $q = 0$ (pink), $q = 0.005$ (blue), $q = 0.01$ (purple) with $\lambda = -0.1$ and the right graph is for $\lambda = -0.1$ (brown), $\lambda = -0.15$ (red), $\lambda = -0.2$ (yellow) with $q = 0.01$.

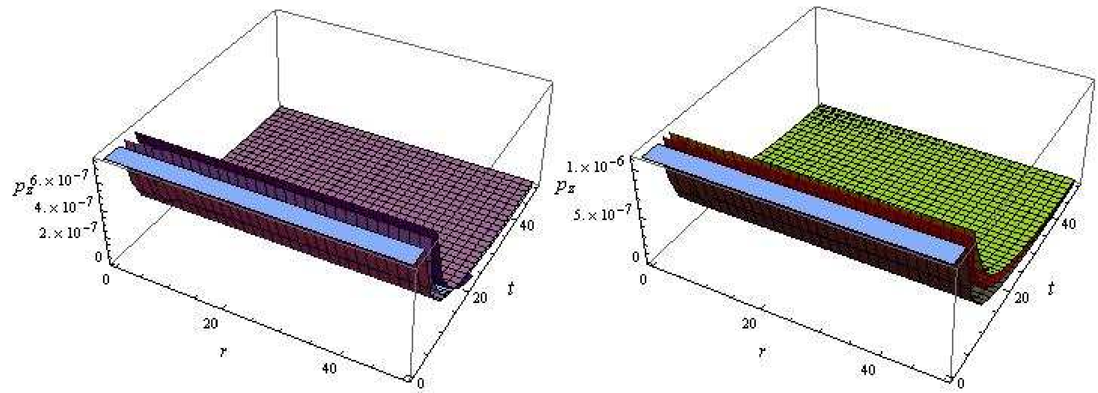

Figure 3.19: Plots of p_z versus r and t for $\gamma_2 = -1.5$, $\alpha_2 = 0.1$. The left graph is for $q = 0$ (pink), $q = 0.01$ (blue), $q = 0.02$ (purple) with $\lambda = -0.1$ and the right graph is for $\lambda = -0.1$ (brown), $\lambda = -0.2$ (red), $\lambda = -0.3$ (yellow) with $q = 0.01$.

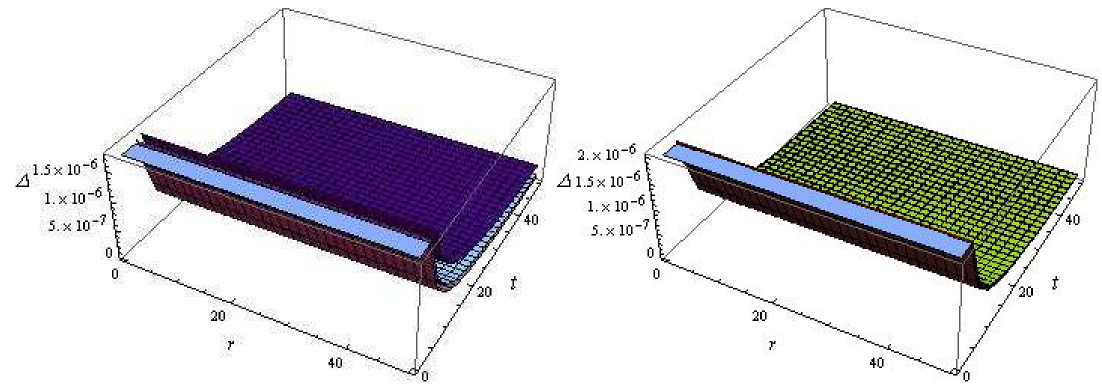

Figure 3.20: Plots of $\triangle$ versus r and t for $\gamma_2 = -1.5$, $\alpha_2 = 0.1$. The left graph is for $q = 0$ (pink), $q = 0.01$ (blue), $q = 0.02$ (purple) with $\lambda = -0.1$ and the right graph is for $\lambda = -0.1$ (brown), $\lambda = -0.2$ (red), $\lambda = -0.3$ (yellow) with $q = 0.01$.

Table **6**: Effects of q and λ for the collapse solution

Parameter	ρ	p_r	p_θ	p_z	$\triangle$	m
As q increases	increases	increases	decreases	decreases	increases	increases
As λ decreases	increases	increases	increases	increases	increases	no change

For charged cylindrical anisotropic source, the energy conditions are

- NEC: $\rho + p_r - A_t \geq 0,\ \rho + p_\theta + \frac{q^2}{4\pi C^2} - A_t \geq 0,\ \rho + p_z + \frac{q^2}{4\pi C^2} - \mathcal{A} \geq 0,$
- WEC: $\rho + \frac{q^2}{8\pi C^2} - A_t \geq 0,\ \rho + p_r - \mathcal{A} \geq 0,\ \rho + p_\theta + \frac{q^2}{4\pi C^2} - A_t \geq 0,\ \rho + p_z + \frac{q^2}{4\pi C^2} - A_t \geq 0,$
- SEC: $\rho + p_r + p_\theta + p_z + \frac{q^2}{4\pi C^2} - A_t \geq 0.$
- DEC: $\rho - p_r + \frac{q^2}{4\pi C^2} - A_t \geq 0,\ \rho + p_\theta - A_t \geq 0,\ \rho - p_z - A_t \geq 0,$

The term A_t is obtained as

$$A_t = \frac{1}{B^2}\left[\frac{A''}{A} + \frac{A'}{A}\left(-\frac{B'}{B} + \frac{C'}{C} + \frac{A'}{A}\right)\right] + \frac{\dot{A}^2}{A^4}.$$

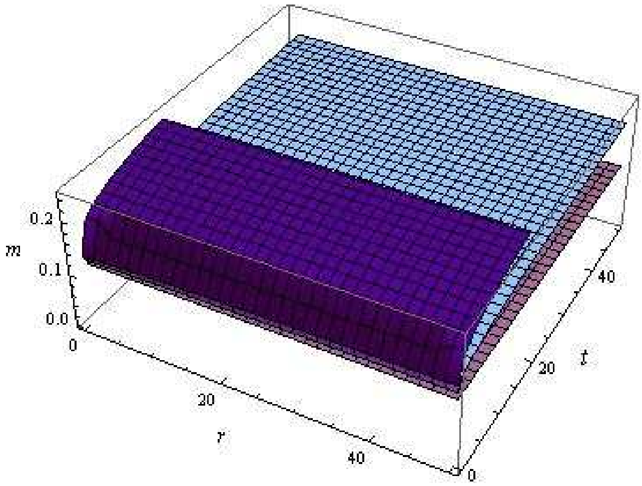

Figure 3.21: Plot of m versus r and t for $\gamma_2 = -1.5$, $\alpha_2 = 0.1$, $q = 0$ (pink), $q = 0.01$ (blue), $q = 0.02$ (purple).

For the collapse solution, we have

$$A_t = \frac{4\gamma_2^2\alpha_2^6\left(\frac{t}{\alpha_2^2} + r(1-2\gamma_2)\alpha_2^2\right)^{\frac{2\gamma_2}{-1+2\gamma_2}}}{(t + r(1-2\gamma_2)\alpha_2^4)^2}.$$

All the energy conditions defined above are plotted in Figures **3.22** and **3.23**, the repeated expressions are shown only once. From these plots, it can be easily seen that all the energy conditions are satisfied for the considered values of free parameters of the collapse solution.

3.2.2 Expansion for $\gamma_2 > -1$

In this case, we require an expression of the metric coefficient C for expanding solution. For convenience, we assume it a linear combination of r and t such that the expansion scalar remains positive for the resulting solution as shown in Figure **3.24**.

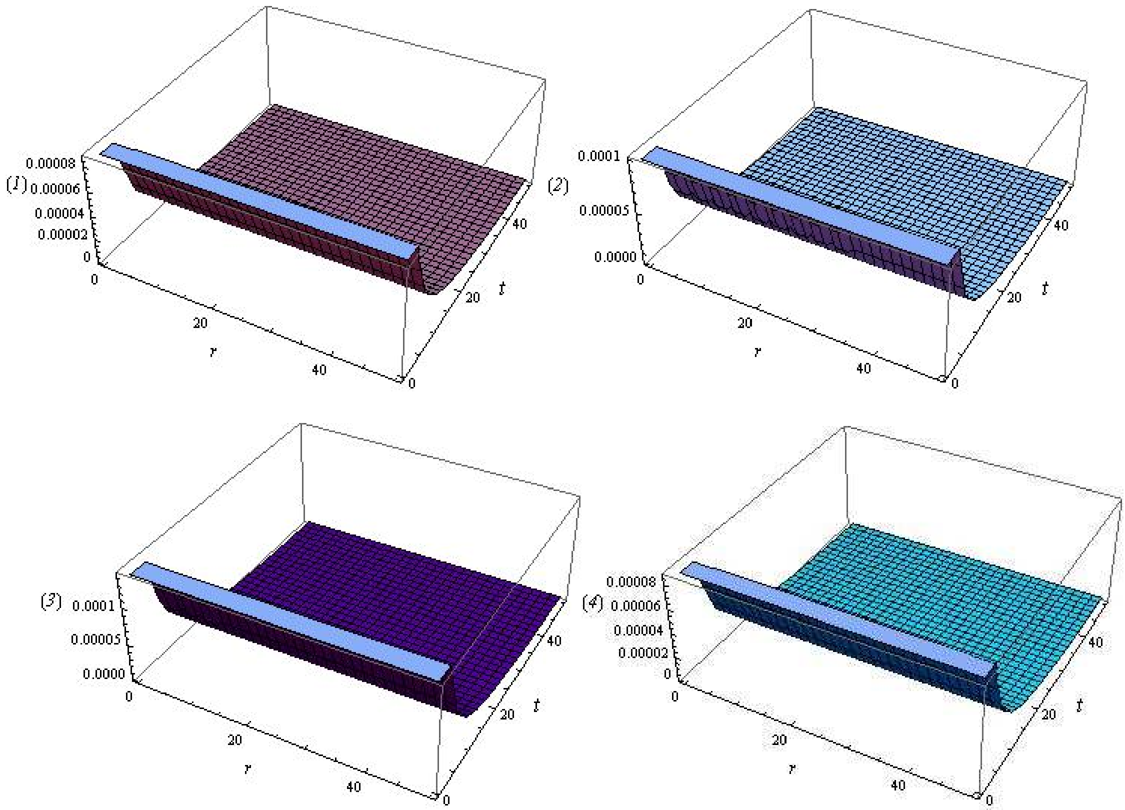

Figure 3.22: Plots of (1) $\rho + p_r - A_t$, (2) $\rho + p_\theta + \frac{q^2}{4\pi C^2} - A_t$, (3) $\rho + p_z + \frac{q^2}{4\pi C^2} - A_t$, (4) $\rho + \frac{q^2}{8\pi C^2} - A_t$ for $\gamma_2 = -1.5$, $\alpha_2 = 0.1$, $q = 0.01$ and $\lambda = -0.1$.

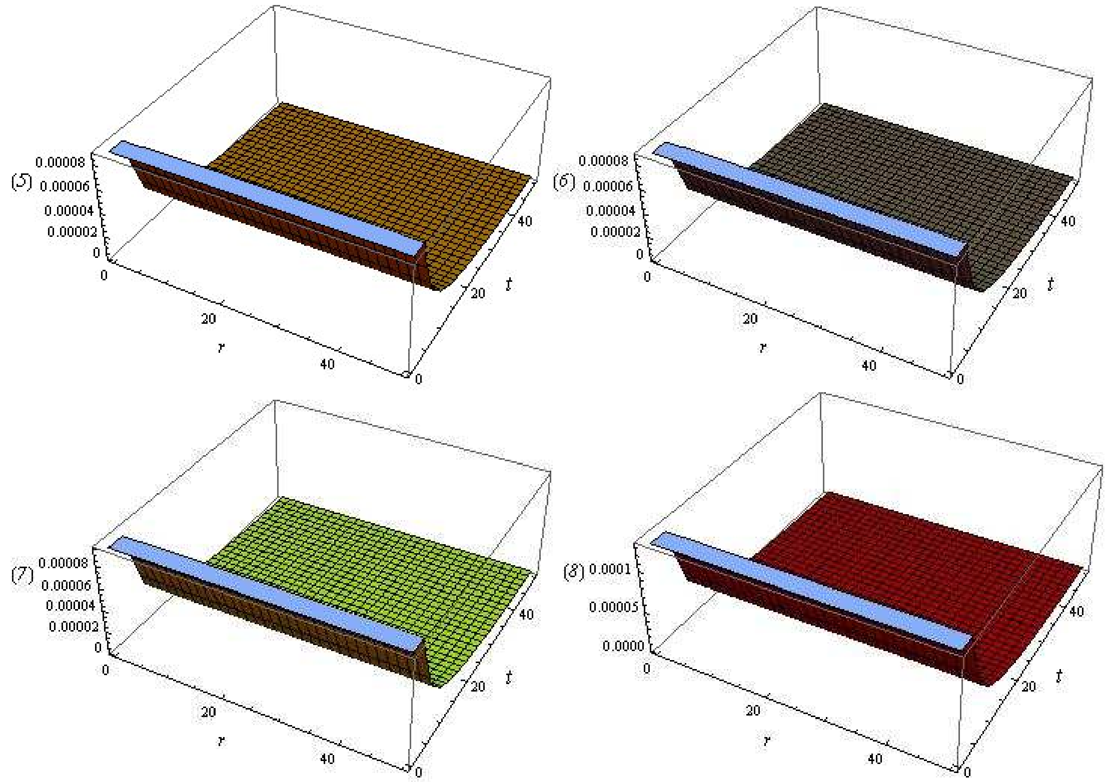

Figure 3.23: Plot of (5) $\rho+p_r+p_\theta+p_z+\frac{q^2}{4\pi C^2}-A_t$, (6) $\rho-p_r+\frac{q^2}{4\pi C^2}-A_t$, (7) $\rho-p_\theta-A_t$, (8) $\rho-p_z-A_t$, for $\gamma_2=-1.5$, $\alpha_2=0.1$, $q=0.01$ and $\lambda=-0.1$.

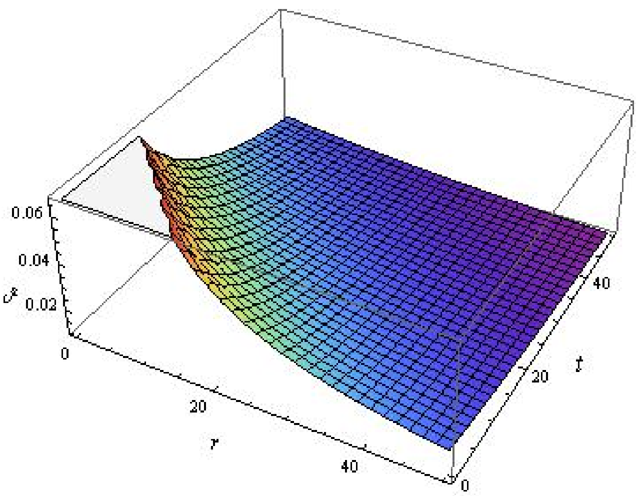

Figure 3.24: Plot of ϑ versus r and t for $\gamma_2=0.0001$, $\alpha_2=1$.

Thus the expanding solution is given by

$$A=\frac{1}{\alpha_2(r+t)^{\gamma_2}},\quad B=\alpha_2(r+t)^{\gamma_2},\quad C=r+t. \tag{3.2.31}$$

Consequently, the expressions of ρ, p_r, p_θ and p_z take the form

$$\begin{aligned}
\rho &= \frac{(r+t)^{-2(2+\gamma_2)}}{8(8\pi^2+6\pi\lambda+\lambda^2)\alpha_2^2}\left[8\pi(r+t)^2(q^2+\gamma_2+(r+t)^{4\gamma_2}\gamma_2C^4)\right.\\
&+ \lambda(q^2(r+t)^2(5-2(r+t)^{2\gamma_2}\alpha_2^2+(r+t)^{4\gamma_2}\alpha_2^4)-\gamma_2(-1-2\gamma_2\\
&+ t^2(-5-2\gamma_2-3(r+t)^{4\gamma_2}\alpha_2^4+4(r+t)^{4\gamma_2}\gamma_2\alpha_2^4)+r^2(-5\\
&- \left.3(r+t)^{4\gamma_2}\alpha_2^4+\gamma_2(-2+4(r+t)^{4\gamma_2}\alpha_2^4))))\right], \qquad (3.2.32)\\
p_r &= \frac{1}{8(r+t)^2(2\pi+\lambda)(4\pi+\lambda)}\left[\frac{-q^2(r+t)^{-2\gamma_2}\lambda}{\alpha_2^2}-\frac{(r+t)^{-2(1+\gamma_2)}\gamma_2}{\alpha_2^2}\right.\\
&\times (8\pi(r+t)^2+(1+2\gamma_2+r^2(5+2\gamma_2)+2rt(5+2\gamma_2)+t^2(5+2\gamma_2))\lambda)\\
&+ 2(r+t)^{2\gamma_2}(-1+\gamma_2)\gamma_2\lambda\alpha_2^2+(r+t)^{2\gamma_2}\gamma_2(-16\pi+(-5+2\gamma_2)\lambda)\alpha_2^2\\
&+ \left.q^2(2\lambda+(r+t)^{2\gamma_2}(8\pi+3\lambda)\alpha_2^2)\right], \qquad (3.2.33)\\
p_\theta &= \frac{1}{8(r+t)^2(2\pi+\lambda)(4\pi+\lambda)}\left[\frac{-q^2(r+t)^{-2\gamma_2}\lambda}{\alpha_2^2}+\frac{(r+t)^{-2(1+\gamma_2)}\gamma_2(1+2\gamma_2)}{\alpha_2^2}\right.\\
&\times (-8\pi+(-3+r^2+2rt+t^2)\lambda)+2(r+t)^{2\gamma_2}(-1+\gamma_2)\gamma_2(4\pi+\lambda)\alpha_2^2\\
&+ \left.(r+t)^{2\gamma_2}\gamma_2(8\pi\gamma_2+(-3+2\gamma_2)\lambda)\alpha_2^2+q^2(8\pi+\lambda(2+(r+t)^{2\gamma_2}\alpha_2^2))\right], \qquad (3.2.34)\\
p_z &= \frac{(r+t)^{-2(2+\gamma_2)}}{8(2\pi+\lambda)(4\pi+\lambda)\alpha_2^2}\left[-8\pi(r+t)^2(q^2(r+t)^{2\gamma_2}\alpha_2^2+(\gamma_2+2\gamma_2^2)(-1\right.\\
&+ (r+t)^{4\gamma_2}\alpha_2^4)-\lambda(q^2(r+t)^2(1+(r+t)^{2\gamma_2}\alpha_2^2)^2+\gamma_2(1+2\gamma_2+t^2\\
&\times (-3-6\gamma_2+3(r+t)^{4\gamma_2}\alpha_2^4+4(r+t)^{4\gamma_2}\gamma_2\alpha_2^4)+(r^2+2rt)(-3\\
&+ \left.3(r+t)^{4\gamma_2}\alpha_2^4+\gamma_2(-6+4(r+t)^{4\gamma_2}\alpha_2^4)))))\right]. \qquad (3.2.35)
\end{aligned}$$

The anisotropic parameter and mass function are obtained as

$$\begin{aligned}
\triangle &= \frac{(r+t)^{-2(2+\gamma_2)}}{2(4\pi+\lambda)\alpha_2^2}\left[q^2(r+t)^{2+2\gamma_2}\alpha_2^2(1+(r+t)^{2\gamma_2}\alpha_2^2)+2\gamma_2^2\right.\\
&\times (-1+(r^2+2rt+t^2)(r+t)^{4\gamma_2}\alpha_2^4)-\gamma_2(1+t^2+3t^2(r+t)^{4\gamma_2}\alpha_2^4
\end{aligned}$$

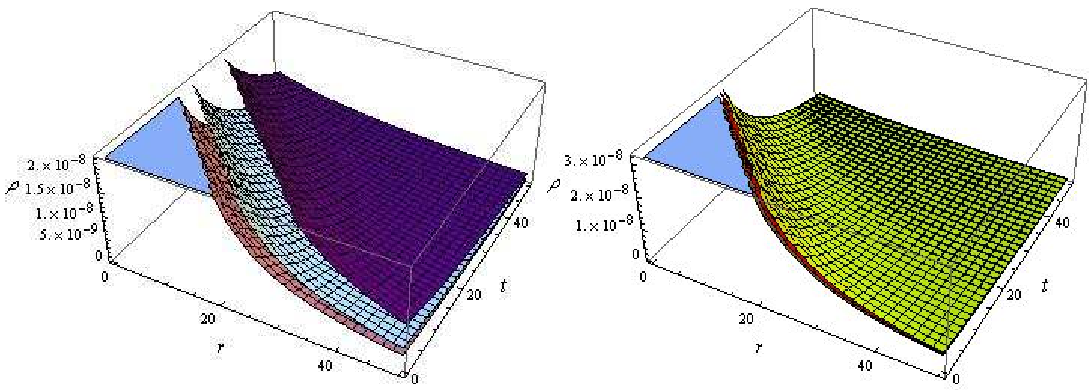

Figure 3.25: Plots of ρ versus r and t for $\gamma_2 = 0.0001$, $\alpha_2 = 1$. The left graph is for $q = 0$ (pink), $q = 0.01$ (blue), $q = 0.02$ (purple) with $\lambda = -0.001$ and the right graph is for $\lambda = -0.001$ (brown), $\lambda = -1$ (red), $\lambda = -2$ (yellow) with $q = 0.01$.

$$+ \quad (r^2 + 2rt)(1 + 3(r+t)^{4\gamma_2}\alpha_2^4))\big], \tag{3.2.36}$$

$$m \quad = \quad \frac{1}{8} + q(r+t). \tag{3.2.37}$$

The evolution of physical parameters during expansion is represented through Figures **3.25-3.30**. It is found that the quantities vary with both time and radial coordinates. The graphical analysis is summarized in Tables **7** and **8**.

Table **7**: Change in parameters with respect to r and t for the expanding solution.

Parameter	ρ	p_r	p_θ	p_z	$\triangle$	m
As r increases	decreases	decreases	increases	increases	decreases	increases
As t increases	decreases	decreases	increases	increases	decreases	increases

Table **8**: Effects of q and λ for the expanding solution.

Parameter	ρ	p_r	p_θ	p_z	$\triangle$	m
As q increases	increases	increases	decreases	decreases	increases	increases
As λ decreases	increases	increases	decreases	decreases	increases	no change

The acceleration term A_t in this case becomes

$$A_t = \frac{(r+t)^{-2(1+\gamma_2)}\gamma_2^2}{\alpha_2^2}(3 + (r+t)^{4\gamma_2}\alpha_2^4).$$

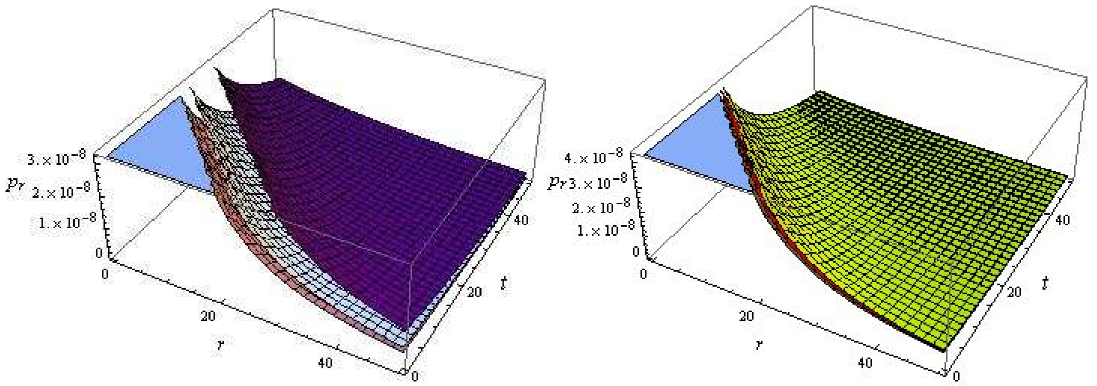

Figure 3.26: Plots of p_r versus r and t for $\gamma_2 = 0.0001$, $\alpha_2 = 1$. The left graph is for $q = 0$ (pink), $q = 0.01$ (blue), $q = 0.02$ (purple) with $\lambda = -0.001$ while the right graph is for $\lambda = -0.001$ (brown), $\lambda = -1$ (red), $\lambda = -2$ (yellow) with $q = 0.01$.

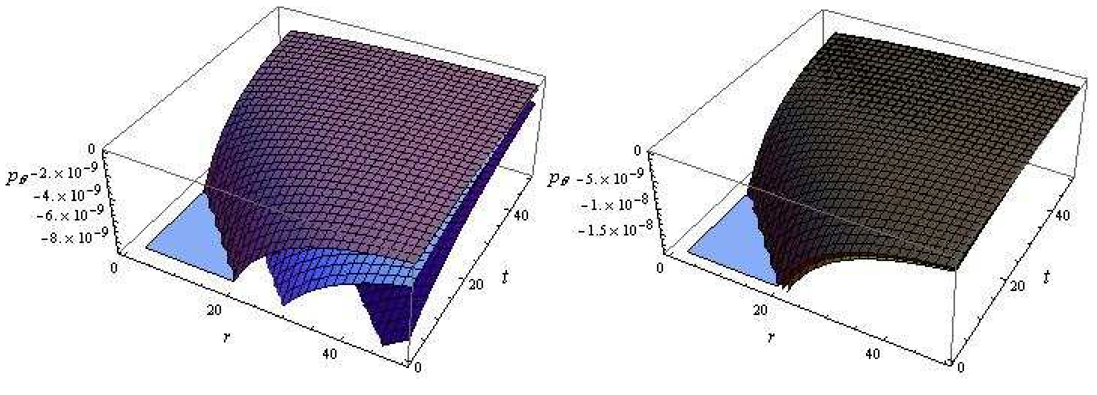

Figure 3.27: Plots of p_θ versus r and t for $\gamma_2 = 0.0001$, $\alpha_2 = 1$. The left graph is for $q = 0$ (pink), $q = 0.01$ (blue), $q = 0.02$ (purple) with $\lambda = -0.001$ while the right graph is for $\lambda = -0.001$ (brown), $\lambda = -1$ (red), $\lambda = -2$ (yellow) with $q = 0.01$.

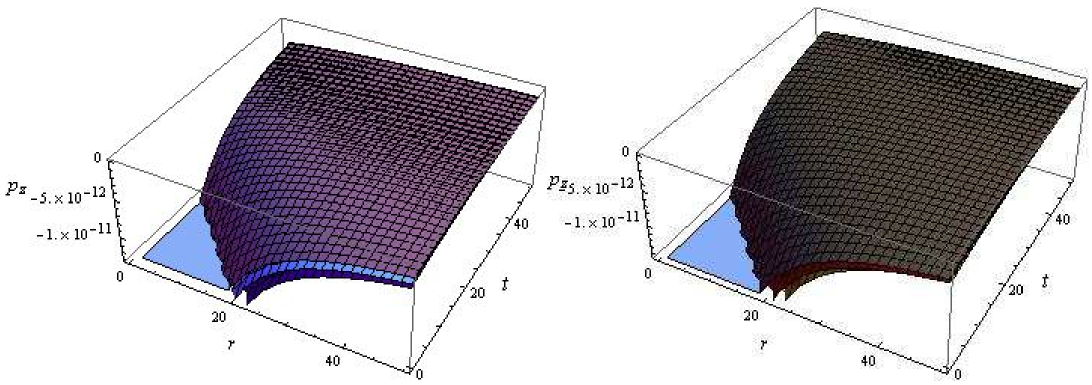

Figure 3.28: Plots of p_z versus r and t for $\gamma_2 = 0.0001$, $\alpha_2 = 1$. The left graph is for $q = 0$ (pink), $q = 0.0001$ (blue), $q = 0.0002$ (purple) with $\lambda = -0.001$ while the right graph is for $\lambda = -0.001$ (brown), $\lambda = -1$ (red), $\lambda = -2$ (yellow) with $q = 0.01$.

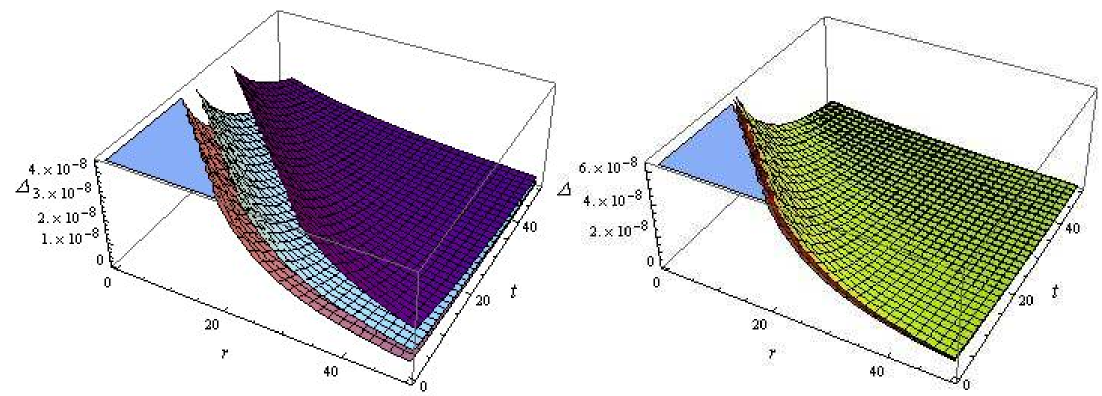

Figure 3.29: Plots of $\triangle$ versus r and t for $\gamma_2 = 0.0001$, $\alpha_2 = 1$. The left graph is for $q = 0$ (pink), $q = 0.01$ (blue), $q = 0.02$ (purple) with $\lambda = -0.001$ while the right graph is for $\lambda = -0.001$ (brown), $\lambda = -1$ (red), $\lambda = -2$ (yellow) with $q = 0.5$.

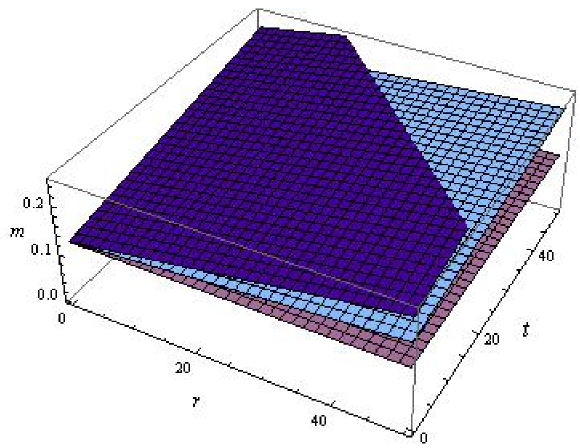

Figure 3.30: Plot of m versus r and t for $\gamma_2 = 0.0001$, $\alpha_2 = 1$, $q = 0$ (pink), $q = 0.001$ (blue), $q = 0.002$ (purple).

The graphs for energy conditions for expanding solutions are given in Figures **3.31** and **3.32** showing that all the energy conditions are satisfied.

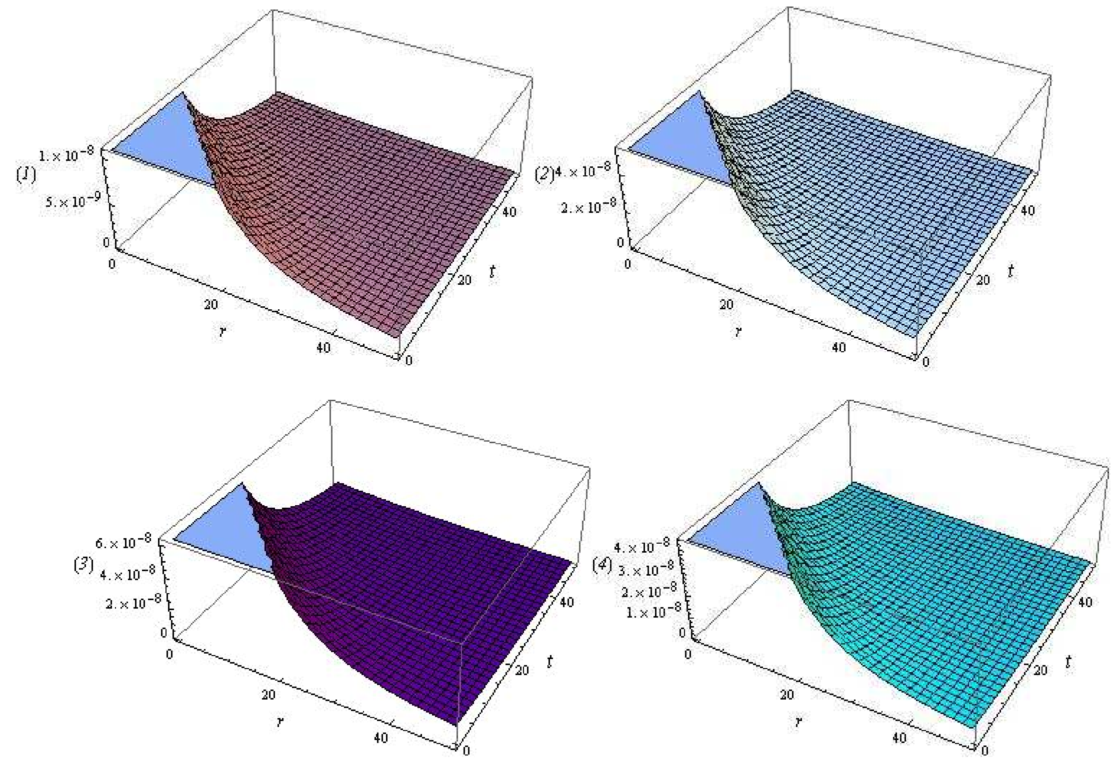

Figure 3.31: Plots of (1) $\rho + p_r - A_t$, (2) $\rho + p_\theta + \frac{q^2}{4\pi C^2} - A_t$, (3) $\rho + p_z + \frac{q^2}{4\pi C^2} - A_t$, (4) $\rho + \frac{q^2}{8\pi C^2} - A_t$ for $\gamma_2 = 0.0001$, $\alpha_2 = 1$, $q = 0.01$ and $\lambda = -0.001$.

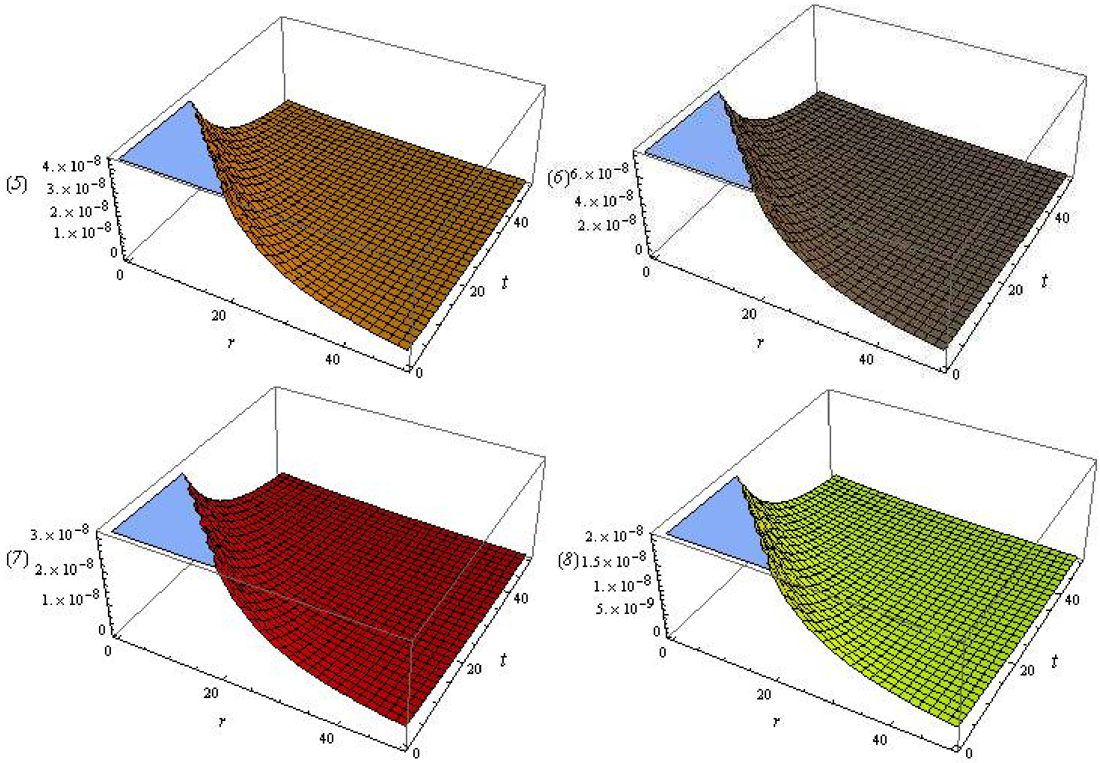

Figure 3.32: Plot of (5) $\rho+p_r+p_\theta+p_z+\frac{q^2}{4\pi C^2}-A_t$, (6) $\rho-p_r+\frac{q^2}{4\pi C^2}-A_t$, (7) $\rho-p_\theta-A_t$, (8) $\rho-p_z-A_t$, for $\gamma_2=0.0001$, $\alpha_2=1$, $q=0.01$ and $\lambda=-0.001$.

Chapter 4

Some Aspects of Gravitational Waves in Modified Theories

This chapter presents PMs of GWs in $f(R)$ theory and a study of axial GWs in $f(R,T)$ theory. The layout of the chapter is as follows. In first section, we find PMs of GWs for some viable $f(R)$ models. In second section, we introduce wave like perturbations in FRW spacetime as well as in the background material field and obtain unknown perturbation parameters by solving the corresponding $f(R,T)$ field equations. The results of this chapter have been published in the form of two papers [71, 72].

4.1 Polarization Modes in $f(R)$ Gravity

To discuss PMs of GWs, one needs to investigate linearized far field vacuum field equations. The vacuum field equations for the $f(R)$ gravity action (1.1.1) are

$$F(R)R_{\mu\nu} - \frac{1}{2}f(R)g_{\mu\nu} - \nabla_\mu\nabla_\nu F(R) + g_{\mu\nu}\Box F(R) = 0. \tag{4.1.1}$$

The trace of the above equation is

$$RF(R) - 2f(R) + 3\Box F(R) = 0. \tag{4.1.2}$$

We assume that waves are traveling in z-direction, i.e., each quantity can be a function of z and t. Amendola *et al.* [73] derived the conditions for cosmological viability of some dark energy models in $f(R)$ gravity. They divided $f(R)$ models into four classes according to the existence of a matter dominated era and the final accelerated expansion phase. They concluded that models of class I are not physical, class II models asymptotically approach to de Sitter universe, class III contains models showing strongly phantom era and models of class IV represent non-phantom acceleration ($\omega > -1$). They argued that only models belonging to class II are observationally acceptable with the final outcome of ΛCDM model. Here we consider these observationally acceptable models among which the model $R + \alpha R^{-n}$ has already been discussed by Alves *et al.* [36], so we discuss the remaining three.

4.1.1 Polarization Modes for $f(R) = R + \beta R^2 - \Lambda$

We consider the model $f(R) = R + \beta R^2 - \Lambda$, it is assumed that β (an arbitrary constant) and Λ (cosmological constant) have positive values. This model corresponds to ΛCDM model in the limit $\beta \to 0$ and Starobinsky inflationary model for $\Lambda \to 0$. In this case, Eq.(4.1.2) yields

$$R(1 + 2\beta R) - 2(R + \beta R^2 - \Lambda) + 3\Box(1 + 2\beta R) = 0, \tag{4.1.3}$$

which on simplification gives

$$\Box R - \frac{1}{6\beta} R = -\frac{\Lambda}{3\beta}. \tag{4.1.4}$$

Equation (4.1.4) can be interpreted as a non-homogeneous two-dimensional wave equation or Klein-Gordon equation and its solution can be found using different methods like Fourier transform and Green function etc. Here we obtain its solution following the technique used to solve Klein-Gordon and Sine-Gordon equations given in [74] which is simple as compared to other methods. According to this method, any static solution is a wave with zero velocity and for the systems with Lorentz invariance, once a static solution is known, moving solutions are trivially obtained by boosting, i.e., transforming to a moving coordinate frame. Since we are considering the vacuum field equations and the background metric is Minkowski, so we can apply Lorentz transformations to the Ricci scalar R (a Lorentz invariant quantity). Hence static solution of Eq.(4.1.4) is obtained by solving

$$\frac{d^2R}{dz^2} - \frac{1}{6\beta}R = -\frac{\Lambda}{3\beta}, \tag{4.1.5}$$

whose solution is

$$R(z) = c_1 e^{\sqrt{\frac{1}{6\beta}}z} + c_2 e^{-\sqrt{\frac{1}{6\beta}}z} + 2\Lambda, \tag{4.1.6}$$

where c_1, c_2 are constants of integration.

Since our system is Lorentz invariant, the time dependent solution is obtained from the static solution through Lorentz transformation as

$$R(z,t) = c_1 e^{\sqrt{\frac{1}{6\beta}}\frac{z-vt}{\sqrt{1-v^2}}} + c_2 e^{-\sqrt{\frac{1}{6\beta}}\frac{z-vt}{\sqrt{1-v^2}}} + 2\Lambda, \tag{4.1.7}$$

where $\sqrt{1-v^2}$ is the Lorentz factor and v represents the velocity of wave propagation. Also, Eq.(4.1.1) can be rewritten as

$$R_{\mu\nu} = \frac{1}{F(R)}\left[\frac{1}{2}f(R)g_{\mu\nu} + \nabla_\mu\nabla_\nu F(R) - g_{\mu\nu}\Box F(R)\right]. \tag{4.1.8}$$

Replacing the values of $f(R)$ and $F(R)$, we obtain its linearized form as

$$R_{\mu\nu} = \frac{1}{2}(R - \Lambda + 2\beta\Lambda R)g_{\mu\nu} + 2\beta\nabla_\mu\nabla_\nu R - 2\beta g_{\mu\nu}\Box R. \tag{4.1.9}$$

The non-zero components of Ricci tensor are

$$R_{tt} = \frac{1}{6(1-v^2)}[3v^2(R-\Lambda) - (R+3\Lambda)] - \beta\Lambda R, \tag{4.1.10}$$

$$R_{xx} = \frac{1}{6}(R+\Lambda) + \beta\Lambda R = R_{yy}, \tag{4.1.11}$$
$$R_{zz} = \frac{1}{6(1-v^2)}[3(R-\Lambda) - v^2(R+\Lambda)] + \beta\Lambda R, \tag{4.1.12}$$
$$R_{tz} = -\frac{vR}{3(1-v^2)}. \tag{4.1.13}$$

With the help of Eqs.(1.5.5) and (1.5.6), we have

$$\Psi_2 = \frac{1}{12}R, \quad \Psi_3 = \frac{1}{2}R_{l\tilde{n}}, \quad \Phi_{22} = -\frac{1}{2}R_{ll}. \tag{4.1.14}$$

Now, we find the expressions of Ψ_3 and Φ_{22} using Eq.(1.5.4). For Ψ_3, it yields

$$\Psi_3 = \frac{1}{2}R_{l\tilde{n}} = \frac{1}{2}R_{\mu\nu}l^\mu\tilde{n}^\nu, \tag{4.1.15}$$

which can also be written as

$$\Psi_3 = \frac{1}{2}(R_{tt}l^t\tilde{n}^t + R_{xx}l^x\tilde{n}^x + R_{yy}l^y\tilde{n}^y + R_{zz}l^z\tilde{n}^z + R_{tz}l^t\tilde{n}^z). \tag{4.1.16}$$

From Eqs.(1.5.1) and (1.5.2), the component form of vectors k, l, n and $\tilde{n}$ can be written as

$$k^\mu = \frac{1}{\sqrt{2}}(1,0,0,1), \quad l^\mu = \frac{1}{\sqrt{2}}(1,0,0,-1), \tag{4.1.17}$$
$$n^\mu = \frac{1}{\sqrt{2}}(0,1,i,0), \quad \tilde{n}^\mu = \frac{1}{\sqrt{2}}(0,1,-i,0). \tag{4.1.18}$$

Substituting all the required values in Eq.(4.1.16), we obtain $\Psi_3 = 0$. Similarly, Eq.(1.5.4) for Φ_{22} yields

$$\Phi_{22} = -\frac{1}{2}R_{ll} = -\frac{1}{2}R_{\mu\nu}l^\mu l^\nu = -\frac{1}{2}(R_{tt}l^tl^t + 2R_{tz}l^tl^z + R_{zz}l^zl^z).$$

Replacing the Ricci tensor components and components of l^μ, the above equation leads to

$$\Phi_{22} = -\frac{R}{12}\left(\frac{1+v}{1-v}\right) + \frac{\Lambda(2v^2+3)}{12(1-v^2)}. \tag{4.1.19}$$

Notice that $\Psi_4 \neq 0$ represents the tensor modes of GWs. Since there is no expression of Ψ_4 in terms of Ricci tensor, so it cannot be evaluated with the help of available values of the Ricci tensor and Ricci scalar [38]. It can be observed that for ΛCDM model (when $\beta \to 0$) Ψ_2 and Φ_{22} remain non-zero.

The model, $f(R) = R + \beta R^2 - \Lambda$, is always viable and reduces to GR when both β as well as Λ approach to zero. In GR, there are only two tensor modes of polarization associated with $Re\Psi_4$ and $Im\Psi_4$, i.e., we have only Ψ_4 non-zero among six NP parameters. From Eq.(4.1.3), we have $R = 0$ for $\beta \to 0$, $\Lambda \to 0$, hence GR results are retrieved.

4.1.2 Polarization Modes for $f(R) = R^{p_1}(\ln \chi R)^{q_1}$

This model is observationally acceptable for $p_1 = 1$ and $q_1 > 0$. Here we assume that $q_1 = 1$ such that the model becomes $f(R) = R \ln \chi R$. Substituting the values of $f(R)$ and $F(R)$ in Eq.(4.1.2), it gives

$$3\Box \ln \chi R - R \ln \chi R + R = 0. \tag{4.1.20}$$

Assuming $\ln \chi R = \varpi$, this equation transforms to

$$\Box \varpi = \frac{e^{\varpi}}{3\chi}(\varpi - 1), \tag{4.1.21}$$

which can also be written as

$$\Box \varpi = \frac{\partial U}{\partial \varpi}; \quad U(\varpi) = \frac{e^{\varpi}}{3\chi}(\varpi - 2). \tag{4.1.22}$$

First we seek for a static solution, i.e., consider $\varpi = \varpi(z)$ such that integration of Eq.(4.1.22) gives

$$\frac{1}{2}\left(\frac{d\varpi}{dz}\right)^2 = U(\varpi). \tag{4.1.23}$$

Substituting the value of $U(\varpi)$ and then integrating, it follows that

$$\varpi(z)=2\left[1+\text{InverseErf}\left[\frac{ez}{\sqrt{3\chi\pi}}+\frac{ec_3}{\sqrt{2\chi\pi}}\right]^2\right], \tag{4.1.24}$$

where c_3 is a constant of integration, $e=2.71828$ and Erf is defined by

$$Erf(z)=\frac{2}{\sqrt{\pi}}\int_0^z e^{-s^2}ds. \tag{4.1.25}$$

Using Lorentz transformation, we obtain time dependent solution given by

$$\varpi(z,t)=2\left[1+\text{InverseErf}\left[\frac{e(z-vt)}{\sqrt{1-v^2}\sqrt{3\chi\pi}}+\frac{ec_3}{\sqrt{2\chi\pi}}\right]^2\right]. \tag{4.1.26}$$

The expression for Ricci scalar is obtained as

$$R(z,t)=\frac{1}{\chi}\exp\left(2\left[1+\text{InverseErf}\left[\frac{e(z-vt)}{\sqrt{1-v^2}\sqrt{3\chi\pi}}+\frac{ec_3}{\sqrt{2\chi\pi}}\right]^2\right]\right). \tag{4.1.27}$$

The non-zero components of the Ricci tensor have the form

$$\begin{aligned}
R_{tt} &= -\frac{R}{6(v^2-1)}\left[\frac{(3v^2-1)\ln\chi R-2}{\ln\chi R+1}\right],\\
R_{xx} &= \frac{R}{6}\left(\frac{\ln\chi R+2}{\ln\chi R+1}\right)=R_{yy},\\
R_{tz} &= \frac{Rv(\ln\chi R-1)}{3(v^2-1)(\ln\chi R+1)},\\
R_{zz} &= \frac{R}{6(v^2-1)}\left[\frac{(v^2-3)\ln\chi R+2v^2}{\ln\chi R+1}\right].
\end{aligned}$$

Finally, the NP parameters for this case are

$$\Psi_2=\frac{1}{12}R,\quad \Psi_3=0,\quad \Phi_{22}=-\frac{R}{12}\left(\frac{1+v}{1-v}\right)\frac{(\ln\chi R-1)}{\ln\chi R+1}. \tag{4.1.28}$$

Here Ψ_4 is also a non-vanishing NP parameter as discussed in the previous case.

4.1.3 Polarization Modes for $f(R) = R^{p_2} e^{\frac{q_2}{R}}$

This model is observationally acceptable for $p_2 = 1$, so we take $f(R) = Re^{\frac{q_2}{R}}$. This model reduces to GR when $q_2 = 0$ and consequently gives no additional PMs. Thus to find extra PMs, we consider $q_2 \neq 0$ in further calculations. For this model, the trace equation (4.1.2) becomes

$$Re^{\frac{q_2}{R}}\left(1 - \frac{q_2}{R}\right) - 2Re^{\frac{q_2}{R}} + 3\Box\left(e^{\frac{q_2}{R}}\left(1 - \frac{q_2}{R}\right)\right) = 0. \tag{4.1.29}$$

In low curvature regime, we have $R << q_2$ which reduces the above equation to the following

$$\Box\left(\frac{1}{R}e^{\frac{q_2}{R}}\right) + \frac{1}{3}e^{\frac{q_2}{R}} = 0. \tag{4.1.30}$$

Replacing $\frac{1}{R} = \tilde{u}$ and $\tilde{u} = \tilde{u}(z)$ for static solution, we obtain

$$\frac{d^2}{dz^2}(\tilde{u}e^{q_2\tilde{u}}) + \frac{1}{3}e^{q_2\tilde{u}} = 0. \tag{4.1.31}$$

Solving the double derivative of the above equation, it becomes

$$(1 + q_2\tilde{u})\frac{d^2\tilde{u}}{dz^2} + q_2(q_2\tilde{u} + 2)\left(\frac{d\tilde{u}}{dz}\right)^2 + \frac{1}{3} = 0.$$

This is a non-homogeneous non-linear second order differential equation and does not provide an exact analytic solution unless we make some assumptions to simplify it. Since we are working in the weak-field regime, so R is very small. Assuming q_2 to be very large, we have $q_2\tilde{u} = \frac{q_2}{R}$ (as $\tilde{u} = \frac{1}{R}$) to be very large such that $(q_2\tilde{u} + 1) \approx q_2\tilde{u}$ as well as $(q\tilde{u} + 2) \approx q\tilde{u}$ and the above equation reduces to

$$\tilde{u}\frac{d^2\tilde{u}}{dz^2} + q_2\tilde{u}\left(\frac{d\tilde{u}}{dz}\right)^2 + \frac{1}{3q_2} = 0.$$

Here $\frac{1}{3q_2} \to 0$ as q_2 is very large, hence it reduces to

$$\tilde{u}\frac{d^2\tilde{u}}{dz^2} + q_2\tilde{u}\left(\frac{d\tilde{u}}{dz}\right)^2 = 0, \tag{4.1.32}$$

whose solution yields ($\tilde{u} = 1/R$)

$$R(z) = \left(\frac{1}{q_2}\ln[q_2(c_4 z + c_5)]\right)^{-1}, \tag{4.1.33}$$

where c_4 and c_5 are integration constants. The non-static solution becomes

$$R(z,t) = \left(\frac{1}{q_2}\ln\left[q_2\left(c_4\frac{(z-vt)}{\sqrt{1-v^2}} + c_5\right)\right]\right)^{-1}. \tag{4.1.34}$$

The non-vanishing components of the Ricci tensor are

$$\begin{aligned} R_{tt} &= \frac{q_2\left[q_2(z-vt)^2 + 2\ln\left[q_2\left(c_4\frac{(z-vt)}{\sqrt{1-v^2}} + c_5\right)\right]\right]c_4^2}{2(\ln\left[q_2\left(c_4\frac{(z-vt)}{\sqrt{1-v^2}} + c_5\right)\right])^2((tv-z)c_4 - \sqrt{1-v^2}c_5)^2} \\ &+ \frac{q_2\left[2q_2\sqrt{1-v^2}(z-vt)c_4c_5 - q_2c_5^2(v^2-1)\right]}{2(\ln\left[q_2\left(c_4\frac{(z-vt)}{\sqrt{1-v^2}} + c_5\right)\right])^2((tv-z)c_4 - \sqrt{1-v^2}c_5)^2}, \end{aligned} \tag{4.1.35}$$

$$\begin{aligned} R_{xx} = R_{yy} &= \frac{-q_2\left[q_2(z-vt)^2 - 2(v^2-1)\ln\left[q_2\left(c_4\frac{(z-vt)}{\sqrt{1-v^2}} + c_5\right)\right]\right]c_4^2}{2(\ln\left[q_2\left(c_4\frac{(z-vt)}{\sqrt{1-v^2}} + c_5\right)\right])^2((tv-z)c_4 - \sqrt{1-v^2}c_5)^2} \\ &- \frac{q_2\left[2q_2\sqrt{1-v^2}(z-vt)c_4c_5 - q_2c_5^2(v^2-1)\right]}{2(\ln\left[q_2\left(c_4\frac{(z-vt)}{\sqrt{1-v^2}} + c_5\right)\right])^2((tv-z)c_4 - \sqrt{1-v^2}c_5)^2}, \end{aligned} \tag{4.1.36}$$

$$\begin{aligned} R_{zz} &= \frac{-q_2\left[q_2(z-vt)^2 - 2v^2\ln\left[q_2\left(c_4\frac{(z-vt)}{\sqrt{1-v^2}} + c_5\right)\right]\right]c_4^2}{2(\ln\left[q_2\left(c_4\frac{(z-vt)}{\sqrt{1-v^2}} + c_5\right)\right])^2((tv-z)c_4 - \sqrt{1-v^2}c_5)^2} \\ &- \frac{q_2\left[2q_2\sqrt{1-v^2}(z-vt)c_4c_5 - q_2c_5^2(v^2-1)\right]}{2(\ln\left[q_2\left(c_4\frac{(z-vt)}{\sqrt{1-v^2}} + c_5\right)\right])^2((tv-z)c_4 - \sqrt{1-v^2}c_5)^2}, \end{aligned} \tag{4.1.37}$$

$$R_{tz} = -\frac{q_2vc_4^2}{(1-v^2)\left(\frac{(z-vt)}{\sqrt{1-v^2}}c_4 + c_5\right)}. \tag{4.1.38}$$

The corresponding NP parameters are

$$\Psi_2 = \frac{1}{12}R, \quad \Psi_3 = 0, \tag{4.1.39}$$

$$\Phi_{22} = -\frac{Rc_4^2(v-1)^2}{4((tv-z)c_4-\sqrt{1-v^2}c_5)^2}. \tag{4.1.40}$$

Ψ_4 is also non-zero.

4.2 Axial Perturbations in FRW Model

We consider FRW cosmological model for the flat universe in (η, r, θ, ϕ) coordinates

$$ds^2 = a^2(\eta)(-d\eta^2 + dr^2 + r^2 d\theta^2 + r^2 \sin^2\theta d\phi^2), \tag{4.2.1}$$

where η is the conformal time coordinate related to the ordinary time by the relation

$$\eta = \int \frac{dt}{a}, \tag{4.2.2}$$

such that the conformal Hubble parameter $\mathcal{H}$ is related with the ordinary Hubble parameter H by

$$H = \frac{\mathcal{H}}{a}. \tag{4.2.3}$$

We consider perturbations producing odd waves or axial waves in flat FRW universe introduced by Regge and Wheeler [54]. The axially perturbed FRW universe in Regge-Wheeler gauge is given by

$$\begin{aligned} ds^2 &= -a^2(\eta)d\eta^2 + 2\hat{e}k_0\sin\theta\partial_\theta Y_l^m d\eta d\phi + a^2(\eta)dr^2 + 2\hat{e}k_1\sin\theta\partial_\theta Y_l^m dr d\phi \\ &+ a^2(\eta)r^2d\theta^2 + a^2(\eta)r^2\sin^2\theta d\phi^2 + O(\hat{e}^2), \end{aligned} \tag{4.2.4}$$

where $\hat{e}$ is a small parameter (it measures strength of perturbations and the terms involving $O(\hat{e}^2)$ are neglected), $k_0 = k_0(\eta, r)$, $k_1 = k_1(\eta, r)$. Here we are considering the odd waves corresponding to $m = 0$, which are discussed by Regge and Wheeler [54] so that ϕ disappears in calculations. Also, for the wavelike solution the index l exceeds one, i.e., we have $Y_l^0 = Y_{l0}$; $l = 2, 3, ...$

We consider matter as perfect fluid given in Eq.(2.1.2) and the perturbations in the material quantities are defined as follows [42]

$$\rho = \rho_0(1+\hat{e}\Delta(\eta,r)Y_{l0})+O(\hat{e}^2), \tag{4.2.5}$$

$$p = p_0(1+\hat{e}\Pi(\eta,r)Y_{l0})+O(\hat{e}^2), \tag{4.2.6}$$

where ρ_0 and p_0 are the background density and pressure. The fluid may or may not be comoving in the perturbed scenario so the perturbed components of four velocity are taken as [42]

$$V_0 = \frac{2g^{(0)}_{00}+\hat{e}k_{00}}{2a(\eta)}+O(\hat{e}^2), \tag{4.2.7}$$

$$V_1 = \hat{e}a(\eta)u_1(\eta,r)Y_{l0}+O(\hat{e}^2), \tag{4.2.8}$$

$$V_2 = \hat{e}u_2(\eta,r)\partial_\theta Y_{l0}+O(\hat{e}^2), \tag{4.2.9}$$

$$V_3 = \hat{e}\sin\theta u_3(\eta,r)\partial_\theta Y_{l0}+O(\hat{e}^2), \tag{4.2.10}$$

where $V_\mu V^\mu = -1+O(\hat{e}^2)$.

Here, we consider $f(R,T)=R+2\lambda T$ to investigate the role of curvature-matter coupling on the propagation of GWs. The assumption $\mathcal{L}_m = p$ and the model $f(R,T)=R+2\lambda T$ simplify the field equations as

$$G_{\mu\nu} = (8\pi+2\lambda)T_{\mu\nu}-2\lambda p g_{\mu\nu}+\lambda T g_{\mu\nu}. \tag{4.2.11}$$

This yields the following independent field equations for the metric (4.2.1)

$$3\mathcal{H}^2 = (8\pi+3\lambda)\rho_0 a^2-\lambda p_0 a^2, \tag{4.2.12}$$

$$-2\partial_\eta\mathcal{H}-\mathcal{H}^2 = (8\pi+3\lambda)p_0 a^2-\lambda\rho_0 a^2. \tag{4.2.13}$$

The field equations for the perturbed metric (4.2.4) are

$$3\mathcal{H}^2 = [(8\pi+3\lambda)\rho_0-\lambda p_0+(8\pi+3\lambda)\rho_0\hat{e}\Delta Y_{l0}-\lambda p_0 e\Pi Y_{l0}]a^2, \tag{4.2.14}$$

$$u_1(8\pi + 2\lambda)(\rho_0 + p_0) = 0, \tag{4.2.15}$$

$$u_2(8\pi + 2\lambda)(\rho_0 + p_0) = 0, \tag{4.2.16}$$

$$-2\partial_\eta \mathcal{H} - \mathcal{H}^2 = a^2[(8\pi + 3\lambda)p_0 - \lambda\rho_0 + (8\pi + 3\lambda)p_0\hat{e}\Pi Y_{l0} - \lambda\rho_0\hat{e}\Delta Y_{l0}], \tag{4.2.17}$$

$$k_1' = \partial_\eta k_0, \tag{4.2.18}$$

$$\begin{aligned}&\partial_\eta k_1' - k_0'' + \frac{2}{r}\partial_\eta k_1 - 2\mathcal{H}k_1' + \frac{4}{r}k_1\mathcal{H} - 4k_0\partial_\eta\mathcal{H} - 2\mathcal{H}^2 k_0 + \frac{k_0}{r^2}l(l+1)\\ &= -2a^3(8\pi + 2\lambda)u_3(\rho_0 + p_0) + [(8\pi + 3\lambda)p_0 - \lambda\rho_0]2a^2k_0\\ &+2a^2\hat{e}(8\pi + 4\lambda)k_0p_0\Pi Y_{l0} - 2a^2\hat{e}\lambda k_0\rho_0\Delta,\end{aligned} \tag{4.2.19}$$

$$\begin{aligned}&\partial_\eta\partial_\eta k_1 - \partial_\eta k_0' + \frac{2}{r}\partial_\eta k_0 - \frac{2}{r^2}k_1 - 2\mathcal{H}\partial_\eta k_1 - 6\partial_\eta\mathcal{H}k_1 - 2\mathcal{H}^2k_1 + \frac{k_1}{r^2}l(l+1)\\ &= 2a^2k_1p_0(8\pi + 2\lambda) + 2\lambda a^2k_1(-\rho_0 + p_0) - 2a^2\hat{e}\lambda k_1\rho_0\Delta\\ &+2a^2\hat{e}(8\pi + 4\lambda)k_1p_0\Pi Y_{l0},\end{aligned} \tag{4.2.20}$$

where we have used the relation

$$\partial_\theta\partial_\theta Y_{l0} = -l(l+1)Y_{l0} - \cot\theta\partial_\theta Y_{l0}.$$

4.2.1 Rotation Induced by Axial GWs

In this section, we find expressions for the perturbation parameters k_0, k_1, Δ, Π, u_1, u_2 and u_3. Equation (2.1.6) implies that either the factor $(8\pi+2\lambda) = 0$, i.e., $\lambda = -4\pi$ or $u_1(\rho_0 + p_0) = 0$. However, the viability conditions for $f(R,T)$ gravity models are

$$f_R > 0, \quad 1 + \frac{f_T}{8\pi} > 0 \quad \text{and} \quad f_{RR} > 0,$$

and give the constraint $\lambda > -4\pi$ for our model implying that $(8\pi + 2\lambda) \neq 0$. Hence Eqs.(4.2.15) and (4.2.16) yield that $u_1 = 0$ and $u_2 = 0$. Substituting the unperturbed field equations in perturbed one, we obtain the following equations from (4.2.14), (4.2.17), (4.2.19) and (4.2.20), respectively.

$$(8\pi+3\lambda)\rho_0\Delta-\lambda p_0\Pi=0, \tag{4.2.21}$$

$$(8\pi+3\lambda)p_0\Pi-\lambda\rho_0\Delta=0, \tag{4.2.22}$$

$$\begin{aligned}&\partial_\eta k_1'-k_0''+\frac{2}{r}\partial_\eta k_1-2\mathcal{H}k_1'+\frac{4}{r}k_1\mathcal{H}+\frac{k_0}{r^2}l(l+1)\\&=-2a^3(8\pi+2\lambda)u_3(\rho_0+p_0)+2a^2\hat{e}[(8\pi+4\lambda)k_0p_0\Pi Y_{l0}-\lambda k_0\rho_0\Delta],\end{aligned} \tag{4.2.23}$$

$$\begin{aligned}&\partial_\eta\partial_\eta k_1-\partial_\eta k_0'+\frac{2}{r}\partial_\eta k_0-\frac{2}{r^2}k_1-2\mathcal{H}\partial_\eta k_1-2\partial_\eta\mathcal{H}k_1+\frac{k_1}{r^2}l(l+1)\\&=2a^2\hat{e}[-\lambda k_1\rho_0\Delta+(8\pi+4\lambda)k_1p_0\Pi Y_{l0}].\end{aligned} \tag{4.2.24}$$

Solving (4.2.21) and (4.2.22) simultaneously for Π, we obtain

$$((8\pi+3\lambda)^2-\lambda^2)p_0\Pi=0, \tag{4.2.25}$$

which implies that either

$$((8\pi+3\lambda)^2-\lambda^2)=0 \quad \text{or} \quad \Pi=0. \tag{4.2.26}$$

The first factor in the above equation yields $\lambda=-4\pi$ and -2π. However, keeping in mind the viability conditions for the assumed model, we exclude $\lambda=-4\pi$. Hence if $\lambda=-2\pi$, then there is a possibility that $\Pi\neq0$ and similarly $\Delta\neq0$, i.e., the axial GWs can affect the background matter in curvature-matter coupling scenario. Assuming EoS for radiation dominated era $p_0=\frac{1}{3}\rho_0$, we obtain the following relationship between Π and Δ

$$\Pi=3\left(\frac{8\pi}{\lambda}+3\right)\Delta. \tag{4.2.27}$$

Substituting the above relation in Eqs.(4.2.23) and (4.2.24), we are left with four unknowns k_0, k_1, Δ, u_3 with three equations (4.2.18), (4.2.23), (4.2.24). Thus in order to have the system closed, we assume that GWs do not perturb the matter field, i.e., $\Delta = 0 = \Pi$. Now introducing a new quantity $Q(\eta, r)$ such that

$$k_1(\eta, r) = ra(\eta)Q(\eta, r). \tag{4.2.28}$$

Using this equation with Eq.(4.2.18) in (4.2.24), we obtain

$$\partial_\eta\partial_\eta Q - Q'' + \frac{l(l+1)}{r^2}Q - a^2[\frac{(4\pi + 3\lambda)}{3}\rho_0 - \frac{(12\pi + 5\lambda)}{3}p_0]Q = 0. \tag{4.2.29}$$

For $p_0 = \frac{\rho_0}{3}$, the field equations (4.2.12) and (4.2.13) lead to

$$2\partial_\eta \mathcal{H} + \frac{6\pi + \lambda}{3\pi + \lambda}\mathcal{H}^2 = 0,$$

which yields the scale factor

$$a(\eta) = c_6 \eta^{\frac{6\pi + 2\lambda}{6\pi + \lambda}}, \tag{4.2.30}$$

where c_6 is a constant of integration.

The covariant derivative of the field equations is

$$\nabla^\mu T_{\mu\nu} = \frac{f_T}{8\pi - f_T}\left[(T_{\mu\nu} + \Theta_{\mu\nu})\nabla^\mu \ln f_T + \nabla^\mu \Theta_{\mu\nu} - \frac{1}{2}g_{\mu\nu}\nabla^\mu T\right]. \tag{4.2.31}$$

Using Eq.(4.2.1), (2.1.2), the model $f(R, T) = R + 2\lambda T$ and $p_0 = \frac{\rho_0}{3}$, Eq.(4.2.31) produces the following differential equation in ρ

$$\partial_\eta \rho_0 + 3\frac{8\pi + \lambda}{6\pi + \lambda}\mathcal{H}\rho_0 = 0,$$

whose solution is

$$\rho_0 = c_7 a^{\frac{-3(8\pi + \lambda)}{6\pi + \lambda}}, \tag{4.2.32}$$

c_7 is another integration constant. Inserting these values of p_0, $a(\eta)$ and ρ_0 in Eq.(4.2.29), it follows that

$$\partial_\eta\partial_\eta Q - Q'' + [\frac{l(l+1)}{r^2} - \frac{4c_6^2 c_7 \hat{b}_1 \lambda}{9}\eta^{\frac{6\pi+2\lambda}{6\pi+\lambda}\frac{(-3)(8\pi+\lambda)}{6\pi+\lambda}}]Q = 0, \tag{4.2.33}$$

where $\hat{b}_1 = c_6^{\frac{-3(8\pi+\lambda)}{6\pi+\lambda}}$. Let us define $\hat{A} = \frac{4c_6^2 c_7 \hat{b}_1 \lambda}{9}$ and take $l = 2$ such that the above equation becomes

$$\partial_\eta \partial_\eta Q - Q'' + [\frac{6}{r^2} - \hat{A}\eta^{\frac{6\pi+2\lambda}{6\pi+\lambda}\frac{(-3)(8\pi+\lambda)}{6\pi+\lambda}}]Q = 0. \tag{4.2.34}$$

This equation can be solved through separation of variables by assuming $Q(\eta, r) = \mathcal{T}(\eta)\mathcal{R}(r)$. Introducing the separation constant $-\digamma^2$, we obtain the following two differential equations

$$\begin{aligned} \partial_\eta \partial_\eta \mathcal{T} - \left(\hat{A}\eta^{\frac{6\pi+2\lambda}{6\pi+\lambda}\frac{(-3)(8\pi+\lambda)}{6\pi+\lambda}} - \digamma^2\right)\mathcal{T} &= 0, && (4.2.35) \\ \mathcal{R}'' - \left(\frac{6}{r^2} - \digamma^2\right)\mathcal{R} &= 0. && (4.2.36) \end{aligned}$$

These are second order homogeneous linear differential equations with variable coefficients. Equation (4.2.35) can yield some solution if the power of η is fixed. So, we consider $\frac{6\pi+2\lambda}{6\pi+\lambda}\frac{(-3)(8\pi+\lambda)}{6\pi+\lambda} = \hat{n}$ and check that for what values of $\hat{n}$ the values of λ are consistent with viability criteria. We find that the values of λ for $\hat{n} > 1$ are not consistent with $\lambda > -4\pi$ (the viability criteria) and $\hat{n} < -2$ yields imaginary values of λ. Hence, $\hat{n}$ can have the values within the limit $-2 \leq \hat{n} < 1$. For $\hat{n} = -2$, we have $\lambda = 0$ which is the case of GR. For the sake of convenience, we take $\hat{n} = 0, -1$, to find the solution of Eq.(4.2.35). For $\hat{n} = 0$, the solution is

$$\mathcal{T}(\eta) = c_8 \cos \digamma\eta + c_9 \sin \digamma\eta, \tag{4.2.37}$$

where c_8 and c_9 are constants of integration and for $\hat{n} = -1$, we have

$$\begin{aligned} \mathcal{T}(\eta) &= c_{10}\eta e^{-i\digamma\eta}\text{Hypergeometric1F1}\left[1 + \frac{\hat{A}}{2i\digamma}, 2, 2i\digamma\eta\right] && (4.2.38) \\ &+ c_{11} t e^{-i\digamma\eta}\text{HypergeometricU}\left[1 + \frac{\hat{A}}{2i\digamma}, 2, 2i\digamma\eta\right], \end{aligned}$$

where c_{10}, c_{11} are constants and Hypergeometric1F1, HypergeometricU are the confluent hypergeometric functions of the first and second kind, respectively. These functions are defined by

$$\begin{aligned}
\text{Hypergeometric1F1}(\alpha;\beta;z) &= \frac{\Gamma(\beta)}{\Gamma(\beta-\alpha)\Gamma(\alpha)}\int_0^1 e^{zt}t(\alpha-1)(1-t)^{\beta-\alpha-1}dt,\\
\text{HypergeometricU}(\alpha,\beta,z) &= \frac{1}{\Gamma(\alpha)}\int_0^\infty e^{-zt}t(\alpha-1)(1+t)^{\beta-\alpha-1}dt,
\end{aligned}$$

where "Γ" indicates the gamma function. The solution of Eq.(4.2.36) is obtained as

$$\begin{aligned}
\mathcal{R}(r) &= \sqrt{\frac{2}{\digamma\pi}}c_{12}\left(\frac{-3\cos\digamma r}{\digamma r}-\sin\digamma r+\frac{3\sin mr}{\digamma^2r^2}\right)\\
&+ \sqrt{\frac{2}{\digamma\pi}}c_{13}\left(\frac{-3\cos\digamma r}{\digamma^2r^2}-\frac{3\sin\digamma r}{\digamma r}+\cos\digamma r\right),
\end{aligned}\tag{4.2.39}$$

where c_{12} and c_{13} are integration constants.

Replacing the values of $Q(\eta,r)$ and $a(\eta)$ in Eq.(4.2.28), we obtain k_1 while the expression for k_0 is obtained from Eq.(4.2.18) as follows

$$k_0=\hat{B}(r)+\int_{\eta_0}^{\eta}k_1'(\tau,r)d\tau,\tag{4.2.40}$$

where η_0 is the conformal time at the hypersurface originating GWs. Assuming $k_0(\eta,r)=0$, we have $\hat{B}(r)=0$ and k_0 becomes

$$k_0=(r\mathcal{R}(r))'\int_{\eta_0}^{\eta}a(\tau)\mathcal{T}(\tau)d\tau.\tag{4.2.41}$$

Finally, replacing the values of k_0, k_1 and $\Delta=0=\Pi$ in Eq.(4.2.23), we obtain for $\hat{n}=0$

$$\begin{aligned}
u_3(\eta,r) &= \frac{\eta^{\frac{\lambda}{6\pi+\lambda}}c_6}{(\digamma r)^{\frac{5}{2}}}\sqrt{\frac{2r}{\pi}}[(3\digamma rc_{12}+\digamma^3r^3c_{12}+3c_{13})\cos\digamma r+(-3c_{12}+\digamma r\\
&(3+\digamma^2r^2)c_{13})\sin\digamma r][(c_8-\digamma\eta c_9)\cos\digamma\eta+(\digamma\eta c_8+c_9)\sin\digamma\eta].
\end{aligned}\tag{4.2.42}$$

For $\hat{n} = -1$, we have

$$\begin{aligned}
u_3(\eta, r) &= \frac{\eta^{\frac{6\pi+2\lambda}{6\pi+\lambda}} e^{-i\digamma\eta} c_6}{(\digamma r)^{\frac{5}{2}}} \sqrt{\frac{r}{2\pi}} \left[(1 - \frac{6\pi + 2\lambda}{6\pi + \lambda} + i\digamma\eta) \{2c_{10} \right. \\
&\times \text{Hypergeometric1F1}\left[1 + \frac{\hat{A}}{2i\digamma}, 2, 2i\digamma\eta\right] + 2c_{11} \\
&\times \text{HypergeometricU}\left[1 + \frac{\hat{A}}{2i\digamma}, 2, 2i\digamma\eta\right]\Big\} + (\hat{A} + 2i\digamma)\eta \\
&\times \Big\{2c_{11}\text{Hypergeometric1F1}\left[1 + \frac{\hat{A}}{2i\digamma}, 3, 2i\digamma\eta\right] - c_{10} \\
&\times \left.\text{Hypergeometric1F1}\left[1 + \frac{\hat{A}}{2i\digamma}, 3, 2i\digamma\eta\right]\Big\}\right] [(3\digamma r c_{12} + \digamma^3 r^3 c_{12} \\
&+ 3c_{13}) \cos\digamma r + (-3c_{12} + \digamma r(3 + \digamma^2 r^2) c_{13}) \sin\digamma r]. \qquad (4.2.43)
\end{aligned}$$

Thus the final expression for four velocity in radiation dominated phase becomes

$$V_\alpha = (-c_6 \eta^{\frac{6\pi+2\lambda}{6\pi+\lambda}}, 0, 0, \hat{e}\partial_\theta Y_{20} u_3(\eta, r) \sin\theta). \qquad (4.2.44)$$

Also, $Y_{20}(\theta) = \frac{1}{4}\sqrt{\frac{5}{\pi}}(3\cos^2\theta - 1)$ leads to $\partial_\eta Y_{20} = \frac{1}{4}\sqrt{\frac{5}{\pi}}\cos\theta\sin\theta$ and hence

$$V_\alpha = (-c_6 \eta^{\frac{6\pi+2\lambda}{6\pi+\lambda}}, 0, 0, \frac{\hat{e}}{4}\sqrt{\frac{5}{\pi}} u_3(\eta, r)\cos\theta\sin^2\theta). \qquad (4.2.45)$$

Thus the azimuthal velocity of any point P having coordinates (η, r, θ, ϕ) is $V_3 = \frac{\hat{e}}{4}\sqrt{\frac{5}{\pi}} u_3(\eta, r)\cos\theta\sin^2\theta$, where $u_3(\eta, r)$ is given in Eq.(4.2.42) and (4.2.43) for $\hat{n} = 0, -1$, respectively. The angular (Ω) and linear rotational (V) velocities of the fluid are

$$\begin{aligned}
\Omega &= \frac{V^3}{V^0} = \frac{\hat{C} u_3}{a r^2}\cos\theta; \quad \hat{C} = \frac{\hat{e}}{4}\sqrt{\frac{5}{\pi}}, \\
V &= a r \sin\theta\Omega = \frac{\hat{C} u_3 \sin 2\theta}{2r}.
\end{aligned}$$

These expressions of velocities show that the fluid remains no more comoving after passing the GW.

Currently, our universe is in expansion phase for which EoS is $p_0 = -\rho_0$. Using this EoS, we can observe how such types of GWs can perturb the flat cosmos in the recent era. For $p_0 = -\rho_0$, the scale factor and density have the expressions

$$a(\eta) = \frac{\tilde{c}_6}{\eta}, \quad \rho = \tilde{c}_7 a^{\frac{-3\lambda}{2\pi}}, \tag{4.2.46}$$

where $\tilde{c}_6$ and $\tilde{c}_7$ are integration constants. It is found that this EoS can yield non-vanishing u_1 and u_2 (from (4.2.15) and (4.2.16)) while the remaining expressions remain the same with $\hat{A} = \frac{8(2\pi+\lambda)}{3}\tilde{c}_6^2\tilde{c}_7\hat{b}_2$, $\hat{b}_2 = \tilde{c}_6^{\frac{-3\lambda}{2\pi}}$ and $\frac{3\lambda-4\pi}{2\pi} = \hat{n}$. In dark energy dominated phase, $\hat{n}$ can take positive and negative values, however, similar to radiation dominated phase, $\hat{n} = -2$ yields the GR case.

Chapter 5

Evolution of Viscous Fluid in $f(R,T)$ Theory

This chapter investigates some aspects of evolution of the universe consisting of viscous fluid. There are two main sections of this chapter. In the next section **5.1**, we study the evolution of bulk viscous MCG interacting with $f(R,T)$ gravity in flat FRW universe. The field equations are formulated for the model $f(R,T) = R + 2\lambda T$ and constraints for the conservation of the energy-momentum tensor are obtained. We discuss the behavior of total energy density, pressure and EoS parameter for emergent, intermediate as well as logamediate scenarios of the universe with two interacting models. In section **5.2**, we study the evolution in the background of LRS Bianchi type-I model with bulk viscous fluid. We discuss scale factors as well as deceleration parameter in dark energy dominated era for different models of bulk viscosity. The occurrence of big-rip singularity is also examined. The results of this chapter have been published in two papers [75, 76].

5.1 Interaction of Viscous MCG with $f(R,T)$ Gravity

The flat FRW universe model is given by

$$ds^2 = -dt^2 + a^2(t)(dx^2 + dy^2 + dz^2). \tag{5.1.1}$$

We consider a matter which consists of MCG with bulk viscosity for which the energy-momentum tensor can be written as [77]

$$T_{\mu\nu} = (\rho + p - 3\xi H)V_\mu V_\nu + (p - 3\xi H)g_{\mu\nu}, \tag{5.1.2}$$

where ρ denotes density of MCG, p represents pressure of MCG and ξ denotes bulk viscosity coefficient. Using Eq.(1.1.4), we obtain the following field equations for the model $f(R,T) = R + 2\lambda T$ and $\kappa^2 = 1$

$$3H^2 = \rho - \lambda T + 2\lambda(\rho + p - 3\xi H) = \rho^{tot}, \tag{5.1.3}$$

$$-2\dot{H} - 3H^2 = p - 3\xi H + \lambda T = p^{tot}, \tag{5.1.4}$$

where $H = \frac{\dot{a}}{a}$ and the trace of energy-momentum tensor is

$$T = -\rho + 3p - 9\xi H. \tag{5.1.5}$$

Also,

$$\rho^{tot} = \rho^{DE} + \rho, \quad p^{tot} = p^{DE} + p. \tag{5.1.6}$$

Consequently, the energy density and pressure of dark energy become

$$\rho^{DE} = -\lambda T + 2\lambda(\rho + p - 3\xi H), \tag{5.1.7}$$

$$p^{DE} = -3\xi H + \lambda T. \tag{5.1.8}$$

The equation of state for MCG is defined in Eq.(1.8.3).

The conservation equation holds in $f(R,T)$ gravity provided that the following constraint holds [78]

$$(\rho + p - 3\xi H)\dot{f}_T - \frac{1}{2}f_T((p - 3\xi H)^{\cdot} - \dot{\rho}) = 0, \tag{5.1.9}$$

with $f = f(T)$. Here $f(T) = \lambda T$ and the above equation gives

$$(p - 3\xi H)^{\cdot} = \dot{\rho} \quad \Rightarrow \quad p - 3\xi H = \rho + c_{14}, \tag{5.1.10}$$

where c_{14} is the constant of integration. Adding Eqs.(1.8.3) and (5.1.10), we have

$$p = \frac{b_1 + 1}{2}\rho - \frac{b_2}{2\rho^\delta} + \frac{3}{2}\xi H + \frac{c_{14}}{2}. \tag{5.1.11}$$

This equation can be written in the form of the EoS of MCG as

$$p = \tilde{b}_1\rho - \frac{\tilde{b}_2}{\rho^\delta}, \tag{5.1.12}$$

where $\tilde{b}_1 = \frac{b_1+1}{2}$, $\tilde{b}_2 = \frac{b_2}{2}$ and

$$\frac{3}{2}\xi H + \frac{c_{14}}{2} = 0, \tag{5.1.13}$$

which gives $\xi(t)$ in terms of H and c_{14}. We take the conservation of $T^{tot}_{\mu\nu}$ with the above mentioned constraints.

The equation of continuity for interacting dark energy and MCG gives

$$\dot{\rho}^{DE} + 3H(\rho^{DE} + p^{DE}) = -\tilde{Q}, \tag{5.1.14}$$

$$\dot{\rho} + 3H(\rho + p) = \tilde{Q}, \tag{5.1.15}$$

where $\tilde{Q}$ is the interaction term. The interaction between $f(R,T)$ and MCG is considered to study the interaction of dark energy and dark matter. The physical significance of considering an interaction between dark energy and dark matter is that it introduces an energy flow between two components of the universe [79, 80]. The interaction term $\tilde{Q}$ is usually considered either $\tilde{Q} = 3Hb\rho$, or $\tilde{Q} = 3Hb\rho^{DE}$, or $\tilde{Q} = 3Hb\rho^{tot}$, where b is the coupling constant [80, 81]. There are also other interacting models containing time derivative of energy density but these interactions cannot change sign. Wei [82] proposed a sign changeable interaction $\tilde{Q} = \tilde{q}(\epsilon\dot{\rho} + 3bH\rho)$, where ϵ is constant. He explored that the cosmological coincidence problem can be alleviated by some scaling attractors and showed that this interaction model can bring new features to cosmology.

In the following, we study the interactions $\tilde{Q} = 3Hb\rho$ as well as $\tilde{Q} = \tilde{q}(\epsilon\dot{\rho}+3bH\rho)$ and compare their results for the following three scenarios.

1. Emergent scenario [83], where the scale factor has the form $a(t) = b_0(b_3 + e^{b_4 t})^{b_5},\ b_0 > 0,\ b_3 > 0,\ b_4 > 0,\ b_5 > 1.$

2. Intermediate scenario [84], where $a(t) = e^{b_6 t^{b_7}}$ with $b_6 > 0,\ 0 < b_7 < 1.$

3. Logamediate scenario [85], where $a(t) = e^{b_8(\ln t)^{b_9}}$ with $b_8 > 0,\ b_9 > 1.$

The sum of Eqs.(5.1.14) and (5.1.15) gives

$$\dot{\rho}^{tot} + 3H(1+\omega^{tot})\rho^{tot} = 0,$$

which shows that for $\omega^{tot} > -1,\ \rho^{tot}$ is decreasing and for $\omega^{tot} < -1,\ \rho^{tot}$ is increasing. For graphical analysis, the parameters in all cases are fixed such that

1. ρ^{tot} and ω^{tot} satisfy the above relation,

2. p^{tot} remains negative,

3. c_{14} is taken negative such that bulk viscosity becomes positive because large positive value of bulk viscosity can produce negative pressure [86].

4. The values of $\tilde{b}_1 = \frac{b_1+1}{2}$ and $\tilde{b}_2 = \frac{b_2}{2}$ are chosen such that the corresponding values of b_1 and b_2 remain positive.

5. The value of b is taken negative to have an energy flow from MCG to dark energy [79].

5.1.1 Interaction $\tilde{Q} = 3Hb\rho$

We replace $\tilde{Q} = 3Hb\rho$ and Eq.(5.1.12) in (5.1.15), it follows that

$$\dot{\rho} + 3H(\rho D - \frac{\tilde{b}_2}{\rho^\delta}) = 0; \quad D = 1 + \tilde{b}_1 - b. \tag{5.1.16}$$

For the emergent universe, the Hubble parameter becomes

$$H = \frac{b_5 b_4 e^{b_4 t}}{(b_3 + e^{b_4 t})}, \tag{5.1.17}$$

and Eq.(5.1.16) gives the solution

$$\rho = \left[\frac{\tilde{b}_2 - e^{D(1+\delta)c_{15}}(b_3 + e^{b_4 t})^{-3Db_5(1+\delta)}}{D}\right]^{\frac{1}{1+\delta}}, \tag{5.1.18}$$

where c_{15} is the constant of integration. Equation (5.1.12) then leads to

$$\begin{aligned} p &= \tilde{b}_1 \left[\frac{\tilde{b}_2 - e^{D(1+\delta)c_{15}}(b_3 + e^{b_4 t})^{-3Db_5(1+\delta)}}{D}\right]^{\frac{1}{1+\delta}} \\ &- \tilde{b}_2 \left[\frac{\tilde{b}_2 - e^{D(1+\delta)c_{15}}(b_3 + e^{b_4 t})^{-3Db_5(1+\delta)}}{D}\right]^{\frac{-\delta}{1+\delta}}. \end{aligned} \tag{5.1.19}$$

Inserting these values in Eqs.(5.1.7) and (5.1.8), we obtain energy density and pressure of dark energy. Consequently, Eq.(5.1.6) gives the values of total energy density and pressure. The total EoS parameter is obtained as

$$\omega^{tot} = \frac{p^{tot}}{\rho^{tot}}. \tag{5.1.20}$$

Equation (5.1.13) yields

$$\xi = \frac{-c_{14}(b_3 + e^{b_4 t})}{3b_5 b_4 e^{b_4 t}}. \tag{5.1.21}$$

The graphs of ρ^{tot}, p^{tot} and ω^{tot} for the emergent universe with first interaction model are shown in Figure **5.1**. We see that the total density decreases while the total pressure increases with time. In all cases, the value of model parameter λ cannot be negative as it leads to negative values of ρ^{tot} which is not physical. The effect of model parameter λ on ρ^{tot}, p^{tot} and ω^{tot} is observed. The first graph shows that ρ^{tot} increases, second indicates a decrease in p^{tot} and third graph depicts that the model has a tendency towards quintessence era with the increase in model parameter. We find that large λ increases ρ^{tot} and decreases p^{tot} but ω^{tot} does not cross the phantom divide line and always lies in matter dominated or quintessence era. Figure **5.2** indicates that the behavior of bulk viscosity with respect to time is decreasing while it decreases with the increase in c_{14}.

For the intermediate scenario, the Hubble parameter is $H = b_6 b_7 t^{b_7 - 1}$ for which Eq.(5.1.16) yields

$$\rho = \left[\frac{\tilde{b}_2 - e^{(-3b_6 t^{b_7} + c_{16})D(1+\delta)}}{D}\right]^{\frac{1}{1+\delta}}, \tag{5.1.22}$$

where c_{16} is another integration constant and Eq.(5.1.13) gives

$$\xi = \frac{-c_{14}}{3b_6 b_7 t^{b_7 - 1}}. \tag{5.1.23}$$

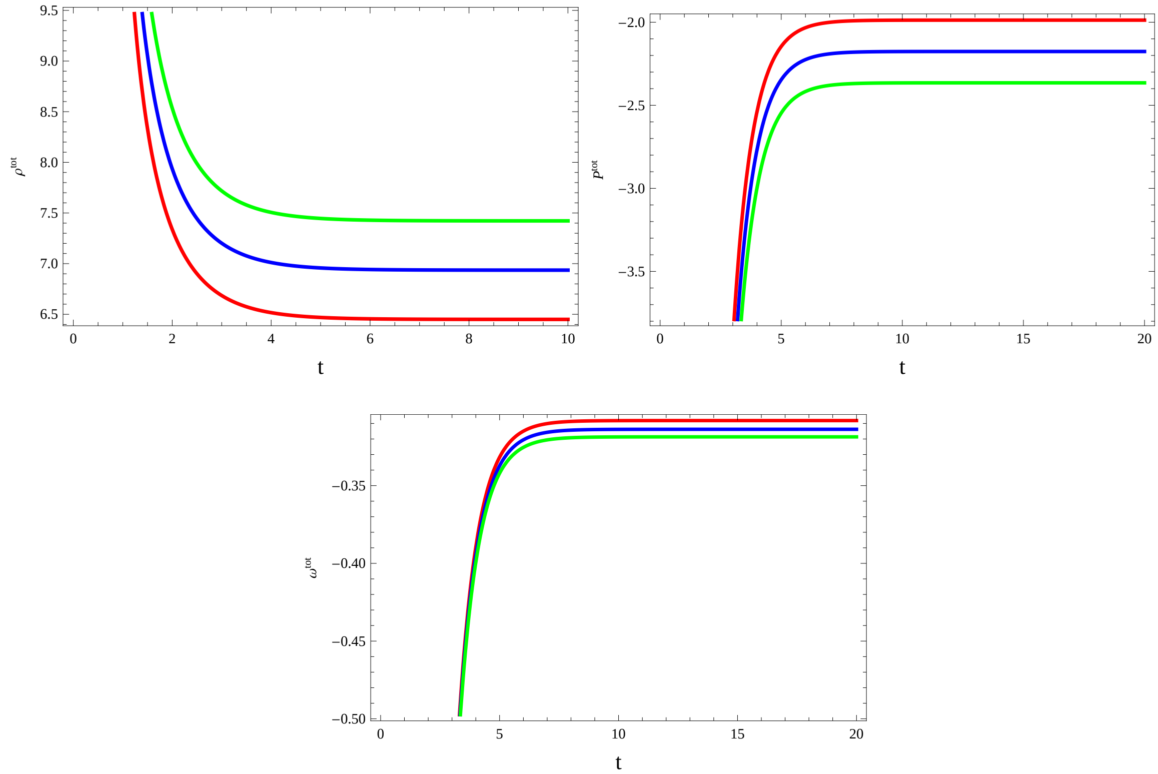

Figure 5.1: Plots of ρ^{tot}, p^{tot} and ω^{tot} versus time in emergent universe for $\tilde{Q} = 3Hb\rho$, $\tilde{b}_1 = 3,\ \tilde{b}_2 = 10,\ \delta = 0.5,\ b = -1,\ b_3 = 0.1,\ b_4 = 0.03,\ b_5 = 15,\ c_{14} = -0.1,\ c_{15} = 1,$ $\lambda = 1$ (red), $\lambda = 1.1$ (blue) and $\lambda = 1.2$ (green).

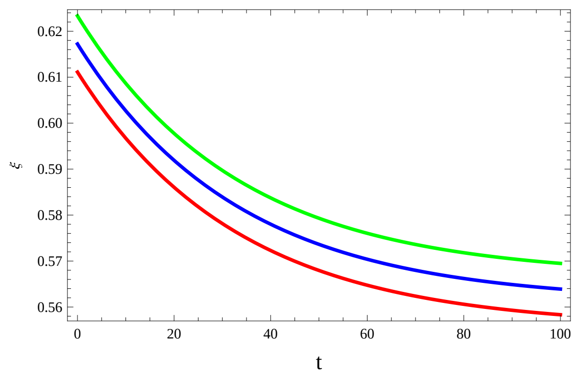

Figure 5.2: Plot of ξ versus time in emergent universe for $\tilde{Q} = 3Hb\rho$, $\tilde{b}_1 = 3,\ \tilde{b}_2 = 10,\ \delta = 0.5,\ b = -1,\ b_3 = 0.1,\ b_4 = 0.03,\ b_5 = 15,\ \lambda = 1,\ c_{15} = 1,$ $c_{14} = -0.1$ (red), $c_{14} = -0.101$ (blue) and $c_{14} = -0.102$ (green).

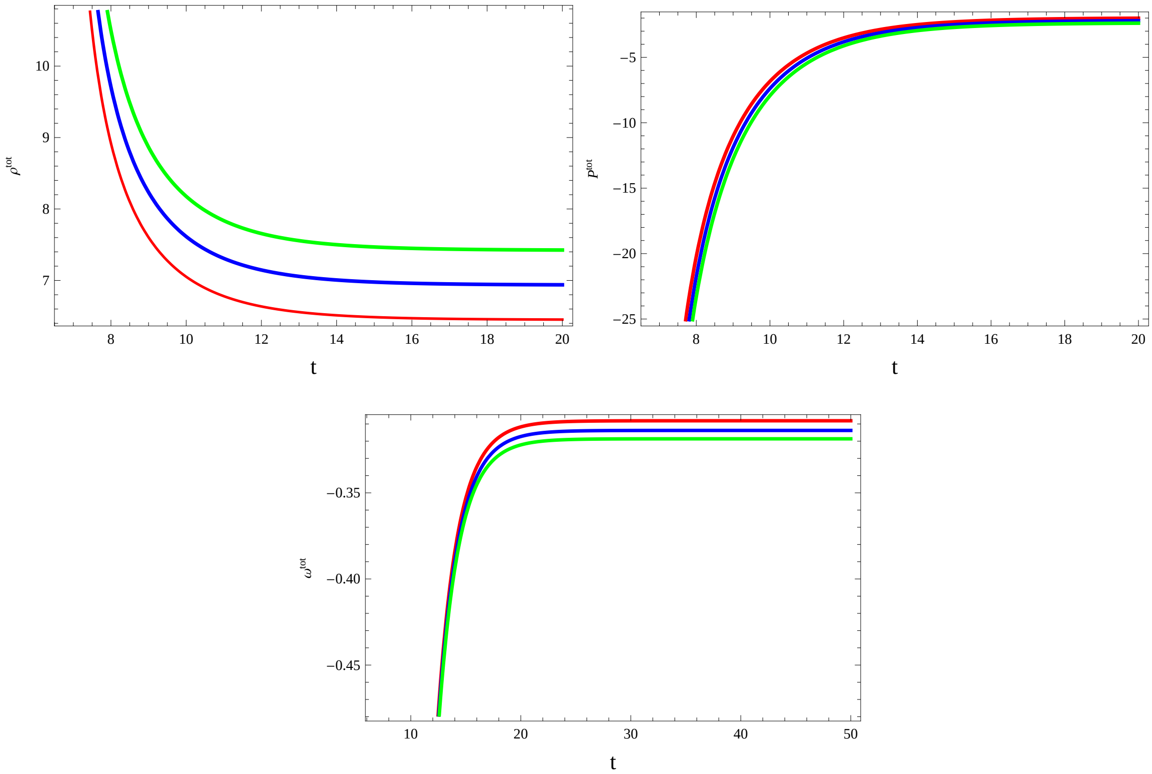

Figure 5.3: Plots of ρ^{tot}, p^{tot}, ω^{tot} and ξ versus time in intermediate universe for $\tilde{Q} = 3Hb\rho$, $\tilde{b}_1 = 3$, $\tilde{b}_2 = 10$, $\delta = 0.5$, $b = -1$, $b_6 = 0.05$, $b_7 = 0.8$, $c_{14} = -0.1$ $c_{16} = 1$, $\lambda = 1$ (red), $\lambda = 1.1$ (blue) and $\lambda = 1.2$ (green).

Following the same procedure as above, we obtain the values of total energy density, pressure and EoS parameter. The graphical behavior is shown in Figure **5.3**. The effect of model parameter remains the same as in emergent while the behavior of ξ observed from Figure **5.4** with respect to time is opposite. It increases with increase in time and decrease in c_{14}.

The Hubble parameter, bulk viscosity and solution of Eq.(5.1.16) for the logamediate universe are given by

$$H = \frac{b_8 b_9 (\ln t)^{b_9 - 1}}{t}, \tag{5.1.24}$$

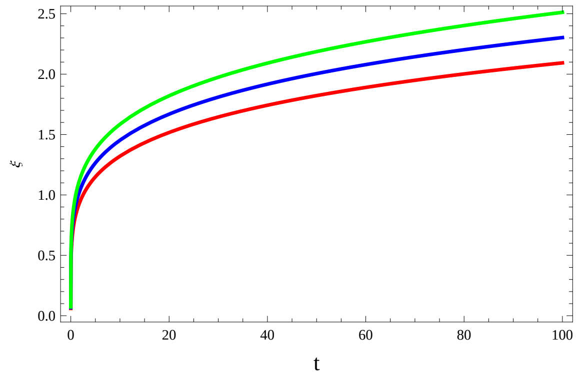

Figure 5.4: Plots of ρ^{tot}, p^{tot}, ω^{tot} and ξ versus time in intermediate universe for $\tilde{Q} = 3Hb\rho$, $\tilde{b}_1 = 3$, $\tilde{b}_2 = 10$, $\delta = 0.5$, $b = -1$, $b_6 = 0.05$, $b_7 = 0.8$, $c_{16} = 1$, $c_{14} = -0.1$ (red), $c_{14} = -0.11$ (blue) and $c_{14} = -0.12$ (green).

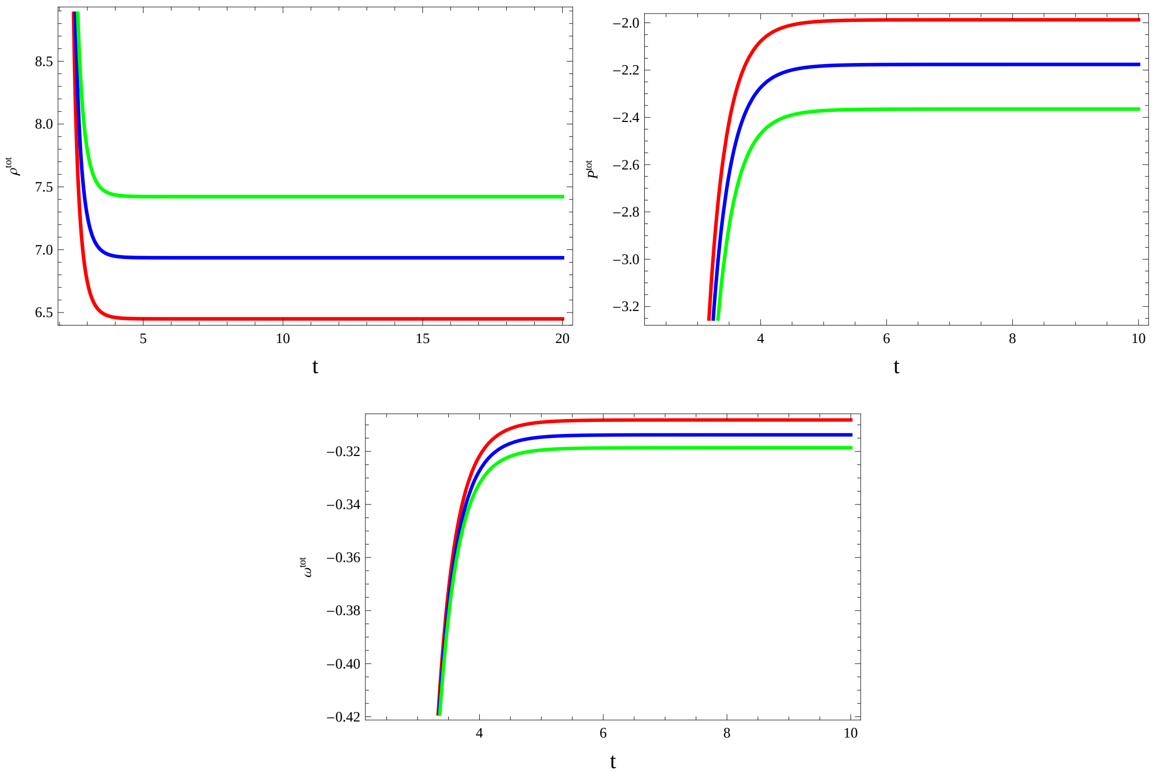

Figure 5.5: Plots of ρ^{tot}, p^{tot} and ω^{tot} versus time in logamediate universe for $\tilde{Q} = 3Hb\rho$, $\tilde{b}_1 = 3$, $\tilde{b}_2 = 10$, $\delta = 0.5$, $b = -1$, $b_8 = 0.3$, $b_9 = 1.5$, $c_{14} = -0.1$ $c_{17} = 1$ $\lambda = 1$ (red), $\lambda = 1.1$ (blue) and $\lambda = 1.2$ (green).

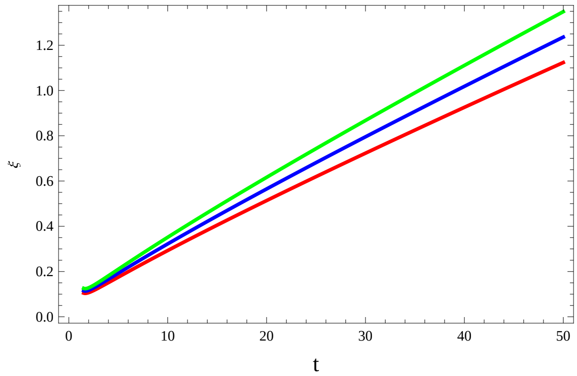

Figure 5.6: Plot of ξ versus time in logamediate universe for $\tilde{Q} = 3Hb\rho$,$\tilde{b}_1 = 3,\ \tilde{b}_2 = 10,\ \delta = 0.5,\ b = -1,\ b_8 = 0.3,\ b_9 = 1.5,\ c_{17} = 1\ c_{14} = -0.1$ (red), $c_{14} = -0.11$ (blue) and $c_{14} = -0.12$ (green).

$$\xi = \frac{-c_{14}t}{3b_8b_9(\ln t)^{b_9-1}} \tag{5.1.25}$$

$$\rho = \left[\frac{\tilde{b}_2 - e^{D(1+\delta)(c_{17}-3b_8(\ln t)^{b_9})}}{D}\right]^{\frac{1}{1+\delta}}, \tag{5.1.26}$$

where c_{17} is the integration constant. In this case, Figure **5.5** indicates the same effect of model parameter as in the previous cases and from Figure **5.6**, it is observed that the behavior of bulk viscosity is increasing with time as in intermediate case but with a rapid rate.

5.1.2 Interaction $\tilde{Q} = \tilde{q}(\epsilon\dot{\rho} + 3bH\rho)$

In this case, we use Eq.(5.1.12) in (5.1.15) and obtain

$$(1 - \tilde{q}\epsilon)\dot{\rho} + 3H(D\rho - \frac{\tilde{b}_2}{\rho^\delta}) = 0. \tag{5.1.27}$$

We evaluate the following solutions of Eq.(5.1.27) for the emergent as well as intermediate universe, respectively

$$\rho=\left[\frac{\tilde{b}_2-e^{\frac{-3De^{b_4t}b_5(1+\delta)}{1+\epsilon}+\frac{3(1+\delta)D\sqrt{b_3b_5\epsilon}\arctan(\frac{e^{b_4t}\sqrt{b_5(1+\epsilon)}}{\sqrt{b_3\epsilon}})}{(1+\epsilon)^{\frac{3}{2}}}+(1+\delta)Dc_{18}}}{D}\right]^{\frac{1}{1+\delta}}, \quad (5.1.28)$$

$$\rho=\left[\frac{\tilde{b}_2-e^{\frac{D(1+\delta)}{b_7(1+\epsilon)^2}(\gamma c_{19}(1+\epsilon)^2-3b_7b_6t^{b_7}(1+\epsilon)+3\epsilon\ln(-(1+b_7)\epsilon+t^{b_7}b_7b_6(1+\epsilon))(b_7-1))}}{D}\right]^{\frac{1}{1+\delta}}, \quad (5.1.29)$$

where c_{18} and c_{19} are constants of integration. For the logamediate scenario, Eq.(5.1.27) gives complicated solution, so we solve it numerically. For this interaction model, the graphical behavior for all cases is shown in Figures **5.7-5.12**. The behavior of ρ^{tot}, p^{tot}, ω^{tot} as well as effect of model parameter λ is similar to the first interaction model for emergent and intermediate scenarios. The behavior of pressure and EoS parameter for logamediate scenario is reversed in this model. Moreover, bulk viscosity also has the same behavior.

5.2 Viscosity Effects on Anisotropic Universe

The LRS Bianchi type-I universe model is taken as

$$ds^2=-dt^2+a_1^2(t)dx^2+a_2^2(t)(dy^2+dz^2). \quad (5.2.1)$$

We assume that shear and expansion scalars are proportional to each other ($\sigma\propto\vartheta$) which gives $a_1=a_2^{\tilde{m}}$ (where $\tilde{m}\neq 0$ is a constant). The mean Hubble parameter then becomes

$$H=\frac{1}{3}\left(\frac{\tilde{m}+2}{\tilde{m}}\right)\frac{\dot{a}_1}{a_1}. \quad (5.2.2)$$

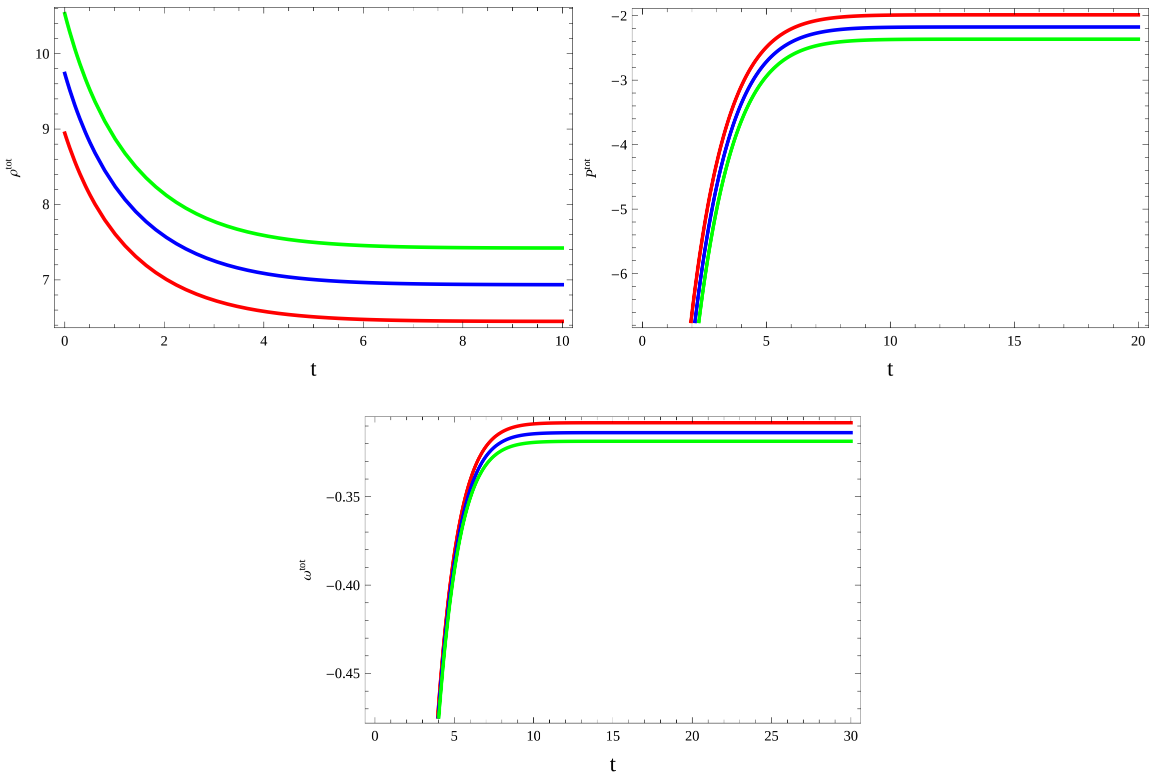

Figure 5.7: Plots of ρ^{tot}, p^{tot} and ω^{tot}versus time in emergent universe for $\tilde{Q} = \tilde{q}(\epsilon\dot{\rho} + 3bH\rho)$ $\tilde{b}_1 = 3,\ \tilde{b}_2 = 10,\ \delta = 0.5,\ b = -1,\ b_3 = 1,\ b_4 = 0.05,\ b_5 = 2,\ \epsilon = 2,\ c_{14} = -0.1,\ c_{18} = 1, \lambda = 1$ (red), $\lambda = 1.1$ (blue) and $\lambda = 1.2$ (green).

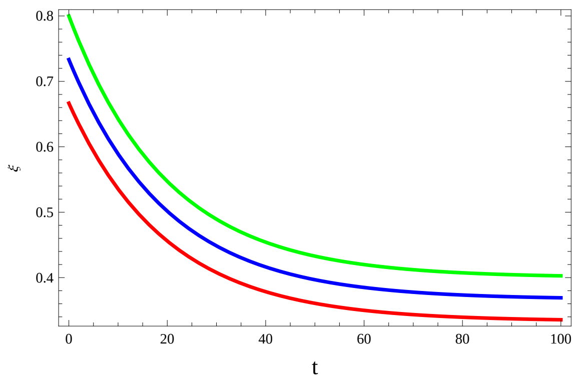

Figure 5.8: Plot of ξ versus time in emergent universe for $\tilde{Q} = \tilde{q}(\epsilon\dot{\rho} + 3bH\rho)$, $\tilde{b}_1 = 3,\ \tilde{b}_2 = 10,\ \delta = 0.5,\ b = -1,\ b_3 = 1,\ b_4 = 0.05,\ b_5 = 2,\ \epsilon = 2,\ c_{18} = 1, c_{14} = -0.1$ (red), $c_{14} = -0.11$ (blue), and $c_{14} = -0.12$ (green).

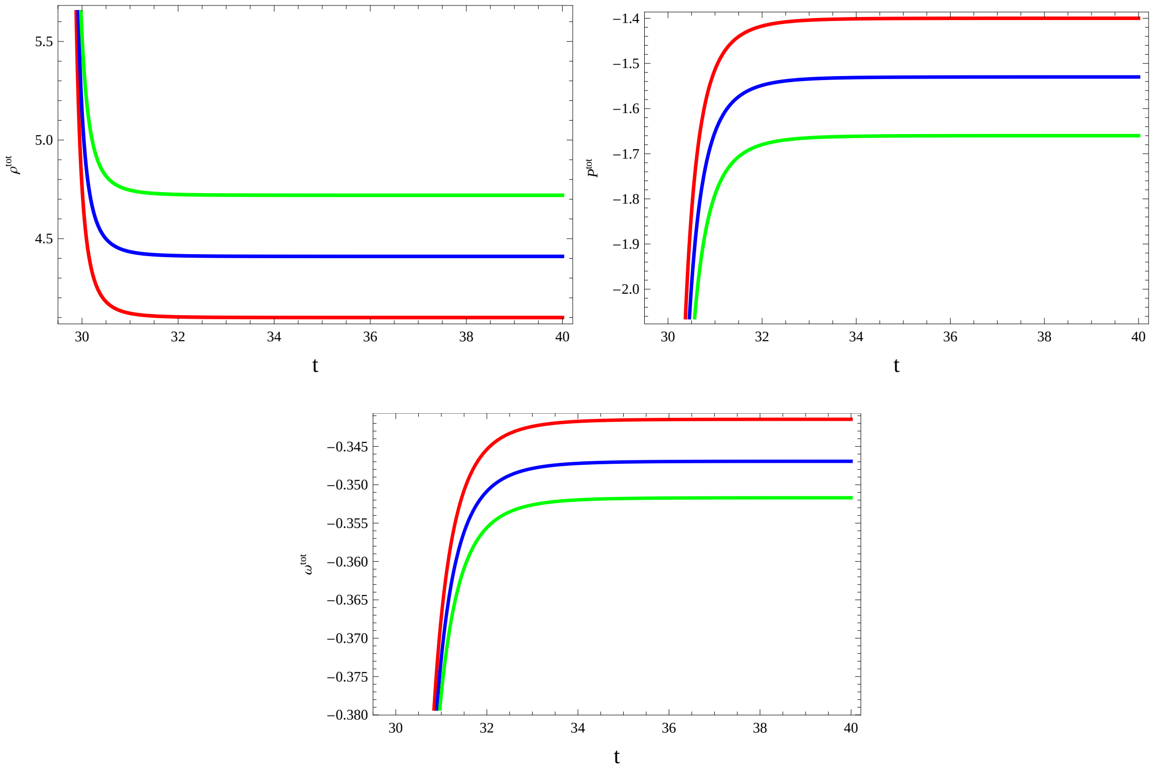

Figure 5.9: Plots of ρ^{tot}, p^{tot} and ω^{tot} versus time in intermediate universe for $\tilde{Q} = \tilde{q}(\epsilon\dot{\rho} + 3bH\rho)$, $\tilde{b}_1 = 8,\ \tilde{b}_2 = 10,\ \delta = 0.5,\ b = -1,\ b_6 = 0.1,\ b_7 = 0.8,\ \epsilon = 2,\ c_{14} = -0.1\ c_{19} = 1$, $\lambda = 1$ (red), $\lambda = 1.1$ (blue) and $\lambda = 1.2$ (green).

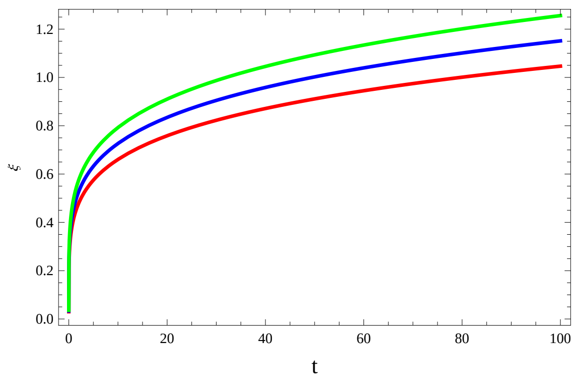

Figure 5.10: Plot of ξ versus time in intermediate universe for $\tilde{Q} = \tilde{q}(\epsilon\dot{\rho} + 3bH\rho)$, $\tilde{b}_1 = 8,\ \tilde{b}_2 = 10,\ \delta = 0.5,\ b = -1,\ b_6 = 0.1,\ b_7 = 0.8,\ \epsilon = 2,\ c_{19} = 1$, $c_{14} = -0.1$ (red), $c_{14} = -0.11$ (blue), and $c_{14} = -0.12$ (green).

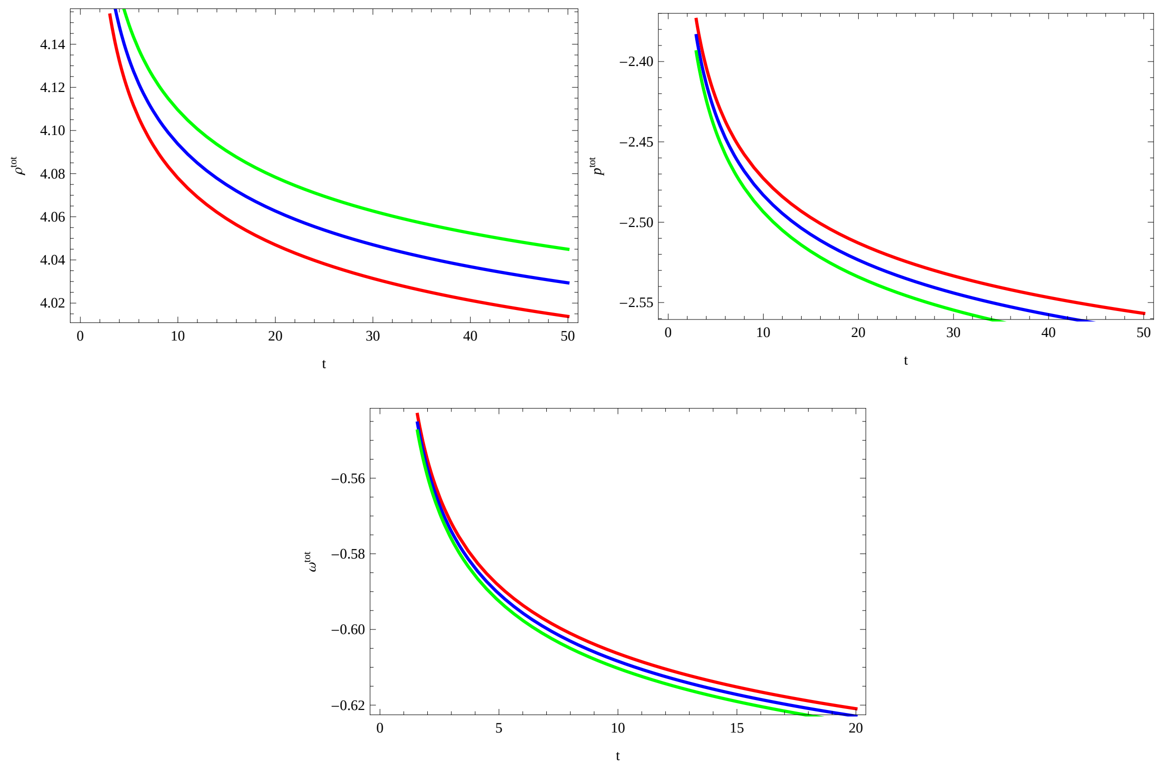

Figure 5.11: Plots of ρ^{tot}, p^{tot} and ω^{tot} versus time in logamediate universe for $\tilde{Q} = \tilde{q}(\epsilon\dot{\rho}+3bH\rho)$, $\tilde{b}_1 = 0.6,\ \tilde{b}_2 = 1,\ \delta = 0.5,\ b = -1,\ b_8 = 0.5,\ b_9 = 1.5,\ \epsilon = 2,\ c_{14} = -0.1$, $\lambda = 1$ (red), $\lambda = 1.005$ (blue) and $\lambda = 1.01$ (green).

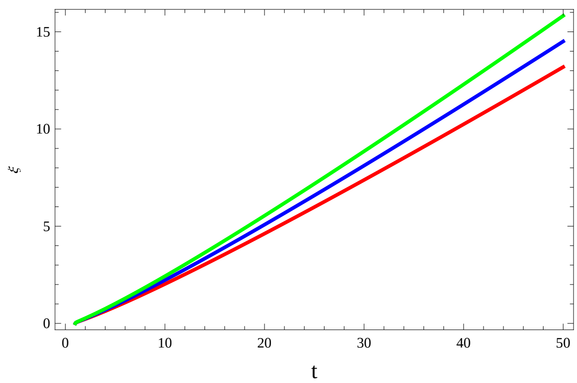

Figure 5.12: Plot of ξ versus time in logamediate universe for $\tilde{Q} = \tilde{q}(\epsilon\dot{\rho} + 3bH\rho)$, $\tilde{b}_1 = 0.6,\ \tilde{b}_2 = 1,\ \delta = 0.5,\ b = -1,\ b_8 = 0.5,\ b_9 = 1.5,\ \epsilon = 2,\ c_{10} = -0.1, c_{14} = -0.1$ (red), $c_{14} = -0.11$ (blue), and $c_{14} = -0.12$ (green).

The energy-momentum tensor of viscous fluid is given in Eq.(5.1.2). The field equations for the metric (5.2.1) are

$$\frac{9(2\tilde{m}+1)}{(\tilde{m}+2)^2}H^2 = (1+3\lambda)\rho - \lambda(p-3\xi H), \tag{5.2.3}$$

$$\frac{-6\dot{H}}{(\tilde{m}+2)} - \frac{9(2\tilde{m}+1)(H)^2}{(\tilde{m}+2)^2} = (1+3\lambda)(p-3\xi H) - \lambda\rho, \tag{5.2.4}$$

$$-(1+\frac{1}{\tilde{m}})\frac{3\tilde{m}\dot{H}}{(\tilde{m}+2)} - (1+\frac{2}{\tilde{m}})\frac{9\tilde{m}^2H^2}{(\tilde{m}+2)^2} = (1+3\lambda)(p-3\xi H) - \lambda\rho. \tag{5.2.5}$$

The anisotropy parameter is given by

$$\mathcal{A}_p = \frac{1}{3}\sum_{i=1}^{3}\left(\frac{\triangle H_i}{H}\right)^2; \quad \triangle H_i = H - H_i, \tag{5.2.6}$$

where H_i represent directional Hubble parameters. We evaluate $\mathcal{A}_p$ as

$$\mathcal{A}_p = \frac{2(\tilde{m}-1)^2}{(\tilde{m}+2)^2}. \tag{5.2.7}$$

The relation between $\tilde{m}$ and $\mathcal{A}_p$ is given in Table **9**.

Table **9**: Relation of $\tilde{m}$ and $\mathcal{A}_p$

Range for $\tilde{m}$	**Behavior of** $\mathcal{A}_p$
$-\infty < \tilde{m} < -2$	increasing
$-2 < \tilde{m} \leq 1$	decreasing
$1 \leq \tilde{m} < \infty$	increasing

The first two field equations produce the differential equation in H

$$\frac{6\dot{H}}{(\tilde{m}+2)} + (\rho+p)(1+2\lambda) - 3\xi H(1+2\lambda) = 0. \tag{5.2.8}$$

To solve this equation for H, we consider the following EoS

$$p = (\gamma-1)\rho; \quad 0 \leq \gamma \leq 2, \tag{5.2.9}$$

and an expression for bulk viscosity of the form [87]

$$\xi = \xi_0 + \xi_1 H, \tag{5.2.10}$$

where ξ_0 and ξ_1 are constants. The matter density is evaluated using Eqs.(5.2.9) and (5.2.10) in (5.2.3) as

$$\rho = \frac{3H}{(1+4\lambda-\gamma\lambda)}\left[\left(\frac{3(2\tilde{m}+1)}{(\tilde{m}+2)^2}-\lambda\xi_1\right)H-\lambda\xi_0\right]. \tag{5.2.11}$$

In the following, we consider four different viscosity models and evaluate the expressions for $H,\ a_1,\ a_2,\ \rho$ and $\tilde{q}$.

5.2.1 Fluid With Zero Viscosity ($\xi = 0$)

For a non-viscous fluid, Eq.(5.2.8) becomes

$$2(\tilde{m}+2)\dot{H}+\frac{3\gamma(1+2\lambda)(2\tilde{m}+1)}{(1+4\lambda-\gamma\lambda)}H^2=0, \tag{5.2.12}$$

where we have used Eqs.(5.2.10) and (5.2.11). The solution of this equation for $\gamma \neq 0$ is given by

$$H = \frac{1}{c_{20}+\frac{3}{2}\frac{\gamma(1+2\lambda)(1+2\tilde{m})t}{(\tilde{m}+2)(1+4\lambda-\gamma\lambda)}}, \tag{5.2.13}$$

where c_{20} is a constant of integration. The Hubble parameter yields

$$a_1 = \left(c_{21}\left[c_{20}+\frac{3}{2}\frac{\gamma(1+2\lambda)(1+2\tilde{m})t}{(\tilde{m}+2)(1+4\lambda-\gamma\lambda)}\right]^{\frac{2(\tilde{m}+2)(1+4\lambda-\gamma\lambda)}{3\gamma(1+2\lambda)(1+2\tilde{m})}}\right)^{\frac{3\tilde{m}}{\tilde{m}+2}}, \tag{5.2.14}$$

here c_{21} is another integration constant. This represents a power-law type solution of the scale factor. The scale factor a_2 can be found using $a_1 = a_2^{\tilde{m}} \Rightarrow a_2 = a_1^{\frac{1}{\tilde{m}}}$. The deceleration parameter is obtained as

$$\tilde{q} = -1-\frac{\dot{H}}{H^2} = -1+\frac{3}{2}\frac{\gamma(1+2\lambda)(1+2\tilde{m})}{(\tilde{m}+2)(1+4\lambda-\gamma\lambda)}. \tag{5.2.15}$$

which is time independent and its value varies with γ, λ and $\tilde{m}$.

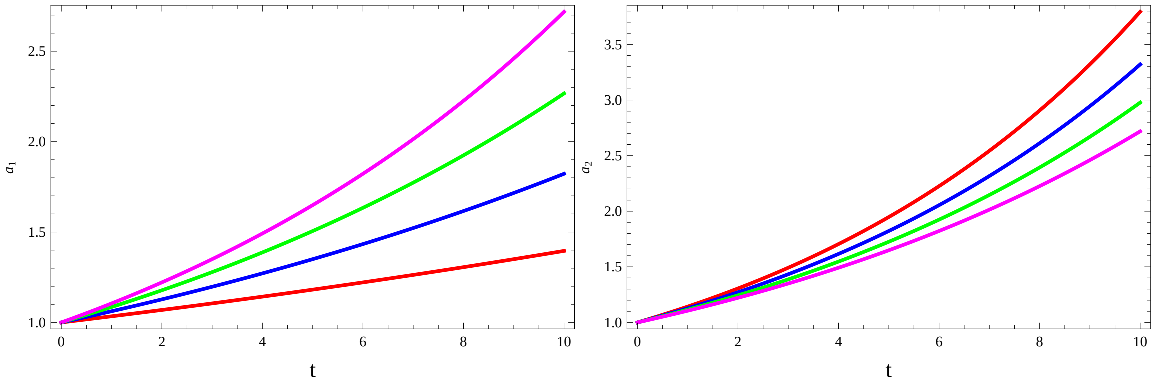

Figure 5.13: Plots of a_1 and a_2 versus t for $\xi = 0$ and fixing $\tilde{c}_{20} = 0.1,\ \tilde{c}_{21} = 1,\ \tilde{m} = 0.25$ (red), $\tilde{m} = 0.5$ (blue), $\tilde{m} = 0.75$ (green) and $\tilde{m} = 1$ (purple).

For different values of γ, we have different evolutionary eras. Here, we present a discussion for the dark energy dominated era corresponding to $\gamma = 0$. Solving Eq.(5.2.12) for $\gamma = 0$, we have

$$H = \tilde{c}_{20}, \quad \tilde{q} = -1, \quad a_1 = (\tilde{c}_{21} e^{\tilde{c}_{20} t})^{\frac{3\tilde{m}}{\tilde{m}+2}}, \quad a_2 = (\tilde{c}_{21} e^{\tilde{c}_{20} t})^{\frac{3}{\tilde{m}+2}}, \tag{5.2.16}$$

$\tilde{c}_{20} > 0$ and $\tilde{c}_{21} > 0$ are constants of integration. The scale factors are of exponential form. For $\tilde{m} = 1$, the above values correspond to the de Sitter universe. The plots for a_1 and a_2 in Eq.(5.2.16) are given in Figure **5.13**. The behavior of both graphs is increasing with time while anisotropy has opposite effects (it increases a_1 and decreases a_2). Equation (5.2.11) yields the expression for density as

$$\rho = \frac{9(2\tilde{m} + 1)\tilde{c}_{20}^2}{(\tilde{m} + 2)^2(1 + 4\lambda)}. \tag{5.2.17}$$

There is a big-rip singularity when $\rho \rightarrow \infty$, i.e., for a non-viscous fluid, a big-rip is expected only if $\tilde{m} = -2$ or $\lambda = -\frac{1}{4}$. For $\tilde{m} = -2$, the anisotropy parameter $\mathcal{A}_p$ defined in (5.2.7) also approaches to infinity.

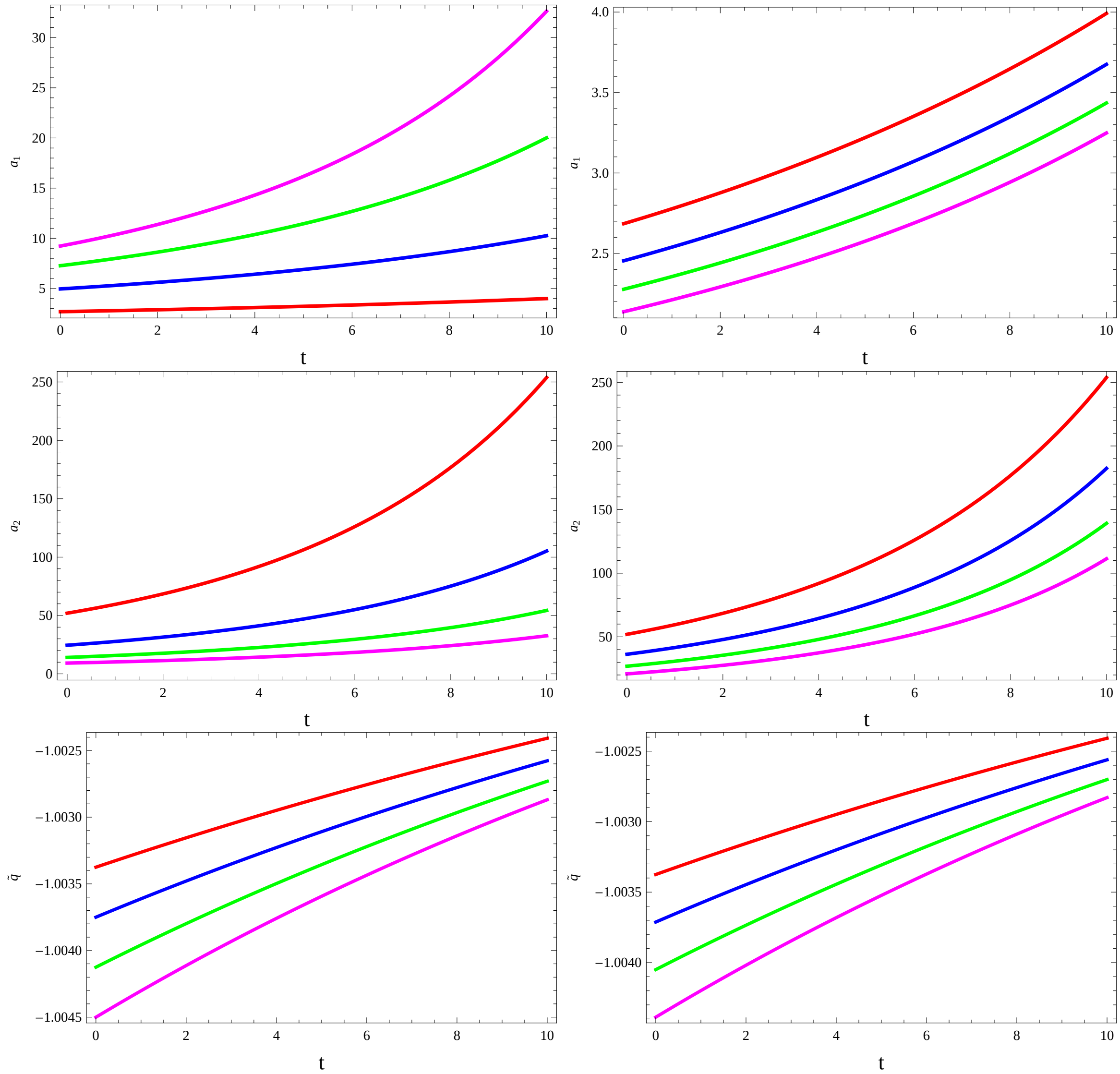

Figure 5.14: Plots of a_1, a_2 and $\tilde{q}$ versus t for $\xi = \xi_0$ and fixing $\lambda = 1,\ \tilde{c}_{22} = 0.1,\ \tilde{c}_{23} = 1,\ \xi_0 = 0.01,\ \tilde{m} = 0.25$ (red), $\tilde{m} = 0.5$ (blue), $\tilde{m} = 0.75$ (green) and $\tilde{m} = 1$ (purple) in the left panel and fixing $\tilde{m} = 0.25,\ \xi_0 = 0.01$ (red), $\xi_0 = 0.011$ (blue), $\xi_0 = 0.012$ (green) and $\xi_0 = 0.013$ (purple) in the right panel.

5.2.2 Fluid With Constant Viscosity ($\xi = \xi_0$)

In this case, for $\gamma \neq 0$ Eq.(5.2.8) yields the solution

$$H = \frac{\left(\frac{\xi_0(1+2\lambda)(1+4\lambda)(\tilde{m}+2)}{2(1+4\lambda-\gamma\lambda)}\right) e^{\frac{\xi_0(1+2\lambda)(1+4\lambda)(\tilde{m}+2)}{2(1+4\lambda-\gamma\lambda)}(t+c_{22})}}{1+\left(\frac{3\gamma(1+2\lambda)(1+2\tilde{m})}{2(\tilde{m}+2)(1+4\lambda-\gamma\lambda)}\right) e^{\frac{\xi_0(1+2\lambda)(1+4\lambda)(\tilde{m}+2)}{2(1+4\lambda-\gamma\lambda)}(t+c_{22})}}, \tag{5.2.18}$$

where c_{22} is an integration constant. Using the above equation, $\tilde{q}$ and a_1 become

$$\tilde{q} = -1 - e^{\frac{-\xi_0(1+2\lambda)(1+4\lambda)(\tilde{m}+2)}{2(1+4\lambda-\gamma\lambda)}(t+c_{22})}, \tag{5.2.19}$$

$$a_1 = \left[c_{23}\left(1+\frac{3\gamma(1+2\lambda)(1+2\tilde{m})}{2(\tilde{m}+2)(1+4\lambda-\gamma\lambda)} \times e^{\frac{\xi_0(1+2\lambda)(1+4\lambda)(\tilde{m}+2)(t+c_{22})}{2(1+4\lambda-\gamma\lambda)}}\right)^{\frac{2(\tilde{m}+2)(1+4\lambda-\gamma\lambda)}{3\gamma(1+2\lambda)(1+2\tilde{m})}}\right]^{\frac{3\tilde{m}}{\tilde{m}+2}}, \tag{5.2.20}$$

where c_{23} is another integration constant. The scale factors become exponential type. For $\gamma = 0$, we have

$$H = \tilde{c}_{22} e^{\frac{\xi_0(1+2\lambda)(\tilde{m}+2)t}{2}}, \tag{5.2.21}$$

$$\tilde{q} = -1 - \frac{\xi_0(1+2\lambda)(\tilde{m}+2)\tilde{c}_{22}}{2e^{\frac{\xi_0(1+2\lambda)(\tilde{m}+2)t}{2}}}, \tag{5.2.22}$$

$$a_1 = \left(\tilde{c}_{23} e^{\frac{2\tilde{c}_{22}}{\xi_0(1+2\lambda)(\tilde{m}+2)} e^{\frac{\xi_0(1+2\lambda)(\tilde{m}+2)t}{2}}}\right)^{\frac{3\tilde{m}}{\tilde{m}+2}}, \tag{5.2.23}$$

here $\tilde{c}_{22}$ and $\tilde{c}_{23}$ are positive constants of integration. The graphical behavior of $\tilde{q}$, a_1 and a_2 are shown in Figure **5.14**. The decrease in anisotropy has the same effects as for zero viscosity fluid while increase in bulk viscosity shows decrease in both a_1 and a_2. The deceleration parameter is negative and does not cross the line $\tilde{q} = -1$. The decrease in $\tilde{m}$ as well as increase in ξ_0 decreases the value of $\tilde{q}$. For a constant viscous fluid, the matter density in dark energy dominated era is obtained as

$$\rho = \frac{3\tilde{c}_{22} e^{\frac{\xi_0(1+2\lambda)(\tilde{m}+2)t}{2}}}{(1+4\lambda)}\left[\frac{3(2\tilde{m}+1)}{(\tilde{m}+2)^2}\tilde{c}_{22} e^{\frac{\xi_0(1+2\lambda)(\tilde{m}+2)t}{2}} - \lambda\xi_0\right]. \tag{5.2.24}$$

Again $\rho \rightarrow \infty$ or big-rip occurs when $\tilde{m} = -2$ or $\lambda = -\frac{1}{4}$. This also holds for the next two cases and we can obtain an expression of time for the big-rip occurrence there.

5.2.3 Fluid With Viscosity Proportional to H ($\xi = \xi_1 H$)

In this case, the solution of Eq.(5.2.8) for $0 \leq \gamma \leq 2$ is

$$H = \frac{1}{\frac{(1+2\lambda)(\tilde{m}+2)}{2(1+4\lambda-\gamma\lambda)}\left[\frac{3(2\tilde{m}+1)\gamma}{(\tilde{m}+2)^2} - \xi_1 - 4\lambda\xi_1\right]t + c_{24}}, \tag{5.2.25}$$

c_{24} represents constant of integration. Similarly, $\tilde{q}$ and a_1 can be obtained as

$$\tilde{q} = -1 + \frac{(1+2\lambda)(\tilde{m}+2)}{2(1+4\lambda-\gamma\lambda)}\left[\frac{3(2\tilde{m}+1)\gamma}{(\tilde{m}+2)^2} - \xi_1 - 4\lambda\xi_1\right], \tag{5.2.26}$$

$$\begin{aligned} a_1 &= \left[c_{25}\left(\frac{(1+2\lambda)(\tilde{m}+2)}{2(1+4\lambda-\gamma\lambda)}\left[\frac{3(2\tilde{m}+1)\gamma}{(\tilde{m}+2)^2} - \xi_1 - 4\lambda\xi_1\right]t\right.\right. \\ &+ \left.\left. c_{24}\right)^{\frac{2(1+4\lambda-\gamma\lambda)}{(1+2\lambda)(\tilde{m}+2)}\left[\frac{3(2\tilde{m}+1)\gamma}{(\tilde{m}+2)^2}-\xi_1-4\lambda\xi_1\right]}\right]^{\frac{3\tilde{m}}{\tilde{m}+2}}, \end{aligned} \tag{5.2.27}$$

c_{25} denotes another integration constant. We see that $\tilde{q}$ has a time independent expression as in the first case and a_1 is of power-law type. The scale factor a_2 is obtained in a similar manner. For $\gamma = 0$, the above expressions reduce to

$$H = \frac{1}{c_{24} - \frac{(1+2\lambda)(\tilde{m}+2)\xi_1 t}{2}}, \tag{5.2.28}$$

$$\tilde{q} = -1 - \frac{(1+2\lambda)(\tilde{m}+2)\xi_1}{2}, \tag{5.2.29}$$

$$a_1 = \left[c_{25}\left(c_{24} - \frac{(1+2\lambda)(\tilde{m}+2)\xi_1 t}{2}\right)^{\frac{-2}{(1+2\lambda)(\tilde{m}+2)\xi_1}}\right]^{\frac{3\tilde{m}}{\tilde{m}+2}}. \tag{5.2.30}$$

The value of $\tilde{q}$ depends on λ, $\tilde{m}$ as well as ξ_1 and remains less than -1 for positive values of all these constants. The plots of a_1 are shown in Figure **5.15**. Here, the decrease in $\tilde{m}$ and increase in ξ_1 yield an increase in a_1. We see that the effects of

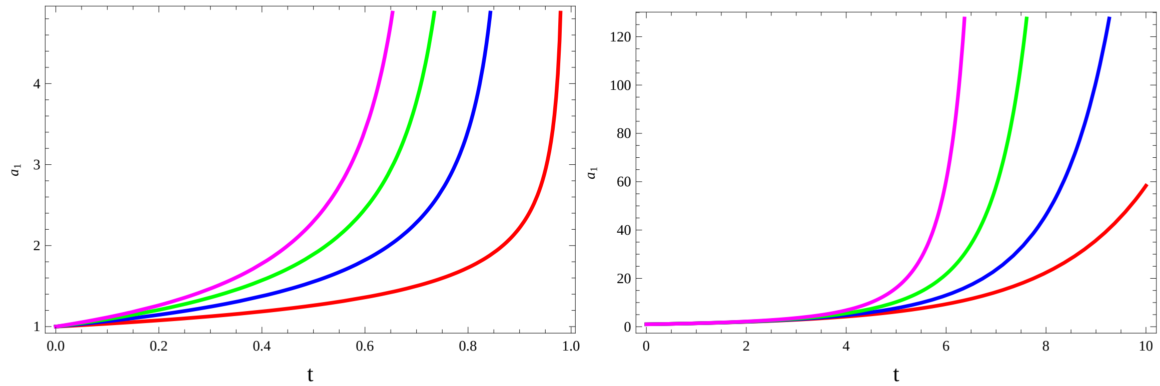

Figure 5.15: Plots of a_1 versus t for $\xi = \xi_1 H$ and fixing $\lambda = 1,\ c_{24} = 1,\ c_{25} = 1,\ \xi_1 = 0.01,\ \tilde{m} = 0.25$ (red), $\tilde{m} = 0.5$ (blue), $\tilde{m} = 0.75$ (green) and $\tilde{m} = 1$ (purple) in the left graph and fixing $\tilde{m} = 0.25,\ \xi_1 = 0.01$ (red), $\xi_1 = 0.012$ (blue), $\xi_1 = 0.014$ (green) and $\xi_1 = 0.016$ (purple) in the right graph.

viscosity are same on both a_1 and a_2 while anisotropy has opposite effects on both. So, we only show the graphs of a_1 in this case as well as in next one. For this viscosity model and $\gamma = 0$, ρ becomes

$$\rho = \frac{1}{1+4\lambda}\left[\frac{9(2\tilde{m}+1)}{(\tilde{m}+2)^2} - 3\lambda\xi_1\right]\frac{1}{\left(c_{24} - \frac{(1+2\lambda)(\tilde{m}+2)\xi_1 t}{2}\right)^2}. \tag{5.2.31}$$

In this case, there is an additional term as compared to the previous cases whose zero value makes density infinite i.e.,

$$\left(c_{24} - \frac{(1+2\lambda)(\tilde{m}+2)\xi_1 t}{2}\right)^2 = 0,$$

giving the time of big-rip occurrence

$$t_{br} = \frac{2c_{24}}{(\tilde{m}+2)(1+2\lambda)\xi_1}.$$

5.2.4 Fluid With Viscosity of the Form $\xi = \xi_0 + \xi_1 H$

For this viscosity model and $0 \leq \gamma \leq 2$, Eq.(5.2.8) has the following solution

$$H = \frac{\frac{\xi_0(1+2\lambda)(1+4\lambda)(\tilde{m}+2)}{2(1+4\lambda-\gamma\lambda)} e^{\frac{\xi_0(1+2\lambda)(1+4\lambda)(\tilde{m}+2)(t+c_{26})}{2(1+4\lambda-\gamma\lambda)}}}{1+\frac{(1+2\lambda)(\tilde{m}+2)\left(\frac{3(2\tilde{m}+1)\gamma}{(\tilde{m}+2)^2}-\xi_1-4\lambda\xi_1\right)}{2(1+4\lambda-\gamma\lambda)} e^{\frac{\xi_0(1+2\lambda)(1+4\lambda)(\tilde{m}+2)(t+c_{26})}{2(1+4\lambda-\gamma\lambda)}}}, \tag{5.2.32}$$

leading the expressions of $\tilde{q}$ and a_1 to

$$\tilde{q} = -1 - e^{\frac{-\xi_0(1+2\lambda)(1+4\lambda)(\tilde{m}+2)(t+c_{26})}{2(1+4\lambda-\gamma\lambda)}}, \tag{5.2.33}$$

$$a_1 = \left[c_{27}\left(1+\frac{(1+2\lambda)(\tilde{m}+2)\left(\frac{3(2\tilde{m}+1)\gamma}{(\tilde{m}+2)^2}-\xi_1-4\lambda\xi_1\right)}{2(1+4\lambda-\gamma\lambda)} \times e^{\frac{\xi_0(1+2\lambda)(1+4\lambda)(\tilde{m}+2)(t+c_{26})}{2(1+4\lambda-\gamma\lambda)}}\right)^{\frac{2(1+4\lambda-\gamma\lambda)}{(1+2\lambda)(\tilde{m}+2)\left(\frac{3(2\tilde{m}+1)\gamma}{(\tilde{m}+2)^2}-\xi_1-4\lambda\xi_1\right)}}\right]^{\frac{3\tilde{m}}{\tilde{m}+2}}, \tag{5.2.34}$$

where c_{26} and c_{27} are integration constants. Here a_1 has an exponential form and for $\gamma = 0$, we obtain

$$H = \frac{\frac{\xi_0(1+2\lambda)(\tilde{m}+2)}{2} e^{\frac{\xi_0(1+2\lambda)(\tilde{m}+2)(t+c_{26})}{2}}}{1-\frac{(1+2\lambda)(\tilde{m}+2)\xi_1}{2} e^{\frac{\xi_0(1+2\lambda)(\tilde{m}+2)(t+c_{26})}{2}}}, \tag{5.2.35}$$

$$q = -1 - e^{\frac{-\xi_0(1+2\lambda)(\tilde{m}+2)(t+c_{26})}{2}}, \tag{5.2.36}$$

$$a_1 = \left[c_{27}\left(1-\frac{(1+2\lambda)(\tilde{m}+2)\xi_1}{2} e^{\frac{\xi_0(1+2\lambda)(\tilde{m}+2)(t+c_{26})}{2}}\right)^{\frac{-2}{(1+2\lambda)(\tilde{m}+2)\xi_1}}\right]^{\frac{3\tilde{m}}{\tilde{m}+2}}. \tag{5.2.37}$$

The behavior of scale factor a_1 is shown in Figures **5.16** and **5.17**. The effects of anisotropy and viscosity on scale factors are the same as in the previous case. The plots of deceleration parameter in Figure **5.18** indicate that it increases with decrease in anisotropy and increase in viscosity. Also, its value does not cross the line $\tilde{q} = -1$.

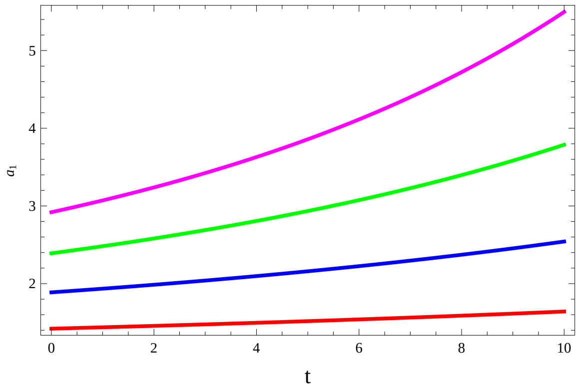

Figure 5.16: Plot of a_1 versus t for $\xi = \xi_0 + \xi_1 H$ and fixing $\lambda = 1,\ c_{26} = 1,\ c_{27} = 1,\ \xi_0 = 0.01,\ \xi_1 = 0.01,\ \tilde{m} = 0.25$ (red), $\tilde{m} = 0.5$ (blue), $\tilde{m} = 0.75$ (green) and $\tilde{m} = 1$ (purple).

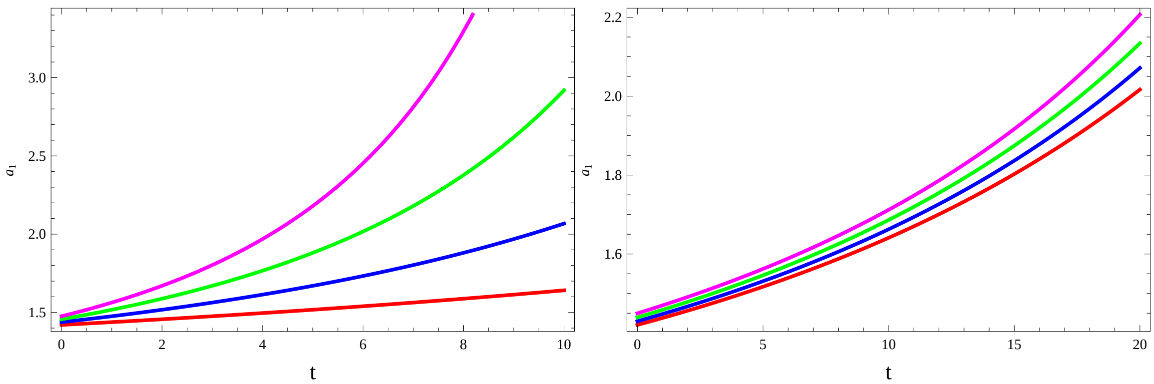

Figure 5.17: Plots of a_1 versus t for $\xi = \xi_0 + \xi_1 H$ and fixing $\lambda = 1,\ c_{26} = 1,\ c_{27} = 1,\ \xi_1 = 0.01,\ \tilde{m} = 0.25,\ \xi_0 = 0.01$ (red), $\xi_0 = 0.02$ (blue), $\xi_0 = 0.03$ (green) and $\xi_0 = 0.04$ (purple) in the left graph and fixing $\tilde{m} = 0.25,\ \xi_0 = 0.01,\ \xi_1 = 0.01$ (red), $\xi_1 = 0.02$ (blue), $\xi_1 = 0.03$ (green) and $\xi_1 = 0.04$ (purple) in the right graph.

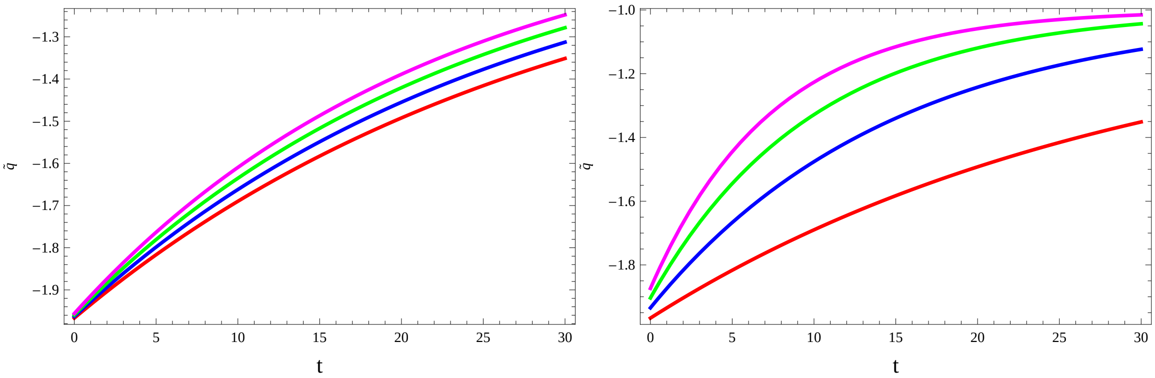

Figure 5.18: Plots of $\tilde{q}$ versus t for $\xi = \xi_0 + \xi_1 H$ and fixing $\lambda = 1,\ c_{26} = 1,\ c_{27} = 1,\ \xi_0 = 0.01,\ \tilde{m} = 0.25$ (red), 0.5 (blue), 0.75 (green) and 1 (purple) in the left graph and fixing $\tilde{m} = 0.25,\ \xi_0 = 0.01$ (red), $\xi_0 = 0.02$ (blue), $\xi_0 = 0.03$ (green) and $\xi_0 = 0.04$ (purple) in the right graph.

Similarly, ρ is obtained as

$$\begin{aligned}\rho \;&=\; \frac{3\dfrac{\frac{\xi_0(1+2\lambda)(\tilde{m}+2)}{2}e^{\frac{\xi_0(1+2\lambda)(\tilde{m}+2)(t+c_{26})}{2}}}{1-\frac{(1+2\lambda)(\tilde{m}+2)\xi_1}{2}e^{\frac{\xi_0(1+2\lambda)(\tilde{m}+2)(t+c_{26})}{2}}}}{(1+4\lambda-\gamma\lambda)}\left[\left(\frac{3(2\tilde{m}+1)}{(\tilde{m}+2)^2}-\lambda\xi_1\right)\right.\\ &\times\left.\frac{\frac{\xi_0(1+2\lambda)(\tilde{m}+2)}{2}e^{\frac{\xi_0(1+2\lambda)(\tilde{m}+2)(t+c_{26})}{2}}}{1-\frac{(1+2\lambda)(\tilde{m}+2)\xi_1}{2}e^{\frac{\xi_0(1+2\lambda)(\tilde{m}+2)(t+c_{26})}{2}}}-\lambda\xi_0\right],\end{aligned} \tag{5.2.38}$$

and the time of big-rip is given by

$$t_{br} = \frac{2}{\xi_0(1+2\lambda)(\tilde{m}+2)}\ln\left[\frac{2}{\xi_1(1+2\lambda)(\tilde{m}+2)}\right] - c_{26}. \tag{5.2.39}$$

The graphical analysis of all cases is summarized in the following tables.

Table **10**: Evolution of scale factors

Viscosity model	**When anisotropy decreases**	**When bulk viscosity increases**
$\xi = 0$	A increases, B decreases	A, B remain the same
$\xi = \xi_0$	A increases, B decreases	A, B decrease
$\xi = \xi_1 H$	A increases, B decreases	A, B increase
$\xi = \xi_0 + \xi_1 H$	A increases, B decreases	A, B increase

Table **11**: Evolution of deceleration parameter

Viscosity Model	**When Anisotropy Decreases**	**When Bulk Viscosity Increases**
$\xi = 0$	constant $(q = -1)$	constant, $(q = -1)$
$\xi = \xi_0$	decreases	decreases
$\xi = \xi_1 H$	decreases	decreases
$\xi = \xi_0 + \xi_1 H$	increases	increases

Chapter 6

Concluding Remarks

This chapter provides a brief summary and conclusions of all the results.

In **Chapter 2**, we have investigated physical features of stellar structures for the model $f(R,T) = R + \alpha R^2 + \lambda T$ via polytropic EoS and MIT bag model as well as characteristics of charged stellar objects for the model $f(R,T) = R + 2\lambda T$ using polytropic EoS. We have solved the system of differential equations numerically assuming some initial conditions. This numerical solution provides the graphical behavior of different geometrical as well as physical quantities of stellar structures. We have also discussed the effect of model parameters on these quantities.

For the first model, with assumed initial conditions and constants, it is found that the star observed through polytropic EoS has approximately radius $R_b \approx 11.4km$, mass $m(R_b) \approx 5M_\odot$, compactness $u(R_b) \approx 0.36$ and gravitational redshift $z_s \approx 0.84$. In the same scenario, MIT bag model leads to a quark star having $R_b \approx 10.2km$, $m(R_b) \approx 3M_\odot$, $u(R_b) \approx 0.30$ and $z_s \approx 0.57$. The redshift parameter and compactness factor for polytropic as well as quark stars lie within the limit defined for perfect fluid configurations [16]. The mass and gravitational redshift tend to decrease with increase in α which is consistent with the behavior of α as discussed in [63].

The mass function grows for quark stars with the increase of λ while for polytropic stars, it first enhances mass but as r increases, it exhibits an opposite behavior. The growing mass with enhancement of λ can cross the observational limits in $f(R,T)$ theory [21]. For both EoS, pressure increases with λ while radius only increases for quark stars and remains the same for polytropic stars. However, for the model $f(R,T) = R + 2\lambda T$, it is observed that [21] for neutron stars, increase in λ enhances mass as well as radius while for quark stars, it produces larger mass but smaller radius. This difference may be due to the presence of the term αR^2 in the model. We have found that the energy conditions are satisfied as well as speed of sound lies between zero and one implying the stability of observed compact stars. We conclude that the observed polytropic star has greater radius, mass and redshift parameter than quark star for the assumed fluid configuration as well as considered values of free parameters.

The model $f(R,T) = R + 2\lambda T$ and the inclusion of electromagnetic field yield the compact star with $R_b \approx 1.5km$, $m(R_b) \approx (0.0094530)M_{\odot}$, $z_s \approx 0.005$ as well as $q(R_b) \approx (-0.0060178)M_{\odot}$ for $p = \sigma_1 \rho^{\frac{5}{3}}$, with same initial conditions but different values of constants. Similarly, for $p = \sigma_2 \rho^2$, the polytropic star has $R_b \approx 0.06km$, $m(R_b) \approx (0.014)M_{\odot}$, $z_s \approx 2$ and $q(R_b) \approx (-0.014)M_{\odot}$. The redshift parameter is less than or equal to two for both cases which lies within the limit defined for perfect fluid configurations [16]. We observed from graphical analysis that any change in λ produces opposite change in mass however in the absence of charge, λ induces similar change in mass as shown in [21].

The resulting electric field intensity is negative causing a force which helps to counter balance the gravity consistent with [24, 26]. The total charge in both cases is negative demonstrating the supremacy of electrons. We have found that the energy conditions are satisfied and speed of sound lies between zero and one implying that the stars are stable. We have found that charged polytropic star with large radius has less mass, charge and surface redshift than the star with small radius. It is observed that the radius of the observed stable charged polytropic star whose matter satisfies the energy conditions is very small as compared to the observed radius of compact objects (white dwarfs and neutron stars). We have also compared our results with those of charged polytropic spheres in $f(R)$ theory [88]. For $f(R,T) = R + 2\lambda T$ gravity model, charged polytropic spheres could have very small masses and radii while for $f(R) = R + \frac{\beta}{2}R^2$, they have very large masses and radii. In [88], the authors deal only with weakly charged spheres however, we have checked that the polytropic charged spheres are stable for our model in strong as well as weak electromagnetic field by assigning large and small values to γ, respectively.

Chapter 3 discusses solutions of the coupled Einstein-Maxwell field equations governing the phenomena of collapse and expansion during stellar evolution in the framework of $f(R,T)$ theory for both spherical as well as cylindrical celestial bodies. In case of spherical systems, the expansion scalar, density, pressures, anisotropy and mass do not change with time for collapse solution. However, for expanding solution, the change remains same for both coordinates, i.e., if one quantity is decreasing with respect to r, it is also decreasing with respect to t. The behavior of these parameters (except expansion scalar) with respect to radius remains the same for both cases. The energy conditions are satisfied for both solutions implying that our solutions are physically acceptable. Also, the graphical analysis for collapsing solution shows that charge slows down the collapsing process by decreasing density and increasing radial pressure. The effect of charge on the collapsing process is consistent with those given in literature [24, 26]. In expansion, the effect of electromagnetic field is very weak as seen in graphs of expanding solution where the effect of charge is not considerable. Abbas and Ahmed [29] discussed the collapsing and expanding solutions without charge and with $H_1(t) = 1$, such that all the quantities are functions of r only. We have taken the effect of charge and dependence of $H_1(t)$ on t. This leads to different behavior of pressures as well as anisotropy but the effect of λ is similar for density while differs for pressures.

For cylindrical system as well as collapse solution, the expansion scalar, density, pressures ($p_r,\ p_\theta$ and p_z), anisotropy and mass do not change with radial coordinate while for expanding solution, change remains the same for both coordinates. For both cases, the behavior of these parameters except p_z remains the same with respect to time. The anisotropy is positive during collapse and expansion which enhances the compactness of the system as discussed in [89]. In both cases, the increase in total charge has the same effects on physical quantities. It is found that the energy conditions are satisfied in both cases showing physical viability of our solutions for the considered values of constants.

Finally, we compare our results with those found in GR or $\lambda = 0$ [27]. For our collapse solution, the change in physical quantities is related with change in time not with radius while in GR, the quantities vary with radial coordinate but do not vary with temporal one. In case of expanding cylinder, physical parameters vary with increase in both time and radius for our solution while in GR, the solution only induces a change with respect to t. In both cases, the anisotropy decreases for our solutions while it increases in GR. The increase in anisotropy can distort the geometry of the system. On the other hand, for our solutions the anisotropy decreases leading to geometry preservation which is due to the dark source terms.

In **Chapter 4**, firstly we have found PMs of GWs for $f(R)$ dark energy models. In each case, we have found four non-zero PMs of GWs Ψ_2 (longitudinal scalar mode), Ψ_4 ($+,\times$ tensorial modes) and Φ_{22} (breathing scalar mode) which is in agreement with the results of [37]. We have non-vanishing Ψ_2 for each model implying that GWs for $f(R)$ dark energy models correspond to class II_6 (as mentioned in Table **1**).

Secondly, we have explored the effects of GWs on the flat universe in the context of curvature-matter coupling. We have found that axial GWs in $f(R,T)$ theory can perturb the background matter in contrast to GR. However, here we suppose Δ and Π equal to zero in order to find the remaining functions k_0, k_1 and u_3. The resulting k_0 and k_1 are different from those of GR and depend upon the coupling constant λ. The function u_3 appearing in the azimuthal velocity component has non-zero expression showing that fluid exhibits a rotation due to axial GWs similar to GR. But the expression of u_3 here depends upon λ and differs from GR. According to velocity memory effect, particles at rest initially gain non-vanishing velocity after passing a GW. We have found that comoving fluid particles (i.e., particles at rest) gain non-zero linear as well as angular velocities after passing the axial GWs. When the expression of $u(\eta, r)$ is continuous at the wave front, the smooth wave profile does not induce any cosmological rotation [42]. Hence we conclude that the axial GW can induce a cosmological rotation if $u(\eta, r)$ is discontinuous at the wave front. If the freely falling particles are displaced by a GW, it is called memory effect of the GW. Hence the axial GW in $f(R,T)$ gravity induces memory effect when the wave profile has discontinuity at the wave front.

In **Chapter 5**, we have investigated cosmological evolution by considering interaction between MCG and $f(R,T)$ gravity. We have discussed the evolution in emergent, intermediate as well as logamediate scenarios and the behavior of bulk viscosity for two interacting models. For the first interaction model, we have found that the bulk viscosity decreases for emergent universe while it increases for intermediate and logamediate cases. For the second interaction model, the bulk viscosity enhances expansion of the universe for intermediate and logamediate scenarios as shown in [86], that large values of bulk viscosity can produce expansion of the universe. We conclude that the interaction of MCG and $f(R,T)$ gravity leads to quintessence phase of dark energy for the three considered scenarios.

We have also observed the evolution for LRS Bianchi type-I model through scale factors and deceleration parameter in dark energy dominated era with different forms of bulk viscosity. The graphical analysis is summarized in Tables **10** and **11**. The evolution of scale factors with the decrease in anisotropy remains the same in all cases as shown in Table **10**. It is observed from Table **11** that decrease in anisotropy as well as increase in viscosity decreases $\tilde{q}$ for second and third bulk viscosity models while increases for the last model. We would like to mention here that for $\tilde{m} = 1$, our results reduce to that of isotropic case [87]. It is concluded that the accelerated expansion is faster for $\xi = \xi_1 H$ as compared to other models.

Related to this thesis, there are several issues which can be taken into account for future research work.

- To study the structure and evolution of stellar objects with tilted congruence in $f(R,T)$ gravity.

- To investigate the effects of polar GWs in modified theories.

- To study the axial GWs in $f(R)$ and other modified theories.
- To study the interactions of viscous cosmic CG with $f(R,T)$ gravity.
- To explore stellar and cosmic evolution for non-minimally coupled models of $f(R,T)$ gravity.

Appendix A

List of Publications

The contents of this thesis are based on the following research papers published or submitted in journals of International repute. These papers are also attached herewith.

1. Sharif, M. and **Siddiqa, A.**: *Study of Stellar Structures in $f(R,T)$ Gravity,*
   Int. J. Mod. Phys. D **27**(2018)1850065.

2. Sharif, M. and **Siddiqa, A.**: *Study of Charged Stellar Structures in $f(R,T)$ Gravity,*
   Eur. Phys. J. Plus **132**(2017)529.

3. Sharif, M. and **Siddiqa, A.**: *Models of Charged Self-Gravitating Source in $f(R,T)$ Theory,*
   Int. J. Mod. Phys. D **27**(2018)1950005.

4. Sharif, M. and **Siddiqa, A.**: *Models of Collapsing and Expanding Cylindrical Source in $f(R,T)$ Theory,*
   Ad. High Energy Phys. **2019**(2019)8702795.

5. Sharif, M. and **Siddiqa, A.**: *Polarization Modes of Gravitational Wave for Viable $f(R)$ Models,*
   Astrophys. Space Sci. **362**(2017)226.

6. Sharif, M. and **Siddiqa, A.**: *Curvature-Matter Coupling Effects on Axial Gravitational Waves,*
   Eur. Phys. J. C **78**(2018)721.

7. Sharif, M. and **Siddiqa, A.**: *Interaction of Viscous Modified Chaplygin Gas with $f(R,T)$ Gravity,*
Mod. Phys. Lett. A **32**(2017)1750151.

8. Sharif, M. and **Siddiqa, A.**: *Viscosity Effects on Anisotropic Universe in Curvature-Matter Coupling Gravity,*
Commun. Theor. Phys. **69**(2018)537.

Also, the following papers related to this thesis have been published.

1. Sharif, M. and **Siddiqa, A.**: *Axial Dissipative Dust as a Source of Gravitational Radiation in $f(R)$ Gravity,*
Phys. Dark Universe **15**(2017)105.

2. Sharif, M. and **Siddiqa, A.**: *Study of Bianchi Type-I Model in $f(R,T^{\psi})$ Gravity,*
Phys. Lett. A **381**(2017)838.

3. Sharif, M. and **Siddiqa, A.**: *Study of Homogeneous and Isotropic Universe in $f(R,T^{\varphi})$ Gravity,*
Ad. High Energy Phys. **2018**(2018)9534279.

4. Sharif, M. and **Siddiqa, A.**: *Equilibrium Configurations of Anisotropic Polytropes in $f(R,T)$ Gravity,*
Eur. Phys. J. Plus **133**(2018)226.

5. Sharif, M. and **Siddiqa, A.**: *Propagation of Polar Gravitational Waves in $f(R,T)$ Scenario,*
Submitted for Publication.

Bibliography

[1] Riess, A.G. *et al.*: *Observational Evidence from Supernovae for an Accelerating Universe and a Cosmological Constant,* Astron. J. **116**(1998)1009.

[2] Perlmutter, S. *et al.*: *Measurement of* Ω *and* Λ *from 42 High-Redshift Supernovae,* Astrophys. J. **517**(1999)565.

[3] Amendola, L. and Tsujikawa, S.: *Drak Energy: Theory and Observations* (Cambridge University Press, 2010).

[4] Starobinsky, A.A.: *A New Type of Isotropic Cosmological Models Without Singularity,* Phys. Lett. B **91**(1980)99.

[5] Hu, W. and Sawicki, I.: *Models of Cosmic Acceleration that Evade Solar System Tests,* Phys. Rev. D **76**(2007)064004; Tsujikawa, S.: *Observational Signatures of Dark Energy Models that Satisfy Cosmological and Local Gravity Constraints,* Phys. Rev. D **77**(2008)023507.

[6] Bamba, K., Geng, C.Q. and Lee, C.C.: *Cosmological Evolution in Exponential Gravity,* J. Cosmol. Astropart. Phys. **08**(2010)021.

[7] De Felice, A. and Tsujikawa, S.: *$f(R)$ Theories,* Living Rev. Rel. **13**(2010)3; Nojiri, S.I. and Odintsov, S.D.: *Unified Cosmic History in Modified Gravity: From $f(R)$ Theory to Lorentz Non-Invariant Models,* Phys. Rep. **505**(2011)59.

[8] Harko, T., Lobo, F.S.N., Nojiri, S. and Odintsov, S.D.: *$f(R,T)$ Gravity,* Phys. Rev. D **84**(2011)024020.

[9] Harko, T. and Lobo, F.S.N.: *Generalized Curvature-Matter Couplings in Modified Theories,* Galaxies **2**(2014)410.

[10] Papantonopoulos, E.: *Modifications of Einstein's Theory of Gravity at Large Distances* (Springer, 2014).

[11] Oppenheimer, J.R. and Snyder, H.: *On Continued Gravitational Contraction,* Phys. Rev. **56**(1939)455.

[12] Misner, C.W. and Sharp, D.H.: *Relativistic Equations for Adiabatic, Spherically Symmetric Gravitational Collapse,* Phys. Rev. **136**(1964)B571.

[13] Misner, C.W. and Sharp, D.H.: *Spherical Gravitational Collapse with Energy Transport by Radiative Diffusion,* Phys. Lett. **15**(1965)279.

[14] Herrera, L., Santos, N.O. and Le Denmat, G.: *Dynamical Instability for Non-Adiabatic Spherical Collapse,* Mon. Not. R. Astron. Soc. **237**(1989)257; Herrera, L. and Santos, N.O.: *Local Anisotropy in Self-Gravitating Systems,* Phys. Rep. **286** (1997)53; Di Prisco, A., Herrera, L., MacCallum, M.A.H. and Santos, N.O.: *Shearfree Cylindrical Gravitational Collapse,* Phys. Rev. D **80**(2009)064031.

[15] Glass, E.N.: *Generating Anisotropic Collapse and Expansion Solutions of Einstein's Equations,* Gen. Relativ. Gravit. **45**(2013)266.

[16] Buchdahl, H.A.: *General Relativistic Fluid Spheres,* Phys. Rev. **116**(1959)1027.

[17] Shapiro, S.L. and Teukolsky, S.A.: *Black Holes, White Dwarfs and Neutron Stars: The Physics of Compact Objects* (John Wiley and Sons, 1983).

[18] Bombaci, I.: *The Maximum Mass of a Neutron Star,* Astron. Astrophys. **305**(1996)871.

[19] Ivanov, B.V.: *Maximum Bounds on the Surface Redshift of Anisotropic Stars,* Phys. Rev. D **65**(2002)104011.

[20] Zubair, M., Abbas, G. and Noureen, I.: *Possible Formation of Compact Stars in $f(R,T)$ Gravity,* Astrophys. Space Sci. **361**(2016)8.

[21] Moraes, P.H.R.S., José D.V.A. and Malheiro, M.: *Stellar Equilibrium Configurations of Compact Stars in $f(R,T)$ Theory of Gravity,* J. Cosmol. Astropart. Phys. **06**(2016)005.

[22] Carvalho, G.A. *et al.*: *Stellar Equilibrium Configurations of White Dwarfs in the $f(R,T)$ Gravity,* Eur. Phys. J. C **77**(2017)871.

[23] Rosseland, S. and Eddington, A.S.: *Electrical State of a Star,* Mon. Not. R. Astron. Soc. **84**(1924)720.

[24] Sharif, M. and Abbas, G.: *Dynamics of Charged Radiating Collapse in Modified Gauss-Bonnet Gravity,* Eur. Phys. J. Plus **128**(2013)102.

[25] Abbas, G.: *Collapse and Expansion of Anisotropic Plane Symmetric Source,* Astrophys. Space Sci. **350**(2014)307.

[26] Abbas, G.: *Effects of Electromagnetic Field on the Collapse and Expansion of Anisotropic Gravitating Source,* Astrophys. Space Sci. **352**(2014)955.

[27] Mahmood, T., Shah, S.M. and Abbas, G.: *Gravitational Collapse and Expansion of Charged Anisotropic Cylindrical Source,* Astrophys. Space Sci. **357**(2015)56.

[28] Bhatti, M.Z. and Yousaf, Z.: *Influence of Electric Charge and Modified Gravity on Density Irregularities,* Eur. Phys. J. C **76**(2016)219.

[29] Abbas, G. and Ahmed, R.: *Models of Collapsing and Expanding Anisotropic Gravitating Source in $f(R,T)$ Theory of Gravity,* Eur. Phys. J. C **77**(2017)441.

[30] Abbott, B.P. *et al.*: *Observation of Gravitational Waves from a Binary Black Hole Merger,* Phys. Rev. Lett. **116**(2016)061102.

[31] Abbott, B.P. *et al.*: *GW170104: Observation of a 50-Solar-Mass Binary Black Hole Coalescence at Redshift 0.2,* Phys. Rev. Lett. **118**(2017)221101.

[32] Abbott, B.P. *et al.*: *GW170817: Observation of Gravitational Waves from a Binary Neutron Star Inspiral,* Phys. Rev. Lett. **119**(2017)161101.

[33] Newman, E. and Penrose, R.: *An Approach to Gravitational Radiation by a Method of Spin Coefficients,* J. Math Phys. **3**(1962)566.

[34] Eardley, D.M., Lee, D.L. and Lightman, A.P.: *Gravitational Wave Observations as a Tool for Testing Relativistic Gravity,* Phys. Rev. D **8**(1973)3308.

[35] Capozziello, S., Corda, C. and De Laurentis, M.F.: *Massive Gravitational Waves from $f(R)$ Theories of Gravity: Potential Detection with LISA,* Phys. Lett. B **669**(2008)255.

[36] Alves, M.E.S., Miranda, O.D. and de Araujo, J.C.N.: *Probing the $f(R)$ Formalism Through Gravitational Wave Polarizations,* Phys. Lett. B **679**(2009)401.

[37] Kausar, H.R., Philippoz, L. and Jetzer, P.: *Gravitational Wave Polarization Modes in $f(R)$ Theories,* Phys. Rev. D **93**(2016)124071.

[38] Alves, M.E., Moraes, P.H., de Araujo, J.C. and Malheiro, M. *Gravitational Waves in $f(R,T)$ and $f(R,T^{\phi})$ Theories of Gravity,* Phys. Rev. D **94**(2016)024032.

[39] Kausar, H.R.: *Polarization States of Gravitational Waves in Modified Theories,* Int. J. Mod. Phys. D **26**(2017)1741010.

[40] Malec, E. and Wylężek, G.: *The Huygens Principle and Cosmological Gravitational Waves in the Regge-Wheeler Gauge,* Class. Quantum Grav. **22**(2005)3549.

[41] Kulczycki, W. and Malec, E.: *Gravitational Waves in Friedman-Lemaitre-Robertson-Walker Cosmology, Material Perturbations and Cosmological Rotation, and the Huygens Principle,* Class. Quantum Grav. **34**(2017)135014.

[42] Kulczycki, W. and Malec, E.: *Axial Gravitational Waves in FLRW Cosmology and Memory Effects,* Phys. Rev. D **96**(2017)063523.

[43] Sharif, M. and Bhatti, M.Z.: *Stability of the Expansion-Free Charged Cylinder,* J. Cosmol. Astropart. Phys. **10**(2013)056.

[44] Sharif, M. and Farooq, N.: *Charged Cylindrically Symmetric Collapse in $f(R)$ Gravity,* Eur. Phys. J. Plus **132**(2017)355.

[45] Sharif, M. and Farooq, N.: *Charged Bulk Viscous Cylindrical Collapse in $f(R)$ Theory,* Int. J. Mod. Phys. D **27**(2018)1850013.

[46] Dolgov, A.D. and Kawasaki, M.: *Can Modified Gravity Explain Accelerated Cosmic Expansion*? Phys. Lett. B **573**(2003)1.

[47] Faraoni, V.: *Lagrangian Description of Perfect Fluids and Modified Gravity with an Extra Force,* Phys. Rev. D **80**(2009)124040.

[48] Dadhich, N.: *Derivation of the Raychaudhuri Equation,* arXiv:gr-qc/0511123; Kar, S. and Sengupta, S.: *The Raychaudhuri Equations: A Brief Review,* Pramana J. Phys. **69**(2007)49.

[49] Poisson, P.: *A Relativist's Toolkit: The Mathematics of Black-Hole Mechanics* (Cambridge University Press, 2004).

[50] Haensel, P., Zdunik, J.L. and Schaeffer, R.: *Strange Quark Stars,* Astron. Astrophys. **160**(1986)121; Glendenning, N.K.: *First-Order Phase Transitions with More Than One Conserved Charge: Consequences for Neutron Stars,* Phys. Rev. D **46**(1992)1274.

[51] Madarassy, E.J.M. and Toth, V.T.: *Evolution and Dynamical Properties of Bose-Einstein Condensate Dark Matter Stars,* Phys. Rev. D **91**(2015)044041.

[52] Bogolioubov, P.N.: *Sur un Modéle á Quarks Quasi-Indépendants,* Ann. Inst. Henry Poincaré **8**(1968)163.

[53] Chodos, A., Jaffe, B.L., Johnson, K., Thorn, C.B. Weisskopf, V.F.: *New Extended Models of Hydrons,* Phys. Rev. D **9**(1974)3471.

[54] Regge, T. and Wheeler, J.A.: *Stability of a Schwarzschild Singularity,* Phys. Rev. **108**(1957)1063.

[55] Ellis, G.F.R., Maartens, R. and MacCallum, M.A.H.: *Relativitis Cosmology* (Cambridge University Press, 2012).

[56] Chaplygin, S.: *Gas Jets,* Sci. Mem. Mosc. Univ. Math. Phys. **21**(1904)1.

[57] Kamenshchik, A.Yu, Moschella, U. and Pasquier, V.: *An Alternative to Quintessence,* Phys. Lett. B **511**(2001)265.

[58] Bento, M.C., Bertolami, O. and Sen, A.A.: *Generalized Chaplygin Gas, Accelerated Expansion and Dark-Energy-Matter Unification,* Phys. Rev. D **66**(2002)043507.

[59] Benaoum, H.B.: *Accelerated Universe from Modified Chaplygin Gas and Tachyonic Fluid,* arXiv:hep-th/0205140.

[60] Sharif, M. and Siddiqa, A.: *Study of Stellar Structures in $f(R,T)$ Gravity,* Int. J. Mod. Phys. D **27**(2018)1850065.

[61] Sharif, M. and Siddiqa, A.: *Study of Charged Stellar Structures in $f(R,T)$ Gravity,* Eur. Phys. J. Plus **132**(2017)529.

[62] Moraes, P.H.R.S., Correa, R.A.C. and Ribeiro, G.: *The Starobinsky Model Within the $f(R,T)$ Formalism as a Cosmological Model,* arXiv:1701.01027.

[63] Astachenok, A.V., de la Cruz-Dombriz, A. and Odinstov, S.D.: *The Realistic Models of Relativistic Stars in $R+\alpha R^2$ Gravity,* Class. Quantum Gravit. **34**(2017)205008.

[64] Barrientos, J. and Rubilar, G.F.: *Comment on "$f(R,T)$ Gravity,"* Phys. Rev. D **90**(2014)028501.

[65] Sharif, M. and Siddiqa, A.: *Dynamics of Charged Plane Symmetric Gravitational Collapse,* Gen. Relativ. Gravit. **43**(2011)73.

[66] Arbañil, J.D.V., Lemos, J.P.S. and Zanchin, V.T.: *Polytropic Spheres with Electric Charge: Compact Stars, the Oppenheimer-Volkoff and Buchdahl Limits, and Quasiblack Holes,* Phys. Rev. D **88**(2013)084023.

[67] Sharif, M. and Siddiqa, A.: *Models of Charged Self-Gravitating Source in $f(R,T)$ Theory,* Int. J Mod. Phys. D **27**(2018)1950005.

[68] Sharif, M. and Siddiqa, A.: *Models of Collapsing and Expanding Cylindrical Source in $f(R,T)$ Theory,* Ad. High Energy Phys. **2019**(2019)8702795.

[69] Booth, I.: *Evolutions from Extremality,* Phys. Rev. D **93**(2016)084005.

[70] Mahmood, A., Siddiqui, A.A. and Feroze, T.: *Non-Static Spherically Symmetric Exact Solution of the Einstein-Maxwell Field Equations,* J. Korean Phys. Soc. **71**(2017)396; Qadir, A. and Ziad, M.: *The Classification of Spherically Symmetric Spacetimes,* Nuovo Cimento B **110**(1995)317.

[71] Sharif, M. and Siddiqa, A.: *Polarization Modes of Gravitational Wave for Viable $f(R)$ Models,* Astrophys. Space Sci. **362**(2017)226.

[72] Sharif, M. and Siddiqa, A.: *Curvature-Matter Coupling Effects on Axial Gravitational Waves,* Eur. Phys. J. C **78**(2018)721.

[73] Amendola, L., Gannouji, R., Polarski, D. and Tsujikawa, S.: *Conditions for the Cosmological Viability of* $f(R)$ *Dark Energy Models,* Phys. Rev. D **75**(2007)083504.

[74] Rajaraman, R.: *An Introduction to Solitons and Instantons in Quantum Field Theory* (Elsevier, 1982).

[75] Sharif, M. and Siddiqa, A.: *Interaction of Viscous Modified Chaplygin Gas with* $f(R,T)$ *Gravity,* Mod. Phys. Lett. A **32**(2017)1750151.

[76] Sharif, M. and Siddiqa, A.: *Viscosity Effects on Anisotropic Universe in Curvature-Matter Coupling Gravity,* Commun. Theor. Phys. **69**(2018)537.

[77] Amani, A.R. and Pourhassan, B.: *Viscous Generalized Chaplygin Gas with Arbitrary* α*,* Int. J. Theor. Phys. **52**(2013)1309; Floerchinger, S., Tetradis, N. and Wiedemann, U.A.: *Accelerating Cosmological Expansion from Shear and Bulk Viscosity,* Phys. Rev. Lett. **114**(2015)091301.

[78] Shabani, H. and Ziaie, A.H.: *Stability of the Einstein Static Universe in* $f(R,T)$ *Gravity,* Eur. Phys. J. C **77**(2017)31.

[79] Abdalla, E., Abramo, L.R., Sodre, L. and Wang, B: *Signature of the Interaction Between Dark Energy and Dark Matter in Galaxy Clusters,* Phys. Lett. B **673**(2009)107.

[80] Naji, J., Pourhassan, B. and Amani, A.R.: *Effect of Shear and Bulk Viscosities on Interacting Modified Chaplygin Gas Cosmology,* Int. J. Mod. Phys. D **23**(2014)1450020.

[81] Sadeghi, J. and Farahani, H.: *Interaction Between Viscous Varying Modified Cosmic Chaplygin Gas and Tachyonic Fluid,* Astrophys. Space Sci. **347**(2013)209.

[82] Wei, H.: *Cosmological Evolution of Quintessence and Phantom with a New Type of Interaction in Dark Sector,* Nucl. Phys. B **845**(2011)381.

[83] Ellis, G.F.R. and Maartens, R.: *The Emergent Universe: Inflationary Cosmology with no Singularity,* Class. Quantum Grav. **21**(2004)223.

[84] Barrow, J.D.: *Graduated Inflationary Universes,* Phys. Lett. B **235**(1990)40.

[85] Barrow, J.D. and Nunes, N. J.: *Dynamics of "Logamediate" Inflation,* Phys. Rev. D **76**(2007)043501.

[86] Gagnon, J.S. and Lesgourgues, J.: *Dark Goo: Bulk Viscosity as an Alternative to Dark Energy,* J. Cosmol. Astropart. Phys. **09**(2011)026.

[87] Singh, C.P. and Kumar, P.: *Friedmann Model with Viscous Cosmology in Modified $f(R,T)$ Gravity Theory,* Eur. Phys. J. C **74**(2014)3070.

[88] Mansour, H., Lakhal, B.S. and Yanallah,A.: *Weakly Charged Compact Stars in $f(R)$ Gravity,* arXiv:1710.09294.

[89] Maurya, S.K., Ray, S., Ghosh, S., Manna, S. and Smitha T.T.: *A Generalized Family of Anisotropic Compact Object in General Relativity,* Ann. Phys. **395**(2018)152.

International Journal of Modern Physics D
Vol. 27, No. 7 (2018) 1850065 (15 pages)
© World Scientific Publishing Company
DOI: 10.1142/S0218271818500657

Study of stellar structures in $f(R,T)$ gravity

M. Sharif* and Aisha Siddiqa†

Department of Mathematics, University of the Punjab,
Quaid-e-Azam Campus, Lahore 54590, Pakistan
**msharif.math@pu.edu.pk*
†aisha.siddiqa17@yahoo.com

Received 5 September 2017
Revised 15 December 2017
Accepted 10 January 2018
Published 7 February 2018

This paper is devoted to study the compact objects whose pressure and density are related through polytropic equation-of-state (EoS) and MIT bag model (for quark stars) in the background of $f(R,T)$ gravity. We solve the field equations together with the hydrostatic equilibrium equation numerically for the model $f(R,T) = R + \alpha R^2 + \lambda T$ and discuss physical properties of the resulting solution. It is observed that for both types of stars (polytropic and quark stars), the effects of model parameters α and λ remain the same. We also obtain that the energy conditions are satisfied and stellar configurations are stable for both EoS.

Keywords: $f(R,T)$ gravity; compact objects; equation-of-state.

PACS Number(s): 04.40.Dg, 04.50.Kd

1. Introduction

Compact objects are remanent of gravitational collapse of massive stars. The final outcome of the collapse depends upon the initial mass of the star. Stars having mass less than $8M_\odot$ ($M_\odot$ denotes solar mass) form a white dwarf while more massive stars form neutron stars and black holes after collapse. White dwarfs and neutron stars exist in our universe and can be observed directly but the existence of black holes is confirmed by some ground-based observations. Astronomers provided the first evidence of the existence of black holes in Andromeda galaxy and later in M104, NGC3115, M106 and Milky Way galaxies.[1]

The pair of these compact objects (accreting each other) can merge together and produce gravitational waves. Hawking[2] found an upper bound for the energy of gravitational radiation emitted by the collision of two black holes. Wagoner[3] investigated gravitational radiation emitted by accreting neutron stars. The electromagnetic radiation are redshifted or reduced in frequency when observed in a region at higher gravitational potential. This phenomenon is named as surface gravitational redshift (z_s) which helps to understand physics of the strong interaction between particles inside the star and its equation-of-state (EoS).[4] Another important quantity for the compact objects is the mass-radius ratio called the compactness factor ($u(r)$). For a compact object having isotropic fluid distribution, the mass-radius ratio of a compact object cannot exceed $\frac{4}{9}$.[5] For static spherical configurations, the maximum bound for the surface redshift parameter is found as $z_s \leq 2$ for perfect fluid distributions[5] while for anisotropic models it is $z_s \leq 5.211$.[6] Böhmer and Harko[7] evaluated the upper and lower bounds for some physical parameters in the background of anisotropic matter distribution as well as in the presence of cosmological constant. They obtained redshift and total energy bounds in terms of anisotropic parameter and claimed that the redshift parameter is $2 \leq z_s \leq 5$ for anisotropic configurations. Boshkayev *et al.*[8] found an approximate analytic solution to the field equations for a slightly deformed and slowly rotating stellar object.

A direct generalization of general relativity (GR) is the $f(R)$ gravity, the Ricci scalar R in the Einstein–Hilbert action is replaced by its generic function $f(R)$. De Felice and Tsujikawa[9] presented a comprehensive study on various applications of $f(R)$ theory in cosmology and astrophysics. Harko *et al.*[10] proposed $f(R,T)$ gravity as a generalized modified theory, where T denotes trace of the energy–momentum tensor. The coupling of curvature and matter leads to a source term which may yield interesting results. It can produce a matter-dependent deviation from geodesic motion and also help to study dark energy, dark matter interactions as well as late-time acceleration.[11] Jamil *et al.*[12] introduced some cosmic models and found that ΛCDM model is reproduced by dust fluid in this gravity. Sharif and Zubair[13] explored validity of the second law of thermodynamics for phantom as well as nonphantom phases. Sharif and Nawazish[14] worked on the existence of Noether symmetries interacting with generalized scalar field model in the same gravity. They found that dust fluid leads to decelerated expansion while perfect fluid yields current cosmic expansion for quintessence model.

The stability of compact objects is a key issue in astrophysics and cosmology. There are different methods to discuss stable fluid configurations like perturbation technique and speed of sound. The matter is in stable state if $0 \leq v_s^2 \leq 1$, where v_s is the speed of sound.[15] Abreu *et al.*[16] provided an alternative approach to check the instability of anisotropic matter distributions. They showed that for unstable regions, the radial speed of sound is less than its tangential part. Jiang and Gleiser[17] found an accuracy in stability regions of astrophysical compact objects using configurational entropy greater than those obtained via perturbation method.

Abbas and Sarwar[18] investigated the stability of expansion-free self-gravitating systems in the context of Einstein Gauss–Bonnet gravity and showed that stability holds for chosen values of parameters otherwise it is disturbed. Sharif and Yousaf[19] discussed the stability of spherically symmetric stellar objects through perturbation technique in $f(R,T)$ gravity and also investigated the role of matter variables. Noureen and Zubair[20] investigated stability of anisotropic spherical star in this gravity yielding some constraints for physical quantities. Zubair *et al.*[21] studied stability, energy conditions and surface redshift for three observed models of compact stars in the same gravity using Krori and Barua solution. Yousaf *et al.*[22] investigated the stability of cylindrical symmetric stellar configurations by inducing perturbations and found that it depends on the stiffness parameter, matter variables as well as $f(R,T)$ dark source terms.

The hydrostatic equilibrium equation is of fundamental importance in the study of celestial objects. Moraes *et al.*[23] studied hydrostatic equilibrium condition for neutron stars with a specific form of EoS and found that the extreme mass can cross observational limits. Astashenok *et al.*[24] examined the existence of realistic models of stars for $f(R) = R + \alpha R^2$ gravity model. Carvalho *et al.*[25] examined white dwarfs for the model $f(R,T) = R + 2\lambda T$ and found that mass can cross the Chandrasekhar limit.

In this paper, we study compact objects and their physical features in the framework of $f(R,T)$ gravity. The behavior of Ricci scalar, pressure, density, mass function, compactness factor and gravitational redshift of stellar objects are discussed. We also study energy conditions and stability of the resulting solution. The paper is organized as follows. In the next section, the field equations and hydrostatic equilibrium equation are formulated for $f(R,T) = R + \alpha R^2 + \lambda T$ gravity model. Section 3 investigates physical features using two EoS. Finally, we conclude our results.

2. Field Equations in $f(R,T)$ Gravity

The action for $f(R,T)$ theory is defined as

$$S = \int d^4x\sqrt{-g}\left[\frac{1}{16\pi}f(R,T) + \mathcal{L}_m\right]. \tag{1}$$

The field equations are obtained by varying this action with respect to $g^{\mu\nu}$

$$f_R R_{\mu\nu} - \frac{1}{2}g_{\mu\nu}f + (g_{\mu\nu}\Box - \nabla_\mu\nabla_\nu)f_R = 8\pi T_{\mu\nu} - f_T(T_{\mu\nu} + \Theta_{\mu\nu}), \tag{2}$$

where $f = f(R,T)$, $f_R = \frac{\partial f}{\partial R}$, $f_T = \frac{\partial f}{\partial T}$ and $\Theta_{\mu\nu}$ is evaluated by

$$\Theta_{\mu\nu} = g^{\gamma\sigma}\frac{\delta T_{\gamma\sigma}}{\delta g^{\mu\nu}}, \quad T_{\mu\nu} = g_{\mu\nu}\mathcal{L}_m - \frac{\partial \mathcal{L}_m}{\partial g^{\mu\nu}}. \tag{3}$$

We consider a spherically symmetric compact object whose geometry is described by the metric

$$ds^2 = -B(r)dt^2 + A(r)dr^2 + r^2(d\theta^2 + \sin^2\theta d\phi^2). \tag{4}$$

The energy–momentum tensor of perfect fluid in comoving coordinates is

$$T_{\mu\nu} = (\rho + p)V_\mu V_\nu + p g_{\mu\nu}, \tag{5}$$

where ρ represents energy density, p denotes pressure of the fluid, V_μ is the four velocity satisfying $V_\mu V^\mu = -1$ and $T = 3p - \rho$. We take $\mathcal{L}_m = p$ and consequently

$\Theta_{\mu\nu} = -2T_{\mu\nu} + pg_{\mu\nu}$. Considering $f(R,T) = f_1(R) + f_2(T)$ as introduced by Harko *et al.*[10] as well as the Starobinsky model[26] for f_1 and λT for f_2, we have the model $f(R,T) = f_1(R) + f_2(T) = R + \alpha R^2 + \lambda T$.[27]

The $f(R,T)$ theory is reduced to $f(R)$ gravity for $T = 0$ which happens in the radiation dominated era. Thus, the discussion of this era in the evolution of the universe within $f(R,T)$ scenario is an issue. It is shown[27] that the model $f(R,T) = R + \alpha R^2 + \lambda T$ solves this issue and describes the radiation dominated era. This model is reduced to GR when α and λ approach zero and $f(R)$ Starobinsky model when $\lambda = 0$ only. In this paper, we consider this model to study stable configurations of compact objects in $f(R,T)$ gravity. It simplifies the field equations as

$$\begin{aligned}(1+2\alpha R)G_{\mu\nu} + 2\alpha(g_{\mu\nu}\Box R - \nabla_\mu\nabla_\nu R) + \frac{\alpha}{2}R^2 g_{\mu\nu}\\ = 8\pi T_{\mu\nu} + \lambda T_{\mu\nu} - \lambda p g_{\mu\nu} + \frac{\lambda}{2}T g_{\mu\nu},\end{aligned} \tag{6}$$

and the trace equation is

$$6\alpha\Box R - R = 8\pi T + 3\lambda T - 4\lambda p, \tag{7}$$

which indicates the propagation of a new degree of freedom, i.e. R. Thus, in the present work, we consider R as an independent dynamical variable.[24] We have also checked the alternative when R is not taken independently rather its value in terms of metric coefficients is replaced. However, the procedure to solve the differential equations becomes complicated in this way. Equation (6) leads to the following field equations:

$$\begin{aligned}&\frac{A'}{rA^2} + \frac{1}{r^2} - \frac{1}{r^2 A} - \frac{R(3\alpha R+2)}{6(1+2\alpha R)} + \frac{\alpha R' B'}{AB(1+2\alpha R)}\\ &= \frac{1}{1+2\alpha R}\left[\frac{16}{3}\pi\rho + 8\pi p + \frac{11}{6}\lambda\rho + \frac{7}{6}\lambda p\right],\end{aligned} \tag{8}$$

$$\begin{aligned}&\frac{B'}{rAB} - \frac{1}{r^2} + \frac{1}{r^2 A} + \frac{2\alpha R'}{(1+2\alpha R)}\left(\frac{B'}{2AB} - \frac{2}{rA}\right) + \frac{\alpha R^2}{2(1+2\alpha R)}\\ &= \frac{1}{(1+2\alpha R)}\left[8\pi p + \frac{\lambda}{2}(3p-\rho)\right],\end{aligned} \tag{9}$$

$$\begin{aligned}&\frac{r^2}{2A}\left(\frac{B'}{B}\right)' - \frac{r^2 A'}{A^2}\left(\frac{2}{r} + \frac{B'}{4B}\right) + \frac{r^2 B'}{2AB}\left(\frac{1}{r} + \frac{B'}{2B}\right)\\ &+ \frac{2\alpha r^2}{(1+2\alpha R)}\left[\frac{A^2}{4} + \frac{R}{6\alpha} - \frac{A'}{Ar}\right]\\ &= \frac{r^2}{(1+2\alpha R)}\left[\frac{-2}{3}\lambda p + \frac{1}{2}\lambda\rho + \frac{8}{3}\pi\rho\right].\end{aligned} \tag{10}$$

In further calculations, we substitute $\varphi = \frac{B'}{B}$. Adding Eqs. (8) and (9), we obtain

$$A' = \frac{2rA^2}{3(1+2\alpha R)}\left[8\pi(\rho+3p) + 2\lambda(\rho+2p) + R\left(\frac{1}{2} - \frac{3\alpha\varphi}{rA}\right)\right.$$
$$\left. - \frac{3\varphi}{2rA} - \frac{3\alpha R'}{A}\left(\varphi - \frac{2}{r}\right)\right]. \tag{11}$$

Similarly, Eq. (10) can be rewritten as

$$\varphi' = \frac{2A'}{A}\left(\frac{2}{r} + \frac{\varphi}{4}\right) - \varphi\left(\frac{1}{r} + \frac{\varphi}{2}\right) - \frac{4\alpha A}{(1+2\alpha R)}\left[\frac{A^2}{2} - \frac{A'}{Ar} + \frac{R}{6\alpha}\right]$$
$$+ \frac{2A}{(1+2\alpha R)}\left[\frac{8}{3}\pi\rho + \lambda\left(\frac{\rho}{2} - \frac{2p}{3}\right)\right], \tag{12}$$

while the trace equation gives

$$R'' = \left(\frac{A'}{2A} - \frac{\varphi}{2} - \frac{2}{r}\right)R' + \frac{A}{6\alpha}\left(R + 2(4\pi+\lambda)(3p-\rho) - (\rho+p)\lambda\right). \tag{13}$$

The covariant divergence of the field equations yields[28]

$$\nabla^\mu T_{\mu\nu} = \frac{f_T}{8\pi - f_T}\left[(T_{\mu\nu} + \Theta_{\mu\nu})\nabla^\mu \ln f_T + \nabla^\mu\Theta_{\mu\nu} - \frac{1}{2}g_{\mu\nu}\nabla^\mu T\right].$$

For the model $f(R,T) = R + \alpha R^2 + \lambda T$, this gives

$$\nabla^\mu T_{\mu\nu} = \frac{\lambda}{8\pi - \lambda}\left[\nabla^\mu\Theta_{\mu\nu} - \frac{1}{2}g_{\mu\nu}\nabla^\mu T\right],$$

which yields the hydrostatic equilibrium equation as

$$p' + (\rho+p)\frac{\varphi}{2} = \frac{\lambda}{2(8\pi-\lambda)}(\rho' - p').$$

This can also be written as

$$p' = -\frac{(\rho+p)\varphi}{2\left[1 - \frac{\lambda}{2(8\pi-\lambda)}\left(\frac{d\rho}{dp} - 1\right)\right]}. \tag{14}$$

3. Physical Features of Compact Objects

White dwarfs have masses close to solar mass as well as radii that are 100 times less than that of the sun while neutron stars can have masses upto $3M_\odot$ and radii close to 10 km.[15] In white dwarfs, the gravitational attraction is balanced by the degeneracy pressure of electrons while in neutron stars, it is balanced by neutrons' degeneracy pressure. A neutron star can also collapse to form a black hole if it is dense enough. If it is not much dense to form a black hole, there is a possibility of it turning into a quark star. The transition of neutron stars into quark stars has been discussed in the literature.[29] Quark stars are hypothetical compact objects composed of up, down and strange quarks. It is supposed that due to extreme temperature and pressure the nuclear matter dissolves into quarks.

In white dwarfs and neutron stars, pressure against the gravitational pull has the same origin, namely quantum pressure (Pauli principle). To study the compact objects in the framework of $f(R,T)$ gravity, we consider polytropic EoS $p=\omega\rho^{\frac{5}{3}}$, where ω is a constant (for white dwarfs and neutron stars) and MIT bag model $p=a(\rho-4\mathcal{B})$, where a and $\mathcal{B}$ are constants (for quark stars). These are the frequently used EoS for such compact objects in the literature.[23,24,30] In the following subsection, we discuss physical properties of these stars. Since we have a set of four differential equations (11)–(14) in five unknowns A, B, R, p and ρ, so EoS will be helpful to reduce one unknown.

3.1. *Equilibrium configuration of polytropic stars*

Here we discuss a polytropic star having EoS $p=\omega\rho^{\frac{5}{3}}$ and the constant ω is assigned the value $\omega=1.475\times10^{-3}(\mathrm{fm}^3/\mathrm{MeV})^{\frac{2}{3}}$.[23] Equations (11)–(14) for $\rho=(\frac{p}{\omega})^{\frac{3}{5}}$ become

$$A'=\frac{2rA^2}{3(1+2\alpha R)}\left[8\pi\left(\left(\frac{p}{\omega}\right)^{\frac{3}{5}}+3p\right)+2\lambda\left(\left(\frac{p}{\omega}\right)^{\frac{3}{5}}+2p\right)\right.$$
$$\left.+R\left(\frac{1}{2}-\frac{3\alpha\varphi}{rA}\right)-\frac{3\varphi}{2rA}-\frac{3\alpha R'}{A}\left(\varphi-\frac{2}{r}\right)\right], \tag{15}$$

$$\varphi'=\frac{2A'}{A}\left(\frac{2}{r}+\frac{\varphi}{4}\right)-\varphi\left(\frac{1}{r}+\frac{\varphi}{2}\right)-\frac{4\alpha A}{(1+2\alpha R)}\left[\frac{A^2}{2}-\frac{A'}{Ar}+\frac{R}{6\alpha}\right]$$
$$+\frac{2A}{(1+2\alpha R)}\left[\frac{8}{3}\pi\left(\frac{p}{\omega}\right)^{\frac{3}{5}}+\lambda\left(\frac{1}{2}\left(\frac{p}{\omega}\right)^{\frac{3}{5}}-\frac{2p}{3}\right)\right], \tag{16}$$

$$R''=\left(\frac{A'}{2A}-\frac{\varphi}{2}-\frac{2}{r}\right)R'+\frac{A}{6\alpha}\left(R+2(4\pi+\lambda)\left(3p-\left(\frac{p}{\omega}\right)^{\frac{3}{5}}\right)\right.$$
$$\left.-\left(\left(\frac{p}{\omega}\right)^{\frac{3}{5}}+p\right)\lambda\right), \tag{17}$$

$$p'=\frac{-\left(\left(\frac{p}{\omega}\right)^{\frac{3}{5}}+p\right)\varphi}{2\left[1-\frac{\lambda}{2(8\pi+\lambda)}\left(\frac{3}{5\omega}\left(\frac{p}{\omega}\right)^{\frac{-2}{5}}-1\right)\right]}. \tag{18}$$

Now, we discuss the initial conditions required to integrate the above system of differential equations. The pressure and density of a compact object are regular and finite at all points. Imposing this condition at the center $r=0$, we have from the field equations $A(0) = 1, A'(0) = 0, \varphi(0) = 0$ and $R'(0) = 0$.[24] Also, $\rho(0) = \rho_i$ and $p(0) = p_i$, where ρ_i and p_i are some initial values at the center which we fix for numerical analysis. To solve the system, we also require the value of Ricci scalar at the center, i.e. $R(0)$. Thus, we have three free initial conditions, $\rho(0)$, $p(0)$ and $R(0)$. Consideration of EoS reduce one condition such that we require only the values of $p(0)$ and $R(0)$. For both cases, we use the following initial conditions

$$\begin{aligned} &A(0) = 1, \quad \varphi(0) = 0, \quad P(0) = 100\,\mathrm{MeV/fm}^3, \\ &R(0) = 10^4\,\mathrm{MeV/fm}^3, \quad R'(0) = 0. \end{aligned} \tag{19}$$

Throughout this paper, we are taking the units of radius as km, mass as $M_\odot$ and density (pressure, Ricci scalar) as MeV/fm^3.[23]

We solve Eqs. (15)–(18) numerically using the above-mentioned initial conditions and investigate the effects of model parameters α and λ. The plots of metric function, Ricci scalar, energy density, pressure, dominant energy condition, mass function, redshift parameter and speed of sound for this EoS are shown in Figs. 1–3.

In the left columns of these figures, $\lambda = -10$ and α is varied whereas in the right columns, $\alpha = 10(\mathrm{MeV/fm}^3)^{-1}$ and λ is varied. The initial conditions and the values of constants are chosen such that we have positive values of density, pressure and mass as well as maximum values of density, pressure and curvature scalar at the center of the star. The plots of the metric functions A, B and Ricci scalar R are shown in Fig. 1. From the first row, we observe that B decreases as α increases while increase in λ yields larger values of B, but as the radial coordinate increases, B attains smaller values for larger λ. Similarly, the second row shows that A decreases with increase in α and increases with increase in λ. The Ricci scalar decreases with increase in radius of star but it decreases rapidly till the boundary of star as compared to the exterior of star. Also, it increases for an increase in α as well as λ.

The first row of Fig. 2 shows that energy density increases with the increase in α while it decreases with increase in λ. The plots in the second row show that $p = 0$ for $\alpha = 10(\mathrm{MeV/fm}^3)^{-1}$ and $\lambda = -10$ at $r \approx 11.4\,\mathrm{km}$. Thus, the polytropic star with $\alpha = 10(\mathrm{MeV/fm}^3)^{-1}$ and $\lambda = -10$ has the radius approximately 11.4 km. The authors[23] showed that the star has the radius approximately $r \approx 12\,\mathrm{km}$ for the same EoS with model $f(R,T) = R + 2\lambda T$ with different values of λ. For our model, pressure increases with increase in α and decreases with increase in λ. However, the radius of the star remains the same for different values of λ and vary as α varies. The energy conditions are $\rho + p \geq 0$ (null energy condition), $\rho \geq 0, \rho + p \geq 0$ (weak energy condition), $\rho - p \geq 0$ (dominant energy condition) and $\rho + 3p \geq 0$ (strong energy condition) which confirm the viability of matter. The null, weak and strong energy conditions are satisfied in this case because ρ and p are positive as shown in first and second rows of Fig. 2. Moreover, the dominant energy condition is also satisfied as observed from the last row of Fig. 2.

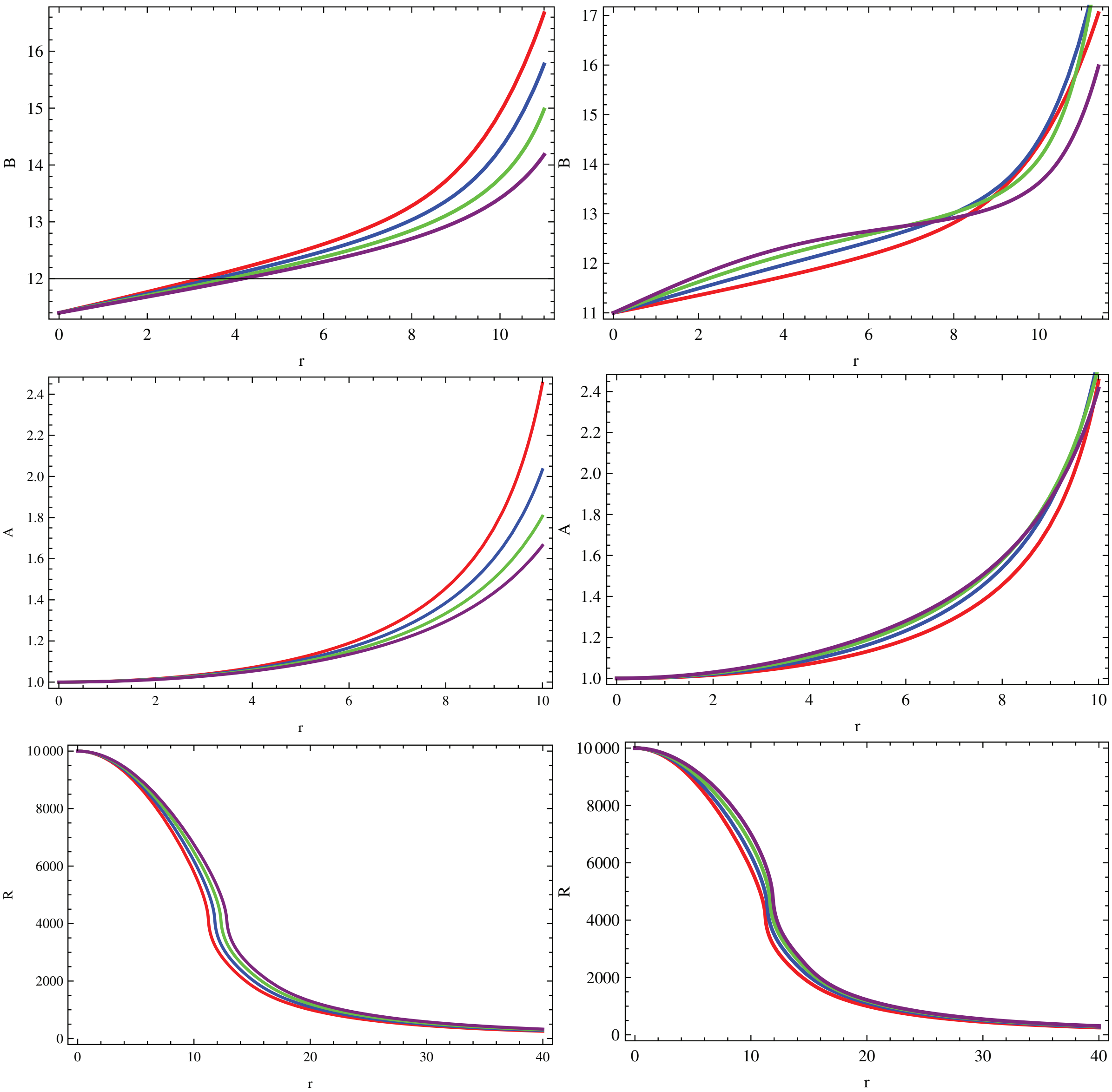

Fig. 1. (Color online) Plots of A, B and R versus r for $p = \omega\rho^{\frac{5}{3}}$, $\omega = 1.475 \times 10^{(-3)}$ $(\mathrm{fm}^3/\mathrm{MeV})^{(2/3)}$. In the left column $\lambda = -10$, $\alpha = 10(\mathrm{MeV}/\mathrm{fm}^3)^{-1}$ (red), $\alpha = 11(\mathrm{MeV}/\mathrm{fm}^3)^{-1}$ (blue), $\alpha = 12(\mathrm{MeV}/\mathrm{fm}^3)^{-1}$ (green) and $\alpha = 13(\mathrm{MeV}/\mathrm{fm}^3)^{-1}$ (purple) while in the right column $\alpha = 10(\mathrm{MeV}/\mathrm{fm}^3)^{-1}$, $\lambda = -10$ (red), $\lambda = -9$ (blue), $\lambda = -8$ (green) and $\lambda = -7$ (purple).

The first row of Fig. 3 indicates the behavior of mass function

$$m(r) = \frac{r}{2}\left(1 - \frac{1}{A(r)}\right), \tag{20}$$

which increases with radius of the star. Also, mass of the star decreases with increase in α while for increase in λ, it first shows an increase but for larger values of r, it shows an opposite behavior. The compactness factor and surface gravitational redshift are defined as

$$u(r) = \frac{m(r)}{r}, \tag{21}$$

$$z_s = (1 - 2u(R_b))^{-\frac{1}{2}} - 1, \tag{22}$$

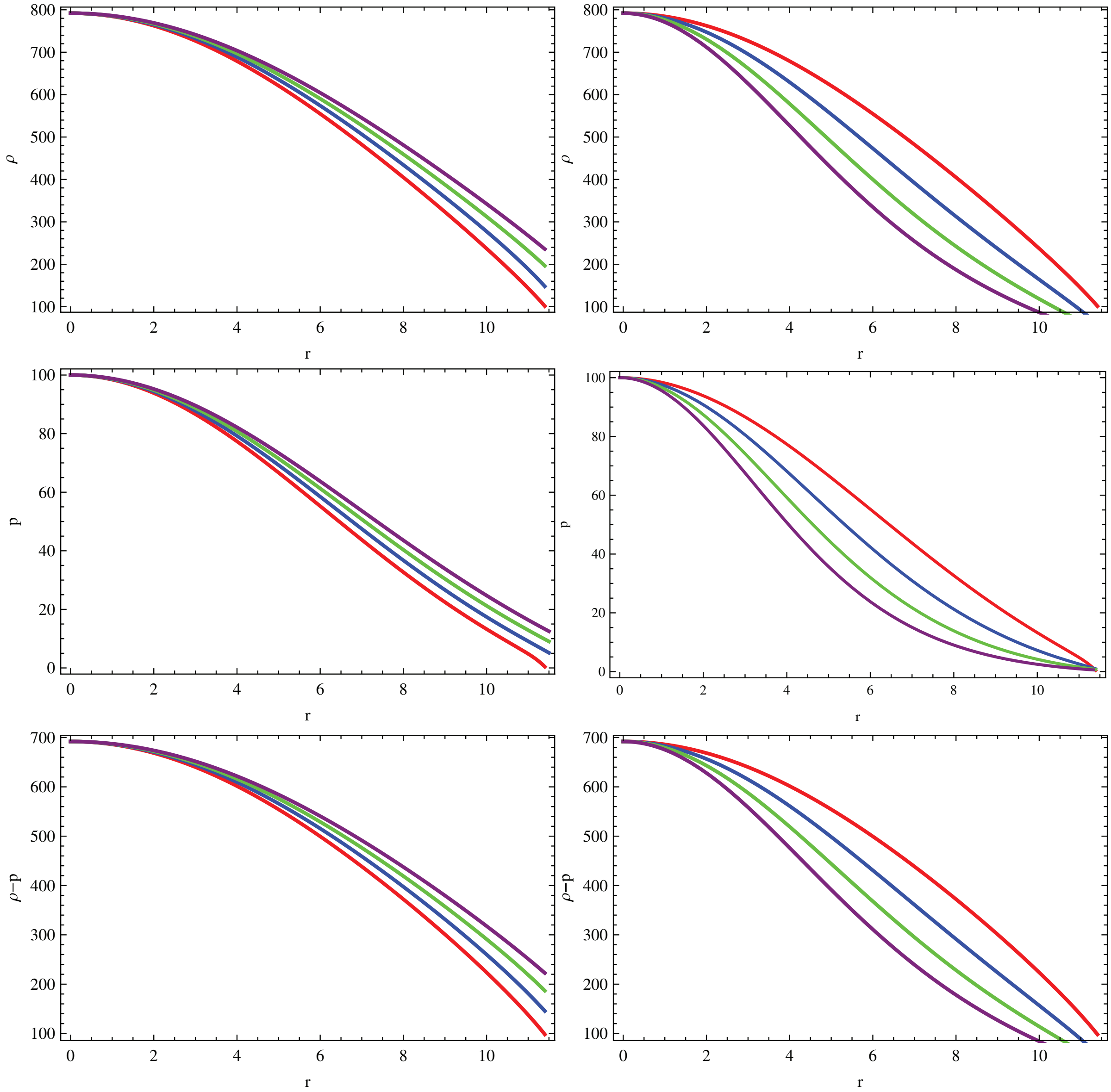

Fig. 2. (Color online) Plots of ρ, p and $\rho - p$ versus r for $p = \omega\rho^{\frac{5}{3}}$, $\omega = 1.475 \times 10^{(-3)}$ $(\text{fm}^3/\text{MeV})^{(2/3)}$. In the left column $\lambda = -10$, $\alpha = 10(\text{MeV/fm}^3)^{-1}$ (red), $\alpha = 11(\text{MeV/fm}^3)^{-1}$ (blue), $\alpha = 12(\text{MeV/fm}^3)^{-1}$ (green) and $\alpha = 13(\text{MeV/fm}^3)^{-1}$ (purple) while in the right column $\alpha = 10(\text{MeV/fm}^3)^{-1}$, $\lambda = -10$ (red), $\lambda = -9$ (blue), $\lambda = -8$ (green) and $\lambda = -7$ (purple).

here R_b is the total radius of the star. The second and third rows of this figure give the behavior of compactness $u(r)$ and surface gravitational redshift z_s, respectively. Both increase with radial coordinate and λ while decrease with α. The speed of sound ($v_s^2 = \frac{dp}{d\rho}$) for this EoS lies within the range $0 \leq v_s^2 \leq 1$ as shown in Fig. 4 implying that the polytropic stars are stable (for the chosen initial conditions and model parameters) in $f(R,T)$ gravity.

3.2. *Equilibrium configuration of quark stars*

This section deals with the physical properties of quark stars governed by EoS $p = a(\rho - 4\mathcal{B})$ with constants $a = 0.28$ and $\mathcal{B} = 60\,\text{MeV/fm}^3$.[23] Substituting

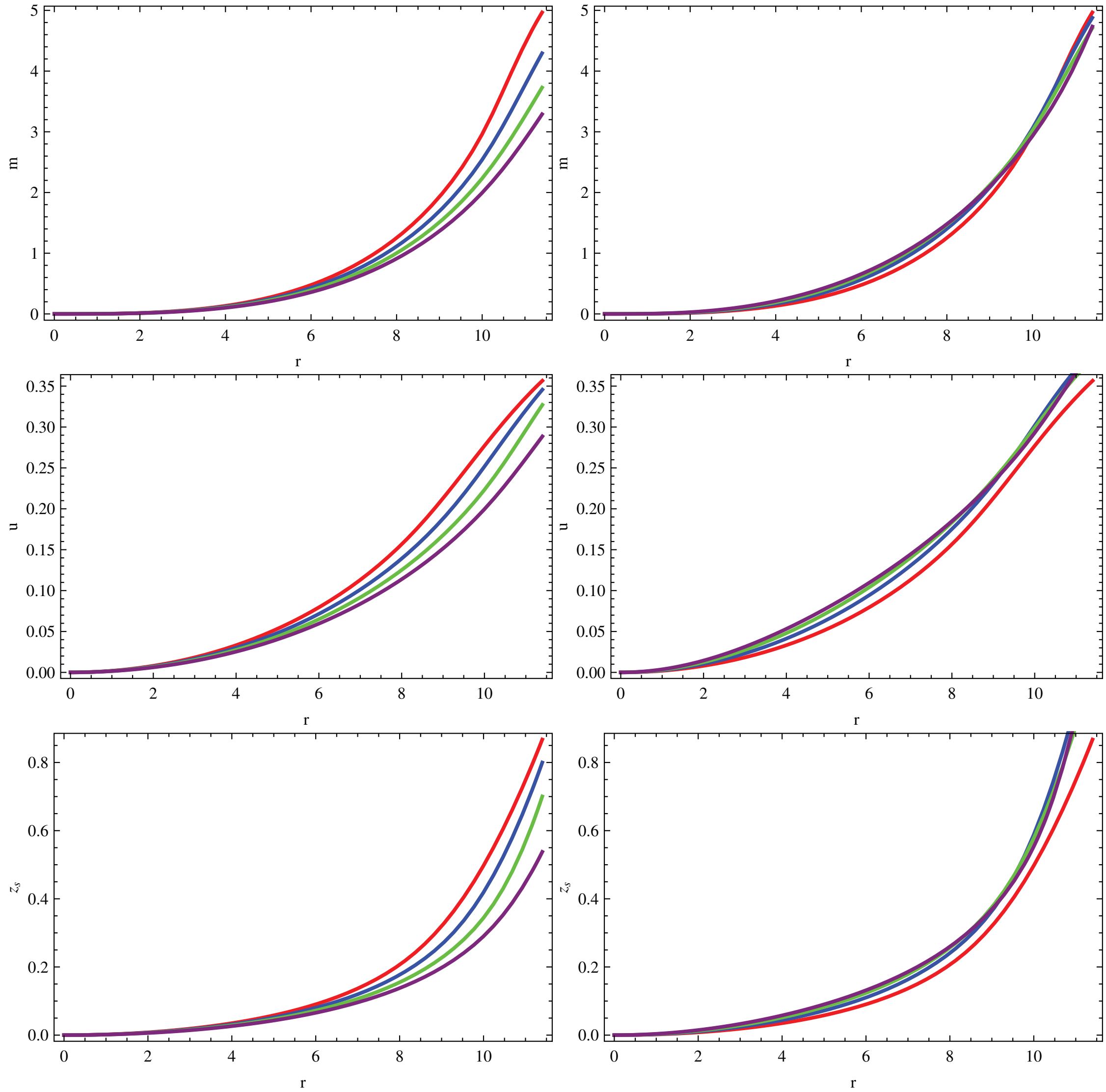

Fig. 3. (Color online) Plots of m, u and z_s versus r for $p = \omega\rho^{\frac{5}{3}}$, $\omega = 1.475 \times 10^{(-3)}$ $(\mathrm{fm}^3/\mathrm{MeV})^{(2/3)}$. In the left column $\lambda = -10$, $\alpha = 10(\mathrm{MeV}/\mathrm{fm}^3)^{-1}$ (red), $\alpha = 11(\mathrm{MeV}/\mathrm{fm}^3)^{-1}$ (blue), $\alpha = 12(\mathrm{MeV}/\mathrm{fm}^3)^{-1}$ (green) and $\alpha = 13(\mathrm{MeV}/\mathrm{fm}^3)^{-1}$ (purple) while in the right column $\alpha = 10(\mathrm{MeV}/\mathrm{fm}^3)^{-1}$, $\lambda = -10$ (red), $\lambda = -9$ (blue), $\lambda = -8$ (green) and $\lambda = -7$ (purple).

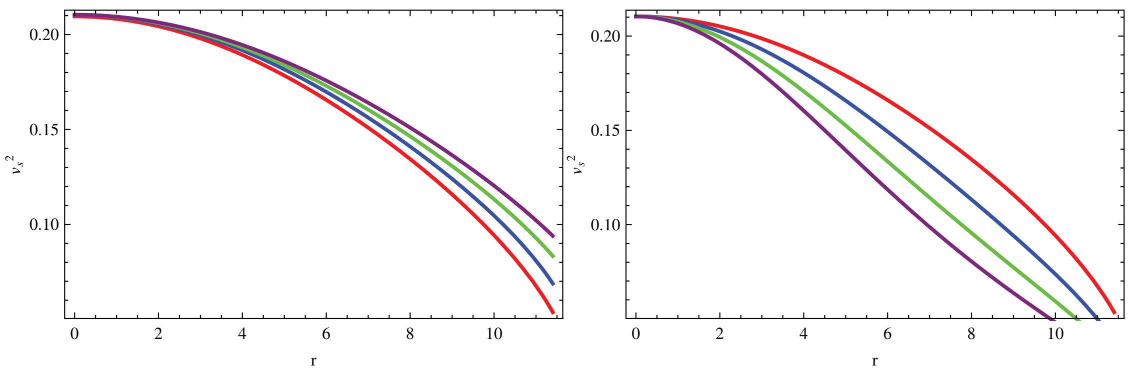

Fig. 4. (Color online) Plots of v_s^2 versus r for $p = \omega\rho^{\frac{5}{3}}$, $\omega = 1.475 \times 10^{(-3)}(\mathrm{fm}^3/\mathrm{MeV})^{(2/3)}$. In the left graph $\lambda = -10$, $\alpha = 10(\mathrm{MeV}/\mathrm{fm}^3)^{-1}$ (red), $\alpha = 11(\mathrm{MeV}/\mathrm{fm}^3)^{-1}$ (blue), $\alpha = 12(\mathrm{MeV}/\mathrm{fm}^3)^{-1}$ (green) and $\alpha = 13(\mathrm{MeV}/\mathrm{fm}^3)^{-1}$ (purple) while in the right graph $\alpha = 10(\mathrm{MeV}/\mathrm{fm}^3)^{-1}$, $\lambda = -10$ (red), $\lambda = -9$ (blue), $\lambda = -8$ (green) and $\lambda = -7$ (purple).

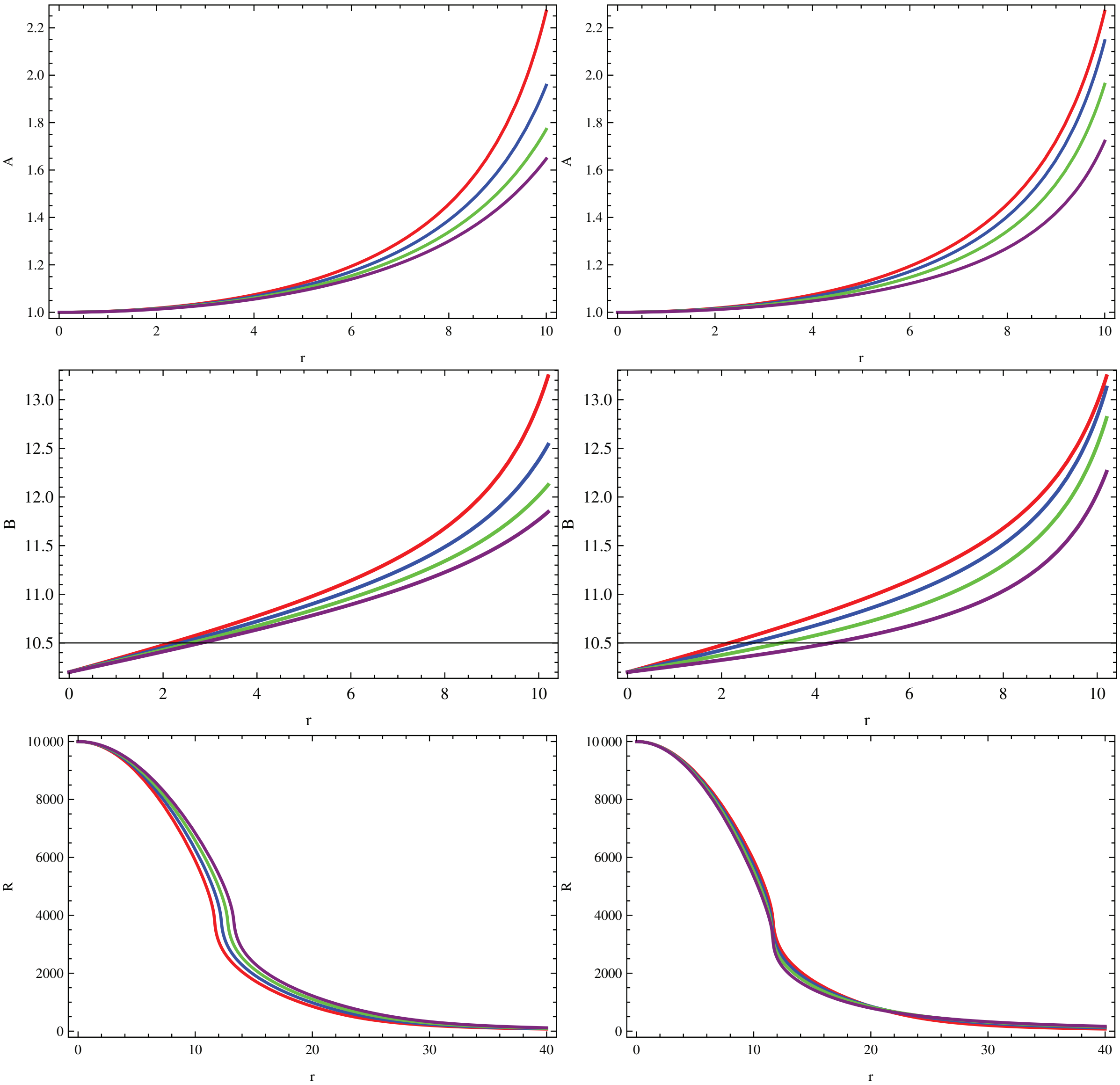

Fig. 5. (Color online) Plots of A, B and R versus r for $p = a(\rho - 4\mathcal{B})$, $a = 0.28$, $\mathcal{B} = 60\,\mathrm{MeV/fm^3}$. In left column $\lambda = -10$, $\alpha = 10(\mathrm{MeV/fm^3})^{-1}$ (red), $\alpha = 11(\mathrm{MeV/fm^3})^{-1}$ (blue), $\alpha = 12(\mathrm{MeV/fm^3})^{-1}$ (green) and $\alpha = 13(\mathrm{MeV/fm^3})^{-1}$ (purple) while in right column $\alpha = 10(\mathrm{MeV/fm^3})^{-1}$, $\lambda = -10$ (red), $\lambda = -10.5$ (blue), $\lambda = -11$ (green) and $\lambda = -11.5$ (purple).

$\rho = (\frac{p}{a} + 4\mathcal{B})$, Eqs. (11)–(14) give

$$A' = \frac{2rA^2}{3(1+2\alpha R)}\left[8\pi\left(\left(\frac{p}{a}+4\mathcal{B}\right)+3p\right)+2\lambda\left(\left(\frac{p}{a}+4\mathcal{B}\right)+2p\right)\right.$$
$$\left. + R\left(\frac{1}{2}-\frac{3\alpha\varphi}{rA}\right)-\frac{3\varphi}{2rA}-\frac{3\alpha R'}{A}\left(\varphi-\frac{2}{r}\right)\right], \tag{23}$$

$$\varphi' = \frac{2A'}{A}\left(\frac{2}{r}+\frac{\varphi}{4}\right)-\varphi\left(\frac{1}{r}+\frac{\varphi}{2}\right)-\frac{4\alpha A}{(1+2\alpha R)}\left[\frac{A^2}{2}-\frac{A'}{Ar}+\frac{R}{6\alpha}\right]$$
$$+\frac{2A}{(1+2\alpha R)}\left[\frac{8}{3}\pi\left(\frac{p}{a}+4\mathcal{B}\right)+\lambda\left(\frac{1}{2}\left(\frac{p}{a}+4\mathcal{B}\right)-\frac{2p}{3}\right)\right], \tag{24}$$

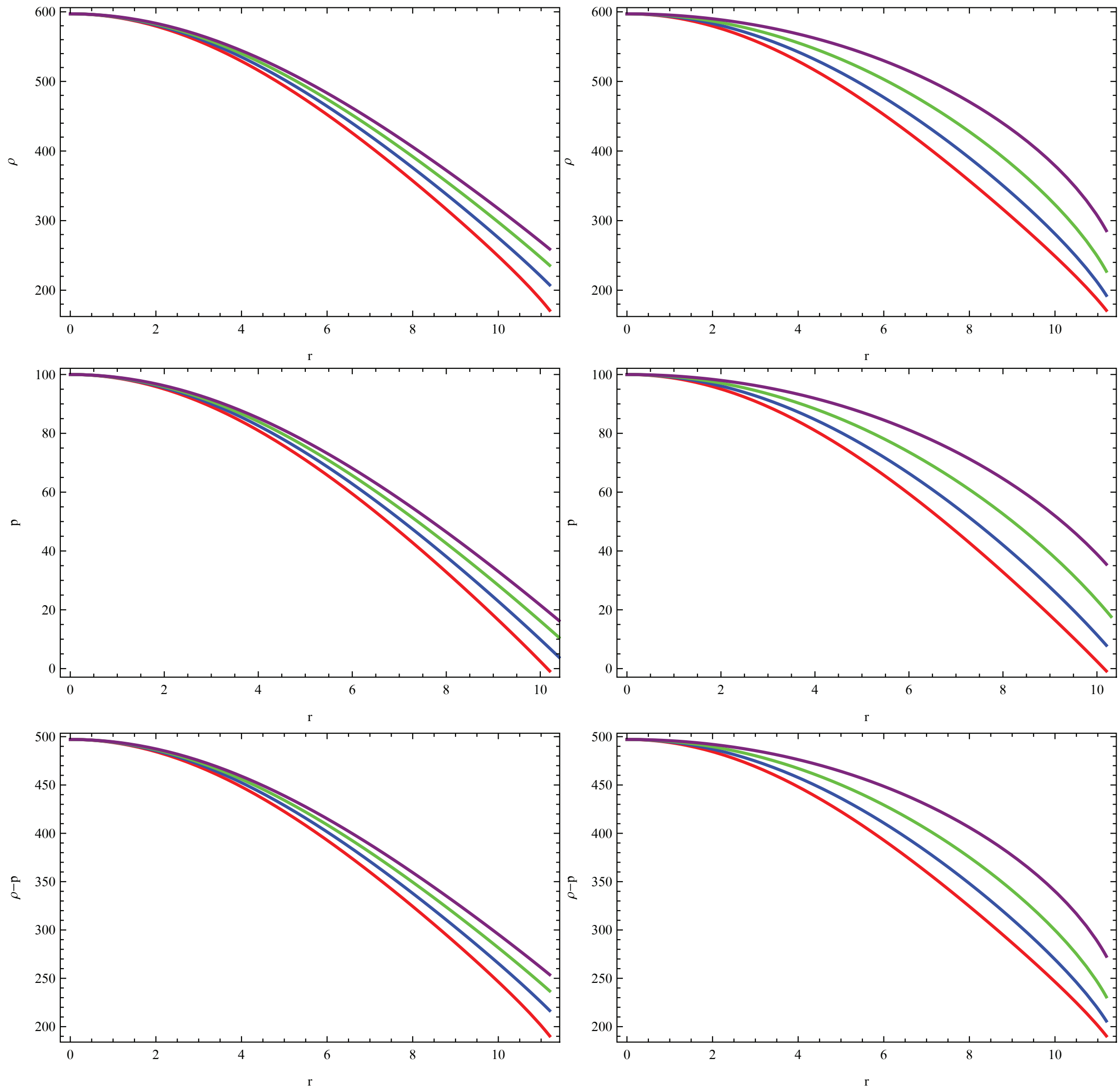

Fig. 6. (Color online) Plots of ρ, p and $\rho - p$ versus r for $p = a(\rho - 4\mathcal{B})$, $a = 0.28$, $\mathcal{B} = 60\,\mathrm{MeV/fm^3}$. In left column $\lambda = -10$, $\alpha = (\mathrm{MeV/fm^3})^{-1}$ (red), $\alpha = 11(\mathrm{MeV/fm^3})^{-1}$ (blue), $\alpha = 12(\mathrm{MeV/fm^3})^{-1}$ (green) and $\alpha = 13(\mathrm{MeV/fm^3})^{-1}$ (purple) while in right column $\alpha = 10(\mathrm{MeV/fm^3})^{-1}$, $\lambda = -10$ (red), $\lambda = -10.5$ (blue), $\lambda = -11$ (green) and $\lambda = -11.5$ (purple).

$$R'' = \left(\frac{A'}{2A} - \frac{\varphi}{2} - \frac{2}{r}\right) R' + \frac{A}{6\alpha}\left(R + 2(4\pi + \lambda)\left(3p - \left(\frac{p}{a} + 4\mathcal{B}\right)\right)\right.$$
$$\left. - \left(\left(\frac{p}{a} + 4\mathcal{B}\right) + p\right)\lambda\right), \tag{25}$$

$$p' = \frac{-\left(\left(\frac{p}{a} + 4\mathcal{B}\right) + p\right)\varphi}{2\left[1 - \frac{\lambda}{2(8\pi + \lambda)}\left(\frac{1}{a} - 1\right)\right]}. \tag{26}$$

Imposing the same initial conditions, we obtain numerical solution of the above system of differential equations. The values of model parameter α remain the same while the values of λ are taken different from the previous case so that we have

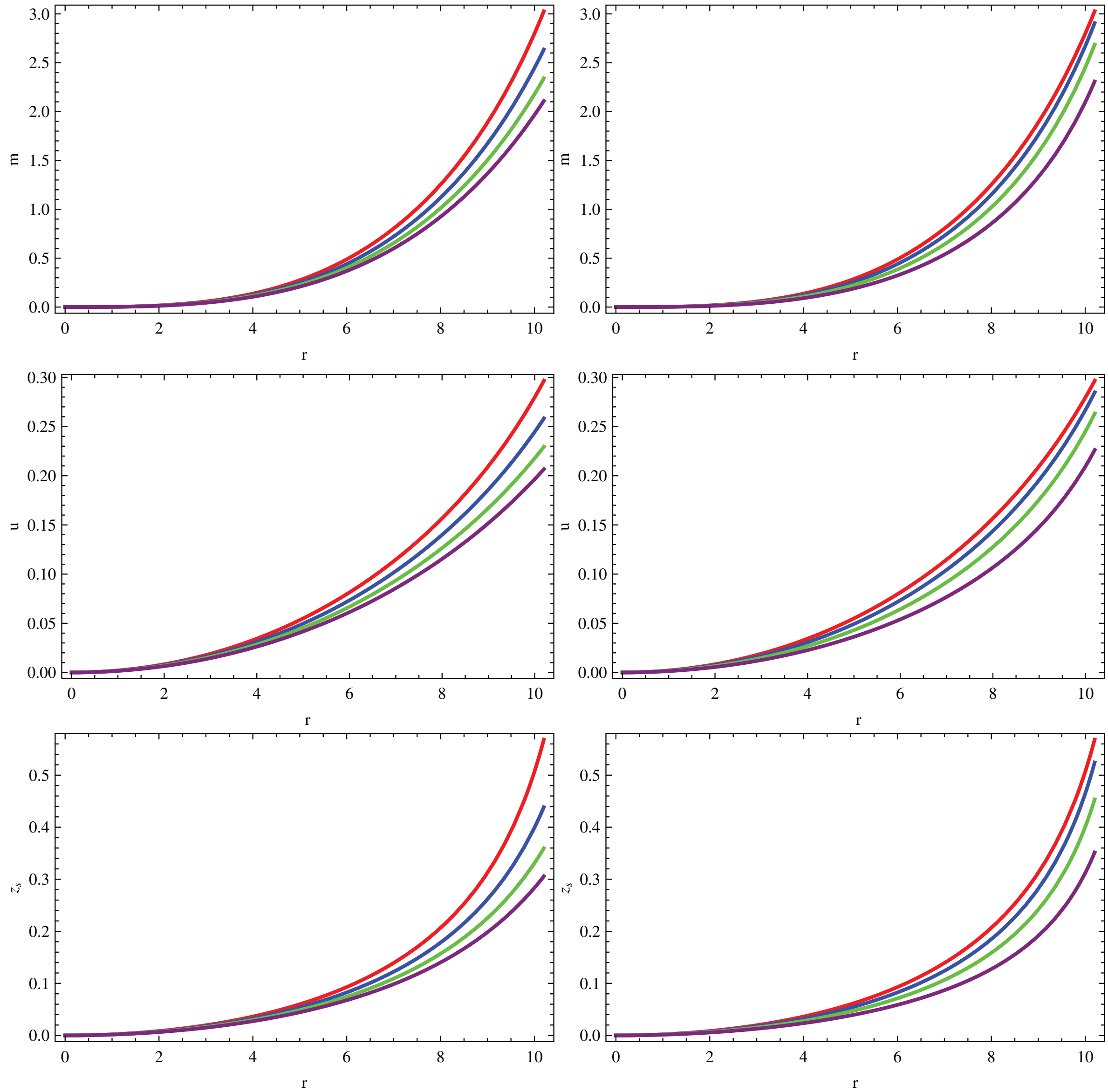

Fig. 7. (Color online) Plots of m, u and z_s versus r for $p = a(\rho - 4\mathcal{B})$, $a = 0.28$, $\mathcal{B} = 60\,\text{MeV/fm}^3$. In left column, $\lambda = -10$, $\alpha = 10(\text{MeV/fm}^3)^{-1}$ (red), $\alpha = 11(\text{MeV/fm}^3)^{-1}$ (blue), $\alpha = 12(\text{MeV/fm}^3)^{-1}$ (green) and $\alpha = 13(\text{MeV/fm}^3)^{-1}$ (purple) while in right column, $\alpha = 10(\text{MeV/fm}^3)^{-1}$, $\lambda = -10$ (red), $\lambda = -10.5$ (blue), $\lambda = -11$ (green) and $\lambda = -11.5$ (purple).

viable pressure, density and curvature scalar. The effect of model parameters (α, λ) on A, B and R is similar to the previous case as shown in Fig. 5. The pressure is zero at $r \approx 10.2\,\text{km}$ as observed from the first row of Fig. 6 for $\alpha = 10(\text{MeV/fm}^3)^{-1}$ and $\lambda = -10$. This indicates that increase in α increases density and pressure while increase in λ produces opposite effects by decreasing pressure and density. This also shows that energy conditions are satisfied for quark star EoS with the considered model. The behavior of mass function, compactness and gravitational redshift are shown in Fig. 7 where the model parameters affect in the same way as in the previous case. However, the speed of sound remains constant ($v_s^2 \approx 0.28$) with respect to radius for $\alpha = 10(\text{MeV/fm}^3)^{-1}$ as well as $\lambda = -10$ and increase or decrease in these parameters does not affect v_s^2.

4. Concluding Remarks

This paper is devoted to explore physical features of compact objects for $f(R,T) = R + \alpha R^2 + \lambda T$ gravity model with two EoS (polytropic and MIT bag model). The geometrical and physical quantities for polytropic as well as quark stars have been examined for different values of model parameters. The mass function grows for quark stars with the increase of λ while for polytropic stars, it first enhances mass but as r increases, it exhibits an opposite behavior. In both cases, pressure increases with λ while radius only increases for quark stars but remains the same for polytropic stars. However, for the model $f(R,T) = R + 2\lambda T$, it is observed that[23] for neutron star, larger values of λ enhance mass as well as radius while for quark star, it produces larger mass but smaller radius. This difference may be due to the presence of the term αR^2 in our model. The values of constants appearing in EoS of polytropic (white dwarfs and neutron stars) and quark stars remain the same as in Ref. 23 for the sake of comparison. The mass and gravitational redshift tend to decrease with increase in α which is consistent with the behavior of α as discussed in Ref. 24.

It is found that the star observed through polytropic EoS has approximately the radius $R_b \approx 11.4\,\text{km}$, mass $m(R_b) = 5M_\odot$, compactness $u(R_b) \approx 0.36$ and gravitational redshift $z_s \approx 0.84$ (for $\alpha = 10(\text{MeV/fm}^3)^{-1}$ and $\lambda = -10$). On the other hand, the MIT bag model in the same scenario leads to a quark star having radius $R_b = 10.2\,\text{km}$, mass $m(R_b) = 3M_\odot$, $u(R_b) \approx 0.30$ and $z_s \approx 0.57$. The redshift parameter and compactness factor for polytropic as well as quark stars lies within the limit defined for perfect fluid configurations.[5] We have found that the energy conditions are satisfied for both EoS and speed of sound is between zero and one. This means that the stars for both cases are stable. We conclude that the polytropic star has greater radius, mass and redshift parameter than quark star for the assumed fluid configuration as well as initial conditions in this theory.

There are upper limits on the masses of white dwarfs and neutron stars in GR. According to Chandrasekhar,[15] the maximum mass limit of a white dwarf to produce sufficient electron degeneracy pressure against collapse is $1.4M_\odot$. Similar to this, the Tolman–Oppenheimer–Volkoff limit[31] gives an upper bound of $3M_\odot$ for the mass of a neutron star to counter balance gravity by neutron degeneracy pressure. However, our analysis provides a possibility that there may exist stable stellar structures having masses above these limits. Also, it is shown in Ref. 23 that the growing mass with enhancement of λ can cross the observational limits in $f(R,T)$ theory.

Acknowledgment

We would like to thank the Higher Education Commission, Islamabad, Pakistan for its financial support through the *Indigenous Ph.D. Fellowship for 5000 Scholars, Phase-II, Batch-III.*

References

1. D. J. Eicher, *The New Cosmos Answering Astronomy's Big Questions* (Cambridge University Press, 2015), p. 208.
2. S. W. Hawking, *Phys. Rev. Lett.* **26** (1971) 1344.
3. R. V. Wagoner, *Astrophys. J.* **278** (1984) 345.
4. J. Herman, M. Cuesta and J. M. Salim, *Astrophys. J.* **608** (2004) 925.
5. H. A. Buchdahl, *Phys. Rev.* **116** (1959) 1027.
6. B. V. Ivanov, *Phys. Rev. D* **65** (2002) 104011.
7. G. Böhmer and T. Harko, *Class. Quantum Grav.* **23** (2006) 6479.
8. K. Boshkayev, H. Quevedo and R. Ruffini, *Phys. Rev. D* **86** (2012) 064043.
9. A. De Felice and S. Tsujikawa, *Living Rev. Rel.* **13** (2010) 3.
10. T. Harko, F. S. N. Lobo, S. Nojiri and S. D. Odintsov, *Phys. Rev. D* **84** (2011) 024020.
11. T. Harko and F. S. N. Lobo, *Galaxies* **2** (2014) 410.
12. M. Jamil *et al.*, *Eur. Phys. J. C* **72** (2012) 1999.
13. M. Sharif and M. Zubair, *J. Cosmol. Astropart. Phys.* **03** (2012) 28.
14. M. Sharif and I. Nawazish, *Eur. Phys. J. C* **77** (2017) 198.
15. S. L. Shapiro and S. A. Teukolsky, *Black Holes, White Dwarfs and Neutron Stars The Physics of Compact Objects* (John Wiley and Sons, 1983), p. 258.
16. H. Abreu, H. Hernández and L. A. Núñez, *Class. Quantum Grav.* **24** (2007) 4631.
17. N. Jiang and M. Gleiser, *Entropy* **20** (2015) 2.
18. G. Abbas and S. Sarwar, *Astrophys. Space Sci.* **352** (2014) 769.
19. M. Sharif and Z. Yousaf, *Astrophys. Space Sci.* **354** (2014) 471.
20. I. Noureen and M. Zubair, *Astrophys. Space Sci.* **356** (2015) 103.
21. M. Zubair, G. Abbas and I. Noureen, *Astrophys. Space Sci.* **361** (2016) 8.
22. Z. Yousaf, M. Z. Bhatti and U. Farwa, *Class. Quantum Grav.* **34** (2017) 145002.
23. P. H. R. S. Moraes, D. V. A. José and M. Malheiro, *J. Cosmol. Astropart. Phys.* **06** (2016) 005.
24. A. V. Astashenok, A. de la Cruz-Dombriz and S. D. Odintsov, *Class. Quantum Grav.* **34** (2017) 205008.
25. G. A. Carvalho *et al.*, *Eur. Phys. J. C* **77** (2017) 871.
26. A. A. Starobinsky, *Phys. Lett. B* **91** (1980) 99.
27. P. H. R. S. Moraes, R. A. C. Correa and G. Ribeiro, arXiv:1701.01027.
28. J. Barrientos and G. F. Rubilar, *Phys. Rev. D* **90** (2014) 028501.
29. P. Haensel, J. L. Zdunik and R. Schaeffer, *Astron. Astrophys.* **160** (1986) 121; N. K. Glendenning, *Phys. Rev. D* **46** (1992) 1274; J. M. Lattimer and M. Prakash, *Astrophys. J.* **550** (2001) 426.
30. M. K. Mak and T. Harko, *Int. J. Mod. Phys. D* **13** (2004) 149; F. Özel, G. Baym and T. Güver, *Phys. Rev. D* **82** (2010) 101301.
31. I. Bombaci, *Astron. Astrophys.* **305** (1996) 871.

Eur. Phys. J. Plus (2017) **132**: 529
DOI 10.1140/epjp/i2017-11810-4

THE EUROPEAN PHYSICAL JOURNAL PLUS

Regular Article

Study of charged stellar structures in f(R, T) gravity

M. Sharif[a] and Aisha Siddiqa[b]

Department of Mathematics, University of the Punjab, Quaid-e-Azam Campus, Lahore - 54590, Pakistan

Received: 25 October 2017 / Revised: 24 November 2017
Published online: 20 December 2017 – © Società Italiana di Fisica / Springer-Verlag 2017

Abstract. This paper explores charged stellar structures whose pressure and density are related through polytropic equation of state ($p = \omega\rho^\sigma$; ω is polytropic constant, p is pressure, ρ denotes density and σ is polytropic exponent) in the scenario of $f(R,T)$ gravity (where R is the Ricci scalar and T is the trace of energy-momentum tensor). The Einstein-Maxwell field equations are solved together with the hydrostatic equilibrium equation for $f(R,T) = R + 2\lambda T$ where λ is the coupling constant, also called model parameter. We discuss different features of such configurations (like pressure, mass and charge) using graphical behavior for two values of σ. It is found that the effects of model parameter λ on different quantities remain the same for both cases. The energy conditions are satisfied and stellar configurations are stable in each case.

1 Introduction

A star is a luminous sphere of plasma held together by its self-gravitation that undergoes gravitational collapse when it burns up its nuclear fuel. The end product of this collapse is a compact object depending upon the initial mass of the star. The compact object does not burn nuclear fuel and has extremely small size as compared to normal star. Stars with mass less than $8M_\odot$ ($M_\odot$ denotes solar mass) form a white dwarf while more massive stars form a neutron star or a black hole after collapse. White dwarfs and neutron stars exist in our universe and can be observed directly while the existence of black holes is confirmed by some ground based observations. Two compact objects orbiting each other can merge together and produce gravitational waves. Hawking [1] studied the gravitational radiation emitted by two merging black holes while Wagoner [2] explored the radiation produced by accreting neutron stars.

A polytropic star is a spherical symmetric self-gravitating stellar object satisfying the equation of state (EoS) $p = \omega\rho^\sigma$. These polytropic models provide a better approximation to reality in some situations like when the system is adiabatic (no heat transfer). In compact objects, there is a degeneracy pressure (a form of quantum degeneracy pressure following the Pauli exclusion principle that no two identical half-integer spin particles can have the same quantum state) of electrons or neutrons instead of thermal pressure to counter balance gravity. Thus polytropic EoS can be used to study compact objects. Tooper [3] was the first who discussed polytropic stars by formulating differential equations governing the stellar structure. He used the numerical method to solve these equations and found mass, pressure and density of polytropes. Polytropic EoS has frequently been discussed to study compact objects in literature [4–7].

Rosseland and Eddington [8] were the first who figured out that stars may have a net electric charge. After that many researchers explored the effects of an electromagnetic field on self-gravitating systems [9–11]. The electromagnetic radiations are redshifted or reduced in frequency if the observer is in a stronger gravitational field than the source producing the radiation. The maximum bound for the surface redshift parameter of static spherical configuration with perfect fluid is found to be $z \leq 2$ [12] while it is $z \leq 5.211$ for anisotropic models [13]. Böhmer and Harko [14] evaluated the upper and lower bounds for some physical parameters in the background of anisotropic matter distribution as well as in the presence of cosmological constant. They obtained redshift and total energy bounds in terms of anisotropic parameter and claimed that the redshift parameter is $2 \leq z \leq 5$ for anisotropic configurations.

A simple generalization of general relativity (GR) is the $f(R)$ gravity in which the Einstein-Hilbert action is modified by replacing the Ricci scalar with $f(R)$. Harko *et al.* [15] proposed $f(R,T)$ gravity as a generalized modified theory. The coupling of curvature and matter leads to a source term which may yield interesting results. It can produce a matter-dependent deviation from geodesic motion and also helps to study dark energy, dark matter interactions as well as

[a] e-mail: `msharif.math@pu.edu.pk`
[b] e-mail: `aisha.siddiqa17@yahoo.com`

late-time acceleration [16]. Sharif and Nawazish [17] worked on Noether symmetries interacting with a generalized scalar field model in this gravity. They found that dust fluid leads to decelerated expansion while perfect fluid yields current cosmic expansion for the quintessence model. We have studied the interaction of a modified Chaplygin gas with $f(R,T)$ gravity and found that the expansion is enhanced by bulk viscosity in intermediate as well as logamediate scenarios [18].

The stability of compact objects is an important issue in astrophysics and different methods like perturbation technique as well as speed of sound have been proposed to discuss stable fluid configurations. The matter is in stable state if $0 \leq v_s^2 \leq 1$, where v_s is the speed of sound [19]. Abreu *et al.* [20] provided an alternative approach to check the instability of anisotropic matter distributions. They showed that for unstable regions, the radial speed of sound is less than its tangential part. Sharif and Yousaf [21] investigated the stability of spheres in $f(R,T)$ gravity through perturbation technique and also discussed the role of matter variables. Jiang and Gleiser [22] found an accuracy in stability regions of astrophysical compact objects using configurational entropy than those obtained via perturbation method. Noureen and Zubair [23] explored the stability of anisotropic spherical star in the context of $f(R,T)$ yielding some constraints on physical quantities. Zubair *et al.* [24] studied stability, energy conditions and surface redshift for three observed models of compact stars in the same gravity using the Krori and Barua solution.

The physical features of compact objects in modified theories have widely been observed. Moraes *et al.* [25] studied the equilibrium configurations of neutron as well as quark stars and found that the extreme mass can cross observational limits. Astashenok *et al.* [26] discussed the existence of realistic models of stars in $f(R) = R + \alpha R^2$ gravity model. Carvalho *et al.* [27] investigated white dwarfs for the model $f(R,T) = R + 2\lambda T$ and found that mass can cross the Chandrasekhar limit.

In this paper, we study the physical features of charged compact objects having polytropic EoS in the framework of $f(R,T)$ gravity. The behavior of pressure, density, mass function, charge, electric field intensity and gravitational redshift of stellar objects is discussed. We also study energy conditions and stability of the resulting solution. The paper is organized as follows. In the next section, the Einstein-Maxwell equations are formulated for $f(R,T) = R+2\lambda T$ gravity. Section 3 investigates physical features of stellar objects considering polytropic EoS. Finally, we conclude our results in the last section.

2 Einstein-Maxwell field equations

The action for $f(R,T)$ theory in the presence of an electromagnetic field is defined as

$$S = \int \mathrm{d}^4x\sqrt{-g}\left[\frac{1}{16\pi}f(R,T) + \mathcal{L}_m + \mathcal{L}_e\right]. \tag{1}$$

Here $\mathcal{L}_e = mF_{\mu\nu}F^{\mu\nu}$, m is an arbitrary constant, $F_{\mu\nu} = \phi_{\nu,\mu} - \phi_{\mu,\nu}$ stands for electromagnetic field tensor, ϕ_μ represents the four-potential. The following field equations are obtained by varying this action with respect to $g_{\mu\nu}$:

$$f_R R_{\mu\nu} - \frac{1}{2}g_{\mu\nu}f + (g_{\mu\nu}\Box - \nabla_\mu\nabla_\nu)f_R = 8\pi T_{\mu\nu} - f_T(T_{\mu\nu} + \Theta_{\mu\nu}) + 8\pi E_{\mu\nu}, \tag{2}$$

where $f = f(R,T)$, $f_R = \frac{\partial f}{\partial R}$, $f_T = \frac{\partial f}{\partial T}$, $\Theta_{\mu\nu}$ is evaluated by

$$\Theta_{\mu\nu} = g^{\gamma\sigma}\frac{\delta T_{\gamma\sigma}}{\delta g^{\mu\nu}}, \qquad T_{\mu\nu} = g_{\mu\nu}\mathcal{L}_m - \frac{\partial\mathcal{L}_m}{\partial g^{\mu\nu}} \tag{3}$$

and $E_{\mu\nu}$ is the electromagnetic energy-momentum tensor defined by

$$E_{\mu\nu} = \frac{1}{4\pi}\left(F_\mu{}^\alpha F_{\nu\alpha} - \frac{1}{4}F^{\alpha\beta}F_{\alpha\beta}g_{\mu\nu}\right). \tag{4}$$

The spherically symmetric stellar configuration is described by the metric

$$\mathrm{d}s^2 = -B(r)\mathrm{d}t^2 + A(r)\mathrm{d}r^2 + r^2(\mathrm{d}\theta^2 + \sin^2\theta\mathrm{d}\phi^2), \tag{5}$$

the energy-momentum tensor of a perfect fluid is

$$T_{\mu\nu} = (\rho + p)V_\mu V_\nu + pg_{\mu\nu}, \tag{6}$$

where p denotes pressure and ρ represents energy density of the fluid, V_μ is the four-velocity satisfying $V_\mu V^\mu = -1$ and $T = 3p - \rho$. We take $\mathcal{L}_m = p$ and consequently $\Theta_{\mu\nu}$ becomes $\Theta_{\mu\nu} = -2T_{\mu\nu} + pg_{\mu\nu}$.

The Maxwell field equations are given by

$$F^{\mu\nu}{}_{;\nu} = 4\pi j^\mu, \tag{7}$$

where j^μ represents the four-current. We are considering a comoving frame in which charges are at rest and hence no magnetic field is produced. The four-potential and four-current in comoving coordinates are defined as

$$\phi_\mu = \phi(r)\delta^0_\mu, \qquad j_\mu = \xi(r)V^\mu, \tag{8}$$

$\phi(r)$ stands for electric scalar potential and $\xi(r)$ represents charge density. For the metric (5), the Maxwell field equations give

$$\phi'' + \phi'\left(\frac{2}{r} - \frac{A'}{2A} - \frac{B'}{2B}\right) = 4\pi\xi(r)A\sqrt{B}, \tag{9}$$

whose integration yields

$$\phi' = \frac{\sqrt{AB}q}{r^2}, \quad q = 4\pi\int_0^r \xi(r)\sqrt{A}r^2\mathrm{d}r, \tag{10}$$

where q denotes the total charge on the sphere with $\phi'(0) = 0$ [28].

We consider the model $R + 2\lambda T$ (which reduces to GR for $\lambda = 0$) proposed by Harko *et al.* [15] to study the effects of curvature-matter coupling. The term $2\lambda T$ induces time-dependent coupling (interaction) between curvature and matter. It also corresponds to ΛCDM model with a time-dependent cosmological constant. This model simplifies the field equations as

$$G_{\mu\nu} = 8\pi T_{\mu\nu} + 2\lambda T_{\mu\nu} - 2\lambda p g_{\mu\nu} + T g_{\mu\nu} + 8\pi E_{\mu\nu}, \tag{11}$$

which leads to the following set of field equations:

$$\frac{A'}{rA^2} + \frac{1}{r^2} - \frac{1}{r^2A} = 8\pi\rho + \frac{\phi'^2}{AB} + \lambda(3\rho - p), \tag{12}$$

$$\frac{B'}{rAB} - \frac{1}{r^2} + \frac{1}{r^2A} = 8\pi p - \frac{\phi'^2}{AB} + \lambda(3p - \rho), \tag{13}$$

$$\frac{-1}{4rA^2B^2}\left(2A'B^2 - 2B'AB - 2rB''BA + rB'^2A + rB'A'B\right) = 8\pi p + \frac{\phi'^2}{AB} + \lambda(3p - \rho). \tag{14}$$

The first two field equations can be written as

$$A' = rA^2\left[\frac{1}{r^2A} - \frac{1}{r^2} + 8\pi\rho + \lambda(3\rho - p) + \frac{\phi'^2}{AB}\right], \tag{15}$$

$$B' = rAB\left[-\frac{1}{r^2A} + \frac{1}{r^2} + 8\pi p + \lambda(3p - \rho) - \frac{\phi'^2}{AB}\right]. \tag{16}$$

The covariant divergence of the field equations yields [29]

$$\nabla^\mu T_{\mu\nu} = \frac{f_T}{8\pi - f_T}\left[(T_{\mu\nu} + \Theta_{\mu\nu})\nabla^\mu \ln f_T + \nabla^\mu\Theta_{\mu\nu} - \frac{1}{2}g_{\mu\nu}\nabla^\mu T - \frac{8\pi}{f_T}\nabla^\mu E_{\mu\nu}\right]. \tag{17}$$

For the model $f(R,T) = R + 2\lambda T$, the above equation gives

$$\nabla^\mu T_{\mu\nu} = \frac{\lambda}{8\pi + 2\lambda}\left[\nabla^\mu\Theta_{\mu\nu} - \frac{1}{2}g_{\mu\nu}\nabla^\mu T - \frac{4\pi}{\lambda}\nabla^\mu E_{\mu\nu}\right],$$

which yields the equation of hydrostatic equilibrium

$$p' + (\rho + p)\frac{B'}{2B} = \frac{\lambda}{(8\pi + 2\lambda)}\left[\rho' - p' + \frac{2\phi'}{r^2\sqrt{AB}}\left(\frac{r^2\phi'}{\sqrt{AB}}\right)'\right].$$

This can also be written as

$$p' = \frac{-(\rho + p)\frac{B'}{2B} + \frac{2\lambda}{(8\pi+2\lambda)}\frac{\phi'}{r^2\sqrt{AB}}\left(\frac{r^2\phi'}{\sqrt{AB}}\right)'}{\left[1 - \frac{\lambda}{(8\pi+2\lambda)}(\frac{d\rho}{dp} - 1)\right]}. \tag{18}$$

We have four eqs. (9), (15), (16) and (18) in six unknowns A, B, ρ, p, ϕ' and ξ. The charge density in terms of energy density can be expressed as [30]

$$\xi = \gamma\rho, \tag{19}$$

where γ is a constant. Further, the energy density is written in terms of pressure via EoS so that we have four differential equations in four unknowns (A, B, p and ϕ'). Now we discuss the initial conditions required to solve this system of eqs. (9), (15), (16) and (18). The pressure and density of a compact object are regular and finite at all points. Imposing this condition at the center $r=0$, we have from the field equations $A(0)=1$, $A'(0)=0$ and $B'(0)=0$. We have already defined the initial condition for ϕ', *i.e.*, $\phi'(0)=0$. So, We have two initial conditions $A(0)=1$ and $\phi'(0)=0$ while $B(0)$ and $p(0)$ are free to choose. For both cases, we use the following initial conditions

$$\begin{aligned} A(0) &= 1, \\ B(0) &= 5, \\ p(0) &= 100, \\ \phi'(0) &= 0. \end{aligned} \tag{20}$$

Throughout this paper, we are taking the units of radius as km, mass (and charge) as $M_\odot$ and density (and pressure) as MeV/fm^3 [25].

3 Polytropic stars

The polytropic EoS represents different stellar structures by varying σ. In this section, we consider the polytropic EoS for $\sigma=\frac{5}{3}$ and 2, to investigate the evolution of charged spherically symmetric configurations in $f(R,T)$ scenario. In general, for $\sigma=\frac{5}{3}$, it can correspond to stars in adiabatic convective equilibrium and the range $2\leq\sigma\leq 3$ can well describe the neutron stars [31]. We study the stellar structures modeled by these values in $f(R,T)$ theory.

3.1 Polytropic star for $\sigma=\frac{5}{3}$

Here we discuss polytropic star having EoS $p=\omega\rho^{\frac{5}{3}}$. Equations (9), (15), (16) and (18) for $\rho=(\frac{p}{\omega})^{\frac{3}{5}}$ become

$$\phi''+\phi'\left(\frac{2}{r}-\frac{A'}{2A}-\frac{B'}{2B}\right)=4\pi\gamma\left(\frac{p}{\omega}\right)^{\frac{3}{5}}A\sqrt{B}, \tag{21}$$

$$A'=rA^2\left[\frac{1}{r^2A}-\frac{1}{r^2}+8\pi\left(\frac{p}{\omega}\right)^{\frac{3}{5}}+\lambda\left(3\left(\frac{p}{\omega}\right)^{\frac{3}{5}}-p\right)+\frac{\phi'^2}{AB}\right], \tag{22}$$

$$B'=rAB\left[-\frac{1}{r^2A}+\frac{1}{r^2}+8\pi p+\lambda\left(3p-\left(\frac{p}{\omega}\right)^{\frac{3}{5}}\right)-\frac{\phi'^2}{AB}\right], \tag{23}$$

$$p'=\frac{-\left((\frac{p}{\omega})^{\frac{3}{5}}+p\right)\frac{B'}{2B}+\frac{2\lambda}{(8\pi+2\lambda)}\frac{\phi'}{r^2\sqrt{AB}}\left(\frac{r^2\phi'}{\sqrt{AB}}\right)'}{\left[1-\frac{\lambda}{(8\pi+2\lambda)}\left(\frac{3}{5\omega}(\frac{p}{\omega})^{\frac{-2}{5}}-1\right)\right]}. \tag{24}$$

We solve eqs. (21)–(24) numerically using the above-mentioned initial conditions and investigate the effects of model parameter λ. The plots of the metric functions, energy density, pressure, speed of sound, mass function, redshift parameter, charge, electric field intensity and energy conditions for this EoS are shown in figs. 1–4.

The initial conditions and values of constants are chosen such that we have positive values of density, pressure and mass as well as maximum values of density and pressure at the center of the star. The viability condition for our model yields $\lambda>-4\pi$, hence for graphical analysis we consider values of λ within this range. The plots of the metric functions B, A, ρ, p and v_s are shown in fig. 1. The first graph shows that B increases with increase in radial coordinate and decrease in λ. The scale in the plot of A is greater than 1 but $A(0)=1$, so it first increases and then starts decreasing with the radius. Also, as λ decreases, A increases. The pressure is zero at $r\approx 1.5$ suggesting that this is the radius of a charged polytropic star in this case. The speed of sound ($v_s^2=\frac{\mathrm{d}p}{\mathrm{d}\rho}$) for this EoS lies within the range $0\leq v_s^2\leq 1$ implying that the polytropic star with $\sigma=\frac{5}{3}$ is stable (for the chosen initial conditions and model parameters) for our model. The decrease in model parameter increases the quantities ρ, p and v_s.

The energy conditions for the curvature-matter coupled gravity are modified as [32] $\rho+p-\mathcal{A}\geq 0$ (null energy condition), $\rho-\mathcal{A}\geq 0$, $\rho+p-\mathcal{A}\geq 0$ (weak energy condition), $\rho-p-\mathcal{A}\geq 0$ (dominant energy condition) and $\rho+3p\geq 0$ (strong energy condition) which confirm the viability of matter. The term $\mathcal{A}$ is the covariant derivative of acceleration which appears due to non-geodesic trajectories of massive particles (due to the presence of non-gravitational force).

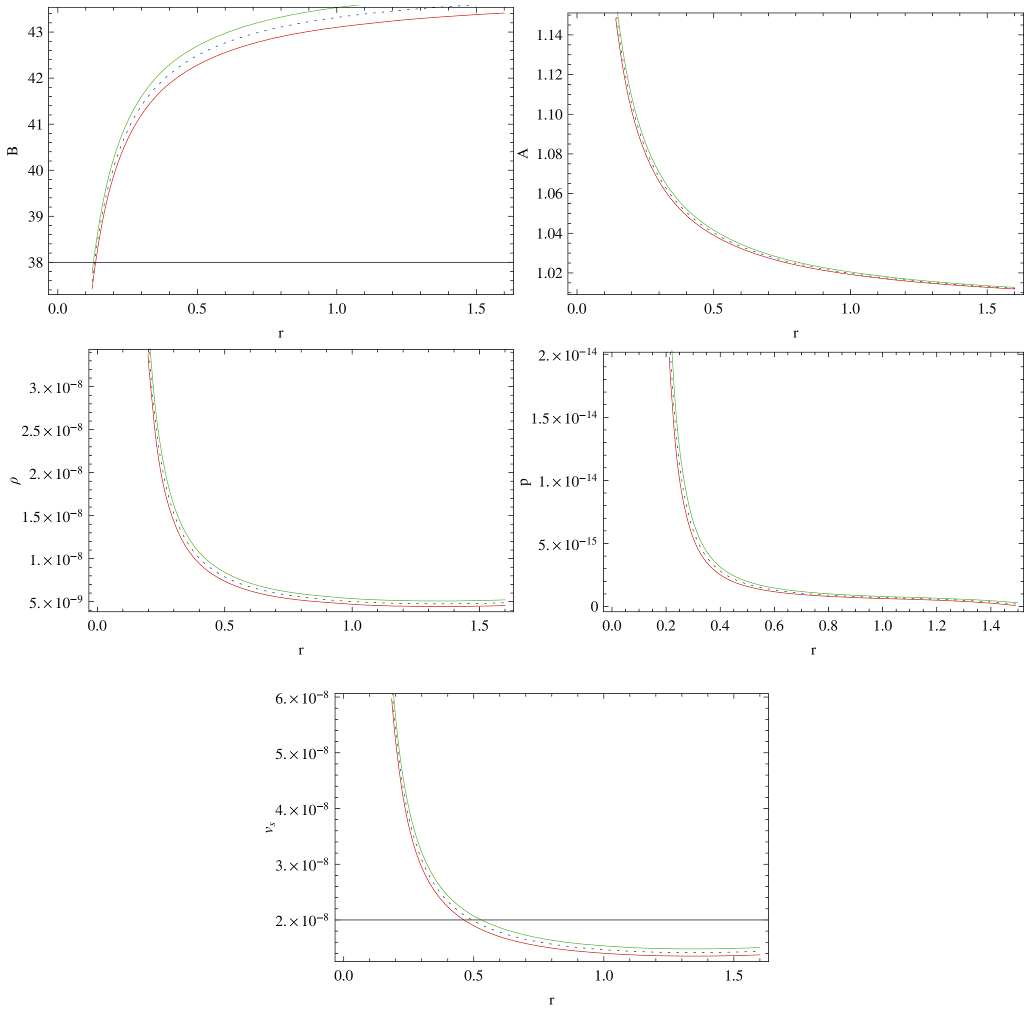

Fig. 1. Plots of B, A, ρ, p and v_s *versus* r for $p=\omega\rho^{\frac{5}{3}}$, $\omega=0.003$, $\gamma=1$, $\lambda=-0.3$ (red), $\lambda=-0.301$ (blue) and $\lambda=-0.302$ (green).

Here we obtain $\mathcal{A}$

$$\mathcal{A}=\frac{1}{2AB}\left[B''-\frac{B'^2}{2B}-\frac{A'B'}{2A}+\frac{B'}{r}\right]. \tag{25}$$

We have checked that all energy conditions are satisfied and their graphs are almost the same as well as overlap. Thus we show only the graph of null energy condition in fig. 2.

The second graph in the first row of fig. 3 indicates the behavior of the mass function obtained by

$$m(r)=\frac{r}{2}\left(1-\frac{1}{A}\right)+\frac{r^3\phi'^2}{2AB}\,, \tag{26}$$

which increases with the radius of star as well as with the decrease in λ. The surface gravitational redshift (denoted by z)

$$z=\left(1-\frac{2M}{R}\right)^{-\frac{1}{2}}-1 \tag{27}$$

(M and R are total mass and radius of the star) increases with increase in radial coordinate and decrease in λ as shown in the first graph of fig. 3. The left graph in the second row of fig. 3 indicates that the derivative of the electric scalar potential is negative and increasing while the right graph shows that the total charge of a polytropic star is also negative but decreasing. The relation between electric field intensity E_α and the electromagnetic field tensor is defined as [33]

$$E_\alpha=F_{\alpha\beta}V^\beta. \tag{28}$$

We have only one non-zero component of $F_{\alpha\beta}$, *i.e.*, $F_{10}=\phi'$ yielding only one component of electric field intensity $E_1=\frac{\phi'}{\sqrt{B}}$ or we can simply write $E=\frac{\phi'}{\sqrt{B}}$. Figure 4 shows that E has negative values. Since the electric field (E)

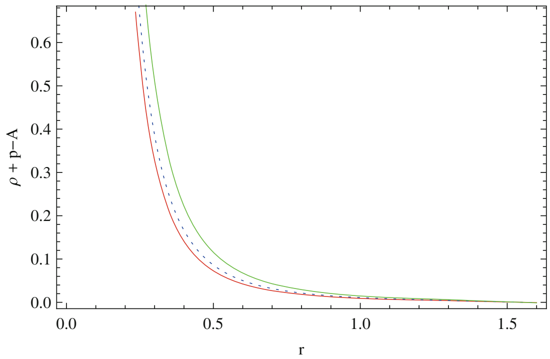

Fig. 2. Plots of null energy condition *versus* r for $p = \omega\rho^{\frac{5}{3}}$, $\omega = 0.003$, $\gamma = 1$, $\lambda = -0.3$ (red), $\lambda = -0.35$ (blue) and $\lambda = -0.4$ (green).

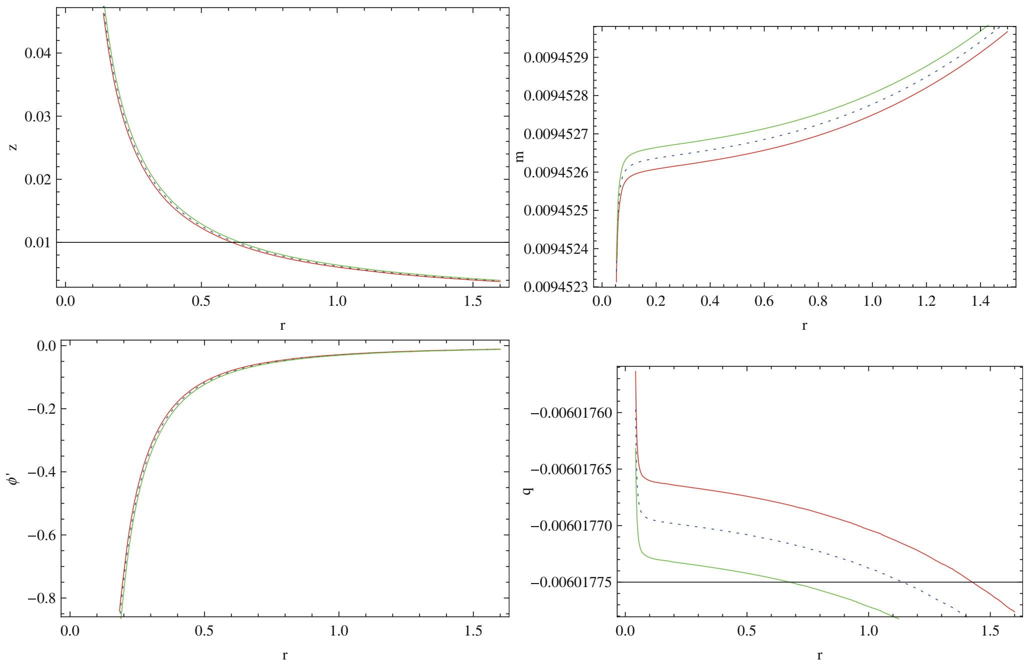

Fig. 3. Plots of z, m, ϕ' and q *versus* r for $p = \omega\rho^{\frac{5}{3}}$, $\omega = 0.003$ and $\gamma = 1$. In the left column $\lambda = -0.3$ (red), $\lambda = -0.35$ (blue), $\lambda = -0.4$ (green) while in the right column $\lambda = -0.3$ (red), $\lambda = -0.30001$ (blue), $\lambda = -0.30002$ (green).

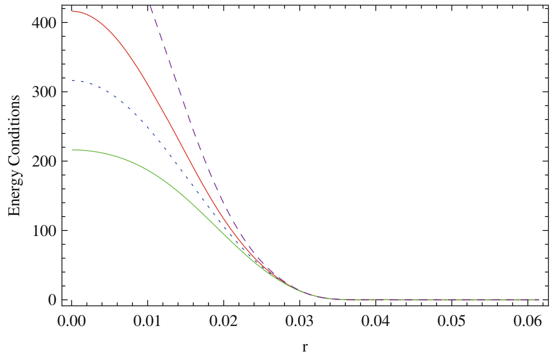

Fig. 4. Plot of electric field intensity *versus* r for $p = \omega\rho^{\frac{5}{3}}$, $\omega = 0.003$, $\gamma = 1$, $\lambda = -0.3$ (red), $\lambda = -0.301$ (blue) and $\lambda = -0.302$ (green).

and gravitational field are analogous, it can be interpreted that negative E is opposite to gravitational pull and can resist or slow down the collapse. Moreover, the negative charge shows a dominance of electrons. Thus cumulatively we can say that the star is stable because electron degeneracy pressure balances gravity. The charge density has the same behavior as energy density (using eq. (19)) because we consider the constant $\gamma = 1$ for graphical analysis.

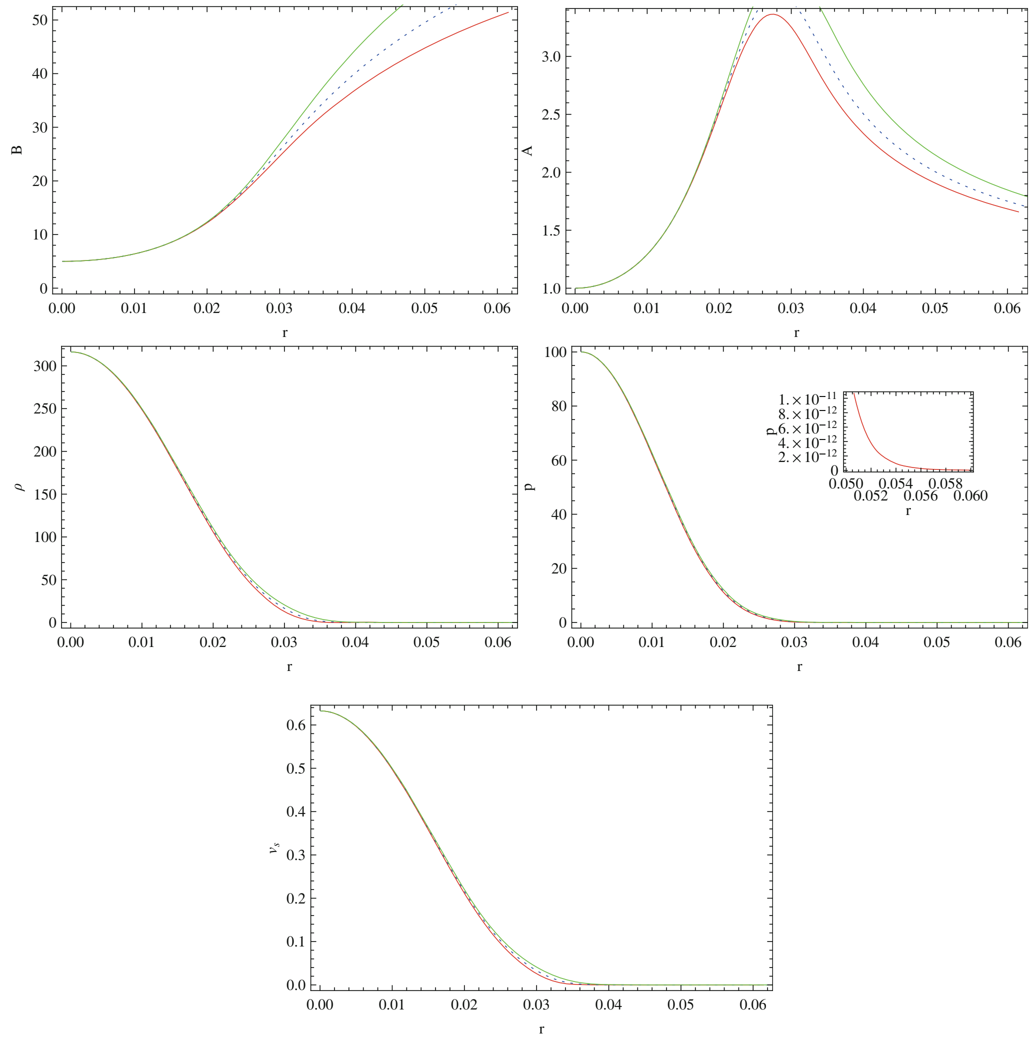

Fig. 5. Plots of B, A, ρ, p and v_s *versus* r for $p = \omega\rho^2$, $\omega = 0.001$, $\gamma = 1$, $\lambda = -0.3$ (red), $\lambda = -0.32$ (blue) and $\lambda = -0.34$ (green).

3.2 Polytropic star for $\sigma = 2$

In this case, the density takes the form $\rho = (\frac{p}{\omega})^{\frac{1}{2}}$ and eqs. (9), (15), (16) and (18) become

$$\phi'' + \phi'\left(\frac{2}{r} - \frac{A'}{2A} - \frac{B'}{2B}\right) = 4\pi\gamma\left(\frac{p}{\omega}\right)^{\frac{1}{2}} A\sqrt{B}, \tag{29}$$

$$A' = rA^2\left[\frac{1}{r^2A} - \frac{1}{r^2} + 8\pi\left(\frac{p}{\omega}\right)^{\frac{3}{5}} + \lambda\left(3\left(\frac{p}{\omega}\right)^{\frac{1}{2}} - p\right) + \frac{\phi'^2}{AB}\right], \tag{30}$$

$$B' = rAB\left[-\frac{1}{r^2A} + \frac{1}{r^2} + 8\pi p + \lambda\left(3p - \left(\frac{p}{\omega}\right)^{\frac{1}{2}}\right) - \frac{\phi'^2}{AB}\right], \tag{31}$$

$$p' = \frac{-\left((\frac{p}{\omega})^{\frac{1}{2}} + p\right)\frac{B'}{2B} + \frac{2\lambda}{(8\pi+2\lambda)}\frac{\phi'}{r^2\sqrt{AB}}\left(\frac{r^2\phi'}{\sqrt{AB}}\right)'}{\left[1 - \frac{\lambda}{(8\pi+2\lambda)}\left(\frac{1}{2\omega}(\frac{p}{\omega})^{\frac{-1}{2}} - 1\right)\right]}. \tag{32}$$

Imposing the same initial conditions, the numerical solution of the above system of equations is obtained for this case. The first row of fig. 5 shows the similar change in metric functions with radius and model parameter λ as in the previous case. The second row of this figure represents decreasing energy density and pressure. The zoomed graph of pressure indicates that it is zero at $r \approx 0.06$. Also, the speed of sound lies between zero and one showing the stability of stellar structure in this case. The plots of four energy conditions are combined in fig. 6.

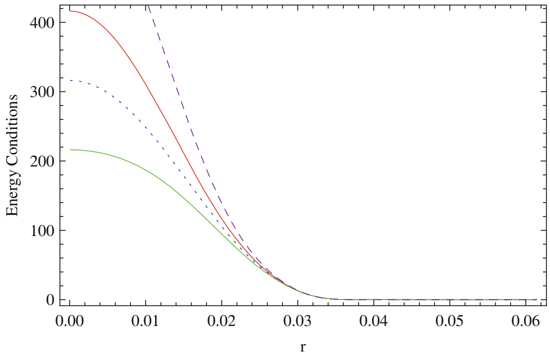

Fig. 6. Plots of NEC (red), WEC (blue), DEC (green), SEC (purple) for $p = \omega\rho^2$, $\omega = 0.001$, $\gamma = 1$ and $\lambda = -0.3$.

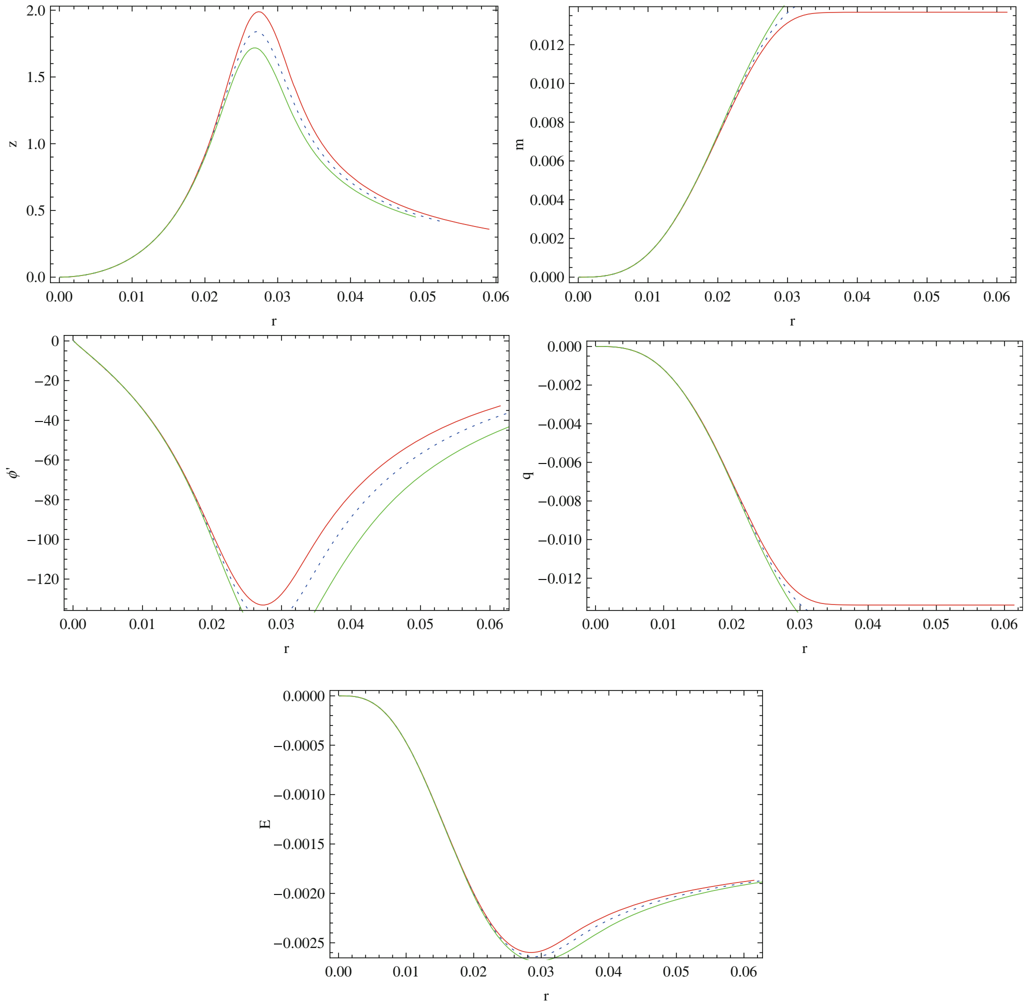

Fig. 7. Plots of z, m, ϕ', q and E *versus* r for $p = \omega\rho^2$, $\omega = 0.003$, $\gamma = 1$. In first graph $\lambda = -0.3$ (red), $\lambda = -0.29$ (blue) and $\lambda = -0.28$ (green) while in remaining three $\lambda = -0.3$ (red), $\lambda = -0.32$ (blue) and $\lambda = -0.34$ (green).

Figure 7 represents how redshift parameter, mass function, derivative of electric scalar potential, charge and electric field intensity grow with radius and exhibit change with parameter λ. Mass and redshift parameter are inversely related with λ while ϕ', q as well as E have a direct relation with λ. These behaviors are in agreement with the previous case. Here again ϕ' yields a negative electric field to counteract the gravitational pull and the charge is negative showing that the origin of this force is electron degeneracy pressure.

4 Concluding remarks

This paper is devoted to study the physical features of charged polytropic stars (with $\sigma = \frac{5}{3}, 2$) for $f(R,T) = R + 2\lambda T$ gravity model. The equation of hydrostatic equilibrium for such configuration is affected by the model parameter (as in [25]) and electromagnetic field. Our analysis shows that mass increases with decrease in λ while in the absence of electromagnetic field, mass and λ are directly proportional as given in [25]. The model parameter produces different changes in the physical features of stars but these changes are similar in both cases. The resulting electric field intensity is negative, causing a force which counterbalances the gravity consistent with [34,35]. The total charge in both cases is negative, demonstrating the supremacy of electrons.

For the first case, the star has radius $r \approx 1.5\,\text{km}$, mass $M \approx (0.0094530)M_{\odot}$, gravitational redshift $z_s \approx 0.005$ as well as $q \approx (-0.0060178)M_{\odot}$ under the assumed initial conditions and constants. In the second case, under the same initial conditions but with different ω, the polytropic star has $r \approx 0.06\,\text{km}$, $M \approx (0.014)M_{\odot}$, $z_s \approx 2$ and $q \approx (-0.014)M_{\odot}$. The redshift parameter is less than or equal to two for both cases which lies within the limit defined for perfect fluid configurations [12,13]. We have found that the energy conditions are satisfied and speed of sound lies between zero and one, implying that the stars are stable. A realistic toy model $\zeta = 2\chi + 5.29355$ has been considered for neutron stars in $f(R)$ gravity [36]. We have also checked this model in our framework and found that it is not stable.

We have found that a charged polytropic star with a large radius (first case) has less mass, charge and surface redshift than the star with a small radius (second case). It is observed that in this gravity, the radius of a stable charged polytropic star whose matter satisfies the energy conditions is very small as compared to the observed radius of compact objects (white dwarfs and neutron stars). We conclude that this analysis provides a possibility of the existence of such small compact objects which have not been observed until today due to their small sizes. We have also compared our results with those of charged polytropic spheres in $f(R)$ theory [37]. In contrast with [37], we deal with ϕ' instead of q in the set of equations and explored the behavior of total charge as well as electric field intensity of the sphere. For $f(R,T) = R + 2\lambda T$ gravity model, charged polytropic spheres could have very small masses and radii while for $f(R) = R + \frac{\beta}{2}R^2$, they have very large masses and radii. In [37], the authors deal only with weakly charged spheres; however, we have checked that the polytropic charged spheres are stable for our model in a strong as well as weak electromagnetic field by assigning large and small values to γ, respectively.

We would like to thank the Higher Education Commission, Islamabad, Pakistan for its financial support through the *Indigenous PhD 5000 Fellowship Program Phase-II, Batch-III.*

References

1. S.W. Hawking, Phys. Rev. Lett. **26**, 1344 (1971).
2. R.V. Wagoner, Astrophys. J. **278**, 345 (1984).
3. R. Tooper, Astrophys. J. **140**, 434 (1964).
4. M.K. Mak, T. Harko, Int. J. Mod. Phys. D **13**, 149 (2004).
5. F. Özel, G. Baym, T. Güver, Phys. Rev. D **82**, 101301 (2010).
6. L. Herrera, W. Barreto, Phys. Rev. D **88**, 084022 (2013).
7. L. Herrera, A. Di Prisco, W. Barreto, J. Ospino, Gen. Relativ. Gravit. **46**, 1827 (2014).
8. S. Rosseland, A.S. Eddington, Mon. Not. R. Astron. Soc. **84**, 720 (1924).
9. J.D. Bekenstein, Phys. Rev. D **4**, 2185 (1960).
10. W.B. Bonnor, Mon. Not. R. Astron. Soc. **129**, 443 (1964).
11. M. Azam, S.A. Mardan, M.A. Rehman, Adv. High Energy Phys. **2015**, 865086 (2015).
12. H.A. Buchdahl, Phys. Rev. **116**, 1027 (1959).
13. B.V. Ivanov, Phys. Rev. D **65**, 104011 (2002).
14. G. Böhmer, T. Harko, Class. Quantum Grav. **23**, 6479 (2006).
15. T. Harko, F.S.N. Lobo, S. Nojiri, S.D. Odintsov, Phys. Rev. D **84**, 024020 (2011).
16. T. Harko, F.S.N. Lobo, Galaxies **2**, 410 (2014).
17. M. Sharif, I. Nawazish, Eur. Phys. J. C **77**, 198 (2017).
18. M. Sharif, A. Siddiqa, Mod. Phys. Lett. A **32**, 1750151 (2017).
19. S.L. Shapiro, S.A. Teukolsky, *Black Holes, White Dwarfs and Neutron Stars* (John Wiley and Sons, 1983).
20. H. Abreu, H. Hernández, L.A. Núñez, Class. Quantum Grav. **24**, 4631 (2007).
21. M. Sharif, Z. Yousaf, Astrophys. Space Sci. **354**, 471 (2014).
22. N. Jiang, M. Gleiser, Entropy **20**, 2 (2015).
23. I. Noureen, M. Zubair, Astrophys. Space Sci. **356**, 103 (2015).
24. M. Zubair, G. Abbas, I. Noureen, Astrophys. Space Sci. **361**, 8 (2016).
25. P.H.R.S. Moraes, D.V.A. José, M. Malheiro, J. Cosmol. Astropart. Phys. **06**, 005 (2016).

26. A.V. Astashenok, A. de la Cruz-Dombriz, S.D. Odintsov, Class. Quantum Grav. **34**, 205008 (2017).
27. G.A. Carvalho *et al.*, Eur. Phys. J. C **77**, 871 (2017).
28. M. Sharif, A. Siddiqa, Gen. Relativ. Gravit. **43**, 73 (2011).
29. J. Barrientos, G.F. Rubilar, Phys. Rev. D **90**, 028501 (2014).
30. J.D.V. Arbañil, J.P.S. Lemos, V.T. Zanchin, Phys. Rev. D **88**, 084023 (2013).
31. W.J. Maciel, *Introduction to Stellar Structure* (Springer, 2016).
32. M. Sharif, A. Ikram, `https://doi.org/10.1142/S0218271817501826`.
33. C.G. Tsagas, Class. Quantum Grav. **22**, 393 (2005).
34. M. Sharif, G. Abbas, Eur. Phys. J. Plus **128**, 102 (2013).
35. M. Azam, S.A. Mardan, M.A. Rehman, Adv. High Energy Phys. **2015**, 865086 (2015).
36. M. Orellana, F. Garcia, F.A.T. Pannia, G.E. Romero, Gen. Relativ. Gravit. **45**, 771 (2013).
37. H. Mansour, B.S. Lakhal, A. Yanallah, arXiv:1710.09294.

Accepted manuscript to appear in IJMPD

Accepted Manuscript

International Journal of Modern Physics D

Article Title: Models of Charged Self-Gravitating Source in $f(R,T)$ Theory

Author(s): M. Sharif, Aisha Siddiqa

DOI: 10.1142/S0218271819500056

Received: 27 February 2018

Accepted: 05 July 2018

To be cited as: M. Sharif, Aisha Siddiqa, Models of Charged Self-Gravitating Source in $f(R,T)$ Theory, *International Journal of Modern Physics D*, doi: 10.1142/S0218271819500056

Link to final version: https://doi.org/10.1142/S0218271819500056

This is an unedited version of the accepted manuscript scheduled for publication. It has been uploaded in advance for the benefit of our customers. The manuscript will be copyedited, typeset and proofread before it is released in the final form. As a result, the published copy may differ from the unedited version. Readers should obtain the final version from the above link when it is published. The authors are responsible for the content of this Accepted Article.

World Scientific
www.worldscientific.com

Manuscript
Click here to download Manuscript mcssfRT.pdf
Accepted manuscript to appear in IJMPD

Models of Charged Self-Gravitating Source in $f(R,T)$ Theory

M. Sharif *and Aisha Siddiqa †
Department of Mathematics, University of the Punjab,
Quaid-e-Azam Campus, Lahore-54590, Pakistan.

Abstract

We discuss anisotropic non-static charged spherical source describing the phenomena of collapse and expansion in the context of $f(R,T)$ theory (R is the Ricci scalar and T is the trace of energy momentum tensor). The Einstein-Maxwell field equations are formulated and an auxiliary solution is considered. We evaluate the corresponding expansion scalar (Θ) and investigate the cases of collapse ($\Theta < 0$) and expansion ($\Theta > 0$). In both cases, we explore the influence of charge as well as model parameter on density, radial/tangential pressure, anisotropic parameter and mass through graphs. It is observed that the physical parameters vary with time for expansion while remain constant for collapse, however the change with respect to radial coordinate is same for both cases. The model parameter has the same impact in both cases while charge affects only in the case of collapse. The energy conditions are satisfied for both solutions with particular values of the parameters.

Keywords: $f(R,T)$ gravity; Self-gravitating objects; Electromagnetic theory.
PACS: 04.50.Kd; 04.40.Dg; 04.20Jb; 04.40.Nr.

*msharif.math@pu.edu.pk
†aisha.siddiqa17@yahoo.com

ACCEPTED MANUSCRIPT

Accepted manuscript to appear in IJMPD

ACCEPTED MANUSCRIPT

1 Introduction

Gravitational force is amenable for governing many astrophysical phenomena like formation of stars, keeping stars together in galaxies, gravitational collapse and restricting the heavenly bodies in their respective orbits. Self-gravitating objects like stars, clusters of stars and galaxies are held together under the influence of mutual gravitation. When a star burns up its nuclear fuel under the fusion reaction, it undergoes gravitational collapse whose end product is called compact object. Two compact objects orbiting each other can produce gravitational waves by loosing their energy and merging together under the gravitational pull. In a self-gravitating system, if the pressure (directing opposite to gravity) exceeds gravity, the system expands.

General relativity (GR) is the most effective theory of gravity described by curvature of spacetime rather than a force. The discovery of accelerating expansion of cosmos leads to the existence of an unknown force called dark energy. Another challenging issue is dark matter expected to exist in clusters of galaxies. To resolve these puzzles, alternative approaches including modification of GR are proposed. A simple generalization of GR is the $f(R)$ gravity in which the Einstein-Hilbert action is modified by replacing the Ricci scalar with $f(R)$. Various applications of this theory to astrophysics and cosmology are discussed in literature [1]. Cembranos *et al.* [2] investigated spherical dust collapse and showed that collapsing process slows down due to the contribution of $f(R)$ terms. Sharif and Yousaf [3] discussed the collapse with metric and Palatini $f(R)$ gravity by considering early and late time models.

Harko *et al.* [4] proposed $f(R,T)$ gravity as a generalized modified theory. The coupling of curvature and matter leads to a source term which may yield interesting results. It can produce a matter dependent deviation from geodesic motion and also helps to study dark energy, dark matter interactions as well as late-time acceleration [5]. Sharif and Zubair [6] explored thermodynamics of this gravity and concluded that the generalized second law of thermodynamics is valid for phantom as well as non-phantom phases. The evolution process for different symmetries with different conditions (expansion-free, shear-free) have been studied by different authors [7]. In literature [8]-[10], the higher dimensions are also explored in this framework. Moraes *et al.* [11] studied the equilibrium configurations of neutron as well as quark stars and found that the extreme mass can cross observational limits. Sharif and Nawazish [12] explored Noether symmetries interacting

ACCEPTED MANUSCRIPT

with generalized scalar field model. They found that dust fluid leads to decelerated expansion while perfect fluid yields current cosmic expansion for quintessence model. We have studied the interaction of modified Chaplygin gas with $f(R,T)$ gravity and found that expansion is enhanced by bulk viscosity in intermediate as well as logamediate scenarios [13].

Rosseland and Eddington [14] were the first who figured out that stars may have a net electric charge. After that many researchers explored the effects of electromagnetic field on self-gravitating systems. Bekenstein [15] discussed charged spherical collapse with perfect fluid and hydrostatic equilibrium. The effects of charge on spherical collapse [16] as well as on the stability of compact objects [17] have been investigated with the conclusion that presence of charge halts the collapse and increases the stability regions. The impact of electromagnetic field on various astrophysical phenomena has also been discussed in modified theories. Sharif and Abbas [18] explored the effects of charge on collapse in modified Gauss-Bonnet gravity and concluded that gravity is much stronger than GR as well as charge term does not act as a source of gravity. Bhatti and Yousaf [19] investigated the effects of charge on anisotropic dissipative plane symmetric fluid configuration in Palatini $f(R)$ gravity. They found that matter inhomogeneity is increased with charge while decreased due to modified gravity terms. The same authors [20] studied the influence of electromagnetic field on the evolution of cylindrical compact objects in $f(R)$ theory and observed more massive objects with small radii as compared to GR for three different models.

In [21], the collapsing and expanding solutions for a non-static anisotropic source have been found while the effects of charge for these solutions are discussed in [22] within the scenario of GR. Abbas and Ahmed [23] explored these solutions in the framework of $f(R,T)$ gravity. In this paper, we investigate the electromagnetic effects on the evolution of collapsing as well as expanding non-static source. We study some physical features of charged spherical stellar object for positive and negative expansion. The paper is organized as follows. In the next section, we formulate the Einstein-Maxwell equations for $f(R,T) = R+2\lambda T$ (λ is the coupling constant, also called model parameter) gravity model and discuss the cases of collapse and expansion. We conclude our results in the last section.

ACCEPTED MANUSCRIPT

2 Einstein-Maxwell Field Equations

The action for $f(R,T)$ theory in the presence of electromagnetic field is defined as

$$S=\int d^4x\sqrt{-g}\left[\frac{1}{16\pi}f(R,T)+\mathcal{L}_m+\mathcal{L}_e\right]. \qquad (1)$$

Here $\mathcal{L}_e=mF_{\mu\nu}F^{\mu\nu}$, m is an arbitrary constant, $F_{\mu\nu}=\phi_{\nu,\mu}-\phi_{\mu,\nu}$ stands for electromagnetic field tensor, ϕ_μ represents the four potential. The following field equations are obtained by varying this action with respect to $g_{\mu\nu}$

$$f_RR_{\mu\nu}-\frac{1}{2}g_{\mu\nu}f+(g_{\mu\nu}\Box-\nabla_\mu\nabla_\nu)f_R=8\pi T_{\mu\nu}-f_T(T_{\mu\nu}+\Theta_{\mu\nu})+8\pi E_{\mu\nu}, \quad (2)$$

where $f=f(R,T),\ f_R=\frac{\partial f}{\partial R},\ f_T=\frac{\partial f}{\partial T}$, $\Theta_{\mu\nu}$ is evaluated by

$$\Theta_{\mu\nu}=g^{\gamma\alpha}\frac{\delta T_{\gamma\alpha}}{\delta g^{\mu\nu}},\quad T_{\mu\nu}=g_{\mu\nu}\mathcal{L}_m-\frac{\partial\mathcal{L}_m}{\partial g^{\mu\nu}}, \qquad (3)$$

and $E_{\mu\nu}$ is the electromagnetic energy-momentum tensor defined by

$$E_{\mu\nu}=\frac{1}{4\pi}\left(F_\mu^{\ \alpha}F_{\nu\alpha}-\frac{1}{4}F^{\alpha\beta}F_{\alpha\beta}g_{\mu\nu}\right). \qquad (4)$$

The non-static spherically symmetric spacetime is taken as

$$ds^2=-W^2(t,r)dt^2+X^2(t,r)dr^2+Y^2(t,r)(d\theta^2+\sin^2\theta d\phi^2). \qquad (5)$$

The energy-momentum tensor of anisotropic source (with no thermal conduction) is given by

$$T_{\mu\nu}=(\rho+p_t)V_\mu V_\nu+p_\perp g_{\mu\nu}+(p_r-p_t)X_\mu X_\nu, \qquad (6)$$

where V_μ, X_μ, ρ, p_r and p_t stand for four velocity, four-vector, density, radial and tangential pressures, respectively. For the above metric, the four-vectors V_μ and X_μ have the expressions

$$V^\mu=(W^{-1},0,0,0),\quad X^\mu=(0,X^{-1},0,0), \qquad (7)$$

satisfying the following relation

$$V^\mu V_\nu=-1,\quad X^\mu X_\nu=1. \qquad (8)$$

The Maxwell equations are given by

$$F^{\mu\nu}_{\ ;\nu} = 4\pi j^{\mu}, \tag{9}$$

where j^{μ} represents the four current. We are considering comoving frame in which charges are at rest and hence no magnetic field is produced. The four potential and four current in comoving coordinates are defined as

$$\phi_{\mu} = (\phi, 0, 0, 0), \quad j_{\mu} = (\xi, 0, 0, 0), \tag{10}$$

ϕ, ξ (both are functions of t and r) represent electric scalar potential and charge density. For the metric (5), the Maxwell equations give

$$\phi'' + \phi' \left(\frac{2Y'}{Y} - \frac{X'}{X} - \frac{W'}{W}\right) = 4\pi\xi W X^2, \tag{11}$$

$$\dot{\phi}' + \phi' \left(\frac{2\dot{Y}}{Y} - \frac{\dot{X}}{X} - \frac{\dot{W}}{W}\right) = 0. \tag{12}$$

Integration of Eq.(11) gives

$$\phi' = \frac{\sqrt{XW}q}{Y^2}, \quad q = 4\pi \int_0^r \xi X Y^2 dr, \tag{13}$$

q denotes the total charge on the sphere with $\phi'(0) = 0$ [24]. We consider the model $f(R,T) = R + 2\lambda T$ proposed by Harko *et al.* [4] to study the effects of curvature-matter coupling on stellar evolution. This model has been frequently used in literature [11, 13, 25]. It yields a power-law type scale factor [4] and is able to discuss the accelerated expansion of the universe. It also corresponds to ΛCDM model with trace dependent cosmological constant or $\Lambda(T)$ gravity discussed by Poplawski [26]. This model and the assumption $\mathcal{L}_m = -\rho$ simplify the field equations as

$$G_{\mu\nu} = (8\pi + 2\lambda)T_{\mu\nu} + 2\lambda\rho g_{\mu\nu} + \lambda T g_{\mu\nu} + 8\pi E_{\mu\nu}, \tag{14}$$

which leads to the following set of field equations

$$\frac{1}{Y^2} - \frac{1}{X^2}\left[\frac{2Y''}{Y} - \frac{2X'Y'}{XY} + \frac{Y'^2}{Y^2}\right] + \frac{1}{W^2}\left[\frac{\dot{X}\dot{Y}}{XY} + \frac{\dot{Y}^2}{Y^2}\right]$$
$$= (8\pi + \lambda)\rho - \lambda p_r - 2\lambda p_t + \frac{q^2}{Y^4}, \tag{15}$$

ACCEPTED MANUSCRIPT

$$\frac{\dot{Y}'}{Y}-\frac{\dot{Y}}{Y}\frac{W'}{W}-\frac{\dot{X}}{X}\frac{Y'}{Y}=0, \tag{16}$$

$$\frac{1}{X^2}\left[\frac{2Y'W'}{YW}+\frac{Y'^2}{Y^2}\right]-\frac{1}{Y^2}+\frac{1}{W^2}\left[\frac{2\dot{Y}\dot{W}}{YW}-\frac{\dot{Y}^2}{Y^2}-\frac{2\ddot{Y}}{Y}\right]$$
$$=(8\pi+3\lambda)p_r+\lambda\rho+2\lambda p_t-\frac{q^2}{Y^4}, \tag{17}$$

$$\frac{1}{X^2}\left[\frac{W''}{W}+\frac{Y''}{Y}+\frac{Y'W'}{YW}-\frac{X'Y'}{XY}-\frac{X'W'}{XW}\right]+\frac{1}{W^2}\left[\frac{\dot{X}\dot{W}}{XW}+\frac{\dot{Y}\dot{W}}{YW}\right.$$
$$\left.-\frac{\dot{X}\dot{Y}}{XY}-\frac{\ddot{X}}{X}-\frac{\ddot{Y}}{Y}\right]=(8\pi+4\lambda)p_t+\lambda\rho+\lambda p_r+\frac{q^2}{Y^4}, \tag{18}$$

where dot and prime denote differentiation with respect to t and r, respectively.

Solving the field equations simultaneously, we obtain the following explicit expressions of density, radial and tangential pressures

$$\begin{aligned}
\rho &= \frac{1}{8(2\pi+\lambda)(4\pi+\lambda)W^3X^3Y^4}\left[2\lambda X^2Y^3\dot{W}(Y\dot{X}+2X\dot{Y})+WX^2Y^2\right.\\
&\times \left\{4(2\pi+\lambda)X\dot{Y}^2-2\lambda Y^2\ddot{X}+Y(8\pi+3\lambda)\dot{x}\dot{y}-4\lambda X\ddot{Y}\right\}+2\lambda W^2Y^3\\
&\times \left\{2XW'Y'+Y(XW''-W'X')\right\}-2W^3\left\{X^3\left\{q^2(4\pi+3\lambda)-2(2\pi+\right.\right.\\
&\times \left.\left.\left.\lambda)Y^2\right\}-4(2\pi+\lambda)Y^3X'Y'+2(2\pi+\lambda)XY^2(Y'^2+2YY'')\right\}\right], \qquad (19)\\
p_r &= \frac{1}{8(2\pi+\lambda)(4\pi+\lambda)W^3X^3Y^4}\left[2X^2Y^3\dot{W}(2(4\pi+\lambda)X\dot{Y}-\lambda Y\dot{X})\right.\\
&+ WX^2Y^2\left\{-4(2\pi+\lambda)X\dot{Y}^2+2\lambda Y^2\ddot{X}+Y(\lambda\dot{X}\dot{Y}-4(4\pi+\lambda)X\ddot{Y})\right\}\\
&+ 2W^3X\left\{X^2(q^2(4\pi+3\lambda)-2(2\pi+\lambda)Y^2)+2(2\pi+\lambda)Y^2Y'^2\right\}\\
&+ \left.2W^2Y^3\left\{2(4\pi+\lambda)XW'Y'+\lambda Y(W'X'-XW'')\right\}\right], \qquad (20)\\
p_t &= \frac{1}{8(2\pi+\lambda)(4\pi+\lambda)W^3X^3Y^4}\left[2X^2Y^3\dot{W}\left\{(4\pi+\lambda)Y\dot{X}+4\pi X\dot{Y}\right\}\right.\\
&- WX^2Y^3\left\{(8\pi+3\lambda)\dot{X}\dot{Y}+2(4\pi+\lambda)Y\ddot{X}+8\pi X\ddot{Y}\right\}\\
&+ 2W^2Y^3\left\{4\pi X\dot{W}\dot{Y}-(4\pi+\lambda)Y(W'X'-XW'')\right\}\\
&- \left.2W^3\left\{q^2(4\pi+\lambda)X^3+2(2\pi+\lambda)Y^3X'Y'-2(2\pi+\lambda)XY^3Y''\right\}\right].(21)
\end{aligned}$$

ACCEPTED MANUSCRIPT

The anisotropic parameter is defined as

$$\triangle = p_r - p_t. \tag{22}$$

To discuss the phenomena of collapse and expansion, we evaluate the expansion scalar given by

$$\Theta = \frac{1}{WXY}\left(\dot{X}Y + 2X\dot{Y}\right). \tag{23}$$

We take an auxiliary solution of Eq.(16) as

$$W = \frac{\dot{Y}}{\alpha Y^{\gamma}}, \quad X = \alpha Y^{\gamma}, \tag{24}$$

where γ and $\alpha > 0$ are arbitrary constants, which leads to

$$\Theta = \alpha(2+\gamma)Y^{\gamma-1}. \tag{25}$$

When Θ is positive we have an expanding solution otherwise a collapsing one. The value of Θ depends on α, γ and Y in which α and Y are always positive implying that we have collapse for $\gamma < -2$ and expansion for $\gamma > -2$. We discuss these cases in the following subsections.

2.1 Collapse for $\gamma < -2$

If the collapse of a self-gravitating object results into a black hole, trapped surfaces (horizons) are formed. We assume that collapse of our spherically symmetric charged source results into a charged black hole. This concept is further used to find the unknown metric coefficient Y. The mass function for the considered source is given by [27]

$$m(t,r) = \frac{Y}{2X^2W}\left(X^2W^2 + X^2\dot{Y}^2 - W^2Y'^2\right) + \frac{q^2}{2Y}. \tag{26}$$

The solution (24) simplifies the mass expression as

$$m(t,r) = \frac{Y}{2}\left(1 + \alpha^2Y^{2\gamma} - \frac{Y'^2}{\alpha^2Y^{2\gamma}} + \frac{q^2}{Y^2}\right). \tag{27}$$

When $Y' = \alpha^2Y^{2\gamma}$, this implies that we have inner and outer horizons $Y^- = m - \sqrt{m^2-q^2}$, $Y^+ = m + \sqrt{m^2-q^2}$, respectively which are consistent with

ACCEPTED MANUSCRIPT

the horizons of regular Reissner-Nordström and Vaidya-Reissner-Nordström spacetimes, also known as marginally trapped tubes [28]. The expression $Y' = \alpha^2 Y^{2\gamma}$ yields

$$Y_{trap} = \left(\alpha^2(1-2\gamma)r + H(t)\right)^{\frac{1}{1-2\gamma}}, \tag{28}$$

where $H(t)$ is an integration function. Hence the collapsing solution has the form

$$\begin{aligned} W &= \frac{1}{\alpha(1-2\gamma)}\dot{H}\left(\alpha^2(1-2\gamma)r + H(t)\right)^{\frac{\gamma}{1-2\gamma}}, && (29)\\ X &= \alpha\left(\alpha^2(1-2\gamma)r + H(t)\right)^{\frac{1}{1-2\gamma}}, && (30)\\ Y_{trap} &= \left(\alpha^2(1-2\gamma)r + H(t)\right)^{\frac{1}{1-2\gamma}}. && (31) \end{aligned}$$

We take $H(t) = \frac{t}{\alpha^2}$ and obtain the following values of ρ, p_r and p_t for the collapse solution

$$\begin{aligned} \rho &= \frac{-\left(\frac{t}{\alpha^2} + r(1-2\gamma)\alpha^2\right)^{\frac{2(2+\gamma)}{2\gamma-1}}}{8(2\pi+\lambda)(4\pi+\lambda)(t+r(1-2\gamma)\alpha^4)^2}\left[8\pi\left\{-\left(\frac{t+r(1-2\gamma)\alpha^4}{\alpha^2}\right)^{\frac{2\gamma}{1-2\gamma}}\right.\right.\\ &\times \left(-q^2 + \left(\frac{t+r(1-2\gamma)\alpha^4}{\alpha^2}\right)^{\frac{2}{1-2\gamma}}\right)(4\gamma^2\alpha^8 r^2 + (t+r\alpha^4)^2)\\ &+ \gamma\alpha^4\left\{\alpha^2\left(\frac{t+r(1-2\gamma)\alpha^4}{\alpha^2}\right)^{\frac{4}{1-2\gamma}} + \left(\frac{t+r(1-2\gamma)\alpha^4}{\alpha^2}\right)^{\frac{2\gamma}{1-2\gamma}}\right.\\ &\times \left.\left.\left(-q^2 + \left(\frac{t+r(1-2\gamma)\alpha^4}{\alpha^2}\right)^{\frac{2}{1-2\gamma}}\right)(4rt + 4r^2\alpha^4)\right\}\right\} + \lambda\\ &\times \left\{-\left(\frac{t+r(1-2\gamma)\alpha^4}{\alpha^2}\right)^{\frac{2\gamma}{1-2\gamma}}\left(-q^2 + \left(\frac{t+r(1-2\gamma)\alpha^4}{\alpha^2}\right)^{\frac{2}{1-2\gamma}}\right)\right.\\ &\times (8\gamma^2\alpha^8 r^2 + 2(t+r\alpha^4)^2) + r\alpha^4\left\{5\alpha^2\left(\frac{t+r(1-2\gamma)\alpha^4}{\alpha^2}\right)^{\frac{4}{1-2\gamma}}\right.\\ &+ \left(\frac{t+r(1-2\gamma)\alpha^4}{\alpha^2}\right)^{\frac{2\gamma}{1-2\gamma}}\left(-q^2 + \left(\frac{t+r(1-2\gamma)\alpha^4}{\alpha^2}\right)^{\frac{2}{1-2\gamma}}\right)\\ &\times \left.\left.\left.(8rt + 8r^2\alpha^4)\right\}\right\}\right], \end{aligned} \tag{32}$$

ACCEPTED MANUSCRIPT

Accepted manuscript to appear in IJMPD

$$\begin{aligned}
p_r &= \frac{-\left(\frac{t}{\alpha^2}+r(1-2\gamma)\alpha^2\right)^{\frac{2(2+\gamma)}{2\gamma-1}}}{8(2\pi+\lambda)(4\pi+\lambda)(t+r(1-2\gamma)\alpha^4)^2}\left[-(8\gamma^2\alpha^8r^2+2(t+r\alpha^4)^2)\right.\\
&\times \left\{-4\pi q^2-3\lambda q^2+(4\pi+2\lambda)\left(\frac{t+r(1-2\gamma)\alpha^4}{\alpha^2}\right)^{\frac{2}{1-2\gamma}}\right\}+\gamma\alpha^4\\
&\times \left\{32\pi r\left(\frac{t+r(1-2\gamma)\alpha^4}{\alpha^2}\right)^{\frac{2\gamma}{1-2\gamma}}\left(-q^2+\left(\frac{t+r(1-2\gamma)\alpha^4}{\alpha^2}\right)^{\frac{2}{1-2\gamma}}\right)\right.\\
&\times (t+r\alpha^4)+\lambda\left\{\alpha^2\left(\frac{t+r(1-2\gamma)\alpha^4}{\alpha^2}\right)^{\frac{4}{1-2\gamma}}+\left(\frac{t+r(1-2\gamma)\alpha^4}{\alpha^2}\right)^{\frac{2\gamma}{1-2\gamma}}\right.\\
&\times \left.\left.\left.\left(-3q^2+\left(\frac{t+r(1-2\gamma)\alpha^4}{\alpha^2}\right)^{\frac{2}{1-2\gamma}}\right)(8rt+8r^2\alpha^4)\right\}\right\}\right], \qquad (33)\\
p_t &= \frac{-\left(\frac{t}{\alpha^2}+r(1-2\gamma)\alpha^2\right)^{\frac{2(2+\gamma)}{2\gamma-1}}}{8(2\pi+\lambda)(4\pi+\lambda)(t+r(1-2\gamma)\alpha^4)^2}\left[-2q^2\left(\frac{t+r(1-2\gamma)\alpha^4}{\alpha^2}\right)^{\frac{2\gamma}{1-2\gamma}}\right.\\
&\times (4\pi+\lambda)(4r^2\gamma^2\alpha^8+(t+r\alpha^4)^2)+\gamma\alpha^4\left\{32\pi rq^2(t+r\alpha^4)\right.\\
&\times \left(\frac{t+r(1-2\gamma)\alpha^4}{\alpha^2}\right)^{\frac{2\gamma}{1-2\gamma}}+\lambda\left\{\alpha^2\left(\frac{t+r(1-2\gamma)\alpha^4}{\alpha^2}\right)^{\frac{4}{1-2\gamma}}\right.\\
&+ \left.\left.\left.8rq^2\left(\frac{t+r(1-2\gamma)\alpha^4}{\alpha^2}\right)^{\frac{2\gamma}{1-2\gamma}}(t+r\alpha^4)\right\}\right\}\right]. \qquad (34)
\end{aligned}$$

For the collapse solution, the anisotropic parameter and mass function take the form

$$\triangle = -\left(\frac{\left(\frac{t+r(1-2\gamma)\alpha^4}{\alpha^2}\right)^{\frac{2}{1-2\gamma}}\left(-1+2q^2\left(\frac{t+r(1-2\gamma)\alpha^4}{\alpha^2}\right)^{\frac{2}{1-2\gamma}}\right)}{2(4\pi+\lambda)}\right), \qquad (35)$$

$$m = \frac{1}{2}\left(\frac{t+r(1-2\gamma)\alpha^4}{\alpha^2}\right)^{\frac{1}{1-2\gamma}}+\frac{q^2}{\left(\frac{t+r(1-2\gamma)\alpha^4}{\alpha^2}\right)^{\frac{1}{1-2\gamma}}}. \qquad (36)$$

Here we discuss the graphical behavior of different physical quantities for this collapse solution. The graph of expansion scalar (Figure **1**) shows increasing behavior with radius but no change with time. Figures **2-5** show

ACCEPTED MANUSCRIPT

ACCEPTED MANUSCRIPT

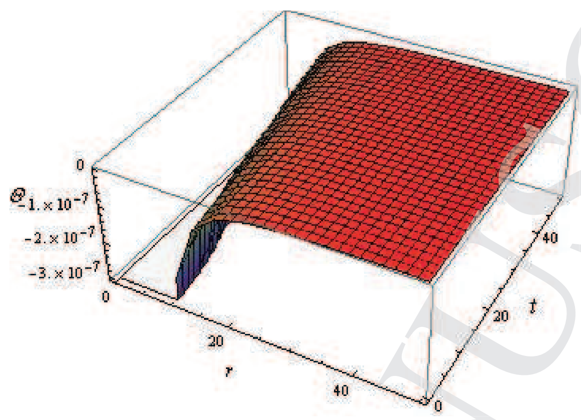

Figure 1: Plot of Θ versus r and t for $\gamma = -2.5$, $\alpha = 1$.

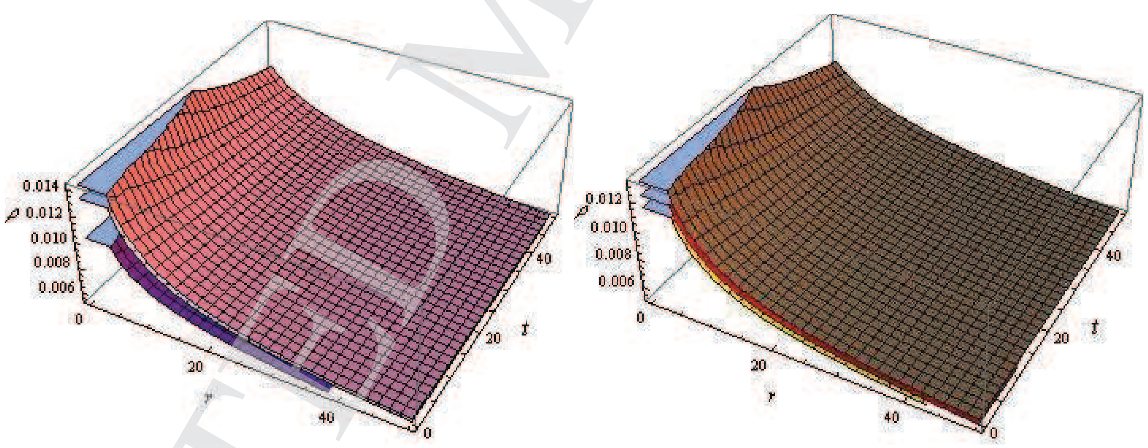

Figure 2: Plots of ρ versus r and t for $\gamma = -2.5$, $\alpha = 1$. The left graph is for $q = 0$ (pink), $q = 0.5$ (blue), $q = 1$ (purple) with $\lambda = 1$ and the right graph is for $\lambda = 1$ (brown), $\lambda = 2$ (red), $\lambda = 3$ (yellow) with $q = 0.5$.

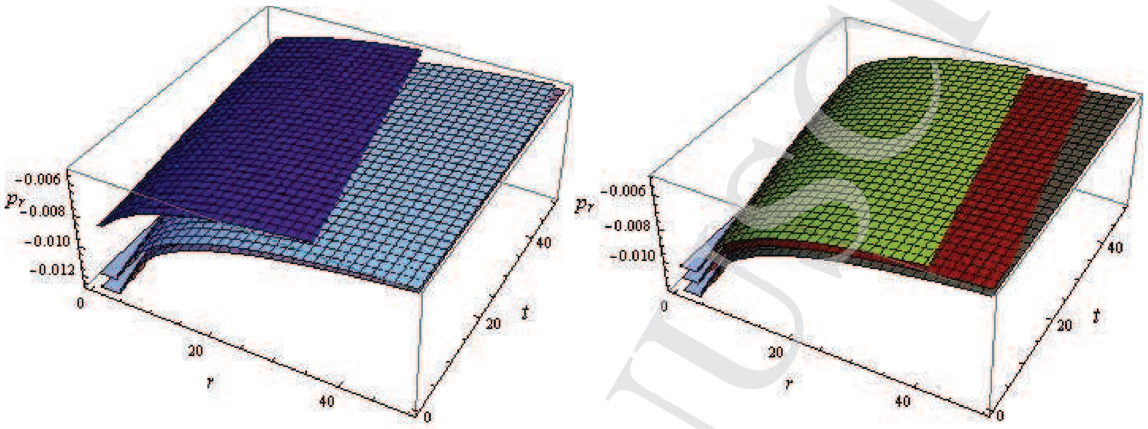

Figure 3: Plots of p_r versus r and t for $\gamma = -2.5$, $\alpha = 1$. The left graph is for $q = 0$ (pink), $q = 0.5$ (blue), $q = 1$ (purple) with $\lambda = 1$ while the right graph is for $\lambda = 1$ (brown), $\lambda = 2$ (red), $\lambda = 3$ (yellow) with $q = 0.5$.

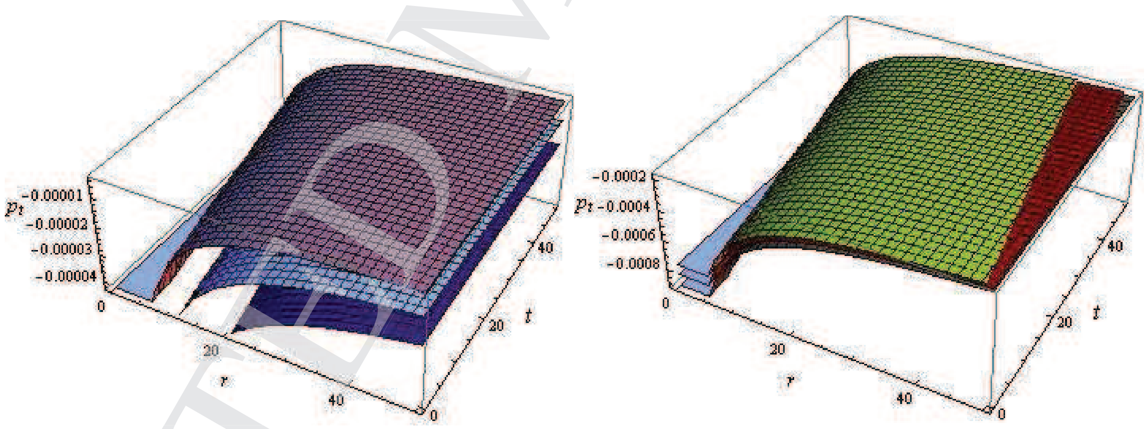

Figure 4: Plots of p_t versus r and t for $\gamma = -2.5$, $\alpha = 1$. The left graph is for $q = 0$ (pink), $q = 0.1$ (blue), $q = 0.15$ (purple) with $\lambda = 1$ and the right graph is for $\lambda = 1$ (brown), $\lambda = 2$ (red), $\lambda = 3$ (yellow) with $q = 0.5$.

ACCEPTED MANUSCRIPT

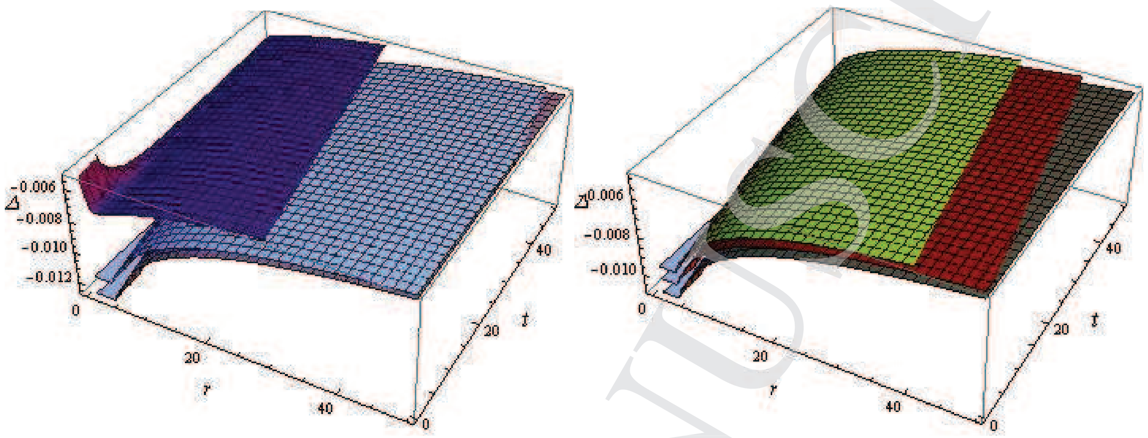

Figure 5: Plots of $\triangle$ versus r and t for $\gamma = -2.5$, $\alpha = 1$. The left graph is for $q = 0$ (pink), $q = 0.4$ (blue), $q = 0.8$ (purple) with $\lambda = 1$ while the right graph is for $\lambda = 1$ (brown), $\lambda = 2$ (red), $\lambda = 3$ (yellow) with $q = 0.5$.

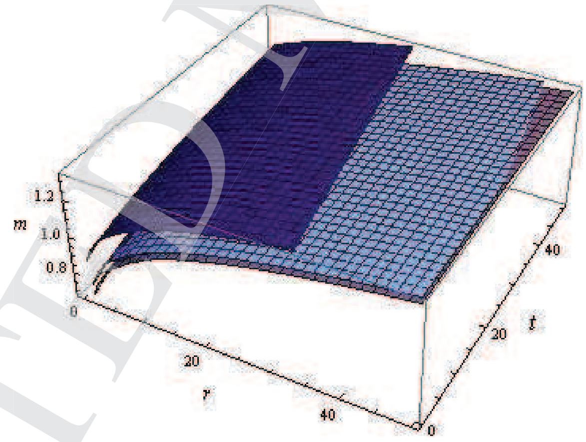

Figure 6: Plot of m versus r and t for $\gamma = -2.5$, $\alpha = 1$, $q = 0$ (pink), $q = 0.4$ (blue), $q = 0.8$ (purple).

ACCEPTED MANUSCRIPT

the graphs of density, radial/tangential pressure and anisotropy. We observe that density is decreasing while radial and tangential pressures as well as anisotropy are increasing with r but remain unchanged with time. The mass function is increasing with radial coordinate as shown in Figure **6**. The effects of charge and model parameter λ are summarized in Table **1**.

Table **1**: Effects of increasing q and λ for collapsing solution

Physical Parameter	ρ	p_r	p_t	$\triangle$	m
As q Increases	decreases	increases	decreases	increases	increases
As λ Increases	decreases	increases	increases	increases	no change

For the curvature-matter coupled gravity, the energy conditions are [29]

- Null energy condition: $\rho + p_r - \mathcal{A} \geq 0,\ \rho + p_t - \mathcal{A} \geq 0,$
- Weak energy condition: $\rho - \mathcal{A} \geq 0,\ \rho + p_r - \mathcal{A} \geq 0,\ \rho + p_t - \mathcal{A} \geq 0,$
- Dominant energy condition: $\rho - p_r - \mathcal{A} \geq 0,\ \rho - p_t - \mathcal{A} \geq 0,$
- Strong energy condition: $\rho + p_r + 2p_t - \mathcal{A} \geq 0.$

The term $\mathcal{A} = (V^\beta V^\alpha_{;\beta})_{;\alpha}$ appears due to non-geodesic motion of massive particles and is found as

$$\mathcal{A} = \frac{1}{X^2}\left[\frac{W''}{W} + \frac{W'^2}{W^2} - \frac{W'}{W}\left(\frac{X'}{X} - \frac{2Y'}{Y}\right)\right] + \frac{\dot{W}^2}{W^4}. \tag{37}$$

The collapsing solution (24) yields

$$\mathcal{A} = \frac{\gamma(1+4\gamma)\alpha^6\left(\frac{t}{\alpha^2 + r(1-2\gamma)\alpha^2}\right)^{\frac{2\gamma}{2\gamma-1}}}{(t + r(1-2\gamma)\alpha^4)^2}. \tag{38}$$

All the expressions of energy conditions defined above are plotted in Figure **7**. These plots show that all the energy conditions are satisfied for the collapse solution as well as considered values of the free parameters.

ACCEPTED MANUSCRIPT

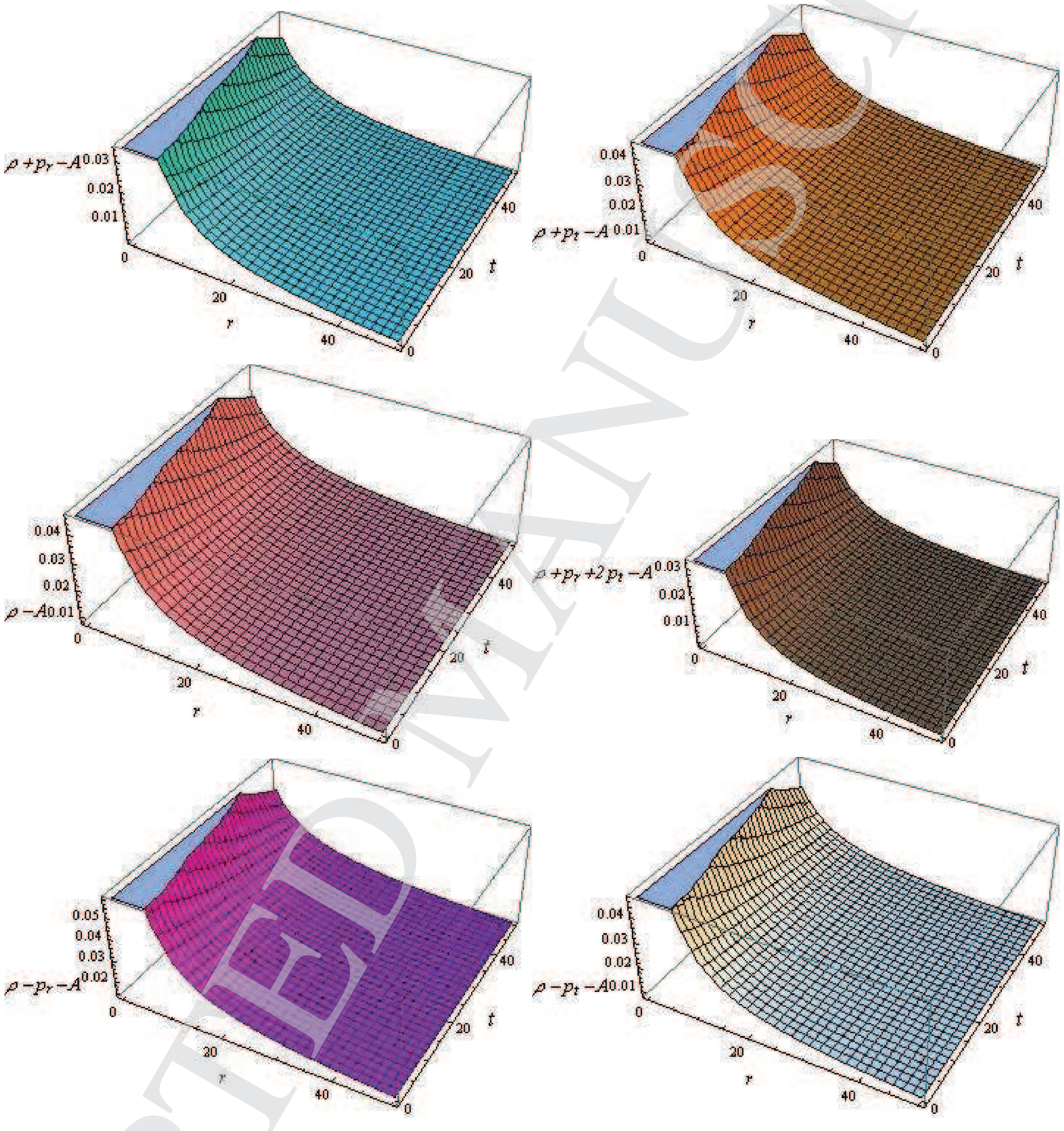

Figure 7: Plots of Energy Conditions versus r and t for $\gamma = -2.5$, $\alpha = 1$, $q = 0.5$ and $\lambda = 1$.

ACCEPTED MANUSCRIPT

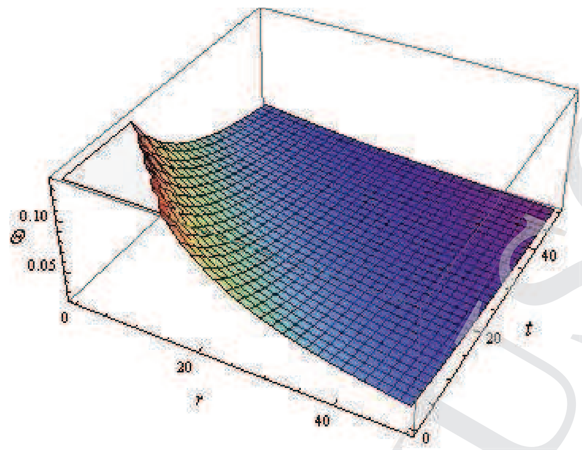

Figure 8: Plot of Θ versus r and t for $\gamma = 0.05$, $\alpha = 1$.

2.2 Expansion for $\gamma > -2$

To discuss the evolution of density and pressures in the expanding case, the value of metric function Y is needed. For non-static spherical symmetric metric, Y can either be a function of $r+t$ or $r-t$ [30]. We consider $Y = r+t$ and check the values of Θ through graph (Figure **8**) which are positive (i.e., the solution is expanding). Thus the expanding solution is given by

$$W = \frac{1}{\alpha(r+t)^{\gamma}}, \quad X = \alpha(r+t)^{\gamma}, \quad Y = r+t. \tag{39}$$

Consequently, the expressions of ρ, p_r and p_t take the form

$$\begin{aligned} \rho &= \frac{1}{8(r+t)^4(2\pi+\lambda)(4\pi+\lambda)}\left[(r+t)^2(8\pi+4\lambda) - q^2(8\pi+6\lambda)\right. \\ &+ \frac{(r+t)^{2-2\gamma}}{\alpha^2}(16\pi\gamma - 8\pi - 4\lambda + 6\gamma\lambda + 4\gamma^2\lambda) + \alpha^2(r+t)^{2+2\gamma} \\ &\times \left.(8\pi + 8\pi\gamma + 4\lambda + \gamma\lambda - 4\gamma^2\lambda)\right], \end{aligned} \tag{40}$$

$$\begin{aligned} p_r &= \frac{1}{8(r+t)^4(2\pi+\lambda)(4\pi+\lambda)}\left[(r+t)^2(8\pi+4\lambda) - q^2(8\pi+6\lambda)\right. \\ &+ \frac{(r+t)^{2-2\gamma}}{\alpha^2}(16\pi\gamma - 8\pi - 4\lambda + 6\gamma\lambda + 4\gamma^2\lambda) + \alpha^2(r+t)^{2+2\gamma} \\ &\times \left.(8\pi + 16\pi\gamma + 4\lambda + 5\gamma\lambda - 4\gamma^2\lambda)\right], \end{aligned} \tag{41}$$

$$p_t = \frac{(r+t)^{-2(2+\gamma)}}{8(\alpha)^2(2\pi+\lambda)(4\pi+\lambda)}\left[-8\pi\left\{q^2(r+t)^{2\gamma}\alpha^2 + \gamma t^2\left\{1-2\gamma\right.\right.\right.$$

ACCEPTED MANUSCRIPT

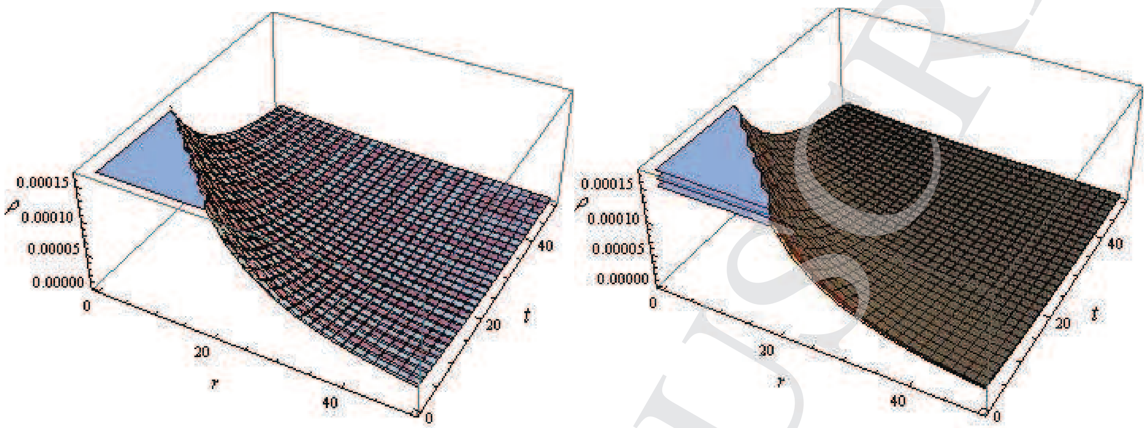

Figure 9: Plots of ρ versus r and t for $\gamma = 0.05$, $\alpha = 1$. The left graph is for $q = 0$ (pink), $q = 0.5$ (blue), $q = 1$ (purple) with $\lambda = 1$ and the right graph is for $\lambda = 1$ (brown), $\lambda = 2$ (red), $\lambda = 3$ (yellow) with $q = 0.5$.

$$\begin{aligned} &+ \quad (r+t)^{4\gamma}\alpha^4(1+2\gamma)\} + r^2\gamma(1+2\gamma rt)\left\{1+(r+t)^{4\gamma}\alpha^4\right. \\ &+ \quad 2\gamma(-1+(r+t)^{4\gamma}\alpha^4)\}\}\left\{2q^2(r+t)^{2\gamma}\alpha^2+\gamma t^2\left\{2-4\gamma\right.\right. \\ &+ \quad (r+t)^{4\gamma}\alpha^4(1+4\gamma)\} + r^2\gamma(1+2\gamma rt)\left\{2+(r+t)^{4\gamma}\alpha^4\right. \\ &+ \quad 4\gamma(-1+(r+t)^{4\gamma}\alpha^4)\}\}\big]. \end{aligned} \tag{42}$$

The anisotropic parameter and mass function for expanding solution are evaluated as

$$\begin{aligned} \triangle &= \frac{(r+t)^{-2(2+\gamma)}}{2(4\pi+\lambda)\alpha^2}\left[-2q^2(r+t)^{2\gamma}\alpha^2+(r^2+t^2)\left\{-1+\gamma\right.\right. \\ &+ \quad (r+t)^{2\gamma}\alpha^2+(r+t)^{4\gamma}\alpha^4(1+\gamma)+\gamma^2(2-2(r+t)^{4\gamma}\alpha^4)\} - 2\gamma t \\ &\times \quad \left\{1-2\gamma^2-\gamma-(r+t)^{2\gamma}\alpha^2+(r+t)^{4\gamma}\alpha^4(2\gamma^2-\gamma-1)\right\}\big], \end{aligned} \tag{43}$$

$$m = \frac{1}{2}\left[(r+t)+\frac{q^2}{r+t}\right]. \tag{44}$$

The evolution of physical parameters during expansion is represented through graphs. Figures **9-13** show the plots of density, radial as well as tangential pressure, anisotropic parameter and mass function, respectively. It is found that in contrast to the collapsing case, here the quantities vary with time coordinate. The increase (or decrease) in charge does not induce a measurable fluctuations in physical quantities. The graphical analysis is summarized in Tables **2** and **3**.

ACCEPTED MANUSCRIPT

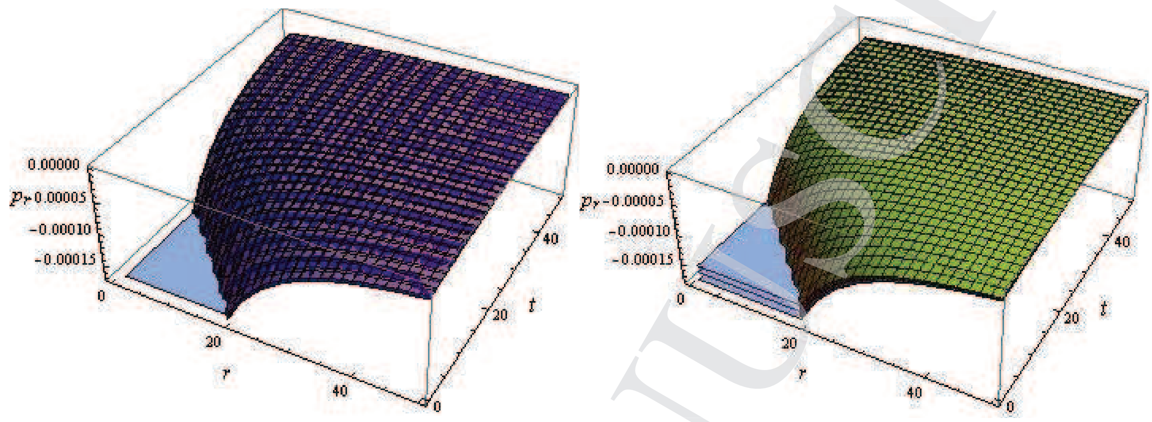

Figure 10: Plots of p_r versus r and t for $\gamma = 0.05$, $\alpha = 1$. The left graph is for $q = 0$ (pink), $q = 0.5$ (blue), $q = 1$ (purple) with $\lambda = 1$ while the right graph is for $\lambda = 1$ (brown), $\lambda = 2$ (red), $\lambda = 3$ (yellow) with $q = 0.5$.

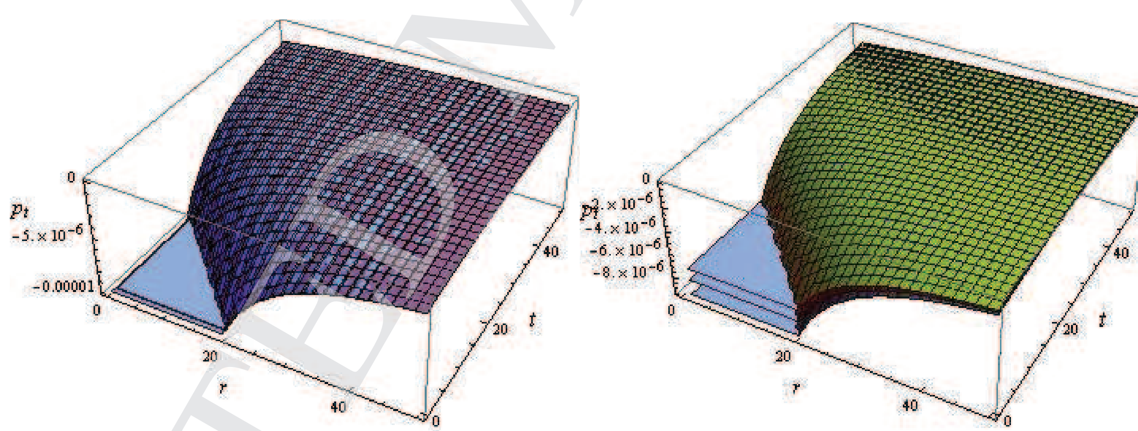

Figure 11: Plots of p_t versus r and t for $\gamma = 0.05$, $\alpha = 1$. The left graph is for $q = 0$ (pink), $q = 0.5$ (blue), $q = 1$ (purple) with $\lambda = 1$ and the right graph is for $\lambda = 1$ (brown), $\lambda = 2$ (red), $\lambda = 3$ (yellow) with $q = 0.5$.

ACCEPTED MANUSCRIPT

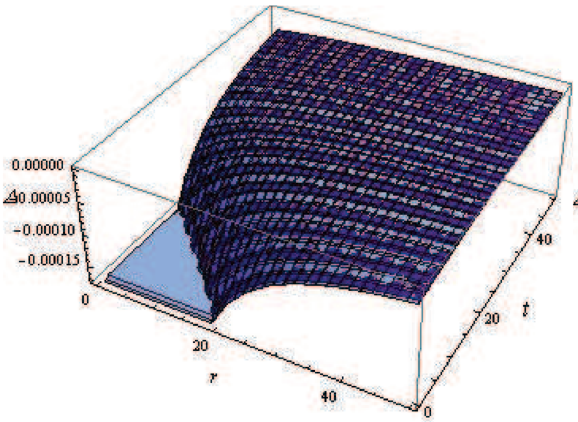

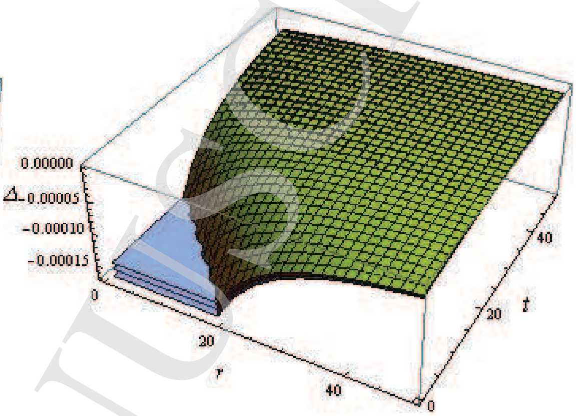

Figure 12: Plots of $\triangle$ versus r and t for $\gamma = 0.05$, $\alpha = 1$. The left graph is for $q = 0$ (pink), $q = 0.5$ (blue), $q = 1$ (purple) with $\lambda = 1$ while the right graph is for $\lambda = 1$ (brown), $\lambda = 2$ (red), $\lambda = 3$ (yellow) with $q = 0.5$.

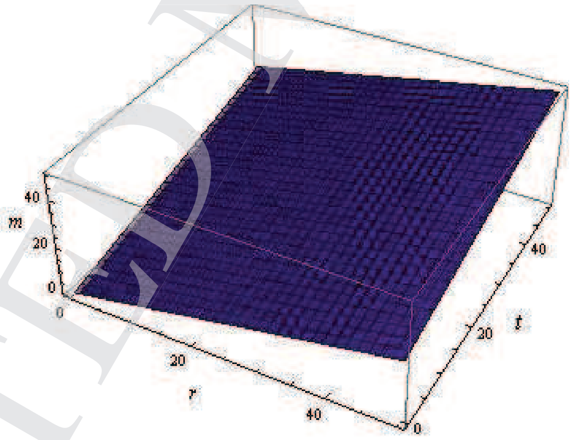

Figure 13: Plot of m versus r and t for $\gamma = 0.05$, $\alpha = 1$, $q = 0$ (pink), $q = 0.5$ (blue), $q = 1$ (purple).

ACCEPTED MANUSCRIPT

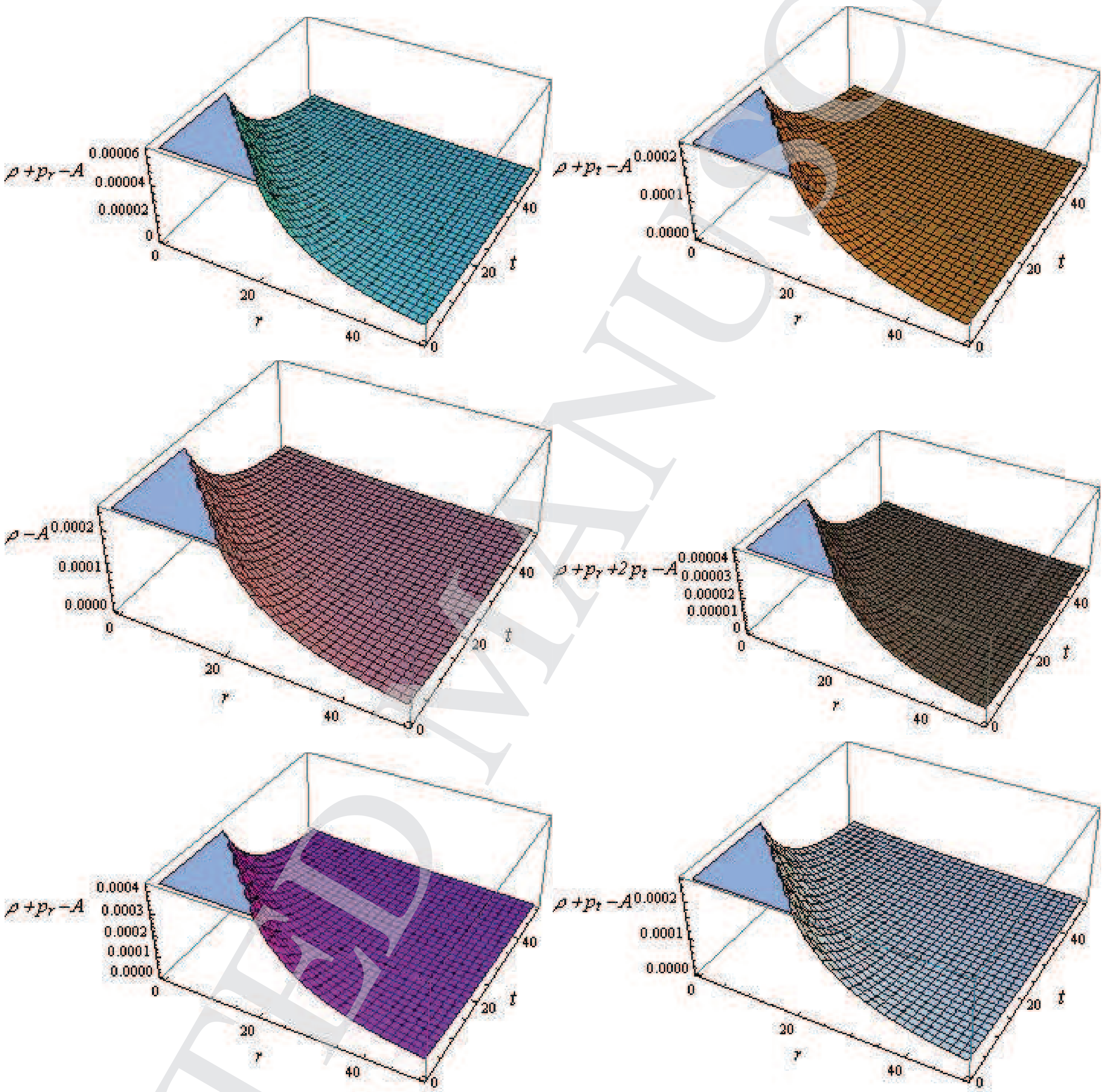

Figure 14: Plots of Energy Conditions versus r and t for $\gamma = 0.05$, $\alpha = 1$, $q = 0.5$ and $\lambda = 1$.

ACCEPTED MANUSCRIPT

Accepted manuscript to appear in IJMPD

ACCEPTED MANUSCRIPT

Table **2**: Change in physical parameters with respect to r and t for the expanding solution

Coordinate	Θ	ρ	p_r	p_t	$\triangle$	m
r	decreases	decreases	increases	increases	increases	increases
t	decreases	decreases	increases	increases	increases	increases

Table **3**: Effects of increasing λ for the expanding solution The solution

Physical Parameter	ρ	p_r	p_t	$\triangle$
As λ Increases	decreases	increases	increases	decreases

(39) yields the value of $\mathcal{A}$ as

$$\mathcal{A} = \frac{(r+t)^{-2(1+\gamma)}\gamma}{\alpha^2}(-1+\gamma(3+(r+t)^{4\gamma}\alpha^4)). \tag{45}$$

The energy conditions for this case are also satisfied as shown in Figure **14**.

3 Concluding Remarks

It is well-known that accelerated expansion of the universe initiates the presence of an unknown force (dark energy) with huge negative pressure. To unveil this mystery of dark energy, alternative theories are of much interest. This dominating factor of our universe could also overwhelm the astrophysical processes. The aim of this analysis is to discuss the solutions of Einstein-Maxwell field equations governing the phenomena of collapse and expansion during stellar evolution in the framework of $f(R,T)$ theory. We study the effects of curvature-matter coupling on the physical features of evolving spherical celestial bodies. We also discuss the consequences of electromagnetic field and the role of model parameter on the physical features.

For collapsing solution, the expansion scalar, density, pressure (radial and tangential), anisotropy and mass do not change with time. For expanding solution, the change remains the same for both coordinates, i.e., if one quantity is decreasing with respect to r, it is also decreasing with respect to t. The behavior of these parameters (except expansion scalar) with respect to radius remains the same for both cases. The energy conditions are satisfied for both solutions implying that our solutions are physically acceptable.

During collapse, charge particles come closer to each other and enhance the electromagnetic field. The graphical analysis for collapsing solution shows that the charge slows down (or it can halt) the collapsing process by decreasing density and increasing radial pressure. The effect of charge on the collapsing process is consistent with those given in literature [18, 22]. In expansion, charge particles move away from each other and consequently, electromagnetic field becomes weaker. This effect could be seen in graphs of expanding solution in which the effect of charge is not considerable (as the graphs overlap for different values of q). In both cases, the increase in model parameter has the same effect on physical quantities. In particular, it reduces density and increases pressure which enhance expansion and diminish collapse. Abbas and Ahmed [23] discussed the collapsing and expanding solutions without charge and with $H(t) = 1$, hence all the quantities are functions of r only. We have taken the effect of charge and $H(t)$ depends on t. This leads to different behavior of pressures as well as anisotropy but the effect of λ is similar for density while differs for pressures.

Acknowledgment

We would like to thank the Higher Education Commission, Islamabad, Pakistan for its financial support through the *Indigenous Ph.D. 5000 Fellowship Program Phase-II, Batch-III.*

References

[1] De Felice, A. and Tsujikawa, S.: Living Rev. Rel. **13**(2010)3; Nojiri, S.I. and Odintsov, S.D.: Phys. Rep. **505**(2011)59.

[2] Cembranos, J.A.R., Cruz-Dombriz, A.D.L. and Núez, B.M.: J. Cosmol. Astropart. Phys. 04(2012)021.

[3] Sharif, M. and Yousaf, Z.: Phys. Rev. D **88**(2013)024020; Eur. Phys. J. C **73**(2013)2633; Astropart. Phys. **56**(2014)19; Mon. Not. R. Astron. Soc. **440**(2014)3479.

[4] Harko, T., Lobo, F.S.N., Nojiri, S. and Odintsov, S.D.: Phys. Rev. D **84**(2011)024020.

ACCEPTED MANUSCRIPT

Accepted manuscript to appear in IJMPD

[5] Harko, T. and Lobo, F.S.N.: Galaxies **2**(2014)410.

[6] Sharif, M. and Zubair, M.: J. Cosmol. Astropart. Phys. **03**(2012)28.

[7] Noureen, I. and Zubair, M.: Eur. Phys. J. C **75**(2015)62; Zubair, M., and Noureen, I.: Eur. Phys. J. C **75**(2015)265; Noureen, I., Zubair, M., Bhatti, A.A. and Abbas, G.: Eur. Phys. J. C **75**(2015)323.

[8] Moraes, P.H.R.S.: Eur. Phys. J. C **75**(2015)168.

[9] Moraes, P.H.R.S. and Correa, R.A.C.: Astrophys. Space Sci. **361**(2016)91.

[10] Correa, R.A.C. and Moraes, P.H.R.S.: Eur. Phys. J. C **76**(2016)100.

[11] Moraes, P.H.R.S., José D.V.A. and Malheiro, M.: J. Cosmol. Astropart. Phys. **06**(2016)005.

[12] Sharif, M. and Nawazish, I.: Eur. Phys. J. C **77**(2017)198.

[13] Sharif, M. and Siddiqa, A.: Mod. Phys. Lett. A **32**(2017)1750151.

[14] Rosseland, S. and Eddington, A.S.: Mon. Not. R. Astron. Soc. **84**(1924)720.

[15] Bekenstein, J.D.: Phys. Rev. D **4**(1960)2185.

[16] Bonnor, W.B.: Mon. Not. R. Astron. Soc. **129**(1964)443.

[17] Azam, M., Mardan, S.A. and Rehman, M.A.: Adv. High Energy Phys. **2015**(2015)865086.

[18] Sharif, M. and Abbas, G.: Eur. Phys. J. Plus **128**(2013)102.

[19] Bhatti, M.Z. and Yousaf, Z.: Eur. Phys. J. C **76**(2016)219.

[20] Yousaf, Z. and Bhatti, M.Z.: Mon. Not. R. Astron. Soc. **458**(2016)1785.

[21] Glass, E.N.: Gen. Relativ. Gravit. **45**(2013)266.

[22] Abbas, G.: Astrophys. Space Sci. **352**(2014)955.

[23] Abbas, G. and Ahmed, R.: Eur. Phys. J. C **77**(2017)441.

ACCEPTED MANUSCRIPT

Accepted manuscript to appear in IJMPD

[24] Sharif, M. and Siddiqa, A.: Gen. Relativ. Gravit. **43**(2011)73.

[25] Moraes, P.H.R.S.: Eur. Phys. J. C **75**(2015)168; Shamir, M.F.: Eur. Phys. J. C **75**(2015)354; Correa, R.A.C. and Moraes, P.H.R.S.: Eur. Phys. J. C **76**(2016)100; Das, A., Rahaman, F., Guha, B.K. and Ray, S.: Eur. Phys. J. C **76**(2016)654; Das, A., Ghosh, S., Guha, B.K., Das, S., Rahaman, F. and Ray, S.: Phys. Rev. D **95**(2017)124011; Shabani, H. and Ziaie, A.H.: Eur. Phys. J. C **77**(2017)31; Gu, B.M., Zhang, Y.P., Yu, H. and Liu, Y.X.: Eur. Phys. J. C **77**(2017)115.

[26] Poplawski, N.J.: arXiv:gr-qc/0608031.

[27] Misner, C.W. and Sharp, D.: Phys. Rev. B **137**(1965)96501360.

[28] Booth, I.: Phys. Rev. D **93**(2016)084005.

[29] Sharif, M. and Ikram, A.: Int. J. Mod. Phys. D **27**(2018)1750182.

[30] Mahmood, A., Siddiqui, A.A. and Feroze, T.: J. Korean Phys. Soc. **71**(2017)396; Qadir, A. and Ziad, M.: Nuovo Cimento B **110**(1995)317.

ACCEPTED MANUSCRIPT

Hindawi
Advances in High Energy Physics
Volume 2019, Article ID 8702795, 16 pages
https://doi.org/10.1155/2019/8702795

Research Article

Models of Collapsing and Expanding Cylindrical Source in $f(R,T)$ Theory

M. Sharif and Aisha Siddiqa

Department of Mathematics, University of the Punjab, Quaid-e-Azam Campus, Lahore 54590, Pakistan

Correspondence should be addressed to M. Sharif; msharif.math@pu.edu.pk

Received 12 November 2018; Revised 9 January 2019; Accepted 9 January 2019; Published 14 February 2019

Academic Editor: Diego Saez-Chillon Gomez

Copyright © 2019 M. Sharif and Aisha Siddiqa. This is an open access article distributed under the Creative Commons Attribution License, which permits unrestricted use, distribution, and reproduction in any medium, provided the original work is properly cited.

We discuss the collapsing and expanding solutions of anisotropic charged cylinder in the context of $f(R,T)$ theory (R represents the Ricci scalar and T denotes the trace of energy-momentum tensor). For this purpose, we take an auxiliary solution of Einstein-Maxwell field equations and evaluate expansion scalar whose negative values lead to collapse and positive values give expansion. For both cases, the behavior of density, pressure, anisotropic parameter, and mass is explored and the effects of charge as well as model parameter on these quantities are examined. The energy conditions are found to be satisfied for both solutions.

1. Introduction

Gravitational force is amenable for governing many astrophysical phenomena like formation of stars, keeping stars together in galaxies, gravitational collapse, and restricting the heavenly bodies in their respective orbits. A star is in equilibrium state under the balance of pressure (directed outward) and gravity (directed inward). It undergoes collapse if gravity exceeds pressure and experiences expansion when pressure overcomes gravity. During the life, a star experiences both of these phenomena. Oppenheimer and Snyder [1] are pioneers to study the gravitational collapse for dust matter. Misner and Sharp worked on the collapse of a star considering isotropic [2] as well as anisotropic fluid [3].

After that, many researchers studied the process of collapse for different configurations. Stark and Piran [4] examined the gravitational waves emitted by the gravitational collapse of rotating relativistic polytropes. Herrera *et al.* [5] examined the dynamical instability of spherical symmetric collapsing fluid suffering heat dissipation and showed that dissipation increases the instability. Harada [6] investigated the final outcome of gravitational collapse of a sphere with perfect fluid distribution and discussed the limits when the singularity is naked or not. Joshi and Dwivedi [7] explored the final outcome of spherical symmetric dust collapse. Depending upon the initial pressure and density distribution, they discussed different new black hole solutions.

The $f(R)$ gravity is a direct generalization of general relativity (GR) obtained by replacing R with $f(R)$ in the Einstein-Hilbert action. Many astrophysical and cosmological phenomena have been explored within the scenario of $f(R)$ theory. The contributions of $f(R)$ terms can lead to different consequences on various phenomena. Sharif and Kausar [8] discussed the perfect fluid collapse in this theory and solved the equations assuming constant Ricci scalar. They showed that $f(R)$ terms play the role of antigravitational force. Cembranos *et al.* [9] worked on spherical dust collapse and showed that the contribution of $f(R)$ terms slows down the collapsing process. Hence in general, it can be deduced that the inclusion of higher order curvature terms reduces the collapse rate. Also in GR, a gravitational wave has two polarization modes while in $f(R)$ theory it is shown that gravitational wave has two extra modes compared to GR [10].

Harko *et al.* [11] proposed a more generalized gravitational theory known as $f(R,T)$ gravity. The curvature-matter coupling produces a deviation from geodesic motion which may yield interesting results and help to explore dark side of the universe [12]. Shabani and Farhoudi [13] investigated cosmological viability of some $f(R,T)$ gravity models using solar system constraints. Moraes *et al.* [14] studied the equilibrium configurations of neutron and quark stars in this theory concluding that mass can cross observational limits. Noureen and Zubair [15] investigated the stability of anisotropic spherical star in the framework of $f(R,T)$ yielding some constraints on physical quantities. Carvalho *et al.* [16] analyzed white dwarfs using an equation of state describing ionized atoms embedded in a relativistic Fermi gas of electrons in curvature-matter coupling scenario. They observed that white dwarfs have larger radius and mass in $f(R,T)$ gravity than those observed in GR and $f(R)$ theory.

Recent detection of gravitational waves has brought motivation to study the collapse phenomenon with the existence of gravitational waves in the exterior. It is well known by Bhirkoff's theorem that a spherical symmetric vacuum spacetime cannot have gravitational radiation. In this context, the next assumption is cylindrical system, because Einstein and Rosen found exact solution of the field equations which models the propagation of cylindrical gravitational waves. Sharif and Bhatti [17] discussed charged expansion-free cylindrical system and found that stability is controlled by charge, density, and pressures. Yousaf *et al.* [18] discussed the stability of cylindrical stellar system through perturbation technique and found its dependence on the stiffness parameter, matter variables, and $f(R,T)$ dark source terms. Sharif and Farooq investigated the dynamics of charged cylindrical collapse in $f(R)$ gravity with perfect [19] as well as bulk viscous dissipative fluid [20] and concluded that collapse rate slows down due to dark source terms.

Rosseland and Eddington [21] were the first who figured out the possibility that stars can have electric charge. After that, the presence of electromagnetic field in self-gravitating systems is explored by many researchers. The effects of charge on spherical collapse [22] and on the stability of compact objects [23] have been investigated with the conclusion that charge halts the collapse and increases the stability regions. Bhatti and Yousaf [24] explored the effects of electromagnetic field on plane symmetric anisotropic dissipative fluid configuration in Palatini $f(R)$ gravity. They concluded that matter inhomogeneity is enhanced with charge while it is decreased due to modified gravity terms. Mansour *et al.* [25] analyzed the features of compact stars in the presence of weak electromagnetic field in $f(R)$ gravity.

Glass [26] studied the collapsing and expanding solutions for a nonstatic anisotropic spherical source within the scenario of GR. Abbas extended this work for plane symmetric configuration [27], for charged spherical source [28], and for charged cylindrical geometry [29] in GR as well as for sphere in $f(R,T)$ gravity [30]. We discussed these solutions for charged spherical configuration in $f(R,T)$ theory [31]. In this paper, we investigate the effects of charge on the evolution of a nonstatic cylindrical source in $f(R,T)$ gravity. The paper is planned as follows. In the coming section, we discuss the outline of work done; then in the next one, we formulate the Einstein-Maxwell equations for $f(R,T) = R + 2\lambda T$ gravity model (where λ is coupling constant also called model parameter) and discuss the cases of collapse and expansion. In the last section, we summarize our results.

2. Physical Goals

In this section, we first discuss physical goals of the research work presented in this paper and then elaborate the technique to achieve these objectives. Here, we would like to explore physical characteristics of a cylindrical star during the phases of collapse and expansion in the dark energy dominated era. When a star starts to loose the hydrostatic equilibrium, firstly, its outer layers expand and it becomes a red-giant. However, after some time, the star suffers a supernova explosion and experiences a collapse. In order to discuss the whole scenario in an expanding universe, we consider $f(R,T)$ theory of gravity as discussed in the Introduction as an alternative to GR. Also, to extend our discussion, we observe the effects of electromagnetic field and consider a charged star. We aim to discuss the behavior of density, pressures, pressure anisotropy, and mass of the star as well as check the energy conditions for the obtained solutions. We also investigate the effects of curvature-matter coupling and presence of charge on the collapse and expansion phases of the star's life.

For this purpose, we generate collapsing and expanding solutions for our cylindrically symmetric model. We then analyze the physical parameters graphically such that the density and mass remain positive. Also, the obtained values of density and pressures must satisfy the energy conditions for the viability of the solution; otherwise there is a possibility of existence of exotic fluid that is an unrealistic situation. The value of curvature-matter coupling constant is taken such that our model $f(R,T) = R + 2\lambda T$ satisfies the viability conditions

$$\begin{gathered} f_R > 0, \\ 1 + \frac{f_T}{8\pi} > 0 \\ \text{and } f_{RR} > 0, \end{gathered} \tag{1}$$

which yield the constraint $\lambda > -4\pi$ for the considered model. In the graphical analysis, free parameters appearing in the solution are fixed such that our solution is physically acceptable; i.e., mass and density are positive and energy conditions are satisfied. In order to examine the effects of electromagnetic field and curvature-matter coupling constant, we vary the values of the total charge and λ in the plots and check the corresponding increase and decrease in the respective quantity.

3. Einstein-Maxwell Field Equations

The $f(R,T)$ gravity action with the contribution of electromagnetic field is defined as

$$S = \int d^4x\sqrt{-g}\left[\frac{1}{16\pi}f(R,T) + \mathscr{L}_m + \mathscr{L}_e\right]. \tag{2}$$

The electromagnetic Lagrangian density $\mathscr{L}_e$ has the form $\mathscr{L}_e = mF_{\mu\nu}F^{\mu\nu}$, m is an arbitrary constant, $F_{\mu\nu} = \phi_{\nu,\mu} - \phi_{\mu,\nu}$ represents the electromagnetic field tensor, and ϕ_μ represents the four potentials. The field equations for the above action are

$$f_R R_{\mu\nu} - \frac{1}{2} g_{\mu\nu} f + \left(g_{\mu\nu}\Box - \nabla_\mu \nabla_\nu\right) f_R = 8\pi T_{\mu\nu} - f_T \left(T_{\mu\nu} + \Theta_{\mu\nu}\right) + 8\pi E_{\mu\nu}, \tag{3}$$

where f_R and f_T denote the derivatives of $f(R,T)$ with respect to R and T, respectively. The expression for $\Theta_{\mu\nu}$ is given by

$$\Theta_{\mu\nu} = g^{\gamma\alpha} \frac{\delta T_{\gamma\alpha}}{\delta g^{\mu\nu}}, \qquad T_{\mu\nu} = g_{\mu\nu} \mathscr{L}_m - \frac{\partial \mathscr{L}_m}{\partial g^{\mu\nu}}, \tag{4}$$

and the electromagnetic energy-momentum tensor $E_{\mu\nu}$ is defined by

$$E_{\mu\nu} = \frac{1}{4\pi} \left(F_\mu{}^\alpha F_{\nu\alpha} - \frac{1}{4} F^{\alpha\beta} F_{\alpha\beta} g_{\mu\nu} \right). \tag{5}$$

The nonstatic cylindrically symmetric spacetime is taken as

$$ds^2 = -A^2(t,r)\, dt^2 + B^2(t,r)\, dr^2 + C^2(t,r)\, d\theta^2 + dz^2. \tag{6}$$

The energy-momentum tensor for anisotropic fluid is given by

$$T_{\mu\nu} = (\rho + p_r) V_\mu V_\nu + p_r g_{\mu\nu} - (p_r - p_z) S_\mu S_\nu - (p_r - p_\theta) K_\mu K_\nu, \tag{7}$$

where V_μ denotes the four velocities, S_μ, K_μ are unit four-vectors, ρ stands for density, and p_r, p_θ, p_z are the pressures in r, θ, and z directions, respectively. The four-vectors V_μ, S_μ, and K_μ have the expressions

$$V^\mu = \left(A^{-1}, 0, 0, 0\right), \quad K^\mu = \left(0, 0, C^{-1}, 0\right), \quad S^\mu = (0, 0, 0, 1), \tag{8}$$

which satisfy the following relations:

$$V^\mu V_\nu = -1, \quad K^\mu K_\nu = S^\mu S_\nu = 1, \quad S^\mu K_\nu = V^\mu K_\nu = V^\mu S_\nu = 0. \tag{9}$$

The Maxwell equations are given by

$$F^{\mu\nu}{}_{;\nu} = 4\pi j^\mu, \tag{10}$$

where j^μ represents the four currents. In comoving frame, the four potentials and four currents are defined as

$$\phi_\mu = (\phi, 0, 0, 0), \quad j_\mu = (\xi, 0, 0, 0), \tag{11}$$

ϕ, ξ (both are functions of t and r) represent electric scalar potential and charge density, respectively. The Maxwell equations for the metric (6) yield

$$\phi'' + \phi' \left(\frac{C'}{C} - \frac{A'}{A} - \frac{B'}{B} \right) = 4\pi \xi A B^2, \tag{12}$$

$$\dot{\phi}' + \phi' \left(\frac{\dot{C}}{C} - \frac{\dot{A}}{A} - \frac{\dot{B}}{B} \right) = 0. \tag{13}$$

Integration of (12) gives

$$\phi' = \frac{AB}{C} q, \quad q = 4\pi \int_0^r \xi B C dr, \tag{14}$$

where q is the total charge of the cylinder. We take $f(R,T) = R + 2\lambda T$ proposed by Harko *et al.* [11] to explore the effects of curvature-matter coupling on collapsing and expanding solutions. This model has frequently been used in literature [32–35] which yields a power-law type scale factor and is able to discuss accelerated expansion of the universe. It corresponds to ΛCDM model with trace dependent cosmological constant or $\Lambda(T)$ gravity discussed by Poplawski [36]. The above-mentioned expression of $f(R,T)$ and $\mathscr{L}_m = -\rho$ simplify the field equations as

$$G_{\mu\nu} = (8\pi + 2\lambda) T_{\mu\nu} + 2\lambda \rho g_{\mu\nu} + \lambda T g_{\mu\nu} + 8\pi E_{\mu\nu}, \tag{15}$$

which produces the following set of equations:

$$\frac{1}{B^2} \left[\frac{B'C'}{BC} - \frac{C''}{C} \right] + \frac{1}{A^2} \frac{\dot{B}\dot{C}}{BC} + \frac{A^2 q^2}{C^2} = 8\pi\rho - \lambda \left(-\rho + p_r + p_\theta + p_z\right), \tag{16}$$

$$\frac{\dot{C}'}{C} - \frac{\dot{C}}{C} \frac{A'}{A} - \frac{\dot{B}}{B} \frac{C'}{C} = 0, \tag{17}$$

$$\frac{1}{A^2} \left[\frac{\dot{A}\dot{C}}{AC} - \frac{\ddot{C}}{C} \right] + \frac{1}{B^2} \frac{A'C'}{AC} + \frac{B^2 q^2}{C^2} = 8\pi p_r + \lambda \left(\rho + 3p_r + p_\theta + p_z\right), \tag{18}$$

$$\frac{1}{A^2} \left[\frac{\dot{A}\dot{B}}{AB} - \frac{\ddot{B}}{B} \right] + \frac{1}{C^2} \left(\frac{\dot{C}}{B} \right)^2 \left[\frac{A''}{A} - \frac{A'B'}{AB} \right] - \frac{q^2}{C^2} = 8\pi p_\theta + \lambda \left(\rho + p_r + 3p_\theta + p_z\right), \tag{19}$$

$$\frac{1}{A^2} \left[-\frac{\ddot{B}}{B} - \frac{\ddot{C}}{C} - \frac{\dot{B}\dot{C}}{BC} + \frac{\dot{A}}{A} \left(\frac{\dot{B}}{B} + \frac{\dot{C}}{C} \right) \right] + \frac{1}{B^2} \left[\frac{A''}{A} + \frac{C''}{C} - \frac{A'B'}{AB} - \frac{C'}{C} \left(\frac{B'}{B} + \frac{A'}{A} \right) \right] - \frac{q^2}{C^2} = 8\pi p_z + \lambda \left(\rho + p_r + p_\theta + 3p_z\right), \tag{20}$$

where dot and prime represent differentiation with respect to t and r, respectively.

A simultaneous solution of the field equations gives the following explicit expressions of density and pressure components:

$$\begin{aligned}\rho = {} & \frac{1}{8\left(8\pi^2+6\pi\lambda+\lambda^2\right)A^3B^3C^2}\left[q^2\left(8\pi+5\lambda\right)A^5B^3\right. \\ & -2AB^2C\left(-2\left(2\pi+\lambda\right)\dot{B}\dot{C}+\lambda\left(C\ddot{B}+B\ddot{C}\right)\right) \\ & +\lambda B^2C\dot{A}\left(2C\dot{B}+B\left(\dot{C}+2C'\right)\right)-\lambda A^2\times\left(C^2+\dot{C}^2\right) \\ & \cdot\left(A'B'-BA''\right)+A^3\left(-2q^2\lambda B^3+q^2\lambda B^5+4\left(2\pi+\lambda\right)\right. \\ & \left.\left.\times CB'C'-4\left(2\pi+\lambda\right)BCC''\right)\right],\end{aligned} \quad (21)$$

$$\begin{aligned}p_r = {} & \frac{1}{8\left(2\pi+\lambda\right)\left(4\pi+\lambda\right)A^3B^3C^2}\left[-q^2\lambda A^5B^3\right. \\ & +q^2A^3B^3\left(2\lambda+\left(8\pi+3\lambda\right)B^2\right)-2AB^2C\left(-\lambda C\ddot{B}\right. \\ & \left.+\left(4\pi+\lambda\right)B\ddot{C}\right)+B^2C\dot{A}\left(-2\lambda C\dot{B}\right. \\ & \left.+B\left(-\lambda\dot{C}+2\left(8\pi+3\lambda\right)C'\right)\right) \\ & +A^2\left(4\left(2\pi+\lambda\right)BCA'C'\right. \\ & \left.\left.+\lambda\left(C^2+\dot{C}^2\right)\left(A'B'-BA''\right)\right)\right],\end{aligned} \quad (22)$$

$$\begin{aligned}p_\theta = {} & \frac{1}{8\left(2\pi+\lambda\right)\left(4\pi+\lambda\right)A^3B^3q^2}\left[-q^2\lambda A^5B^3\right. \\ & -q^2A^3B^3\left(8\pi+2\lambda+\lambda B^2\right)-2AB^2C\left(\left(4\pi+\lambda\right)C\ddot{B}\right. \\ & \left.-\lambda B\ddot{C}\right)+B^2C\dot{A}\left(2\left(4\pi+\lambda\right)C\dot{B}-\lambda B\left(\dot{C}+2C'\right)\right) \\ & \left.+A^2\left(\lambda C^2-\left(8\pi+3\lambda\right)\dot{C}^2\right)\left(A'B'-BA''\right)\right],\end{aligned} \quad (23)$$

$$\begin{aligned}p_z = {} & \frac{-1}{8\left(2\pi+\lambda\right)\left(4\pi+\lambda\right)A^3B^3C^2}\left[q^2\lambda A^5B^3\right. \\ & +2AB^2C\left(2\left(2\pi+\lambda\right)\dot{B}\dot{C}+\left(4\pi+\lambda\right)\left(C\ddot{B}+B\ddot{C}\right)\right) \\ & -B^2C\dot{A}\left(2\left(4\pi+\lambda\right)C\dot{B}+B\left(\left(8\pi+3\lambda\right)\times\dot{C}-2\lambda C'\right)\right) \\ & +A^2\left(4\left(2\pi+\lambda\right)BCA'C'\right. \\ & \left.+\left(8\pi+3\lambda\right)C^2\left(A'B'-BA''\right)+\lambda\dot{C}^2\left(-A'B'+BA''\right)\right) \\ & +A^3\left(2q^2\left(4\pi+\lambda\right)B^3+q^2\lambda B^5+4\left(2\pi+\lambda\right)CB'C'\right. \\ & \left.\left.-4\left(2\pi+\lambda\right)BCC''\right)\right].\end{aligned} \quad (24)$$

The anisotropic parameter is defined as

$$\triangle = p_r - p_\theta. \quad (25)$$

To investigate the collapse and expansion of considered cylindrical source, the expansion scalar is evaluated as

$$\Theta = \frac{1}{A}\left(\frac{\dot{B}}{B}+\frac{\dot{C}}{C}\right), \quad (26)$$

and an auxiliary solution of (17) is

$$A = \frac{\dot{C}}{\alpha C^\gamma}, \qquad B = \alpha C^\gamma, \quad (27)$$

where γ and $\alpha > 0$ are arbitrary constants. The above solution leads to

$$\Theta = \alpha\left(1+\gamma\right)C^{\gamma-1}. \quad (28)$$

The positive values of Θ provide expansion and its negative values correspond to collapse. The value of Θ depends on α, γ, and C in which α and C are always positive implying that we have collapse for $\gamma < -1$ and expansion for $\gamma > -1$. We explore these cases one by one in the following subsections.

3.1. Collapse for $\gamma < -1$. For collapsing solution, we find the unknown metric function C in the solution (27) such that the collapse leads to the formation of trapped surfaces. The mass function for the cylindrically symmetric charged source is obtained as

$$m\left(t,r\right) = \frac{1}{8}\left[1-\left(\frac{C'}{B}\right)^2+\left(\frac{\dot{C}}{A}\right)^2\right]+qC. \quad (29)$$

Equation (27) simplifies the mass expression as

$$m\left(t,r\right) = \frac{1}{8}\left(1+\alpha^2C^{2\gamma}-\frac{C'^2}{\alpha^2C^{2\gamma}}\right)+qC. \quad (30)$$

For trapped surface formation $m = 1/8 + qC$ [29], which yields

$$C_{trap} = \left[\alpha^2\left(1-2\gamma\right)r+g\left(t\right)\right]^{1/(1-2\gamma)}, \quad (31)$$

where $g(t)$ is an integration function and the collapsing solution becomes

$$A = \frac{1}{\alpha\left(1-2\gamma\right)}\dot{g}\left(\alpha^2\left(1-2\gamma\right)r+g\left(t\right)\right)^{\gamma/(1-2\gamma)}, \quad (32)$$

$$B = \alpha\left(\alpha^2\left(1-2\gamma\right)r+g\left(t\right)\right)^{\gamma/(1-2\gamma)}, \quad (33)$$

$$C_{trap} = \left(\alpha^2\left(1-2\gamma\right)r+g\left(t\right)\right)^{1/(1-2\gamma)}. \quad (34)$$

For the sake of simplicity, we consider $g(t)$ as a linear function of t, i.e., $g(t) = t/\alpha^2$, and obtain the following expressions of density and pressures:

$$\rho = \frac{\left(t/\alpha^2 + r(1-2\gamma)\alpha^2\right)^{(2+4\gamma)/(2\gamma-1)}}{8(1-2\gamma)^2(8\pi^2+6\pi\lambda+\lambda^2)\alpha^6}\left[q^2(8\pi+5\lambda)\left(\frac{t}{\alpha^2}+r(1-2\gamma)\alpha^2\right)^{6\gamma/(1-2\gamma)}\right.$$
$$-\frac{1}{\left(t+r(1-2\gamma)\alpha^4\right)^2}\left(2(1-2\gamma)^2\gamma(-4\pi+(-1+3\gamma)\lambda)\alpha^{12}\times\left(\frac{t}{\alpha^2}+r(1-2\gamma)\alpha^2\right)^{(2+2\gamma)/(1-2\gamma)}\right)$$
$$+\frac{\gamma(-1+2\gamma)\lambda\alpha^{12}\left(t/\alpha^2+r(1-2\gamma)\alpha^2\right)^{(2+2\gamma)/(1-2\gamma)}}{\left(t+r(1-2\gamma)\alpha^4\right)^4}\times\left(1+t^2(1-2\gamma)^2-2rt(-1+2\gamma)^3\alpha^4+r^2(1-2\gamma)^4\alpha^8\right)$$
$$-\frac{1}{\left(t+r(1-2\gamma)\alpha^4\right)^2}\times\left((1-2\gamma)^2\gamma\lambda\alpha^{12}\left(\frac{t}{\alpha^2}+r(1-2\gamma)\alpha^2\right)^{(2+2\gamma)/(1-2\gamma)}\left(-1-2\alpha^4+\gamma\left(-2+4\alpha^4\right)\right)\right)+(1-2\gamma)^2 \quad (35)$$
$$\cdot\alpha^3\left(\frac{t}{\alpha^2}+r(1-2\gamma)\alpha^2\right)^{\gamma/(1-2\gamma)}\left\{-2q^2\lambda\alpha^3\left(\frac{t}{\alpha^2}+r(1-2\gamma)\alpha^2\right)^{3\gamma/(1-2\gamma)}+q^2\lambda\alpha^5\left(\frac{t}{\alpha^2}+r(1-2\gamma)\alpha^2\right)^{5\gamma/(1-2\gamma)}+4\gamma(2\pi\right.$$
$$\left.\left.+\lambda)\alpha^5\left(\frac{t}{\alpha^2}+r(1-2\gamma)\alpha^2\right)^{5\gamma/(1-2\gamma)}-\frac{1}{\left(t+r(1-2\gamma)\alpha^4\right)^2}8\gamma(2\pi+\lambda)\alpha^9\left(\frac{t}{\alpha^2}+r(1-2\gamma)\alpha^2\right)^{(2+\gamma)/(1-2\gamma)}\right\}\right],$$

$$p_r = \frac{\left(t/\alpha^2 + r(1-2\gamma)\alpha^2\right)^{(2+4\gamma)/(2\gamma-1)}}{8(1-2\gamma)^2(2\pi^2+\lambda)(4\pi^2+\lambda)\alpha^6}\left[-q^2\lambda\left(\frac{t}{\alpha^2}+r(1-2\gamma)\alpha^2\right)^{6\gamma/(1-2\gamma)}\right.$$
$$+\frac{1}{\left(t+r(1-2\gamma)\alpha^4\right)^2}\left(2(1-2\gamma)^2\gamma(-8\pi+3(-1+\gamma)\lambda)\alpha^{12}\times\left(\frac{t}{\alpha^2}+r(1-2\gamma)\alpha^2\right)^{(2+2\gamma)/(1-2\gamma)}\right)+(q-2q\gamma)^2\alpha^6\left(\frac{t}{\alpha^2}\right.$$
$$\left.+r(1-2\gamma)\alpha^2\right)^{4\gamma/(1-2\gamma)}\times\left(2\lambda+(8\pi+3\lambda)\alpha^2\left(\frac{t}{\alpha^2}+r(1-2\gamma)\alpha^2\right)^{2\gamma/(1-2\gamma)}\right)-\left(-8\pi(-1+2\gamma)\times\left(t+r(1-2\gamma)\alpha^4\right)^2\right. \quad (36)$$
$$\left.+\lambda\left(1+t^2\left(5-12\gamma+4\gamma^2\right)-2rt(1-2\gamma)^2(-5+2\gamma)\alpha^4+r^2(-5+2\gamma)(-1+2\gamma)^3\alpha^3\right)\right)$$
$$\cdot\left(\left(t+r(1-2\gamma)\alpha^4\right)^4\gamma(-1+2\gamma)\alpha^{12}\times\left(\frac{t}{\alpha^2}+r(1-2\gamma)\alpha^2\right)^{(2+2\gamma)/(1-2\gamma)}\right)-\frac{1}{\left(t+r(1-2\gamma)\alpha^4\right)^2}(1-2\gamma)^2\gamma\alpha^{12}\times\left(\frac{t}{\alpha^2}\right.$$
$$\left.\left.+r(1-2\gamma)\alpha^2\right)^{(2+2\gamma)/(1-2\gamma)}\left(16\pi(-1+2\gamma)\alpha^4+\lambda\left(1-6\alpha^4+2\gamma\left(1+6\alpha^4\right)\right)\right)\right],$$

$$p_\theta = \frac{\left(t/\alpha^2 + r(1-2\gamma)\alpha^2\right)^{(2+4\gamma)/(-1+2\gamma)}}{8(1-2\gamma)^2(2\pi+\lambda)(4\pi+\lambda)\alpha^6}\left[-q^2\lambda\left(\frac{t}{\alpha^2}+r(1-2\gamma)\alpha^2\right)^{6\gamma/(1-2\gamma)}\right.$$
$$-\frac{2(1-2\gamma)^2\gamma(4\pi(-1+3\gamma)+3(-1+\gamma)\lambda)\alpha^{12}\left(t/\alpha^2+r(1-2\gamma)\alpha^2\right)^{(2+2\gamma)/(1-2\gamma)}}{\left(t+r(1-2\gamma)\alpha^4\right)^2}$$
$$+\frac{(1-2\gamma)^2\gamma\alpha^{12}\left(t/\alpha^2+r(1-2\gamma)\alpha^2\right)^{(2+2\gamma)/(1-2\gamma)}}{\left(t+r(1-2\gamma)\alpha^4\right)^2}\left(8\pi\gamma+(-1+2\gamma)\lambda\left(1+2\alpha^4\right)\right) \quad (37)$$
$$+\frac{(1-2\gamma)^3\gamma\alpha^{12}\left(t/\alpha^2+r(1-2\gamma)\alpha^2\right)^{(2+2\gamma)/(1-2\gamma)}}{\left(t+r(1-2\gamma)\alpha^4\right)^2}\left(\lambda-\frac{8\pi+3\lambda}{(1-2\gamma)^2\left(t+r(1-2\gamma)\alpha^4\right)^2}-q^2(1-2\gamma)^2\alpha^6\right)\left(\frac{t}{\alpha^2}\right.$$
$$\left.\left.+r(1-2\gamma)\alpha^2\right)^{4\gamma/(1-2\gamma)}\left(8\pi+\lambda\left(2+\alpha^2\times\left(\frac{t}{\alpha^2}+r(1-2\gamma)\alpha^2\right)^{2\gamma/(1-2\gamma)}\right)\right)\right],$$

$$p_z = \frac{\alpha^6 \left(t/\alpha^2 + r(1-2\gamma)\alpha^2\right)^{(2+2\gamma)/(-1+2\gamma)}}{8(1-2\gamma)^2(2\pi+\lambda)(4\pi+\lambda)} \left[8\pi(1-2\gamma)^2 \left(\frac{-2\gamma\left(t/\alpha^2 + r(1-2\gamma)\alpha^2\right)^{2/(1-2\gamma)}}{\left(t + r(1-2\gamma)\alpha^4\right)^2} - \frac{q^2\left(t/\alpha^2 + r(1-2\gamma)\alpha^2\right)^{2\gamma/(1-2\gamma)}}{\alpha^6} \right) + \lambda \left(\frac{-q^2\left(t/\alpha^2 + r(1-2\gamma)\alpha^2\right)^{2\gamma/(1-2\gamma)}}{\alpha^{12}} \times \left(2(1-2\gamma)^2\alpha^6 + \left(\frac{t}{\alpha^2} + r(1-2\gamma)\alpha^2\right)^{2\gamma/(1-2\gamma)} + (1-2\gamma)^2\alpha^6 \times \left(\frac{t}{\alpha^2} + r(1-2\gamma)\alpha^2\right)^{2\gamma/(1-2\gamma)}\right) + \left(-1 + \left(4rt(1-2\gamma)^2\alpha^4 + 2r^2(-1+2\gamma)^3\alpha^8\right) \times \left(-3 + \gamma - \alpha^4 + 2\gamma\alpha^4 + 2t^2\left(3 + \alpha^4 + \gamma^2\left(2+4\alpha^4\right) - \gamma\left(7+4\alpha^4\right)\right)\right)\right) \times \left(\left(t + r(1-2\gamma)\alpha^4\right)^4 \gamma(-1+2\gamma)\left(\frac{t}{\alpha^2} + r(1-2\gamma)\alpha^2\right)^{2/(1-2\gamma)}\right)^{-1} \right) \right]. \quad (38)$$

For the solution (32)-(34), the anisotropic parameter and mass function become

$$\triangle = \frac{\alpha^6 \left(t/\alpha^2 + r(1-2\gamma)\alpha^2\right)^{(2+2\gamma)/(-1+2\gamma)}}{8(1-2\gamma)(4\pi+\lambda)} \left[-q^2(-1+\gamma) \cdot \alpha^{-6}\left(\frac{t}{\alpha^2} + r(1-2\gamma)\alpha^2\right)^{2\gamma/(1-2\gamma)} \times \left(1 + \alpha^2\left(\frac{t}{\alpha^2} + r(1-2\gamma)\alpha^2\right)^{2\gamma/(-1+2\gamma)}\right) + \left(1 - 4rt(1-2\gamma)^2\alpha^4\left(1 - \alpha^4 - \gamma\left(-1+2\alpha^4\right)\right) + 2r^2(-1+2\gamma)^3\alpha^8\left(1 - \alpha^8 - \gamma\left(-1+2\alpha^4\right)\right) + \frac{2t^2\left(-1 + \alpha^4 + \gamma\left(3-4\alpha^4\right) + \gamma^2\left(-2+4\alpha^4\right)\right)}{\left(t + r(1-2\gamma)\alpha^4\right)^4 \gamma\left(t/\alpha^2 + r(1-2\gamma)\alpha^2\right)^{2/(-1+2\gamma)}}\right)\right], \quad (39)$$

$$m = \frac{1}{8} + q\left(\frac{t}{\alpha^2} + r(1-2\gamma)\alpha^2\right)^{1/(1-2\gamma)}. \quad (40)$$

For the collapsing case, the graphical representation of different parameters is given in Figures 1–7. We observe that the quantities are changing with respect to temporal coordinate while no change is observed with respect to radial coordinate. The change in different quantities with respect to time is given in Table 1 and the effects of charge as well as model parameter λ are summarized in Table 2.

To observe physical viability of our solution, we plot the null (NEC), weak (WEC), strong (SEC), and dominant (DEC) energy conditions for the curvature-matter coupled gravity [37]:

(i) NEC: $\rho + p_r - \mathscr{A} \geq 0$, $\rho + p_\theta - \mathscr{A} \geq 0$, $\rho + p_z - \mathscr{A} \geq 0$.

(ii) WEC: $\rho - \mathscr{A} \geq 0$, $\rho + p_r - \mathscr{A} \geq 0$, $\rho + p_\theta - \mathscr{A} \geq 0$, $\rho + p_z - \mathscr{A} \geq 0$.

(iii) SEC: $\rho + p_r + p_\theta + p_z - \mathscr{A} \geq 0$.

(iv) DEC: $\rho - p_r - \mathscr{A} \geq 0$, $\rho + p_\theta - \mathscr{A} \geq 0$, $\rho - p_z - \mathscr{A} \geq 0$.

The term $\mathscr{A} = (V^\beta V^\alpha_{;\beta})_{;\alpha}$ is due to nongeodesic motion of massive particles. We evaluate $\mathscr{A}$ as

$$\mathscr{A} = \frac{1}{B^2}\left[\frac{A''}{A} + \frac{A'}{A}\left(-\frac{B'}{B} + \frac{C'}{C} + \frac{A'}{A}\right)\right] + \frac{\dot{A}^2}{A^4}. \quad (41)$$

For the collapse solution, we have

$$\mathscr{A} = \frac{4\gamma^2\alpha^6\left(t/\alpha^2 + r(1-2\gamma)\alpha^2\right)^{2\gamma/(-1+2\gamma)}}{\left(t + r(1-2\gamma)\alpha^4\right)^2}. \quad (42)$$

All the energy conditions defined above are plotted in Figures 8–11; the repeated expressions are shown only once. From these plots, it can be easily seen that all the energy conditions are satisfied for the considered values of free parameters of the collapse solution.

3.2. Expansion for $\gamma > -1$. In this case, we require an expression of the metric coefficient C for expanding solution. For convenience, We assume it a linear combination of r and t such that the expansion scalar remains positive for the resulting solution as shown in Figure 12. Thus the expanding solution is given by

$$A = \frac{1}{\alpha(r+t)^\gamma}, \quad B = \alpha(r+t)^\gamma, \quad C = r + t. \quad (43)$$

Consequently, the expressions of ρ, p_r, p_θ, and p_z take the form

$$\rho = \frac{(r+t)^{-2(2+\gamma)}}{8(8\pi^2 + 6\pi\lambda + \lambda^2)\alpha^2}\left[8\pi(r+t)^2\left(q^2 + \gamma + (r+t)^{4\gamma}\gamma C^4\right) + \lambda\left(q^2(r+t)^2\left(5 - 2(r+t)^{2\gamma}\alpha^2 + (r+t)^{4\gamma}\alpha^4\right) - \gamma\left(-1 - 2\gamma + t^2\left(-5 - 2\gamma - 3(r+t)^{4\gamma}\alpha^4 + 4(r+t)^{4\gamma}\gamma\alpha^4\right) + r^2\left(-5 - 3(r+t)^{4\gamma}\alpha^4 + \gamma\left(-2 + 4(r+t)^{4\gamma}\alpha^4\right)\right)\right)\right)\right], \quad (44)$$

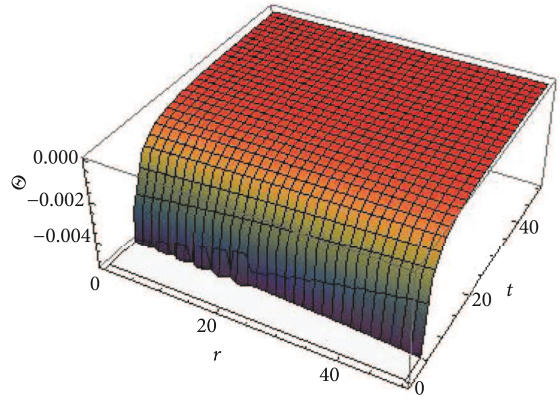

Figure 1: Plot of Θ versus r and t for $\gamma = -1.5$, $\alpha = 0.1$.

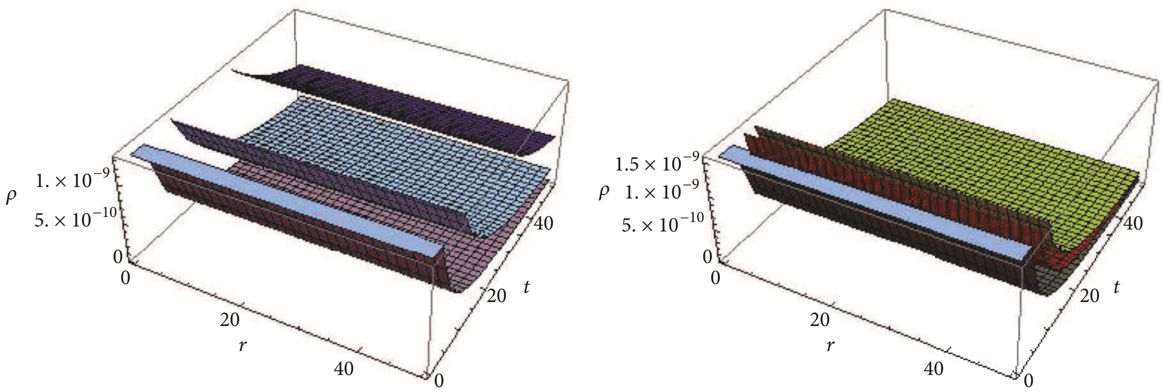

Figure 2: Plots of ρ versus r and t for $\gamma = -1.5$, $\alpha = 0.1$. The left graph is for $q = 0$ (pink), $q = 0.00005$ (blue), and $q = 0.0001$ (purple) with $\lambda = -0.1$ and the right graph is for $\lambda = -0.1$ (brown), $\lambda = -0.2$ (red), and $\lambda = -0.3$ (yellow) with $q = 0.0001$.

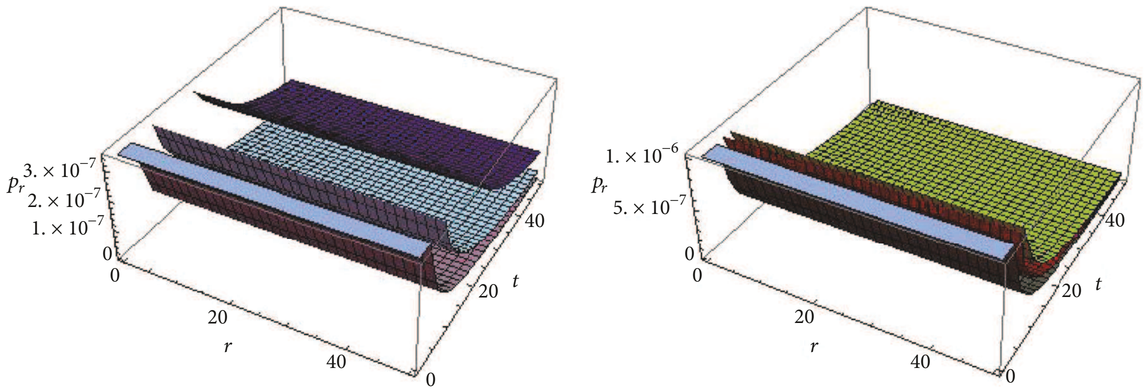

Figure 3: Plots of p_r versus r and t for $\gamma = -1.5$, $\alpha = 0.1$. The left graph is for $q = 0$ (pink), $q = 0.01$ (blue), and $q = 0.02$ (purple) with $\lambda = -0.1$ while the right graph is for $\lambda = -0.1$ (brown), $\lambda = -0.2$ (red), and $\lambda = -0.3$ (yellow) with $q = 0.01$.

Table 1: Change in parameters with respect to t for the collapse solution.

Parameter	ρ	p_r	p_θ	p_z	$\triangle$	m
As t increases	decreases	decreases	increases	decreases	decreases	increases

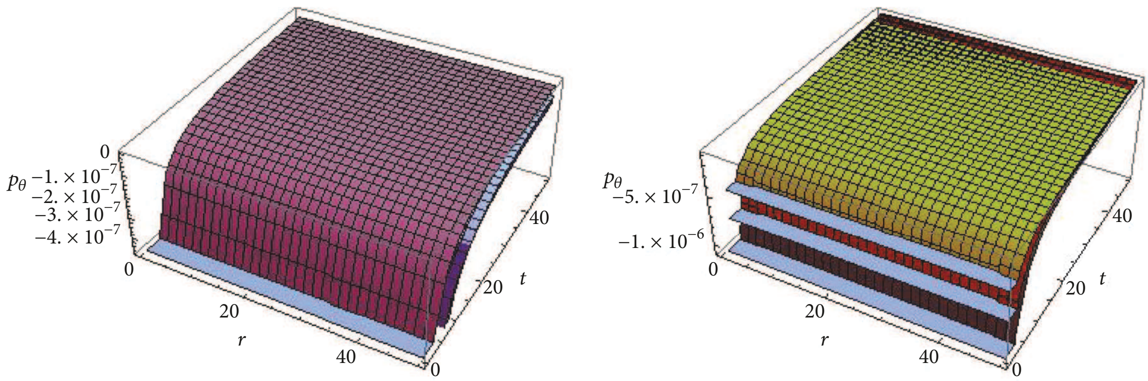

FIGURE 4: Plots of p_θ versus r and t for $\gamma = -1.5$, $\alpha = 0.1$. The left graph is for $q = 0$ (pink), $q = 0.005$ (blue), and $q = 0.01$ (purple) with $\lambda = -0.1$ and the right graph is for $\lambda = -0.1$ (brown), $\lambda = -0.15$ (red), and $\lambda = -0.2$ (yellow) with $q = 0.01$.

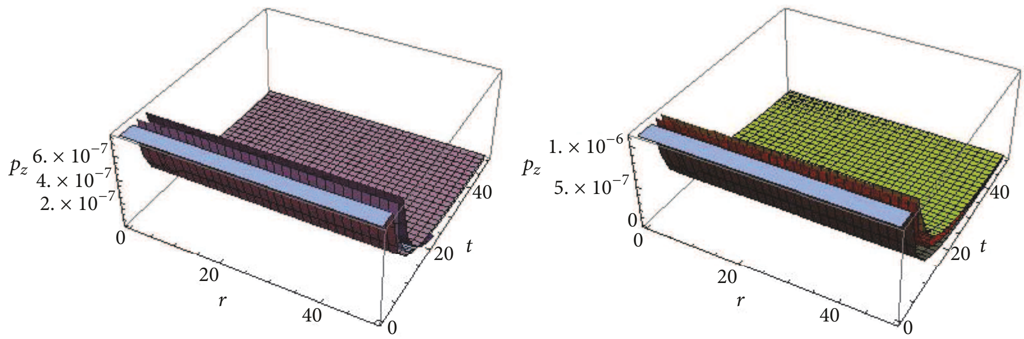

FIGURE 5: Plots of p_z versus r and t for $\gamma = -1.5$, $\alpha = 0.1$. The left graph is for $q = 0$ (pink), $q = 0.01$ (blue), and $q = 0.02$ (purple) with $\lambda = -0.1$ and the right graph is for $\lambda = -0.1$ (brown), $\lambda = -0.2$ (red), and $\lambda = -0.3$ (yellow) with $q = 0.01$.

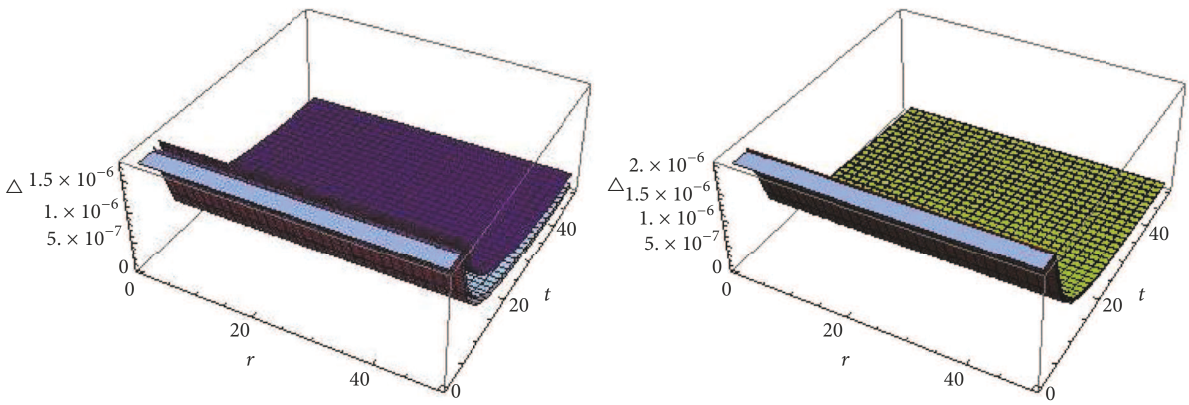

FIGURE 6: Plots of $\triangle$ versus r and t for $\gamma = -1.5$, $\alpha = 0.1$. The left graph is for $q = 0$ (pink), $q = 0.01$ (blue), and $q = 0.02$ (purple) with $\lambda = -0.1$ and the right graph is for $\lambda = -0.1$ (brown), $\lambda = -0.2$ (red), and $\lambda = -0.3$ (yellow) with $q = 0.01$.

TABLE 2: Effects of q and λ for the collapse solution.

Parameter	ρ	p_r	p_θ	p_z	$\triangle$	m
As q increases	increases	increases	decreases	decreases	increases	increases
As λ decreases	increases	increases	increases	increases	increases	no change

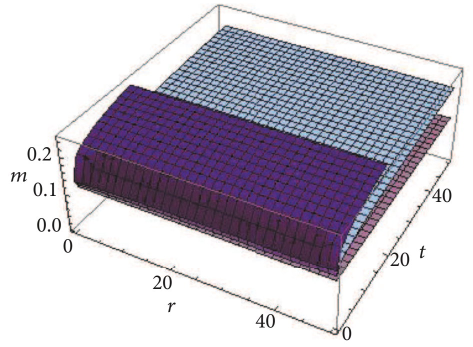

Figure 7: Plot of m versus r and t for $\gamma = -1.5$, $\alpha = 0.1$, $q = 0$ (pink), $q = 0.01$ (blue), and $q = 0.02$ (purple).

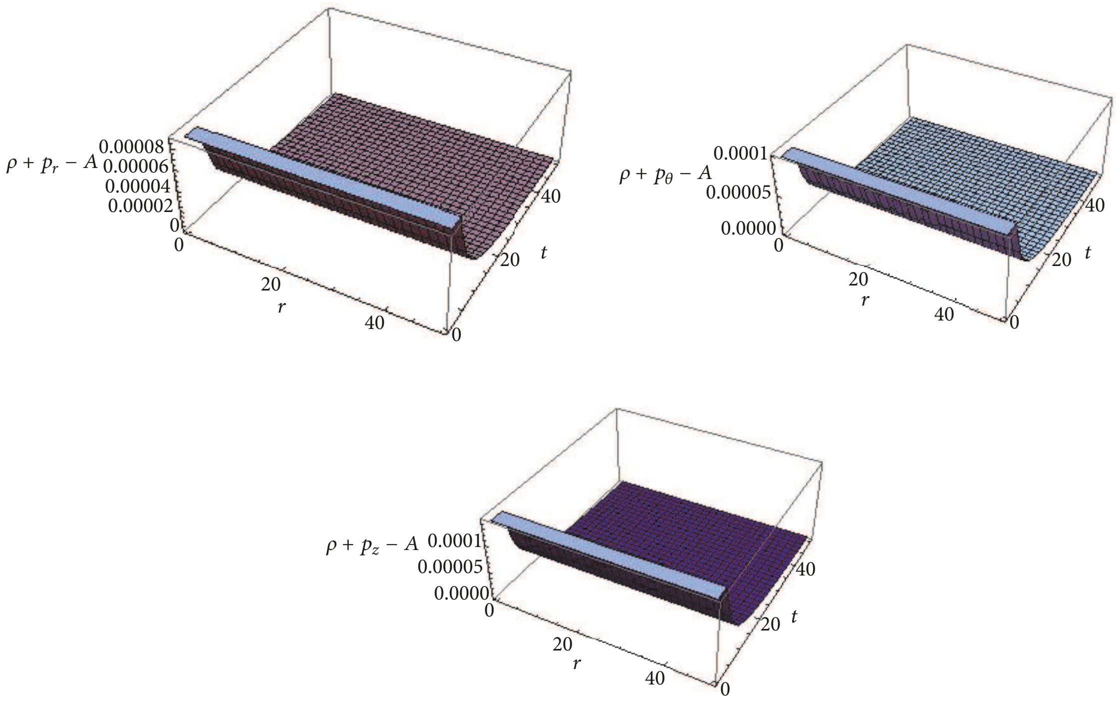

Figure 8: Plots for NEC for $\gamma = -1.5$, $\alpha = 0.1$, $q = 0.01$, and $\lambda = -0.1$.

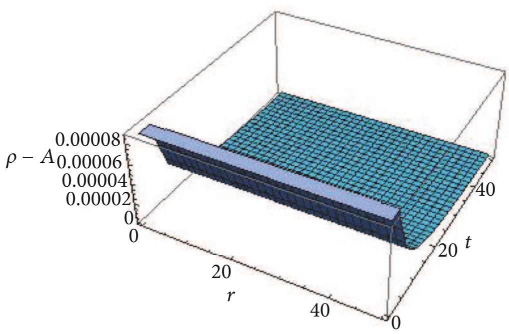

Figure 9: Plot for WEC for $\gamma = -1.5$, $\alpha = 0.1$, $q = 0.01$, and $\lambda = -0.1$.

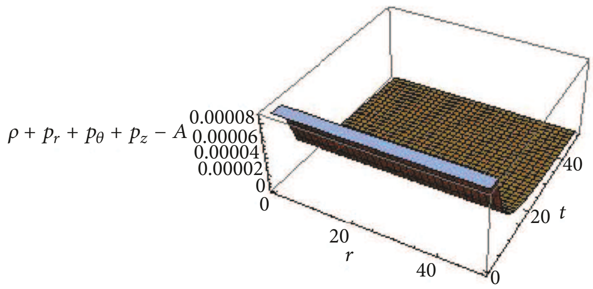

FIGURE 10: Plot for SEC for $\gamma = -1.5$, $\alpha = 0.1$, $q = 0.01$, and $\lambda = -0.1$.

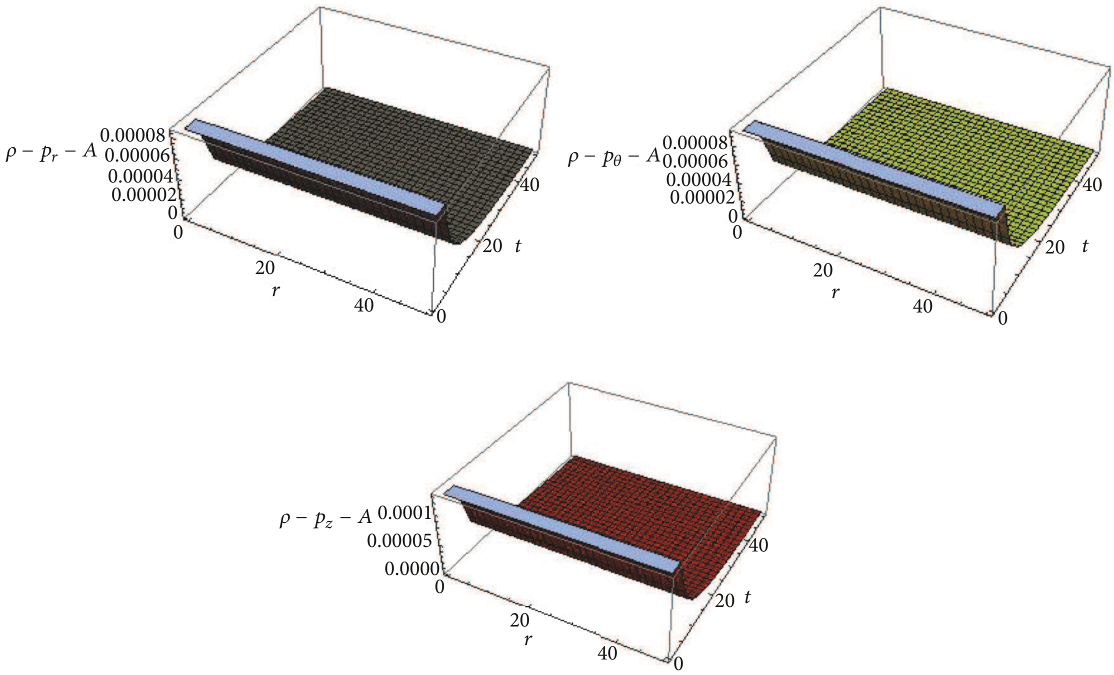

FIGURE 11: Plots for DEC for $\gamma = -1.5$, $\alpha = 0.1$, $q = 0.01$, and $\lambda = -0.1$.

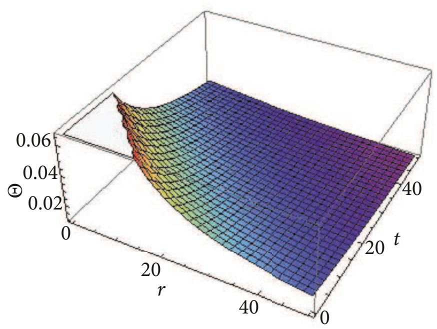

FIGURE 12: Plot of Θ versus r and t for $\gamma = 0.0001$, $\alpha = 1$.

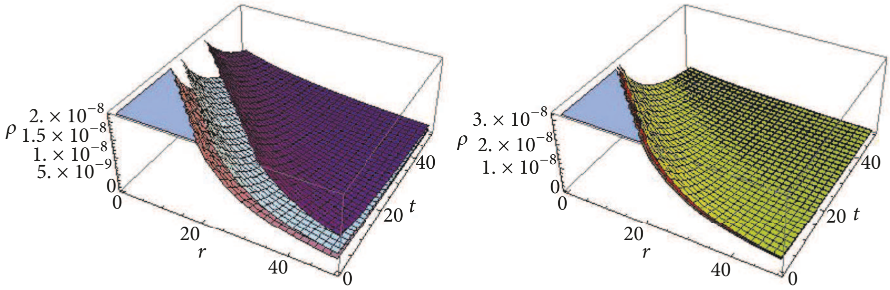

FIGURE 13: Plots of ρ versus r and t for $\gamma = 0.0001$, $\alpha = 1$. The left graph is for $q = 0$ (pink), $q = 0.01$ (blue), and $q = 0.02$ (purple) with $\lambda = -0.001$ and the right graph is for $\lambda = -0.001$ (brown), $\lambda = -1$ (red), and $\lambda = -2$ (yellow) with $q = 0.01$.

TABLE 3: Change in parameters with respect to r and t for the expanding solution.

Parameter	ρ	p_r	p_θ	p_z	$\triangle$	m
As r increases	decreases	decreases	increases	increases	decreases	increases
As t increases	decreases	decreases	increases	increases	decreases	increases

$$p_r = \frac{1}{8(r+t)^2(2\pi+\lambda)(4\pi+\lambda)}\left[\frac{-q^2(r+t)^{-2\gamma}\lambda}{\alpha^2} - \frac{(r+t)^{-2(1+\gamma)}\gamma}{\alpha^2} \times \left(8\pi(r+t)^2 + \left(1+2\gamma+r^2(5+2\gamma)+2rt(5+2\gamma)\right.\right.\right.$$
$$\left.\left.\left. + t^2(5+2\gamma)\right)\lambda\right) + 2(r+t)^{2\gamma}(-1+\gamma)\gamma\lambda\alpha^2 + (r+t)^{2\gamma}\gamma(-16\pi+(-5+2\gamma)\lambda)\alpha^2 + q^2\left(2\lambda+(r+t)^{2\gamma}(8\pi+3\lambda)\alpha^2\right)\right], \tag{45}$$

$$p_\theta = \frac{1}{8(r+t)^2(2\pi+\lambda)(4\pi+\lambda)}\left[\frac{-q^2(r+t)^{-2\gamma}\lambda}{\alpha^2} + \frac{(r+t)^{-2(1+\gamma)}\gamma(1+2\gamma)}{\alpha^2} \times \left(-8\pi+\left(-3+r^2+2rt+t^2\right)\lambda\right) + 2(r+t)^{2\gamma}(-1\right.$$
$$\left. +\gamma)\gamma(4\pi+\lambda)\alpha^2 + (r+t)^{2\gamma}\gamma(8\pi\gamma+(-3+2\gamma)\lambda)\alpha^2 + q^2\left(8\pi+\lambda\left(2+(r+t)^{2\gamma}\alpha^2\right)\right)\right], \tag{46}$$

$$p_z = \frac{(r+t)^{-2(2+\gamma)}}{8(2\pi+\lambda)(4\pi+\lambda)\alpha^2}\left[-8\pi(r+t)^2\left(q^2(r+t)^{2\gamma}\alpha^2+\left(\gamma+2\gamma^2\right)\left(-1+(r+t)^{4\gamma}\alpha^4\right) - \lambda\left(q^2(r+t)^2\left(1+(r+t)^{2\gamma}\alpha^2\right)^2\right.\right.\right.$$
$$\left.\left.\left. +\gamma\left(1+2\gamma+t^2\times\left(-3-6\gamma+3(r+t)^{4\gamma}\alpha^4+4(r+t)^{4\gamma}\gamma\alpha^4\right)+\left(r^2+2rt\right)\left(-3+3(r+t)^{4\gamma}\alpha^4+\gamma\left(-6+4(r+t)^{4\gamma}\alpha^4\right)\right)\right)\right)\right)\right]. \tag{47}$$

The anisotropic parameter and mass function are obtained as

$$\triangle = \frac{(r+t)^{-2(2+\gamma)}}{2(4\pi+\lambda)\alpha^2}\left[q^2(r+t)^{2+2\gamma}\alpha^2\left(1+(r+t)^{2\gamma}\alpha^2\right)\right.$$
$$+2\gamma^2\times\left(-1+\left(r^2+2rt+t^2\right)(r+t)^{4\gamma}\alpha^4\right) - \gamma\left(1+t^2\right.$$
$$\left.\left. +3t^2(r+t)^{4\gamma}\alpha^4+\left(r^2+2rt\right)\left(1+3(r+t)^{4\gamma}\alpha^4\right)\right)\right], \tag{48}$$

$$m = \frac{1}{8} + q(r+t). \tag{49}$$

The evolution of physical parameters during expansion is represented through Figures 13–18. It is found that the quantities vary with both time and radial coordinates. The graphical analysis is summarized in Tables 3 and 4.

The acceleration term $\mathscr{A}$ in this case becomes

$$\mathscr{A} = \frac{(r+t)^{-2(1+\gamma)}\gamma^2}{\alpha^2}\left(3+(r+t)^{4\gamma}\alpha^4\right). \tag{50}$$

The graphs for energy conditions for expanding solutions are given in Figures 19–22 showing that all the energy conditions are satisfied.

4. Concluding Remarks

Accelerated expansion of the universe is an observed phenomenon which can affect astrophysical processes. To study the consequences of the expanding universe on collapsing and expanding scenarios of a stellar object, we consider charged anisotropic cylindrical source in $f(R,T)$ framework. The solutions of Einstein-Maxwell field equations governing the phenomena of collapse and expansion during stellar evolution are discussed. We explore the role of electromagnetic field and model parameter on the physical features.

In case of collapse solution, the expansion scalar, density, pressures (p_r, p_θ, and p_z), anisotropy, and mass do not change with radial coordinate. For expanding solution, the change remains the same for both coordinates. The behavior of these

Table 4: Effects of q and λ for the expanding solution.

Parameter	ρ	p_r	p_θ	p_z	$\triangle$	m
As q increases	increases	increases	decreases	decreases	increases	increases
As λ decreases	increases	increases	decreases	decreases	increases	no change

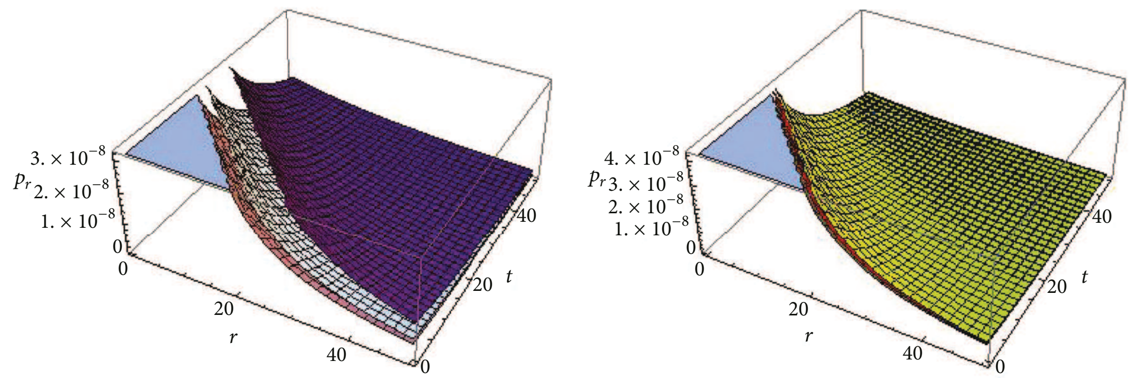

Figure 14: Plots of p_r versus r and t for $\gamma = 0.0001$, $\alpha = 1$. The left graph is for $q = 0$ (pink), $q = 0.01$ (blue), and $q = 0.02$ (purple) with $\lambda = -0.001$ while the right graph is for $\lambda = -0.001$ (brown), $\lambda = -1$ (red), and $\lambda = -2$ (yellow) with $q = 0.01$.

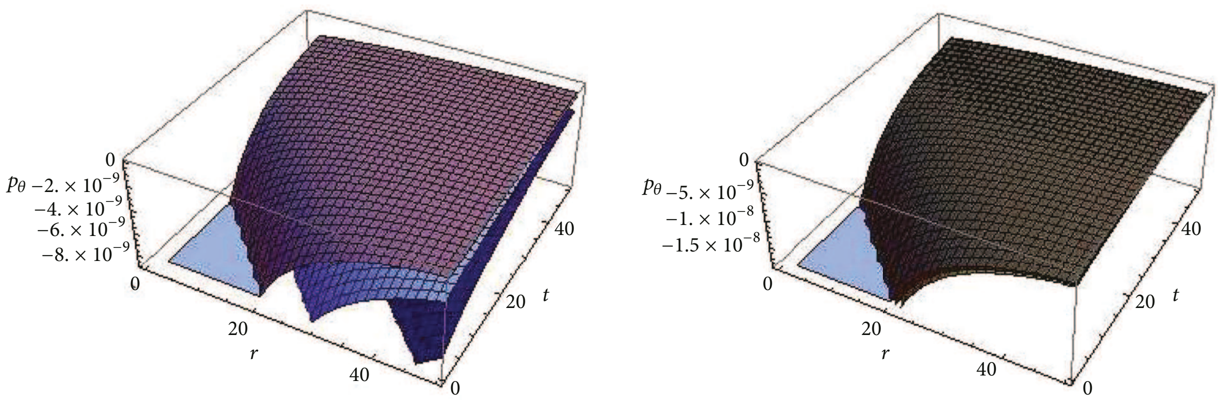

Figure 15: Plots of p_θ versus r and t for $\gamma = 0.0001$, $\alpha = 1$. The left graph is for $q = 0$ (pink), $q = 0.01$ (blue), and $q = 0.02$ (purple) with $\lambda = -0.001$ while the right graph is for $\lambda = -0.001$ (brown), $\lambda = -1$ (red), and $\lambda = -2$ (yellow) with $q = 0.01$.

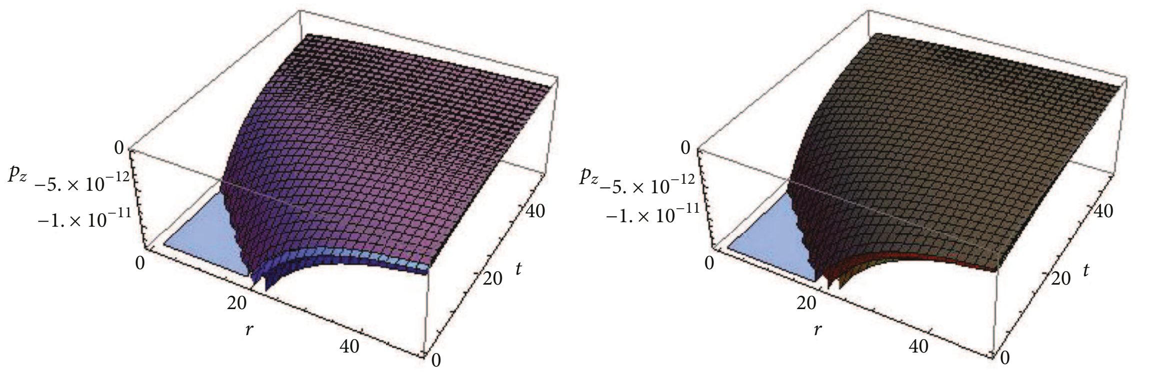

Figure 16: Plots of p_z versus r and t for $\gamma = 0.0001$, $\alpha = 1$. The left graph is for $q = 0$ (pink), $q = 0.0001$ (blue), and $q = 0.0002$ (purple) with $\lambda = -0.001$ while the right graph is for $\lambda = -0.001$ (brown), $\lambda = -1$ (red), and $\lambda = -2$ (yellow) with $q = 0.01$.

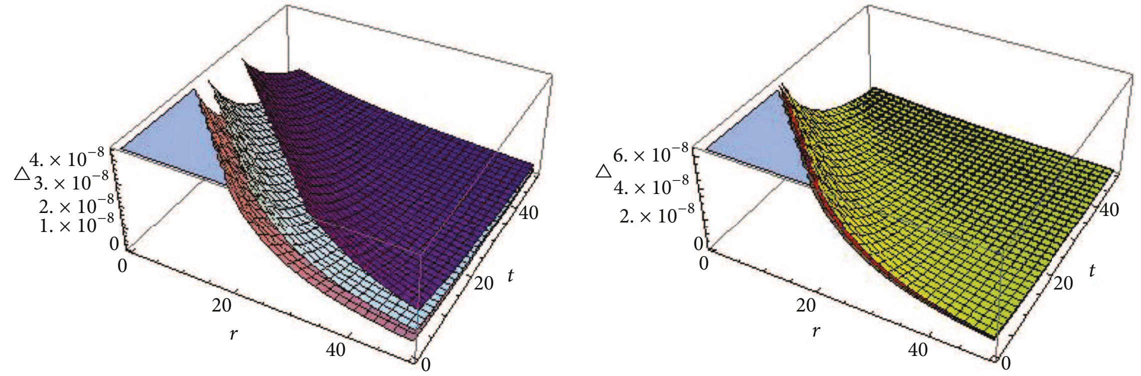

FIGURE 17: Plots of $\triangle$ versus r and t for $\gamma = 0.0001$, $\alpha = 1$. The left graph is for $q = 0$ (pink), $q = 0.01$ (blue), and $q = 0.02$ (purple) with $\lambda = -0.001$ while the right graph is for $\lambda = -0.001$ (brown), $\lambda = -1$ (red), and $\lambda = -2$ (yellow) with $q = 0.5$.

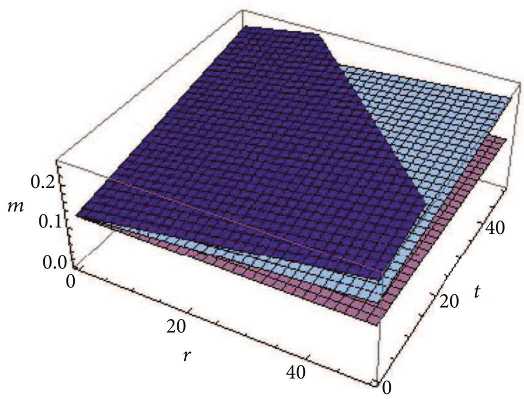

FIGURE 18: Plot of m versus r and t for $\gamma = 0.0001$, $\alpha = 1$, $q = 0$ (pink), $q = 0.001$ (blue), and $q = 0.002$ (purple).

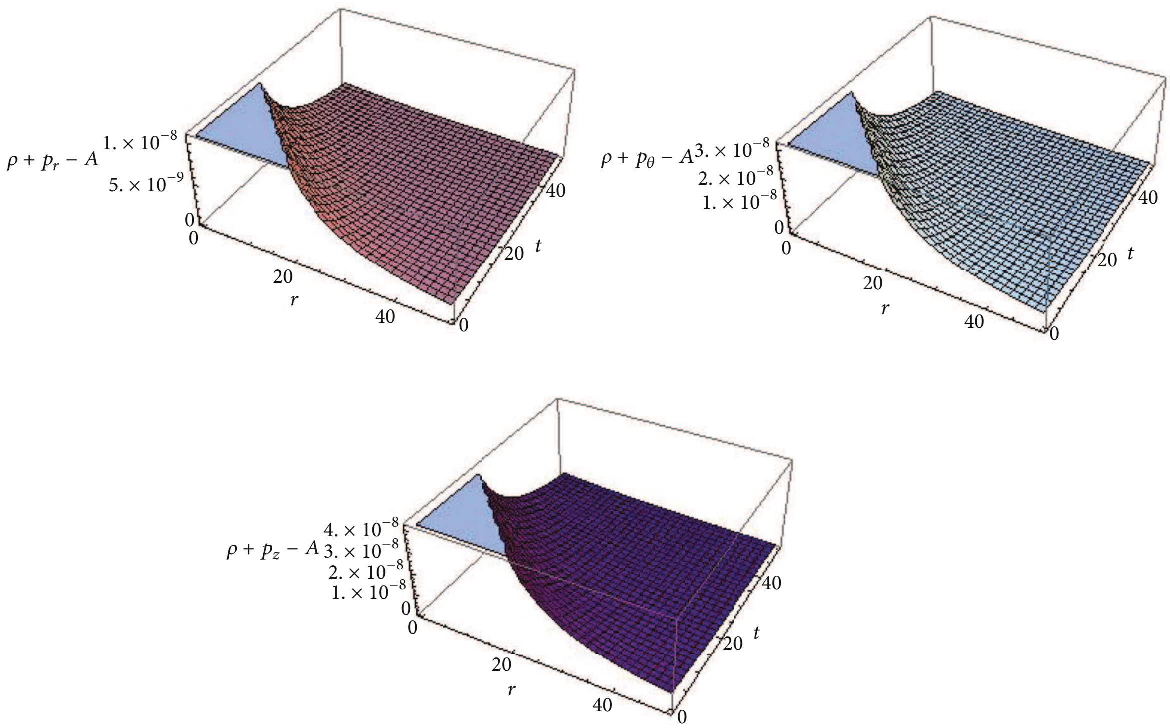

FIGURE 19: Plots for NEC for $\gamma = 0.0001$, $\alpha = 1$, $q = 0.01$, and $\lambda = -0.001$.

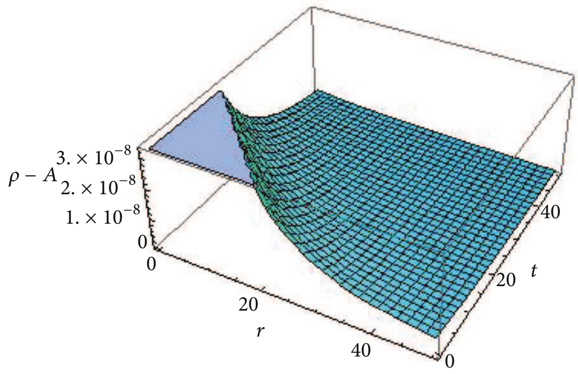

Figure 20: Plot for WEC for $\gamma = 0.0001$, $\alpha = 1$, $q = 0.01$, and $\lambda = -0.001$.

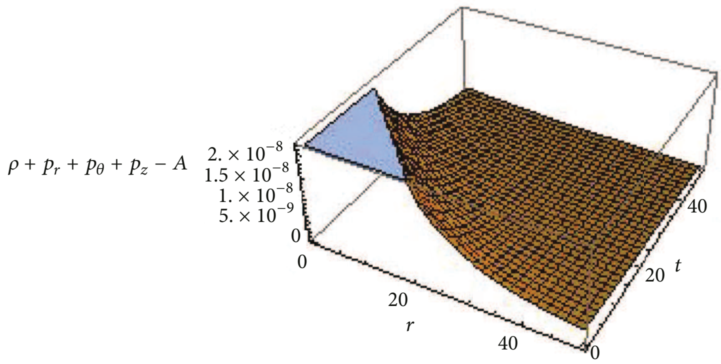

Figure 21: Plot for SEC for $\gamma = 0.0001$, $\alpha = 1$, $q = 0.01$, and $\lambda = -0.001$.

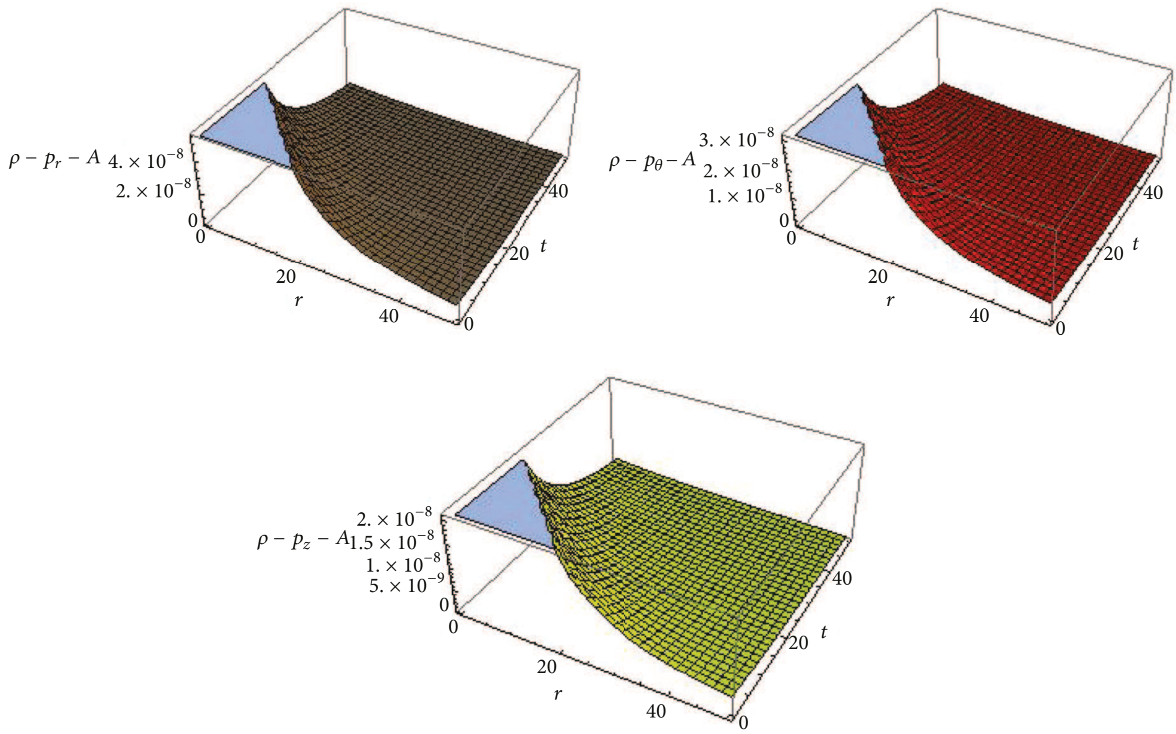

Figure 22: Plots for DEC for $\gamma = 0.0001$, $\alpha = 1$, $q = 0.01$, and $\lambda = -0.001$.

parameters with respect to time remains the same for both cases, except p_z. The anisotropy is positive for both cases which enhances the compactness of the system as discussed in [38]. In both cases, the increase in total charge has the same effects on physical quantities. The effect of model parameter is different for p_θ and p_z in both cases while it is same for the remaining quantities. We conclude that the collapse rate increases for the collapse solution while the expansion rate decreases for the expanding solution. It is found that the energy conditions are satisfied in both cases showing physical viability of our solutions for the considered values of constants.

Finally, we compare our results with those found in GR or $\lambda = 0$ [29]. For our collapse solution, the change in physical quantities is related with increase in time not with radius while in GR the quantities vary with radial coordinate but do not vary with temporal one. In case of expanding cylinder, the physical parameters vary with increase in both time and radius for our solution while in GR the solution only induces a change with respect to t. In both cases, the anisotropy decreases for our solutions while it increases in GR. The increase in anisotropy can distort the geometry of the system; i.e., solutions in GR can deform the shape of the system. On the other hand, for our solutions the anisotropy decreases leading to geometry preservation which is due to the dark source terms. It is worthwhile to mention here that our solutions satisfy the energy condition for chosen values of constants which are not shown in the similar works [26–29].

Data Availability

No data were used to support this study.

Conflicts of Interest

The authors declare that they have no conflicts of interest.

Acknowledgments

We would like to thank the Higher Education Commission, Islamabad, Pakistan, for its financial support through the *Indigenous Ph.D. 5000 Fellowship Program Phase-II, Batch-III*.

References

[1] J. R. Oppenheimer and H. Snyder, “On continued gravitational contraction,” *Physical Review A: Atomic, Molecular and Optical Physics*, vol. 56, no. 5, pp. 455–459, 1939.

[2] C. W. Misner and D. H. Sharp, “Relativistic equations for adiabatic, spherically symmetric gravitational collapse,” *Physical Review A: Atomic, Molecular and Optical Physics*, vol. 136, no. 2, pp. B571–B576, 1964.

[3] C. W. Misner and D. H. Sharp, “Spherical Gravitational Collapse with Energy Transport by Radiative Diffusion,” *Physics Letters*, vol. 15, pp. 279–281, 1965.

[4] R. F. Stark and T. Piran, “Gravitational-Wave Emission from Rotating Gravitational Collapse,” *Physical Review Letters*, vol. 55, no. 8, pp. 891–894, 1985.

[5] L. Herrera, G. le Denmat, and N. O. Santos, “Dynamical instability for nonadiabatic spherical collapse,” *Royal Astronomical Society. Monthly Notices*, vol. 237, no. 2, pp. 257–268, 1989.

[6] T. Harada, “Final fate of the spherically symmetric collapse of a perfect fluid,” *Physical Review D: Particles, Fields, Gravitation and Cosmology*, Article ID 104015, 1998.

[7] P. S. Joshi and I. H. Dwivedi, “Initial data and the end state of spherically symmetric gravitational collapse,” *Classical and Quantum Gravity*, vol. 16, no. 1, pp. 41–59, 1999.

[8] M. Sharif and H. R. Kausar, “Gravitational Perfect Fluid Collapse in f(R) Gravity,” *Astrophysics and Space Science*, vol. 331, p. 281, 2011.

[9] J. A. R. Cembranos, A. D. L. Cruz-Dombriz, and B. M. Núez, “Gravitational collapse in f(R) theories,” *Journal of Cosmology and Astroparticle Physics*, vol. 04, article no. 021, 2012.

[10] H. R. Kausar, L. Philippoz, and P. Jetzer, “Gravitational wave polarization modes in $f(R)$ theories,” *Physical Review D: Particles, Fields, Gravitation and Cosmology*, vol. 93, no. 12, Article ID 124071, 2016.

[11] T. Harko, F. S. N. Lobo, S. Nojiri, and S. D. Odintsov, “$f(R, T)$ gravity,” *Physical Review D: Particles, Fields, Gravitation and Cosmology*, vol. 84, no. 2, Article ID 024020, 2011.

[12] T. Harko and F. S. N. Lobo, “Generalized curvature-matter couplings in modified gravity,” *Galaxies*, vol. 2, no. 3, pp. 410–465, 2014.

[13] H. Shabani and M. Farhoudi, “Cosmological and solar system consequences of f(R,T) gravity models,” *Physical Review D: Particles, Fields, Gravitation and Cosmology*, vol. 90, Article ID 044031, 2014.

[14] P. H. R. S. Moraes, “Cosmological solutions from induced matter model applied to 5D f(R,T) gravity and the shrinking of the extra coordinate,” *The European Physical Journal C*, vol. 75, p. 168, 2015.

[15] I. Noureen and M. Zubair, “On dynamical instability of spherical star in $f(R,T)$ gravity,” *Astrophysics and Space Science*, vol. 356, no. 1, pp. 103–110, 2015.

[16] G. A. Carvalho, R. V. Lobato, P. H. R. S. Moraes et al., “Stellar equilibrium configurations of white dwarfs in the $f(R, T)$ gravity,” *The European Physical Journal C*, vol. 77, p. 871, 2017.

[17] M. Sharif and M. Z. Bhatti, “Stability of the expansion-free charged cylinder,” *Journal of Cosmology and Astroparticle Physics*, vol. 10, article no. 056, 2013.

[18] Z. Yousaf, M. Z. Bhatti, and U. Farwa, “Stability analysis of stellar radiating filaments,” *Classical and Quantum Gravity*, vol. 34, no. 14, Article ID 145002, 2017.

[19] M. Sharif and N. Farooq, “Study of the charged spherical stellar model in f(R) gravity,” *The European Physical Journal Plus*, vol. 132, p. 355, 2017.

[20] M. Sharif and N. Farooq, “Charged bulk viscous cylindrical collapse in $f(R)$ theory,” *International Journal of Modern Physics D*, vol. 27, no. 2, Article ID 1850013, 2018.

[21] S. Rosseland, A. S. Eddington, and R. Astron, “Electrical state of a star,” *Monthly Notices of the Royal Astronomical Society*, vol. 84, pp. 720–728, 1924.

[22] W. B. Bonnor, “The equilibrium of a charged sphere,” *Monthly Notices of the Royal Astronomical Society*, vol. 129, no. 6, pp. 443–446, 1964.

[23] M. Azam, S. A. Mardan, and M. A. Rehman, “Fate of Electromagnetic Field on the Cracking of PSR J1614-2230 in Quadratic Regime,” *Advances in High Energy Physics*, vol. 2015, Article ID 865086, 9 pages, 2015.

[24] M. Z. Bhatti and Z. Yousaf, "Influence of Electric Charge and Modified Gravity on Density Irregularities," *The European Physical Journal C*, vol. 76, p. 219, 2016.

[25] H. Mansour, B. S. Lakhal, and A. Yanallah, "Weakly charged compact stars in $f(R)$ gravity," *Journal of Cosmology and Astroparticle Physics*, vol. 2018, article no. 6, 2018.

[26] E. N. Glass, "Generating anisotropic collapse and expansion solutions of Einstein's equations," *General Relativity and Gravitation*, vol. 45, no. 12, pp. 2661–2670, 2013.

[27] G. Abbas, "Collapse and Expansion of Anisotropic Plane Symmetric Source," *Astrophysics and Space Science*, vol. 350, pp. 307–311, 2014.

[28] G. Abbas, "Effects of Electromagnetic Field on The Collapse and Expansion of Anisotropic Gravitating Source," *Astrophysics and Space Science*, vol. 352, pp. 955–961, 2014.

[29] G. Abbas, A. Kanwal, and M. Zubair, "Anisotropic compact stars in $f(T)$ gravity," *Astrophysics and Space Science*, vol. 357, no. 56, 2015.

[30] G. Abbas and R. Ahmed, "Models of collapsing and expanding anisotropic gravitating source in f(R, T) theory of gravity," *The European Physical Journal C*, vol. 77, no. 441, 2017.

[31] M. Sharif and A. Siddiqa, "Models of charged self-gravitating source in $f(R, T)$ theory," *International Journal of Modern Physics D*, Article ID S0218271819500044, p. 1950005, 2019.

[32] P. H. R. S. Moraes, "Cosmological solutions from induced matter model applied to 5D $f(R,T)$ gravity and the shrinking of the extra coordinate," *The European Physical Journal C*, vol. 75, p. 168, 2015.

[33] R. A. C. Correa and P. H. R. S. Moraes, "Configurational entropy in $f(R,T)$ brane models," *The European Physical Journal C*, vol. 76, no. 100, 2016.

[34] A. Das, F. Rahaman, B. K. Guha, and S. Ray, "Compact stars in $f(R, \mathscr{T})$ gravity," *The European Physical Journal C*, vol. 76, no. 12, Article ID 654, 2016.

[35] A. Das, S. Ghosh, B. K. Guha, S. Das, F. Rahaman, and S. Ray, "Gravastars in $f(R, \mathscr{I})$ gravity," *Physical Review D: Particles, Fields, Gravitation and Cosmology*, vol. 95, no. 12, Article ID 124011, 2017.

[36] N. J. Poplawski, "A Lagrangian description of interacting dark energy," *General Relativity and Quantum Cosmology*, vol. 1, pp. 1–14, 2006.

[37] M. Sharif and A. Ikram, "Existence of static wormholes in $f(\mathscr{G}, T)$ gravity," *International Journal of Modern Physics D: Gravitation, Astrophysics, Cosmology*, vol. 27, no. 1, Article ID 1750182, 2018.

[38] S. K. Maurya, S. Ray, S. Ghosh, S. Manna, and T. T. Smitha, "A generalized family of anisotropic compact object in general relativity," *Annals of Physics*, vol. 395, pp. 152–169, 2018.


Advances in Chemistry
Journal of Engineering
The Scientific World Journal
International Journal of Geophysics
Applied Bionics and Biomechanics
Shock and Vibration
Hindawi
Submit your manuscripts at
www.hindawi.com
Active and Passive Electronic Components
Advances in Mathematical Physics
Advances in Astronomy
Advances in OptoElectronics
International Journal of Rotating Machinery
Advances in Physical Chemistry
Advances in Condensed Matter Physics
Advances in Optical Technologies
Journal of Chemistry
International Journal of Antennas and Propagation
Advances in High Energy Physics
Advances in Acoustics and Vibration
International Journal of Optics

Astrophys Space Sci (2017) 362:226
DOI 10.1007/s10509-017-3207-8

ORIGINAL ARTICLE

Polarization modes of gravitational wave for viable $f(R)$ models

M. Sharif[1] · Aisha Siddiqa[1]

Received: 16 June 2017 / Accepted: 8 November 2017
© Springer Science+Business Media B.V., part of Springer Nature 2017

Abstract In this paper, we study the gravitational wave polarization modes for some particular $f(R)$ models using Newman-Penrose formalism. We find two extra scalar modes of gravitational wave (longitudinal and transversal modes) in addition to two tensor modes of general relativity. We conclude that gravitational waves correspond to class II_6 under the Lorentz-invariant E(2) classification of plane null waves for these $f(R)$ models.

Keywords $f(R)$ gravity · Gravitational wave polarizations

1 Introduction

Gravitational waves (GWs) are fluctuations in the fabric of spacetime produced by the motion of massive celestial objects. The scientific curiosity and struggles to detect these waves by the Earth based detectors lead to the invention of laser interferometer detectors such as LIGO, VIRGO, GEO and LISA (Bassan 2014). The most promising source for these detectors is merging the compact binaries composed of neutron star-neutron star, neutron star-black hole and black hole-black hole. These orbiting systems loose their energy in the form of GWs which speed up their orbital motion and this process ends up at the merging of orbiting objects. Recently, LIGO scientific and Virgo collaborations (Abbott et al. 2016) detected these waves and provided two observational evidences (with signals known as GW150914 and GW151226) for GWs each of which is the result of a pair of colliding black holes.

✉ M. Sharif
msharif.math@pu.edu.pk

A. Siddiqa
aisha.siddiqa17@yahoo.com

1 Department of Mathematics, University of the Punjab, Quaid-e-Azam Campus, Lahore 54590, Pakistan

Polarization of a wave gives information about the geometrical orientation of oscillations. A common method to discuss polarization modes (PMs) of GWs is the linearized theory consisting of metric perturbations around Minkowski background. Newman and Penrose (1962) introduced tetrad and spinor formalism in general relativity (GR) to deal with radiation theory. Eardley et al. (1973) used this formalism for linearized gravity and showed that six Newman-Penrose (NP) parameters for plane null waves represent six polarization modes (amplitudes) of these GWs. They also introduced Lorentz-invariant E(2) classification of plane null waves.

Hawking (1971) found an upper bound for the energy of gravitational radiation emitted by the collision of two black holes. Wagoner (1984) investigated gravitational radiation emitted by accreting neutron stars. Cutler and Flanagan (1994) explored the extent of accuracy of the distance to source and masses as well as spin of two bodies measured by the detectors LIGO and VIRGO from the gravitational wave signal. Turner (1997) worked on GWs produced by inflation and discussed the potential of cosmic microwave background anisotropy as well as laser interferometers (LIGO, VIRGO, GEO and LISA) for the detection of GWs. Langlois et al. (2000) studied the evolution of GWs for a brane embedded in five-dimensional anti-de Sitter universe and showed that a discrete normalizable massless graviton mode exists during slow roll inflation.

Recent indications of accelerated expansion of the universe caused by dark energy introduced much interest in cosmology. The mysteries of dark energy and dark matter (invisible matter) leads to modified theories of gravity obtained by either modifying matter part or geometric part of the Einstein-Hilbert action. A direct generalization of GR is the $f(R)$ theory in which the Ricci scalar R in

Published online: 16 November 2017

the Einstein-Hilbert action is replaced by its generic function $f(R)$. De Felice and Tsujikawa (2010) presented a comprehensive study on various applications of $f(R)$ theory to cosmology and astrophysics. Starobinsky (1980) proposed the first inflationary model in $f(R)$ gravity compatible with anisotropies of cosmic microwave background radiation. Hu and Sawicki (2007) proposed a class of $f(R)$ models without cosmological constant that satisfy cosmological and solar system tests for small field limit of the parameter space. Tsujikawa (2008) explored observational consequences of $f(R)$ models that satisfy the local gravity constraints. Bamba et al. (2010) introduced $f(R)$ model which explains inflation and late cosmic expansion at the same time.

A lot of work has been done for PMs of GWs in $f(R)$ as well as in other modified theories. Capozziello et al. (2008) investigated PMs of GWs in $f(R)$ gravity and concluded that for every $f(R)$ model there is an extra mode than GR called massive longitudinal mode. They also worked out the response function of GWs with LISA. Alves et al. (2009) discussed PMs of GWs for particular $f(R)$ model concluding the same results. They showed that five non-zero PMs exist for a specific form of quadratic gravity. The topic of gravitational radiation for linearized $f(R)$ theory has also been discussed in literature Berry and Gair (2011), Näf and Jetzer (2011). Capozziello and Stabile (2015) studied GWs in the context of general fourth order gravity and discussed the states of polarization and helicity. Kausar et al. (2016) found that for any $f(R)$ model there are two extra modes as compared to GR. Alves et al. (2016) explored these modes in $f(R,T)$ as well as $f(R,T^{\phi})$ theories concluding that the earlier one reduces to $f(R)$ in vacuum while PMs for the later depend on the expression of T^{ϕ}.

Herrera et al. (2015a, 2015b) studied the presence of gravitational radiation in GR for perfect as well as dissipative dust fluid with axial symmetry using super-Poynting vector and showed that both fluids do not produce gravitational radiation. We have investigated that the axial dissipative dust acts as a source of gravitational radiation in $f(R)$ theory (Sharif and Siddiqa 2017). This paper is devoted to find PMs for some viable dark energy models of this gravity. The paper is organized as follows. In the next section, we write down field equations and dark energy models of $f(R)$ gravity. We then find PMs of GWs for three models in its subsections. Finally, we conclude our results.

2 Dark energy models in $f(R)$ gravity

The $f(R)$ gravity action is defined as

$$S=\frac{1}{16\pi}\int\sqrt{-g}f(R)d^4x+S_M, \tag{1}$$

where $S_M=\int\sqrt{-g}L_Md^4x$ denotes the matter action and L_M represents the matter Lagrangian. To discuss PMs of GWs, one needs to investigate the linearized far field vacuum field equations. The vacuum field equations for the action (1) are given by

$$F(R)R_{\beta\gamma}-\frac{1}{2}f(R)g_{\beta\gamma}-\nabla_\beta\nabla_\gamma F(R)+g_{\beta\gamma}\Box F(R)=0, \tag{2}$$

where $F=\frac{df}{dR}=f_R$ and $\Box=\nabla^\alpha\nabla_\alpha$ is the D'Alembertian operator. The trace of this equation is

$$RF(R)-2f(R)+3\Box F(R)=0. \tag{3}$$

We assume that waves are traveling in z-direction, i.e., each quantity can be a function of z and t.

Various models of $f(R)$ gravity have been proposed in literature Starobinsky (1980), Hu and Sawicki (2007), Tsujikawa (2008), Bamba et al. (2010) describing the phenomena of early inflation and late cosmic expansion. The model proposed by Hu and Sawicki (2007) is reduced to the model considered by Alves et al. (2009) in the weak field regime (i.e., when $R\ll m^2$, m stands for mass). Thus Hu and Sawicki model which satisfies the cosmological and solar system tests has been indeed examined for PMs of GWs in the low curvature case or Minkowski background. Similarly, the Starobinsky model having consistency with the temperature anisotropies measured by CMBR (De Felice and Tsujikawa 2010) has also been analyzed for PMs of GWs by Kausar et al. (2016).

Amendola et al. (2007) derived the conditions for cosmological viability of some dark energy models in $f(R)$ gravity. They divided $f(R)$ models into four classes according to the existence of a matter dominated era and the final accelerated expansion phase or geometrical properties of the $m(r)$ curves where $m(r)=\frac{Rf_{,RR}}{f_{,R}}$. They concluded that models of class I are not physical, class II models asymptotically approach to de Sitter universe, class III contains models showing strongly phantom era and models of class IV represent non-phantom acceleration ($\omega>-1$). They argued that only models belonging to class II are observationally acceptable with the final outcome of ΛCDM model. Here we consider these observationally acceptable models having the similar geometry of $m(r)$ curves to discuss the PMs of GW. There are four models among the considered models that fall in class II while the model $R+\alpha R^{-n}$ has already been discussed by Alves et al. (2009) so we discuss the remaining three models in this paper.

2.1 Polarization modes for $f(R)=R+\xi R^2-\Lambda$

We consider the model $f(R)=R+\xi R^2-\Lambda$, it is assumed that ξ (an arbitrary constant) and Λ (cosmological constant) have positive values (Amendola et al. 2007). This model corresponds to ΛCDM model in the limit $\xi \to 0$ and Starobinsky inflationary model for $\Lambda \to 0$. In this case, Eq. (3) yields

$$R(1+2\xi R) - 2\big(R + \xi R^2 - \Lambda\big) + 3\Box(1+2\xi R) = 0, \quad (4)$$

which on simplification gives

$$\Box R - \frac{1}{6\xi}R = -\frac{\Lambda}{3\xi}. \quad (5)$$

For the sake of simplicity, we consider gravitational waves moving in one direction, i.e., z-direction. Thus Eq. (5) can be interpreted as a non-homogeneous two-dimensional wave equation or Klein-Gordon equation and its solution can be found using different methods like Fourier transform and Green's function etc. Here we obtain its solution following the technique used to solve Klein-Gordon and Sine-Gordon equations given in Rajaraman (1982) which is simple as compared to other methods. According to this method, any static solution is a wave with zero velocity and for the systems with Lorentz invariance, once a static solution is known, moving solutions are trivially obtained by boosting, i.e., transforming to a moving coordinate frame. Since we are considering the vacuum field equations and the background metric is Minkowski, so we can apply Lorentz transformations to the Ricci scalar R (a Lorentz invariant quantity). Hence static solution of Eq. (5) is obtained by solving

$$\frac{d^2R}{dz^2} - \frac{1}{6\xi}R = -\frac{\Lambda}{3\xi}, \quad (6)$$

whose solution is

$$R(z) = c_1 e^{\sqrt{m}z} + c_2 e^{-\sqrt{m}z} + 2\Lambda, \quad (7)$$

where c_1, c_2 are constants of integration and $m = \frac{1}{6\xi}$.

Since our system is Lorentz invariant, the time dependent solution is obtained from the static solution through Lorentz transformation as

$$R(z,t) = c_1 e^{\sqrt{m}\frac{z-vt}{\sqrt{1-v^2}}} + c_2 e^{-\sqrt{m}\frac{z-vt}{\sqrt{1-v^2}}} + 2\Lambda, \quad (8)$$

where $\sqrt{1-v^2}$ is the Lorentz factor and v represents the velocity of wave propagation. Also, Eq. (2) can be rewritten as

$$R_{\beta\gamma} = \frac{1}{F(R)}\left[\frac{1}{2}f(R)g_{\beta\gamma} + \nabla_\beta\nabla_\gamma F(R) - g_{\beta\gamma}\Box F(R)\right]. \quad (9)$$

Replacing the values of $f(R)$ and $F(R)$, we obtain its linearized form as

$$R_{\beta\gamma} = \frac{1}{2}(R - \Lambda + 2\xi\Lambda R)g_{\beta\gamma} + 2\xi\nabla_\beta\nabla_\gamma R - 2\xi g_{\beta\gamma}\Box R. \quad (10)$$

The non-zero components of Ricci tensor are

$$R_{tt} = \frac{1}{6(1-v^2)}\big[3v^2(R-\Lambda) - (R+3\Lambda)\big] - \xi\Lambda R, \quad (11)$$

$$R_{xx} = \frac{1}{6}(R+\Lambda) + \xi\Lambda R = R_{yy}, \quad (12)$$

$$R_{zz} = \frac{1}{6(1-v^2)}\big[3(R-\Lambda) - v^2(R+\Lambda)\big] + \xi\Lambda R, \quad (13)$$

$$R_{tz} = -\frac{vR}{3(1-v^2)}. \quad (14)$$

With the help of Eqs. (47) and (48), we have

$$\Psi_2 = \frac{1}{12}R, \qquad \Psi_3 = \frac{1}{2}R_{l\tilde{m}}, \qquad \Phi_{22} = -\frac{1}{2}R_{ll}. \quad (15)$$

Now, we find the expressions of Ψ_3 and Φ_{22} using Eq. (46). For Ψ_3, it yields

$$\Psi_3 = \frac{1}{2}R_{l\tilde{m}} = \frac{1}{2}R_{\mu\nu}l^\mu\tilde{m}^\nu, \quad (16)$$

which can also be written as

$$\Psi_3 = \frac{1}{2}\big(R_{tt}l^t\tilde{m}^t + R_{xx}l^x\tilde{m}^x + R_{yy}l^y\tilde{m}^y + R_{zz}l^z\tilde{m}^z + R_{tz}l^t\tilde{m}^z\big). \quad (17)$$

From Eqs. (43) and (44), the component form of vectors k, l, m and $\tilde{m}$ can be written as

$$k^\mu = \frac{1}{\sqrt{2}}(1,0,0,1), \qquad l^\mu = \frac{1}{\sqrt{2}}(1,0,0,-1), \quad (18)$$

$$m^\mu = \frac{1}{\sqrt{2}}(0,1,i,0), \qquad \tilde{m}^\mu = \frac{1}{\sqrt{2}}(0,1,-i,0). \quad (19)$$

Substituting all the required values in Eq. (17), we obtain

$$\Psi_3 = 0. \quad (20)$$

Similarly, Eq. (46) for Φ_{22} yields

$$\Phi_{22} = -\frac{1}{2}R_{ll} = -\frac{1}{2}R_{\mu\nu}l^\mu l^\nu = -\frac{1}{2}\big(R_{tt}l^tl^t + 2R_{tz}l^tl^z + R_{zz}l^zl^z\big).$$

Replacing the Ricci tensor components and components of l^μ, the above equation leads to

$$\Phi_{22} = -\frac{R}{12}\left(\frac{1+v}{1-v}\right) + \frac{\Lambda(2v^2+3)}{12(1-v^2)}. \quad (21)$$

Notice that $\Psi_4 \neq 0$ represents the tensor modes of GWs. Since there is no expression of Ψ_4 in terms of Ricci tensor, so it cannot be evaluated with the help of available values of Ricci tensor and Ricci scalar (Alves et al. 2016). It can be observed that for ΛCDM model (when $\xi \to 0$) Ψ_2 and Φ_{22} remain non-zero.

The model, $f(R) = R + \xi R^2 - \Lambda$, is always viable and reduces to GR when both ξ as well as Λ approach to zero. In GR, there are only two tensor modes of polarization associated with $\mathrm{Re}\,\Psi_4$ and $\mathrm{Im}\,\Psi_4$, i.e., we have only Ψ_4 non-zero among six NP parameters. From Eq. (4), we have $R = 0$ for $\xi \to 0$, $\Lambda \to 0$, hence GR results are retrieved.

2.2 Polarization modes for $f(R) = R^p(\ln\alpha R)^q$

This model is observationally acceptable for $p = 1$ and $q > 0$ (Amendola et al. 2007). Here we assume that $q = 1$ such that the model becomes $f(R) = R\ln\alpha R$. Substituting the values of $f(R)$ and $F(R)$ in Eq. (3), it gives

$$3\Box\ln\alpha R - R\ln\alpha R + R = 0. \tag{22}$$

Assuming $\ln\alpha R = \phi$, this equation transforms to

$$\Box\phi = \frac{e^{\phi}}{3\alpha}(\phi - 1), \tag{23}$$

which can also be written as

$$\Box\phi = \frac{\partial U}{\partial\phi}; \qquad U(\phi) = \frac{e^{\phi}}{3\alpha}(\phi - 2). \tag{24}$$

First we seek for a static solution, i.e., consider $\phi = \phi(z)$ such that integration of Eq. (24) gives

$$\frac{1}{2}\left(\frac{d\phi}{dz}\right)^2 = U(\phi). \tag{25}$$

Substituting the value of $U(\phi)$ and then integrating, it follows that

$$\phi(z) = 2\left[1 + \mathrm{InverseErf}\left[\frac{ez}{\sqrt{3\alpha\pi}} + \frac{ec_3}{\sqrt{2\alpha\pi}}\right]^2\right], \tag{26}$$

where c_3 is a constant of integration, $e = 2.71828$ and Erf is defined by

$$Erf(z) = \frac{2}{\sqrt{\pi}}\int_0^z e^{-s^2}ds. \tag{27}$$

Using Lorentz transformation, we obtain time dependent solution given by

$$\phi(z,t) = 2\left[1 + \mathrm{InverseErf}\left[\frac{e(z - vt)}{\sqrt{1 - v^2}\sqrt{3\alpha\pi}} + \frac{ec_3}{\sqrt{2\alpha\pi}}\right]^2\right]. \tag{28}$$

The expression for Ricci scalar is obtained as

$$R(z,t) = \frac{1}{\alpha}\exp\left(2\left[1 + \mathrm{InverseErf}\left[\frac{e(z - vt)}{\sqrt{1 - v^2}\sqrt{3\alpha\pi}} + \frac{ec_3}{\sqrt{2\alpha\pi}}\right]^2\right]\right). \tag{29}$$

The non-zero components of the Ricci tensor have the form

$$R_{tt} = -\frac{R}{6(v^2 - 1)}\left[\frac{(3v^2 - 1)\ln\alpha R - 2}{\ln\alpha R + 1}\right],$$
$$R_{xx} = \frac{R}{6}\left(\frac{\ln\alpha R + 2}{\ln\alpha R + 1}\right) = R_{yy},$$
$$R_{tz} = \frac{Rv(\ln\alpha R - 1)}{3(v^2 - 1)(\ln\alpha R + 1)},$$
$$R_{zz} = \frac{R}{6(v^2 - 1)}\left[\frac{(v^2 - 3)\ln\alpha R + 2v^2}{\ln\alpha R + 1}\right].$$

Finally, the NP parameters for this case are

$$\Psi_2 = \frac{1}{12}R, \qquad \Psi_3 = 0,$$
$$\Phi_{22} = -\frac{R}{12}\left(\frac{1 + v}{1 - v}\right)\frac{(\ln\alpha R - 1)}{\ln\alpha R + 1}. \tag{30}$$

Here Ψ_4 is also a non-vanishing NP parameter as discussed in the previous case.

2.3 Polarization modes for $f(R) = R^p e^{\frac{q}{R}}$

This model is observationally acceptable for $p = 1$, so we take $f(R) = Re^{\frac{q}{R}}$ (Amendola et al. 2007). This model reduces to GR when $q = 0$ and consequently gives no additional PMs. Thus to find extra PMs, we consider $q \neq 0$ in further calculations. For this model, the trace equation (3) becomes

$$Re^{\frac{q}{R}}\left(1 - \frac{q}{R}\right) - 2Re^{\frac{q}{R}} + 3\Box\left(e^{\frac{q}{R}}\left(1 - \frac{q}{R}\right)\right) = 0. \tag{31}$$

In low curvature regime, we have $R \ll q$ which reduces the above equation to the following

$$\Box\left(\frac{1}{R}e^{\frac{q}{R}}\right) + \frac{1}{3}e^{\frac{q}{R}} = 0. \tag{32}$$

Replacing $\frac{1}{R} = u$ and $u = u(z)$ for static solution, we obtain

$$\frac{d^2}{dz^2}(ue^{qu}) + \frac{1}{3}e^{qu} = 0. \tag{33}$$

Solving the double derivative of the above equation, it becomes

$$(1 + qu)\frac{d^2u}{dz^2} + q(qu + 2)\left(\frac{du}{dz}\right)^2 + \frac{1}{3} = 0.$$

The is a non-homogeneous non-linear second order differential equation and does not provide an exact analytic solution unless we make some assumptions to simplify it. Since we are working in the weak-field regime, so R is very small. Assuming q to be very large, we have $qu = \frac{q}{R}$ (as $u = \frac{1}{R}$) to be very large such that $(qu+1) \approx qu$ as well as $(qu+2) \approx qu$ and the above equation reduces to

$$u\frac{d^2u}{dz^2} + qu\left(\frac{du}{dz}\right)^2 + \frac{1}{3q} = 0.$$

Here $\frac{1}{3q} \to 0$ as q is very large, hence it reduces to

$$u\frac{d^2u}{dz^2} + qu\left(\frac{du}{dz}\right)^2 = 0 \tag{34}$$

whose solution yields $(u = 1/R)$

$$R(z) = \left(\frac{1}{q}\ln\big[q(c_4 z + c_5)\big]\right)^{-1}, \tag{35}$$

where c_4 and c_5 are integration constants. The non-static solution becomes

$$R(z,t) = \left(\frac{1}{q}\ln\left[q\left(c_4\frac{(z-vt)}{\sqrt{1-v^2}} + c_5\right)\right]\right)^{-1}. \tag{36}$$

The non-vanishing components of the Ricci tensor are

$$R_{tt} = \frac{q[q(z-vt)^2 + 2\ln[q(c_4\frac{(z-vt)}{\sqrt{1-v^2}} + c_5)]]c_4^2}{2(\ln[q(c_4\frac{(z-vt)}{\sqrt{1-v^2}} + c_5)])^2((tv-z)c_4 - \sqrt{1-v^2}c_5)^2} + \frac{q[2q\sqrt{1-v^2}(z-vt)c_4c_5 - qc_5^2(v^2-1)]}{2(\ln[q(c_4\frac{(z-vt)}{\sqrt{1-v^2}} + c_5)])^2((tv-z)c_4 - \sqrt{1-v^2}c_5)^2}, \tag{37}$$

$$R_{xx} = R_{yy} = \frac{-q[q(z-vt)^2 - 2(v^2-1)\ln[q(c_4\frac{(z-vt)}{\sqrt{1-v^2}} + c_5)]]c_4^2}{2(\ln[q(c_4\frac{(z-vt)}{\sqrt{1-v^2}} + c_5)])^2((tv-z)c_4 - \sqrt{1-v^2}c_5)^2} - \frac{q[2q\sqrt{1-v^2}(z-vt)c_4c_5 - qc_5^2(v^2-1)]}{2(\ln[q(c_4\frac{(z-vt)}{\sqrt{1-v^2}} + c_5)])^2((tv-z)c_4 - \sqrt{1-v^2}c_5)^2}, \tag{38}$$

$$R_{zz} = \frac{-q[q(z-vt)^2 - 2v^2\ln[q(c_4\frac{(z-vt)}{\sqrt{1-v^2}} + c_5)]]c_4^2}{2(\ln[q(c_4\frac{(z-vt)}{\sqrt{1-v^2}} + c_5)])^2((tv-z)c_4 - \sqrt{1-v^2}c_5)^2} - \frac{q[2q\sqrt{1-v^2}(z-vt)c_4c_5 - qc_5^2(v^2-1)]}{2(\ln[q(c_4\frac{(z-vt)}{\sqrt{1-v^2}} + c_5)])^2((tv-z)c_4 - \sqrt{1-v^2}c_5)^2}, \tag{39}$$

$$R_{tz} = -\frac{qvc_4^2}{(1-v^2)(\frac{(z-vt)}{\sqrt{1-v^2}}c_4 + c_5)}. \tag{40}$$

The corresponding NP parameters are

$$\Psi_2 = \frac{1}{12}R, \qquad \Psi_3 = 0, \tag{41}$$

$$\Phi_{22} = -\frac{Rc_4^2(v-1)^2}{4((tv-z)c_4 - \sqrt{1-v^2}c_5)^2}. \tag{42}$$

Ψ_4 is also non-zero.

3 Final remarks

Observations suggest that our universe is facing an accelerated expansion phase due to a mysterious factor of dark energy. Moreover, direct observation of GWs opens up a new window of research. It would be worthwhile to discuss combine effect of both dark energy and GWs. In this paper, we have found PMs of GWs in the context of $f(R)$ dark energy models. For each of the three models, we have first obtained a static solution of differential equation in R and then applied Lorentz transformation to obtain a time dependent solution. It is observed that due to Lorentz transformation, a factor of $(\frac{1+v}{1-v})$ appears in the value of Φ_{22} mode in first and second case but it has negligible effect because the speed of GW is comparable with the speed of light. It can be seen that the expressions of Ψ_2 and Φ_{22} in all cases are directly proportional to R implying that increase in R enhances these modes or amplitudes. The mode Φ_{22} for the first model (21) depends directly on the model parameter Λ, for the second model (30), it depends on $\ln\alpha$ (as $\ln\alpha R = \ln\alpha + \ln R$) while for the third model (41), this depends on constants c_4 and c_5.

In each case, we have found four non-zero PMs of GWs Ψ_2 (longitudinal scalar mode), Ψ_4 (+, × tensorial modes) and Φ_{22} (breathing scalar mode) which is in agreement with the results of Kausar et al. (2016). We have non-vanishing Ψ_2 for each model implying that GWs for $f(R)$ dark energy models correspond to class II_6 (as mentioned in Table 1). This is the only observer dependent mode, remaining modes are all observer independent (Eardley et al. 1973). These expressions of NP parameters representing the amplitudes of GWs are significant due to the presence of dark energy dominated era.

Here we elaborate the PMs of GW for some modified theories. The six non-zero PMs are found only for the quadratic gravity with Lagrangian density $\mathcal{L} = R + \alpha R^2 + \gamma R_{\mu\nu}R^{\mu\nu}$ in Alves et al. (2009). For $F(T)$ theory (where T is torsion scalar in teleparallelism), there are no extra PMs from GR as shown in Bamba et al. (2013) and in $f(R, T^{\phi})$ theory the number of PMs of GW depend on the functional form of $f(R, T^{\phi})$ (Alves et al. 2016). On the other hand, the PMs of GW in scalar-tensor theory (Kausar 2017) and massive Brans-Dicke theory (Sathyaprakash and Schutz 2009) are same as in $f(R)$ theory.

The LIGO instruments in Livingston and Hanford have similar orientations and the possibility of extra PMs than GR cannot be excluded. Moreover, with two detectors having no electromagnetic and neutrino counterpart, a large uncertainty is expected about the source of event and consequently in the speed of GW. Thus the possibility that speed of GW is less than the speed of light cannot be excluded. Hence from this perspective, the modified theories of gravity cannot be ruled out. The improvements to automated pipelines and analysis techniques for the detection of future GW events are continuously made for accurate measurements. Recently, two more events of GWs, GW170104 (Abbott et al. 2017a) and GW170817 (Abbott et al. 2017b) have been detected by the advanced interferometers. The event GW170104 is consistent with merging black holes of masses 31 $M_\odot$ and 19 $M_\odot$ in GR while the second one GW170817 is consistent with the binary neutron star inspiral having masses in the range 1.17 $M_\odot$–1.60 $M_\odot$. The signal GW170817, has the association with GRB170817A detected by Fermi-GBM and provides the first direct evidence of a link between these mergers and short γ-ray bursts. It is expected that future GW observations made by a network of the Earth based interferometers could actually measure the polarization of GWs and thus constrain $f(R)$ deviations from GR.

Acknowledgements We would like to thank the Higher Education Commission, Islamabad, Pakistan for its financial support through the *Indigenous Ph.D. 5000 Fellowship Program Phase-II, Batch-III*. We are also grateful to the anonymous referee for his constructive comments.

Appendix

In this appendix, we first briefly describe the Newman-Penrose formalism (Newman and Penrose 1962) to discuss gravitational waves and then PMs as well as classification of null waves is developed (Eardley et al. 1973).

Newman and Penrose developed a new technique in GR with the help of tetrad formalism and applied this to resolve the issue of outgoing gravitational radiation. They defined the following relations between the Cartesian $(\hat{t}, \hat{x}, \hat{y}, \hat{z})$ and null-tetrads $(k, l, m, \tilde{m})$

$$k = \frac{1}{\sqrt{2}}(\hat{t} + \hat{z}), \qquad l = \frac{1}{\sqrt{2}}(\hat{t} - \hat{z}), \tag{43}$$

$$m = \frac{1}{\sqrt{2}}(\hat{x} + i\hat{y}), \qquad \tilde{m} = \frac{1}{\sqrt{2}}(\hat{x} - i\hat{y}), \tag{44}$$

which satisfy the relations

$$-k.l = m.\tilde{m} = 1, \qquad k.m = k.\tilde{m} = l.m = l.\tilde{m} = 0. \tag{45}$$

Any tensor can be transformed from Cartesian to null basis by the formula (Alves et al. 2009)

$$S_{abc\ldots} = S_{\alpha\beta\gamma\ldots}a^\alpha b^\beta c^{\gamma\cdots}, \tag{46}$$

where $(a, b, c, \ldots)$ vary over the set $\{k, l, m, \tilde{m}\}$ and $(\alpha, \beta, \gamma, \ldots)$ vary over the set $\{t, x, y, z\}$. In Newman and Penrose (1962), the irreducible parts of the Riemann tensor, also called the NP parameters, are defined by ten Ψ's, nine Φ's and a term Λ (these are all algebraically independent). Eardley et al. (1973) showed that for plane null

Table 1 The E(2) classes of weak plane null waves

Classes	Condition for NP parameters
II_6	$\Psi_2 \neq 0$
III_5	$\Psi_2 = 0$ and $\Psi_3 \neq 0$
N_3	$\Psi_2 = 0 = \Psi_3$, $\Psi_4 \neq 0$ and $\Phi_{22} \neq 0$
N_2	$\Psi_2 = 0 = \Psi_3 = \Phi_{22}$ and $\Psi_4 \neq 0$
O_1	$\Psi_2 = 0 = \Psi_3 = \Psi_4$ and $\Phi_{22} \neq 0$
O_0	$\Psi_2 = 0 = \Psi_3 = \Phi_{22} = \Psi_4$

waves (due to differential and symmetry properties of the Riemann tensor) these NP quantities are reduced to the set $\{\Psi_2, \Psi_3, \Psi_4, \Phi_{22}\}$. This set consists of six NP parameters or PMs because Ψ_3 and Ψ_4 are complex and thus represent two independent modes. They also give formulas of these NP quantities in terms of null-tetrad components of the Riemann tensor as

$$\begin{aligned} &\Psi_2 = -\frac{1}{6}R_{lklk}, \qquad \Psi_3 = -\frac{1}{2}R_{lkl\tilde{m}}, \\ &\Psi_4 = -R_{l\tilde{m}l\tilde{m}}, \qquad \Phi_{22} = -R_{lml\tilde{m}}. \end{aligned} \tag{47}$$

Following are some helpful relations of null-tetrad components of the Riemann and Ricci tensors

$$\begin{aligned} &R_{lk} = R_{lklk}, \qquad R_{ll} = 2R_{lml\tilde{m}}, \\ &R_{lm} = R_{lklm}, \qquad R_{l\tilde{m}} = R_{lkl\tilde{m}}, \qquad R = -2R_{lk}. \end{aligned} \tag{48}$$

The classification of weak plane null waves (Eardley et al. 1973) obtained for standard observer (i.e., each observer sees the waves traveling in z-direction and each observer measures the same frequency) is given in Table 1.

References

Abbott, B.P., et al.: Phys. Rev. Lett. **116**, 061102 (2016)
Abbott, B.P., et al.: Phys. Rev. Lett. **118**, 221101 (2017a)
Abbott, B.P., et al.: Phys. Rev. Lett. **119**, 161101 (2017b)
Alves, M.E.S., Miranda, O.D., de Araujo, J.C.N.: Phys. Lett. B **679**, 401 (2009)
Alves, M.E.S., Moraes, P.H.R.S., de Araujo, J.C.N., Malheiro, M.: Phys. Rev. D **94**, 024032 (2016)
Amendola, L., Gannouji, R., Polarski, D., Tsujikawa, S.: Phys. Rev. D **75**, 083504 (2007)
Bamba, K., Geng, C.Q., Lee, C.C.: J. Cosmol. Astropart. Phys. **08**, 021 (2010)
Bamba, K., Capozziello, S., De Laurentis, M., Nojiri, S., Sáez-Gómez, D.: Phys. Lett. B **727**, 194 (2013)
Bassan, M.: Advanced Interferometers and the Search for Gravitational Waves. Springer, Berlin (2014)
Berry, C.P.L., Gair, J.R.: Phys. Rev. D **83**, 104022 (2011)
Capozziello, S., Corda, C., De Laurentis, M.F.: Phys. Lett. B **669**, 255 (2008)
Capozziello, S., Stabile, A.: Astrophys. Space Sci. **358**, 27 (2015)
Cutler, C., Flanagan, E.E.: Phys. Rev. D **49**, 2658 (1994)

De Felice, A., Tsujikawa, S.: Living Rev. Relativ. **13**, 3 (2010)
Eardley, D.M., Lee, D.L., Lightman, A.P.: Phys. Rev. D **8**, 3308 (1973)
Hawking, S.W.: Phys. Rev. Lett. **26**, 1344 (1971)
Herrera, L., Di Prisco, A., Ospino, J.: Phys. Rev. D **91**, 024010 (2015a)
Herrera, L., Di Prisco, A., Ospino, J., Carot, J.: Phys. Rev. D **91**, 124015 (2015b)
Hu, W., Sawicki, I.: Phys. Rev. D **76**, 064004 (2007)
Kausar, H.R., Philippoz, L., Jetzer, P.: Phys. Rev. D **93**, 124071 (2016)
Kausar, H.R.: Int. J. Mod. Phys. D **26**, 1741010 (2017)
Langlois, D., Maartens, R., Wands, D.: Phys. Lett. B **489**, 259 (2000)
Näf, J., Jetzer, P.: Phys. Rev. D **84**, 024027 (2011)
Newman, E., Penrose, R.: J. Math. Phys. **3**, 566 (1962)
Rajaraman, R.: An Introduction to Solitons and Instantons in Quantum Field Theory. Elsevier Science Publishers, Amsterdam (1982)
Sathyaprakash, B., Schutz, B.: Living Rev. Relativ. **12**, 2 (2009)
Sharif, M., Siddiqa, A.: Phys. Dark Universe **15**, 105 (2017)
Starobinsky, A.A.: Phys. Lett. B **91**, 99 (1980)
Tsujikawa, S.: Phys. Rev. D **77**, 023507 (2008)
Turner, M.S.: Phys. Rev. D **55**, 435 (1997)
Wagoner, R.V.: Astrophys. J. **278**, 345 (1984)

Eur. Phys. J. C (2018) 78:721
https://doi.org/10.1140/epjc/s10052-018-6201-6

THE EUROPEAN PHYSICAL JOURNAL C

Regular Article - Theoretical Physics

Curvature-matter coupling effects on axial gravitational waves

M. Sharif[a], **Aisha Siddiqa**[b]

Department of Mathematics, University of the Punjab, Quaid-e-Azam Campus, Lahore 54590, Pakistan

Received: 4 June 2018 / Accepted: 28 August 2018
© The Author(s) 2018

Abstract In this paper, we investigate propagation of axial gravitational waves in the background of flat FRW universe in $f(R,T)$ theory. The field equations are obtained for unperturbed as well as axially perturbed FRW metric. These field equations are solved simultaneously to obtain the unknown perturbation parameters. We find that the assumed perturbations can affect matter as well as four velocity. Moreover, ignoring the material perturbations we explicitly obtain an expression for four velocity. It is concluded that axial gravitational waves in the curvature-matter coupling background can produce cosmological rotation or have memory effect if the wave profile has discontinuity at the wave front.

1 Introduction

The discovery of cosmic expansion is a big achievement as well as the most fascinating area of research. Researchers introduced different approaches to investigate the reason behind this phenomenon by modifying matter or geometric part of the Einstein–Hilbert action leading to modified matter models or modified theories of gravity, respectively. Examples of modification in geometric part are $f(R)$ [1], $f(G)$ [2] and $f(R,T)$ [3] theories of gravity where R, G and T denote Ricci scalar, Gauss–Bonnet invariant and trace of the energy-momentum tensor. While examples of modified matter models are quintessence [4,5], phantom [6], K-essence [7], holographic dark energy [8,9] and Chaplygin gas models [10–12].

The simplest generalization of general relativity (GR) is obtained by replacing R with its generic function named as $f(R)$ in the Einstein–Hilbert action leading to $f(R)$ theory. Many astrophysical as well as cosmological aspects have been investigated within the framework of this theory [13,14]. Harko et al. [3] proposed $f(R,T)$ gravity which is a curvature-matter coupling theory. This can produce a matter dependent deviation from geodesic motion and also help to study dark energy, dark matter interactions as well as late-time acceleration [15].

Different aspects of cosmic and stellar evolution have been studied in $f(R,T)$ gravity. Sharif and Zubair [16] investigated the validity of second law of thermodynamics for phantom as well as non-phantom phases. Shabani and Farhoudi [17] explored viability of some $f(R,T)$ gravity models by solar system constraints. Yousaf et al. [18] investigated the stability of cylindrical symmetric stellar configurations by inducing perturbations in this theory. We have studied physical characteristics of charged [19] as well as uncharged stellar structure [20] in this gravity.

The fluctuations in the fabric of spacetime produced by massive celestial objects are known as gravitational waves (GWs). The significance of GWs comes from the fact that they lead to new techniques to explore cosmic issues. The observations of GWs can help us to study the individual sources of GWs that give information about structure as well as kinematics of the cosmos. The observation of a stochastic background of GWs of cosmological origin can provide information about initial structure formation. These detections have inaugurated a new era of astronomy as well as the possibility to investigate gravity in extreme gravity regimes.

After a long history of struggles (from Weber bars to advanced laser interferometers), scientific efforts came true and GWs are finally detected by earth-based detectors. Some of the observed GWs signals by the LIGO-VIRGO collaboration are GW150914 [21], GW170104 [22] and GW170817 [23]. The origin of these signals is the merging binaries of black holes and neutron stars which release energy in the form of GWs. The most recent signal (GW170817) [23] is consistent with the binary neutron star inspiral. It has an association with gamma ray burst signal GRB170817A detected by Fermi-GBM and provides the first direct evidence of gamma ray bursts during the mergence of two neutron stars.

[a] e-mail: msharif.math@pu.edu.pk
[b] e-mail: aisha.siddiqa17@yahoo.com

The phenomenon of GWs has become a topic of central importance in cosmology nowadays. The polarization of a GW provides information for its geometrical orientation. Kausar et al. [24] explored polarization modes of GWs in $f(R)$ theory and found two modes other than GR. Alves et al. [25] evaluated these modes for $f(R,T)$ and $f(R,T^{\phi})$ theories (here ϕ represents scalar field). They concluded that in vacuum the former one produces the same results as $f(R)$ while the polarization modes in $f(R,T^{\phi})$ gravity depend upon the expression of T^{ϕ}. We have shown that axially symmetric dust fluid with dissipation behave as a source of gravitational radiation in $f(R)$ theory [26]. We have also studied polarization modes of GWs for some viable $f(R)$ models [27].

Regge and Wheeler [28] studied the stability of Schwarzschild singularity by introducing small perturbations in the form of spherical harmonics producing odd and even waves. They found that these disturbances oscillate around equilibrium state and do not grow with time showing the stability of Schwarzschild singularity. Zerilli [29] analyzed the emission of gravitational radiation when a black hole swallows a star. He did this analysis by considering the problem of a particle falling into a Schwarzschild black hole and perturbations introduced by Regge and Wheeler as well as corrected the even wave propagation equation derived in [28]. The energy carried by GWs is the gravitational radiation. Hawking [30] investigated gravitational radiation produced by colliding black holes and Wagoner [31] discussed these radiation for accreting neutron stars.

Malec and Wylężek [32] used the wavelike perturbations proposed by Regge and Wheeler in the Schwarzschild spacetime to study the GW propagation in cosmological context. They investigated Huygens principle for cosmological GWs in Regge–Wheeler gauge and found that this principle is satisfied in radiation dominated era while it does not hold in matter dominated universe. Otakar [33] explored the GW propagations in higher dimensions using axial perturbations proposed by Regge–Wheeler. They showed that in braneworld scenario the Huygens principle seems to be satisfied for high multipoles in contrast with four dimensions. Viaggiu [34] studied propagations of axial and polar GWs proposed in [28], in de Sitter universe using the Laplace transformation. Kulczycki and Malec also [35] studied the perturbations induced by axial and polar GWs in FRW universe. They concluded that Huygens principle has the same status for both types of waves, it is valid for radiation era while it is broken elsewhere. The same authors [36] discussed cosmological rotation of radiation matter induced by axial GWs. However, axial and polar perturbations have also been studied using gauge-invariant quantities [37–40]. In [40], the authors investigated the cosmological perturbations in the context of Lemaitre–Tolman spacetime. In case of axial modes, their equations (restricted to FRW metric) coincide with that of [35].

The issues of cosmological rotation induced by GWs and validity of Huygens principle in Regge–Wheeler gauge have not yet been studied in the framework of modified theories. In the present work, we induce the axial perturbations (which change the geometry from spherical to axial) introduced by Regge and Wheeler [28] in the flat cosmological as well as curvature-matter coupling backgrounds. Since the FRW universes are conformally flat, these distortions are linked with the axial GWs. These disturbances are may be the consequence of non-gravitational forces (electromagnetic forces, nuclear forces) associated with brutal astrophysical events. The non-symmetric explosion of a supernova could be an example for the production of such type of waves. We focus on the axial wave perturbations induced in flat cosmos consisting of perfect fluid. The paper is arranged as follows. In the coming section, we discuss the background FRW cosmology in $f(R,T)$ theory. In Sect. 3, we define the perturbations in FRW metric as well as matter variables and formulate the corresponding field equations. The unknown perturbation parameters are found in Sect. 4. Finally, we summarize and conclude the results in the last section.

2 FRW cosmology and $f(R,T)$ gravity

In order to discuss the wave propagation in FRW universe, we consider the FRW metric in conformal coordinates (η,r,θ,ϕ) as

$$ds^2=a^2(\eta)(-d\eta^2+dr^2+r^2d\theta^2+r^2\sin^2\theta d\phi^2), \qquad (1)$$

where η is the conformal time coordinate related to the ordinary time by the relation

$$\eta=\int\frac{dt}{a}, \qquad (2)$$

such that the conformal Hubble parameter H is related with the ordinary Hubble parameter $\mathcal{H}$ by

$$\mathcal{H}=\frac{H}{a}. \qquad (3)$$

We consider matter as perfect fluid defined by the energy-momentum tensor

$$T_{\mu\nu}=(\rho_0+p_0)V_\mu V_\nu+pg_{\mu\nu}, \qquad (4)$$

where V_μ, ρ_0 and p_0 stand for four-velocity as well as background unperturbed density and pressure, respectively.

The action integral for $f(R,T)$ theory is

$$S=\int d^4x\sqrt{-g}\left[\frac{1}{16\pi}f(R,T)+\mathcal{L}_m\right]. \tag{5}$$

where g is the determinant of the metric tensor and $\mathcal{L}_m$ is the matter Lagrangian density. The field equations for this action are

$$f_R R_{\mu\nu}-\frac{1}{2}g_{\mu\nu}f-(\nabla_\mu\nabla_\nu-g_{\mu\nu}\Box)f_R$$
$$=8\pi T_{\mu\nu}-f_T(\Theta_{\mu\nu}+T_{\mu\nu}), \tag{6}$$

where $f_R=\frac{\partial f}{\partial R}$, $f_T=\frac{\partial f}{\partial T}$ and $\Theta_{\mu\nu}=-2T_{\mu\nu}+\mathcal{L}_m g_{\mu\nu}$. In this paper, we consider $f(R,T)=R+2\lambda T$ [3] to investigate the role of curvature-matter coupling on the propagation of GWs. This model can discuss the accelerated expansion by producing a power-law like scale factor. It also has a correspondence with ΛCDM model by considering the cosmological constant as a function of trace T or $\Lambda(T)$ gravity by Poplawski [41]. The choices for matter Lagrangian density $\mathcal{L}_m$ are p_0 or $-\rho_0$. However, it is shown that these two densities yield the same results for minimal curvature-matter coupling if the matter under discussion is perfect fluid [42]. So the assumption $\mathcal{L}_m=p_0$ and the model $f(R,T)=R+2\lambda T$ simplify the field equations as

$$G_{\mu\nu}=(8\pi+2\lambda)T_{\mu\nu}-2\lambda p g_{\mu\nu}+\lambda T g_{\mu\nu}. \tag{7}$$

This yields the following independent field equations for the metric (1)

$$3H^2=(8\pi+3\lambda)\rho_0 a^2-\lambda p_0 a^2, \tag{8}$$
$$-2\dot{H}-H^2=(8\pi+3\lambda)p_0 a^2-\lambda\rho_0 a^2, \tag{9}$$

here dot denote the derivative with respect to the conformal time η.

In further discussion, we consider the GWs in radiation dominated era so using the equation of state (EoS) $p_0=\frac{\rho_0}{3}$, the field equations (8) and (9) give the following differential equation in H

$$2\dot{H}+\frac{6\pi+\lambda}{3\pi+\lambda}H^2=0,$$

which yields the scale factor

$$a(\eta)=c_1\eta^{\frac{6\pi+2\lambda}{6\pi+\lambda}}, \tag{10}$$

where c_1 is constant of integration. The covariant derivative of the field equations is

$$\nabla^\mu T_{\mu\nu}=\frac{f_T}{8\pi-f_T}\left[(T_{\mu\nu}+\Theta_{\mu\nu})\nabla^\mu\ln f_T\right.$$
$$\left.+\nabla^\mu\Theta_{\mu\nu}-\frac{1}{2}g_{\mu\nu}\nabla^\mu T\right]. \tag{11}$$

Using Eqs. (1), (4), the model $f(R,T)=R+2\lambda T$ and $p_0=\frac{\rho_0}{3}$, Eq. (11) produces the following differential equation in ρ_0

$$\dot{\rho}+3\frac{8\pi+\lambda}{6\pi+\lambda}H\rho_0=0,$$

whose solution is

$$\rho_0=c_2 a^{\frac{-3(8\pi+\lambda)}{6\pi+\lambda}}, \tag{12}$$

c_2 is again an integration constant. These values of scale factor and density are used in the further mathematics.

3 Axial perturbations in FRW spacetime

In this section, we first briefly discuss perturbations used to study the effects of GWs. Here, the background metric $g_{\mu\nu}$ is the FRW spacetime and $h_{\mu\nu}$ are the corresponding perturbations in the metric tensor due to GWs such that we have

$$g_{\mu\nu}^{(perturb)}=g_{\mu\nu}^{(flat)}+eh_{\mu\nu}+O(e^2), \tag{13}$$

where e is a small parameter (it measures strength of perturbations and the terms involving $O(e^2)$ are neglected).

We follow the Regge–Wheeler [28] perturbation scheme to investigate the wavelike fluctuations. To obtain explicit expressions for the components of $h_{\mu\nu}$ in terms of four coordinates ($x^0=\eta,\ x^1=r,\ x^2=\theta,\ x^3=\phi$), they expressed them in the form of spherical harmonics. The symmetry of the metric tensor allows the angular momentum to be defined. The angular momentum is discussed by assuming the rotations on a 2D-manifold with $\eta=$ constant and $r=$ constant. The components of $h_{\mu\nu}$ have different transformations under a rotation of the frame. Among the ten independent components of the tensor $h_{\mu\nu}$, the components $h_{00},\ h_{01},\ h_{11}$ transform like scalars (as $x^0=\eta$ and $x^1=r$ are constants and do not change during rotation), $h_{02},\ h_{03},\ h_{12},\ h_{13}$ change like vectors (as x^2 and x^3 are changed during rotation) while $h_{22},\ h_{23},\ h_{33}$ transform like tensors. Further, these scalars, vectors and tensors are expressed in terms of spherical harmonics Y_L^M where L is the angular momentum with the projection M on z-axis. After this, they expressed the perturbation matrix $h_{\mu\nu}$ in terms of odd and even parity waves. In this paper, we only consider the odd or axial wave perturbations defined by the matrix [28]

$$h_{\mu\nu}=\partial_\theta Y\sin\theta\begin{pmatrix}0&0&0&k_0\\0&0&0&k_1\\0&0&0&0\\k_0&k_1&0&0\end{pmatrix}, \tag{14}$$

with $k_0=k_0(\eta,r)$ and $k_1=k_1(\eta,r)$. Here we are considering the odd waves corresponding to $m=0$, which are discussed by Regge and Wheeler [28] so that ϕ disappears in calculations. Also, for the wavelike solution the index l exceeds one, i.e., $Y = Y_{l0};\ l = 2, 3, \ldots$. The resulting axially perturbed FRW spacetime in Regge–Wheeler gauge is defined by

$$\begin{aligned} ds^2 = &-a^2(\eta)d\eta^2 + 2ek_0\partial_\theta Y \sin\theta d\eta d\phi + a^2(\eta)dr^2 \\ &+2ek_1\partial_\theta Y \sin\theta dr d\phi \\ &+a^2(\eta)r^2 d\theta^2 + a^2(\eta)r^2\sin^2\theta d\phi^2 + O(e^2). \end{aligned} \tag{15}$$

The perturbations in the material quantities are defined as follows [35]

$$\rho = \rho_0(1 + e\Delta(\eta, r)Y) + O(e^2), \tag{16}$$

$$p = p_0(1 + e\Pi(\eta, r)Y) + O(e^2), \tag{17}$$

where ρ_0 and p_0 are the background density and pressure. The fluid may or may not be comoving in the perturbed scenario so the perturbed components of four velocity are taken as [35]

$$V_0 = \frac{2g_{00}^{(0)} + ek_{00}}{2a(\eta)} + O(e^2), \tag{18}$$

$$V_1 = ea(\eta)w(\eta, r)Y + O(e^2), \tag{19}$$

$$V_2 = ev(\eta, r)Y' + O(e^2), \tag{20}$$

$$V_3 = e\sin\theta u(\eta, r)Y' + O(e^2), \tag{21}$$

where $V_\alpha V^\alpha = -1 + O(e^2)$. The field equations for the perturbed metric (15) as well as corresponding perturbed matter are

$$\begin{aligned} 3H^2 = &[(8\pi + 3\lambda)\rho_0 - \lambda p_0 + (8\pi + 3\lambda)\rho_0 e\Delta Y \\ &-\lambda p_0 e\Pi Y]a^2, \end{aligned} \tag{22}$$

$$w(8\pi + 2\lambda)(\rho_0 + p_0) = 0, \tag{23}$$

$$v(8\pi + 2\lambda)(\rho_0 + p_0) = 0, \tag{24}$$

$$\begin{aligned} -2\dot{H} - H^2 = &a^2[(8\pi + 3\lambda)p_0 - \lambda\rho_0 \\ &+(8\pi + 3\lambda)p_0 e\Pi Y - \lambda\rho_0 e\Delta Y], \end{aligned} \tag{25}$$

$$k_1' = \dot{k}_0, \tag{26}$$

$$\begin{aligned} &\dot{k}_1' - k_0'' + \frac{2}{r}\dot{k}_1 - 2Hk_1' + \frac{4}{r}k_1 H - 4k_0\dot{H} \\ &\quad -2H^2 k_0 + \frac{k_0}{r^2}l(l+1) \\ &= -2a^3(8\pi + 2\lambda)u(\rho_0 + p_0) \\ &\quad +[(8\pi + 3\lambda)p_0 - \lambda\rho_0]2a^2k_0 \\ &\quad +2a^2e(8\pi + 4\lambda)k_0p_0\Pi Y - 2a^2e\lambda k_0\rho_0\Delta, \end{aligned} \tag{27}$$

$$\begin{aligned} &\ddot{k}_1 - \dot{k}_0' + \frac{2}{r}\dot{k}_0 - \frac{2}{r^2}k_1 - 2H\dot{k}_1 - 6\dot{H}k_1 \\ &\quad -2H^2k_1 + \frac{k_1}{r^2}l(l+1) \\ &= 2a^2k_1p_0(8\pi + 2\lambda) + 2\lambda a^2k_1(-\rho_0 + p_0) \\ &\quad -2a^2e\lambda k_1\rho_0\Delta \\ &\quad +2a^2e(8\pi + 4\lambda)k_1p_0\Pi Y, \end{aligned} \tag{28}$$

where prime indicates the derivative with respect to r and also, we have used the relation [35]

$$\partial_\theta\partial_\theta Y = -l(l+1)Y - \cot\theta\partial_\theta Y.$$

4 Effects of axial gravitational waves

In this section, we find expressions for the perturbation parameters k_0, k_1, Δ, Π, w, v and u. Equation (23) implies that either the factor $(8\pi + 2\lambda) = 0$, i.e., $\lambda = -4\pi$ or $w(\rho_0 + p_0) = 0$. However, the viability conditions for $f(R, T)$ gravity models are

$$f_R > 0, \quad 1 + \frac{f_T}{8\pi} > 0 \quad \text{and} \quad f_{RR} > 0,$$

and give the constraint $\lambda > -4\pi$ for our model implying that $(8\pi + 2\lambda) \neq 0$. Hence Eqs. (23) and (24) yield that $w = 0$ and $v = 0$. Substituting the unperturbed field equations in perturbed one, we obtain the following equations from (22), (25), (27) and (28), respectively.

$$(8\pi + 3\lambda)\rho_0\Delta - \lambda p_0\Pi = 0, \tag{29}$$

$$(8\pi + 3\lambda)p_0\Pi - \lambda\rho_0\Delta = 0, \tag{30}$$

$$\begin{aligned} &\dot{k}_1' - k_0'' + \frac{2}{r}\dot{k}_1 - 2Hk_1' + \frac{4}{r}k_1H + \frac{k_0}{r^2}l(l+1) \\ &= -2a^3(8\pi + 2\lambda)u(\rho_0 + p_0) \\ &\quad +2a^2e[(8\pi + 4\lambda)k_0p_0\Pi Y - \lambda k_0\rho_0\Delta], \end{aligned} \tag{31}$$

$$\begin{aligned} &\ddot{k}_1 - \dot{k}_0' + \frac{2}{r}\dot{k}_0 - \frac{2}{r^2}k_1 - 2H\dot{k}_1 - 2\dot{H}k_1 + \frac{k_1}{r^2}l(l+1) \\ &= 2a^2e[-\lambda k_1\rho_0\Delta + (8\pi + 4\lambda)k_1p_0\Pi Y]. \end{aligned} \tag{32}$$

Solving (29) and (30) simultaneously for Π, we obtain

$$((8\pi + 3\lambda)^2 - \lambda^2)p_0\Pi = 0, \tag{33}$$

which implies either

$$((8\pi + 3\lambda)^2 - \lambda^2) = 0 \quad \text{or} \quad \Pi = 0. \tag{34}$$

The first factor in the above equation yields $\lambda = -4\pi$ and -2π. However, keeping in mind the viability conditions for the assumed model, we exclude $\lambda = -4\pi$. Hence if $\lambda = -2\pi$, then there is a possibility that $\Pi \neq 0$ and similarly $\Delta \neq 0$, i.e., the axial GWs can affect the background matter in curvature-matter coupling scenario. Assuming the EoS for radiation dominated era $p_0 = \frac{1}{3}\rho_0$, we obtain the following relationship between Π and Δ

$$\Pi = 3\left(\frac{8\pi}{\lambda} + 3\right)\Delta. \tag{35}$$

Substituting the above relation in Eqs. (31) and (32), we are left with four unknowns k_0, k_1, Δ, u with three equations (26), (31), (32). Thus in order to have the system closed, we assume that GWs do not perturb the matter field, i.e.,

$\Delta = 0 = \Pi$. Now introducing a new quantity $Q(\eta, r)$ such that

$$k_1(\eta, r) = ra(\eta)Q(\eta, r). \tag{36}$$

Using this equation with Eq. (26) in (32), we obtain

$$\ddot{Q} - Q'' + \frac{l(l+1)}{r^2}Q - a^2 \left[\frac{(4\pi + 3\lambda)}{3}\rho_0 - \frac{(12\pi + 5\lambda)}{3}p_0\right] Q = 0. \tag{37}$$

Inserting $p_0 = \frac{\rho_0}{3}$, the values of $a(\eta)$ as well as ρ_0 from Eqs. (10) and (11) into (37), it follows that

$$\ddot{Q} - Q'' + \left[\frac{l(l+1)}{r^2} - \frac{4c_1^2 c_2 b_1 \lambda}{9}\eta^{\frac{6\pi+2\lambda}{6\pi+\lambda}\frac{(-3)(8\pi+\lambda)}{6\pi+\lambda}}\right] Q = 0, \tag{38}$$

where $b_1 = c_1^{\frac{-3(8\pi+\lambda)}{6\pi+\lambda}}$. Let us define $A = \frac{4c_1^2 c_2 b_1 \lambda}{9}$ and take $l = 2$ such that the above equation becomes

$$\ddot{Q} - Q'' + \left[\frac{6}{r^2} - A\eta^{\frac{6\pi+2\lambda}{6\pi+\lambda}\frac{(-3)(8\pi+\lambda)}{6\pi+\lambda}}\right] Q = 0. \tag{39}$$

This is a wave equation and can be solved through separation of variables by assuming $Q(\eta, r) = \mathcal{T}(\eta)\mathcal{R}(r)$ and the initial conditions.

$$Q(0, r) = \Psi_1(r), \quad \partial_\eta Q(0, r) = \Psi_2(r),$$

Introducing the separation constant $-m^2$, we obtain the following two differential equations

$$\ddot{\mathcal{T}} - \left(A\eta^{\frac{6\pi+2\lambda}{6\pi+\lambda}\frac{(-3)(8\pi+\lambda)}{6\pi+\lambda}} - m^2\right)\mathcal{T} = 0, \tag{40}$$

$$\mathcal{R}'' - \left(\frac{6}{r^2} - m^2\right)\mathcal{R} = 0. \tag{41}$$

These are second order homogeneous linear differential equations with variable coefficients. Equation (40) can yield some solution if the power of η is fixed. So, we consider $\frac{6\pi+2\lambda}{6\pi+\lambda}\frac{(-3)(8\pi+\lambda)}{6\pi+\lambda} = n$ and check that for what values of n, the values of λ are consistent with viability criteria. We find that the values of λ for $n > 1$ are not consistent with $\lambda > -4\pi$ (the viability criteria) and $n < -2$ yields imaginary values of λ. Hence, n can have the values within the limit $-2 \leq n < 1$. For $n = -2$, we have $\lambda = 0$ which is the case of GR. For convenience, we consider the integer values in this interval, i.e., $n = 0, -1$, to find the solution of Eq. (40). For $n = 0$, the solution is

$$\mathcal{T}(\eta) = c_3 \cos m\eta + c_4 \sin m\eta, \tag{42}$$

where c_3 and c_4 are constants of integration and for $n = -1$, we have

$$\mathcal{T}(\eta) = c_5\eta e^{-im\eta}\text{Hypergeometric1F1}\left[1 + \frac{A}{2im}, 2, 2im\eta\right] + c_6\eta e^{-im\eta}\text{HypergeometricU}\left[1 + \frac{A}{2im}, 2, 2im\eta\right],$$

where c_5, c_6 are constants and Hypergeometric1F1, HypergeometricU are the confluent hypergeometric functions of the first and second kind, respectively. These functions are defined by

$$\text{Hypergeometric1F1}(\alpha; \beta; z) = \frac{\Gamma(\beta)}{\Gamma(\beta - \alpha)\Gamma(\alpha)}\int_0^1 e^{zt}t\,(\alpha - 1)(1 - t)^{\beta-\alpha-1}dt,$$

$$\text{HypergeometricU}(\alpha, \beta, z) = \frac{1}{\Gamma(\alpha)}\int_0^\infty e^{-zt}t(\alpha - 1)\,(1 + t)^{\beta-\alpha-1}dt,$$

where "Γ" indicates the gamma function. The solution of Eq. (41) is obtained as

$$\mathcal{R}(r) = \sqrt{\frac{2}{m\pi}}c_7\left(\frac{-3\cos mr}{mr} - \sin mr + \frac{3\sin mr}{m^2r^2}\right) + \sqrt{\frac{2}{m\pi}}c_8\left(\frac{-3\cos mr}{m^2r^2} - \frac{3\sin mr}{mr} + \cos mr\right), \tag{43}$$

where c_7, c_8 are integration constants. Inserting the values of $\mathcal{R}(r)$ and $\mathcal{T}(\eta)$ in $Q(\eta, r) = \mathcal{T}(\eta)\mathcal{R}(r)$, we obtain $Q(\eta, r)$ for both values of n. Furthermore, using initial conditions one can find the expressions for $\Psi_1(r)$ and $\Psi_2(r)$ for $n = 0$ as well as $n = -1$.

Replacing the values of $Q(\eta, r)$ and $a(\eta)$ in Eq. (36), we obtain the value of k_1 while the expression for k_0 is obtained from Eq. (26) as follows

$$k_0 = B(r) + \int_{\eta_0}^{\eta} k_1'(\tau, r)d\tau, \tag{44}$$

where η_0 is the conformal time at the hypersurface originating GWs. Assuming $k_0(\eta, r) = 0$, we have $B(r) = 0$ and k_0 becomes

$$k_0 = (r\mathcal{R}(r))'\int_{\eta_0}^{\eta} a(\tau)\mathcal{T}(\tau)d\tau. \tag{45}$$

Finally, replacing the values of k_0, k_1 and $\Delta = 0 = \Pi$ in Eq. (31), we obtain for $n = 0$

$$u(\eta, r) = \frac{\eta^{\frac{\lambda}{6\pi+\lambda}}c_1}{(mr)^{\frac{5}{2}}}\sqrt{\frac{2r}{\pi}}[(3mrc_7 + m^3r^3c_7 + 3c_8)\cos mr + (-3c_7 + mr(3 + m^2r^2)c_8)\sin mr]\,[(c_3 - m\eta c_4)\cos m\eta + (m\eta c_3 + c_4)\sin m\eta]. \tag{46}$$

For $n = -1$, we have

$$u(\eta, r) = \frac{\eta^{\frac{6\pi+2\lambda}{6\pi+\lambda}} e^{-im\eta} c_1}{(mr)^{\frac{5}{2}}} \sqrt{\frac{r}{2\pi}} \left[\left(1 - \frac{6\pi + 2\lambda}{6\pi + \lambda} + im\eta \right) \right.$$
$$\times \left\{ 2c_5 \text{Hypergeometric1F1} \left[1 + \frac{A}{2im}, 2, 2im\eta \right] \right.$$
$$\left. + 2c_6 \text{HypergeometricU} \left[1 + \frac{A}{2im}, 2, 2im\eta \right] \right\}$$
$$+ (A + 2im)\eta \left\{ 2c_6 \text{HypergeometricU} \right.$$
$$\times \left[2 + \frac{A}{2im}, 3, 2im\eta \right] - c_5$$
$$\left. \left. \times \text{Hypergeometric1F1} \left[2 + \frac{A}{2im}, 3, 2im\eta \right] \right\} \right]$$
$$\times [(3mrc_7 + m^3r^3c_7 + 3c_8) \cos mr$$
$$+ (-3c_7 + mr(3 + m^2r^2)c_8) \sin mr]. \tag{47}$$

Thus the final expression for four velocity in radiation dominated phase becomes

$$V_\alpha = (-c_1\eta^{\frac{6\pi+2\lambda}{6\pi+\lambda}}, 0, 0, e\partial_\theta Y u(\eta, r) \sin\theta). \tag{48}$$

Also, $Y = Y_{20}(\theta) = \frac{1}{4}\sqrt{\frac{5}{\pi}}(3\cos^2\theta - 1)$ leads to $\partial_\theta Y = \frac{1}{4}\sqrt{\frac{5}{\pi}} \cos\theta \sin\theta$ and hence

$$V_\alpha = \left(-c_1\eta^{\frac{6\pi+2\lambda}{6\pi+\lambda}}, 0, 0, \frac{e}{4}\sqrt{\frac{5}{\pi}} u(\eta, r) \cos\theta \sin^2\theta \right). \tag{49}$$

Thus the azimuthal velocity of any point P having coordinates (η, r, θ, ϕ) is $V_3 = \frac{e}{4}\sqrt{\frac{5}{\pi}} u(\eta, r) \cos\theta \sin^2\theta$, where $u(\eta, r)$ is given in Eqs. (46) and (47) for $n = 0, -1$, respectively.

5 Final remarks

According to rough approximate, a pair of massive black holes merge in every $223^{352}_{-115} sec$ and a binary of neutron star merge in every $13^{49}_{-9} sec$ [43]. Among these mergers a small fraction is detected by advance interferometers of LIGO-Virgo collaboration and can be associated to some individual GW event. The rest of the events contribute to make a stochastic background which is a random GW signal originated by various independent, weak and unresolved sources. These sources include for instance, the supernova explosions at the end of a massive star's life (including non-symmetric explosions), a rapidly rotating neutron star, cosmic strings etc. Mathematical and statistical approaches have been developed to observe these stochastic background of GWs and extract information from them [44,45]. These GWs signals have great influence on cosmic evolution and hence the study of different aspect of GW phenomenon is very significant.

The main goal of this manuscript is to explore the changes produced by axial GWs in geometry as well as matter of a flat universe during evolution and in the context of curvature-matter coupling theory. For this purpose, we assume the presence of these waves and find the corresponding geometrical and material changes produced by these waves in $f(R, T)$ gravity. We have introduced axial perturbations in the flat FRW spacetime, the background matter is also perturbed as well as the four velocity is allowed to be non-comoving. We then proceed to find all unknown parameters of perturbations with the help of perturbed and unperturbed field equations. It is mentioned here that all field equations reduce to GR equations [36] for $\lambda = 0$.

The factors w, v, appearing in V_1 and V_2 are zero showing that axial waves do not change these components of velocity which is similar to that in GR. We have found that axial GWs in $f(R, T)$ theory can perturb the background matter in contrast to GR. However, here we suppose Δ and Π equal to zero in order to find the remaining functions k_0, k_1 and u. The resulting k_0 and k_1 are different from those of GR and depend upon the coupling constant λ. The function u appearing in the azimuthal velocity component has non-zero expression showing that fluid exhibits a rotation due to axial GWs similar to GR. But the expression of u here depends upon λ and differs from GR.

Currently, our universe is in expansion phase and it is crucial to investigate the propagation of GWs in this expanding universe. In this regard, we expand our analysis using the EoS $p_0 = -\rho_0$ for expanding matter and observe how such types of GWs can perturb the flat cosmos in the recent era. For $p_0 = -\rho_0$, the scale factor and density have the expressions

$$a(\eta) = \frac{\tilde{c}_1}{\eta}, \quad \rho_0 = \tilde{c}_2 a^{\frac{-3\lambda}{2\pi}}, \tag{50}$$

where $\tilde{c}_1$ and $\tilde{c}_2$ are integration constants. It is found that this EoS can yield non-vanishing w and v (from (23) and (24)) while the remaining expressions remain the same with $A = \frac{8(2\pi+\lambda)}{3} c_1^2 c_2 b_1$, $b_1 = \tilde{c}_6^{\frac{-3\lambda}{2\pi}}$ and $\frac{3\lambda - 4\pi}{2\pi} = n$. In dark energy dominated phase, n can take positive and negative values, however, similar to radiation dominated phase, $n = -2$ yields the GR case.

The angular (Ω) and linear rotational (V) velocities of the fluid are

$$\Omega = \frac{V^3}{V^0} = \frac{Cu}{ar^2} \cos\theta; \quad C = \frac{e}{4}\sqrt{\frac{5}{\pi}},$$
$$V = ar \sin\theta\Omega = \frac{Cu \sin 2\theta}{2r}.$$

When the expression of $u(\eta, r)$ is continuous at the wave front, the smooth wave profile does not induce any cosmological rotation [36]. Hence we conclude that the axial GW can induce a cosmological rotation if $u(\eta, r)$ is discontinuous at the wave front. If the freely falling particles are displaced by a GW, it is called memory effect of the GW. Hence the axial GW in $f(R, T)$ gravity induces memory effect when the wave profile has discontinuity at the wave front. Also, the model considered here describes the simplest curvature-matter coupling and we assume this model to reduce the calculation work. However, this work can be extended for other minimally coupled models containing nonlinear power of R or T or non-minimally coupled models leading to interesting results. Such models may yield the non-vanishing values of the perturbation parameters which are zero in the present scenario.

When a GW without memory passes through a detector, it produces an oscillatory deformation and returns the detector back to its equilibrium state. On the other hand, a GW with memory can induce a permanent deformation in an idealized detector, i.e., a truly free falling detector [46]. The detectors like Weber bars and LIGO are not sensitive to the memory effect. However, the detectors of the type like LISA (Laser interferometry space antenna) or advanced LIGO can detect the memory due to its sensitivity and with strong memory sources [47,48]. Also, the ground-based detectors are not truly free falling and cannot store a memory signal while LISA like detectors are able to maintain the permanent displacement because these are free floating.

Acknowledgements We would like to thank the Higher Education Commission, Islamabad, Pakistan for its financial support through the *Indigenous Ph.D. 5000 Fellowship Program Phase-II, Batch-III.*

Open Access This article is distributed under the terms of the Creative Commons Attribution 4.0 International License (http://creativecommons.org/licenses/by/4.0/), which permits unrestricted use, distribution, and reproduction in any medium, provided you give appropriate credit to the original author(s) and the source, provide a link to the Creative Commons license, and indicate if changes were made.
Funded by SCOAP[3].

References

1. H.A. Buchdahl, Mon. Not. R. Astron. Soc. **150**, 1 (1970)
2. S. Nojiri, S.D. Odintsov, Phys. Lett. B **631**, 1 (2005)
3. T. Harko, F.S.N. Lobo, S. Nojiri, S.D. Odintsov, Phys. Rev. D **84**, 024020 (2011)
4. P. Ratra, L. Peebles, Phys. Rev. D **37**, 3406 (1988)
5. R.R. Caldwell, R. Dave, P.J. Steinhardt, Phys. Rev. Lett. **80**, 1582 (1998)
6. R.R. Caldwell, Phys. Lett. B **545**, 23 (2002)
7. N. Afshordi, D.J.H. Chung, G. Geshnizjani, Phys. Rev. D **75**, 083513 (2007)
8. M.R. Setare, Phys. Lett. B **648**, 329 (2007)
9. M.R. Setare, Phys. Lett. B **653**, 116 (2007)
10. S. Chaplygin, Sci. Mem. Mosc. Univ. Math. Phys. **21**, 1 (1904)
11. AYu. Kamenshchik, U. Moschella, V. Pasquier, Phys. Lett. B **511**, 265 (2001)
12. M.C. Bento, O. Bertolami, A.A. Sen, Phys. Rev. D **66**, 043507 (2002)
13. A. De Felice, S. Tsujikawa, Living Rev. Relativ. **13**, 3 (2010)
14. S.I. Nojiri, S.D. Odintsov, Phys. Rep. **505**, 59 (2011)
15. T. Harko, F.S.N. Lobo, Galaxies **2**, 410 (2014)
16. M. Sharif, M. Zubair, J. Cosmol. Astropart. Phys. **03**, 28 (2012)
17. H. Shabani, M. Farhoudi, Phys. Rev. D **90**, 044031 (2014)
18. Z. Yousaf, M.Z. Bhatti, Ume Farwa, Class. Quantum Gravity **34**, 145002 (2017)
19. M. Sharif, A. Siddiqa, Eur. Phys. J. Plus **132**, 529 (2017)
20. M. Sharif, A. Siddiqa, Int. J. Mod. Phys. D **27**, 1850065 (2018)
21. B.P. Abbott et al., Phys. Rev. Lett. **116**, 061102 (2016)
22. B.P. Abbott et al., Phys. Rev. Lett. **118**, 221101 (2017)
23. B.P. Abbott et al., Phys. Rev. Lett. **119**, 161101 (2017)
24. H.R. Kausar, L. Philippoz, P. Jetzer, Phys. Rev. D **93**, 124071 (2016)
25. M.E.S. Alves, P.H.R.S. Moraes, J.C.N. de Araujo, M. Malheiro, Phys. Rev. D **94**, 024032 (2016)
26. M. Sharif, A. Siddiqa, Phys. Dark Universe **15**, 105 (2017)
27. M. Sharif, A. Siddiqa, Astrophys. Space Sci. **362**, 226 (2017)
28. T. Regge, J.A. Wheeler, Phys. Rev. **108**, 1063 (1957)
29. F.J. Zerilli, Phys. Rev. D **02**, 2141 (1970)
30. S.W. Hawking, Phys. Rev. Lett. **26**, 1344 (1971)
31. R.V. Wagoner, Astrophys. J. **278**, 345 (1984)
32. E. Malec, G. Wylężek, Class. Quantum Gravity **22**, 3549 (2005)
33. O. Svitek, J. Phys. Conf. Ser. **229**, 012070 (2010)
34. S. Viaggiu, Class. Quantum Gravity **34**, 035018 (2017)
35. W. Kulczycki, E. Malec, Class. Quantum Gravity **34**, 135014 (2017)
36. W. Kulczycki, E. Malec, Phys. Rev. D **96**, 063523 (2017)
37. U.H. Gerlach, U.K. Sengupta, Phys. Rev. D **19**, 2268 (1979)
38. U.H. Gerlach, U.K. Sengupta, Phys. Rev. D **22**, 1300 (1980)
39. C. Gundlach, J.M. Martin-Garcia, Phys. Rev. D **61**(2000), 084024 (2000)
40. C. Clarkson, T. Clifton, S. February, J. Cosmol. Astropart. Phys. **06**, 25 (2009)
41. N.J. Poplawski, arXiv:gr-qc/0608031
42. V. Faraoni, Phys. Rev. D **80**, 124040 (2009)
43. B.P. Abbott et al., Phys. Rev. Lett. **120**, 091101 (2018)
44. B. Allen, J.D. Romano, Phys. Rev. D **59**, 102001 (1999)
45. R. Smith, E. Thrane, Phys. Rev. X **8**, 021019 (2018)
46. M. Favata, Class. Quantum Gravity **27**, 084036 (2010)
47. P.D. Lasky, E. Thrane, Y. Levin, J. Blackman, Y. Chen, Phys. Rev. Lett. **117**, 061102 (2016)
48. P.M. Zhang, C. Duval, G.W. Gibbons, P.A. Horvathy, Phys. Lett. B **772**, 743 (2017)

Modern Physics Letters A
Vol. 32, No. 28 (2017) 1750151 (12 pages)
© World Scientific Publishing Company
DOI: 10.1142/S0217732317501516

Interaction of viscous modified Chaplygin gas with $f(R, T)$ gravity

M. Sharif* and Aisha Siddiqa†

Department of Mathematics, University of the Punjab,
Quaid-e-Azam Campus, Lahore 54590, Pakistan
**msharif.math@pu.edu.pk*
†aisha.siddiqa17@yahoo.com

Received 20 March 2017
Revised 14 June 2017
Accepted 24 July 2017
Published 24 August 2017

We study the evolution of viscous modified Chaplygin gas (MCG) interacting with $f(R,T)$ gravity in flat FRW universe, where T is the trace of energy–momentum tensor. The field equations are formulated for a particular model $f(R,T) = R + 2\chi T$ and constraints for the conservation of energy–momentum tensor are obtained. We investigate the behavior of total energy density, pressure and equation of state (EoS) parameter for emergent, intermediate as well as logamediate scenarios of the universe with two interacting models. It is found that the EoS parameter lies in the matter-dominated or quintessence era for all the three scenarios while the bulk viscosity enhances the expansion for the intermediate and logamediate scenarios.

Keywords: $f(R,T)$ gravity; modified Chaplygin gas; viscosity.

PACS Nos.: 04.50.Kd, 95.36.+x, 98.80.Jk

1. Introduction

The most striking and fascinating area in cosmology is the current accelerated expansion of the universe suggested by different observations. The factor generating this expansion is named as dark energy violating the strong energy condition (i.e. $\rho + 3p < 0$). The simplest model explaining this expansion is the Λ cold dark matter (CDM), but it suffers from two issues called fine-tuning (large difference between its observed and theoretical predicted values) and coincidence (between observed vacuum energy and current matter density). This promotes the alternative models of dark energy proposed by either modifying the matter or geometric part of the Einstein–Hilbert action. The modified matter models are quintessence,[1,2] phantom,[3] K-essence,[4] holographic dark energy[5] and Chaplygin gas (CG). Some examples of modification in geometric part are scalar–tensor theory, $f(R)$ and $f(R,T)$ theories of gravity.

Chaplygin[6] introduced an exotic equation of state (EoS) to describe the force on the wing of airplane. After the observational evidences for expansion of the universe, the CG model is used in cosmology[7,8] to describe the exotic fluid causing expansion of the universe. The extended models known as generalized CG (GCG),[9] modified CG (MCG)[10] and generalized cosmic CG (GCCG)[11] are widely investigated in the literature. It is observed that pure CG model is not compatible with the observational data.[12,13]

Sadeghi and Farahani[14] investigated the interaction between viscous varying MCCG and tachyonic fluid for emergent, intermediate as well as logamediate scenarios. They found phantom-like behavior of emergent universe (a universe whose starting point is not a singularity) and quintessence region for the other two scenarios. Naji *et al.*[15] studied MCG interacting with matter and explored the effects of bulk and shear viscosities on cosmological parameters. Sharif and Sarwar[16] examined the stability of GCCG model and found that it is stable adiabatically but it cannot be observed for isothermal condition. CG models are also considered in literature to discuss inflation.[17–19]

Harko *et al.*[20] proposed $f(R,T)$ gravity as a generalized modified theory. Jamil *et al.*[21] introduced some cosmic models in this gravity and found that the ΛCDM model is reproduced by dust fluid. Houndjo[22] discussed the matter-dominated and accelerated phases of the universe for the models linear in T while the power of R depends on input parameters. Sharif and Zubair[23] explored thermodynamics of this gravity and concluded that the second law of thermodynamics is valid for phantom as well as non-phantom phases. The same authors[24] established energy conditions and constraints for the stability of power-law models.

The effects of viscosity cannot be separated from fluids in cosmology and interesting conclusions can be drawn by exploring the effects of bulk as well as shear viscosity on cosmological evolution. Johri and Sudharsan[25] investigated the effects of bulk viscosity on the evolution of FRW universe and found that the time independent bulk viscosity can drive a steady state universe. Ren and Meng[26] presented a study on scalar field with bulk viscosity and proposed a model for which ΛCDM is a special case. They concluded that the bulk viscosity enhances expansion of the universe. Gagnon and Lesgourgues[27] discussed a bulk viscous model as an alternative to dark energy. Baffou *et al.*[28] studied the cosmological evolution of viscous GCG interacting with $f(R,T)$ gravity for power-law model.

The interaction between modified theories and CG models have also been investigated in the literature[28–30] to study the interaction of dark energy and dark matter. The interacting models of dark energy and dark matter may provide a possible solution to the problems associated with the ΛCDM model.[31,32] The physical significance of considering an interaction between dark energy and dark matter is that it introduces an energy flow between the two components of the universe.[33,34] In this paper, we analyze the evolution of MCG interacting with $f(R,T)$ gravity under the effects of viscosity. This analysis is done for three different models of the universe namely emergent universe, intermediate and logamediate scenarios of inflation. The paper has the following format. In Sec. 2, the field equations are formulated for a particular model. Section 3 explores the evolution of interacting MCG and dark energy. The last section contains the concluding remarks.

2. $f(R,T)$ Gravity and Viscous Cosmology

The action for $f(R,T)$ gravity is defined as

$$S = \int d^4x\sqrt{-g}\left[\frac{1}{2\kappa^2}f(R,T) + \mathcal{L}_m\right]. \tag{1}$$

Variation of the above action with respect to $g^{\mu\nu}$ gives the field equations

$$f_R R_{\alpha\beta} - \frac{1}{2}g_{\alpha\beta}f + (g_{\alpha\beta}\Box - \nabla_\alpha\nabla_\beta)f_R = \kappa^2 T_{\alpha\beta} - f_T(T_{\alpha\beta} + \Theta_{\alpha\beta})\,, \tag{2}$$

where $f = f(R,T)$, $f_R = \frac{\partial f}{\partial R}$, $f_T = \frac{\partial f}{\partial T}$ and $\Theta_{\alpha\beta}$ is evaluated by

$$\Theta_{\alpha\beta} = g^{\gamma\mu}\frac{\delta T_{\gamma\mu}}{\delta g^{\alpha\beta}}\,, \qquad T_{\alpha\beta} = g_{\alpha\beta}\mathcal{L}_m - \frac{\partial \mathcal{L}_m}{\partial g^{\alpha\beta}}\,. \tag{3}$$

Harko *et al.*[20] introduced the model $f(R,T) = R + 2f(T)$ while $f(T) = \chi(T)^n$ is taken in Refs. 35 and 36, where χ and n are real constants. Thus we can write $f(R,T) = R + 2\chi T$,[37] which simplifies the field equations as

$$R_{\alpha\beta} - \frac{1}{2}Rg_{\alpha\beta} = \kappa^2 T_{\alpha\beta} - 2\chi(T_{\alpha\beta} + \Theta_{\alpha\beta}) + \chi g_{\alpha\beta}T = T^{\mathrm{tot}}_{\alpha\beta}\,. \tag{4}$$

The flat FRW universe model is given by

$$ds^2 = -dt^2 + a^2(t)(dx^2 + dy^2 + dz^2)\,, \tag{5}$$

where $a(t)$ is the scale factor.

We consider a matter which consists of MCG with bulk viscosity for which the energy–momentum tensor can be written as[38,39]

$$T_{\alpha\beta} = (\rho + p - 3\xi(t)H)V_\alpha V_\beta + (p - 3\xi(t)H)g_{\alpha\beta}\,, \tag{6}$$

where ρ denotes density of MCG, p represents pressure of MCG, V_α is four velocity and $\xi(t)$ denotes the bulk viscosity coefficient. Thus we can write the field equations as ($\kappa^2 = 1$)

$$3H^2 = \rho - \chi T + 2\chi(\rho + p - 3\xi H) = \rho^{\mathrm{tot}}\,, \tag{7}$$

$$-2\dot{H} - 3H^2 = p - 3\xi H + \chi T = p^{\mathrm{tot}}\,, \tag{8}$$

where $H = \frac{\dot{a}}{a}$ is the Hubble parameter and the trace of the energy–momentum tensor is

$$T = -\rho + 3p - 9\xi H\,. \tag{9}$$

Also,

$$\rho^{\mathrm{tot}} = \rho^{\mathrm{DE}} + \rho\,, \qquad p^{\mathrm{tot}} = p^{\mathrm{DE}} + p\,. \tag{10}$$

Consequently the energy density and pressure of dark energy become

$$\rho^{\mathrm{DE}} = -\chi T + 2\chi(\rho + p - 3\xi H)\,, \tag{11}$$

$$p^{\mathrm{DE}} = -3\xi H + \chi T\,. \tag{12}$$

The EoS for MCG is given by[10]

$$p = B\rho - \frac{C}{\rho^{\alpha}}\,, \tag{13}$$

where B, C are positive constants and $0 < \alpha \leq 1$.

3. Viscous Modified Chaplygin Gas Interaction

The conservation equation holds in $f(R,T)$ gravity provided that the following constraint holds:[40]

$$(\rho + p - 3\xi H)\dot{f}_T - \frac{1}{2} f_T((p - 3\xi H)^{\cdot} - \dot{\rho}) = 0\,. \tag{14}$$

When $f(T) = \chi T$, the above equation gives

$$(p - 3\xi H)^{\cdot} = \dot{\rho} \;\Rightarrow\; p - 3\xi H = \rho + c_1\,, \tag{15}$$

where c_1 is constant of integration. Adding Eqs. (13) and (15), we have

$$p = \frac{B+1}{2}\rho - \frac{C}{2\rho^{\alpha}} + \frac{3}{2}\xi H + \frac{c_1}{2}\,. \tag{16}$$

This equation can be written in the form of the EoS of MCG as

$$p = \tilde{B}\rho - \frac{\tilde{C}}{\rho^{\alpha}}\,, \tag{17}$$

where $\tilde{B} = \frac{B+1}{2}$, $\tilde{C} = \frac{C}{2}$ and

$$\frac{3}{2}\xi H + \frac{c_1}{2} = 0\,, \tag{18}$$

which gives $\xi(t)$ in terms of H and c_1. We take the conservation of $T^{\mathrm{tot}}_{\mu\nu}$ with the above mentioned constraints. The equation of continuity for interacting dark energy and MCG gives

$$\dot{\rho}^{\mathrm{DE}} + 3H(\rho^{\mathrm{DE}} + p^{\mathrm{DE}}) = -Q\,, \tag{19}$$

$$\dot{\rho} + 3H(\rho + p) = Q\,, \tag{20}$$

where Q is the interaction term which is usually considered either $Q = 3Hb\rho$, or $Q = 3Hb\rho^{\mathrm{DE}}$, or $Q = 3Hb\rho^{\mathrm{tot}}$, or b is the coupling constant.[14,15] There are also other interacting models containing time derivative of energy density but these interactions cannot change sign.

Wei[41] proposed a sign changeable interaction $Q = q(\mu\dot{\rho} + 3bH\rho)$, were μ is constant and q is the deceleration parameter given by

$$q = -1 - \frac{\dot{H}}{H^2}\,. \tag{21}$$

This is positive for the deceleration phase and negative for the acceleration phase. He explored that the cosmological coincidence problem can be alleviated by some scaling attractors and showed that this interaction model can bring new features to cosmology. In the following, we study the interactions $Q = 3Hb\rho$ as well as $Q = q(\mu\dot{\rho} + 3bH\rho)$ and compare their results for the following three scenarios.

1. Emergent scenario,[42] where the scale factor has the form $a(t) = a_0(A + e^{kt})^m$, $a_0 > 0,\ A > 0,\ k > 0,\ m > 1$.
2. Intermediate scenario,[43] where $a(t) = e^{\lambda t^\gamma}$ with $\lambda > 0$, $0 < \gamma < 1$.
3. Logamediate scenario,[43] where $a(t) = e^{\nu(\ln t)^\sigma}$ with $\nu > 0$, $\sigma > 1$.

The sum of Eqs. (19) and (20) gives

$$\dot{\rho}^{\mathrm{tot}} + 3H(1 + \omega^{\mathrm{tot}})\rho^{\mathrm{tot}} = 0\,,$$

which shows that for $\omega^{\mathrm{tot}} > -1$, ρ^{tot} is decreasing and for $\omega^{\mathrm{tot}} < -1$, ρ^{tot} is increasing. For graphical analysis, the parameters in all cases are fixed such that

1. ρ^{tot} and ω^{tot} satisfy the above relation,
2. p^{tot} remains negative,
3. c_1 is taken negative such that the bulk viscosity becomes positive because large positive value of bulk viscosity can produce negative pressure.[27]
4. The values of $\tilde{B} = \frac{B+1}{2}$ and $\tilde{C} = \frac{C}{2}$ are chosen such that the corresponding values of B and C remain positive.
5. The value of b is taken negative to have an energy flow from MCG to dark energy.[33]

3.1. *Interaction $Q = 3Hb\rho$*

We replace $Q = 3Hb\rho$ and Eq. (17) in (20), it follows that

$$\dot{\rho} + 3H\left(\rho D - \frac{\tilde{C}}{\rho^\alpha}\right) = 0\,, \qquad D = 1 + \tilde{B} - b\,. \tag{22}$$

For the emergent universe, the Hubble parameter becomes

$$H = \frac{mke^{kt}}{(A + e^{kt})} \tag{23}$$

and Eq. (22) gives the solution

$$\rho(t) = \left[\frac{\tilde{C} - e^{D(1+\alpha)c_2}(A + e^{kt})^{-3Dm(1+\alpha)}}{D}\right]^{\frac{1}{1+\alpha}}, \tag{24}$$

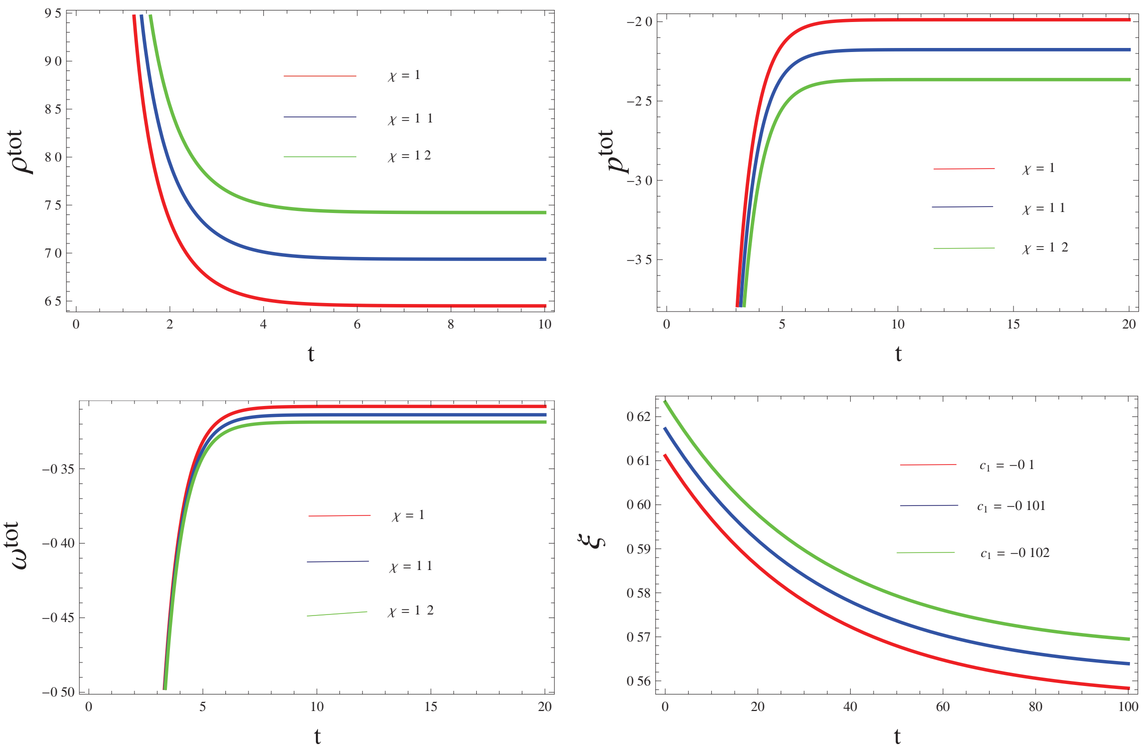

Fig. 1. Plots of $\rho^{\rm tot}$, $p^{\rm tot}$, $\omega^{\rm tot}$ and ξ vs. time in emergent universe for $\tilde{B}=3$, $\tilde{C}=10$, $\alpha=0.5$, $b=-1$, $A=0.1$, $k=0.03$, $m=15$, $c_1=-0.1$, $c_2=1$ and $Q=3Hb\rho$.

where c_2 is the constant of integration. Equation (17) then leads to

$$p(t)=\tilde{B}\left[\frac{\tilde{C}-e^{D(1+\alpha)c_2}(A+e^{kt})^{-3Dm(1+\alpha)}}{D}\right]^{\frac{1}{1+\alpha}} - \tilde{C}\left[\frac{\tilde{C}-e^{D(1+\alpha)c_2}(A+e^{kt})^{-3Dm(1+\alpha)}}{D}\right]^{\frac{-\alpha}{1+\alpha}}. \tag{25}$$

Inserting these values in Eqs. (11) and (12), we obtain the energy density and pressure of dark energy. Consequently, Eq. (10) gives the values of total energy density and pressure. The total EoS parameter is obtained as

$$\omega^{\rm tot}=\frac{p^{\rm tot}}{\rho^{\rm tot}}. \tag{26}$$

Equation (18) yields

$$\xi(t)=\frac{-c_1(A+e^{kt})}{3mke^{kt}}. \tag{27}$$

The graphs of $\rho^{\rm tot}$, $p^{\rm tot}$, $\omega^{\rm tot}$ and ξ for the emergent universe with the first interaction model are shown in Fig. 1. We see that the total density decreases while the total pressure increases with time. In all cases, the value of the model parameter χ cannot be negative as it leads to negative values of $\rho^{\rm tot}$ which is not physical. The effect of the model parameter χ on ρ^{tot}, p^{tot} and ω^{tot} is observed. The first graph shows that ρ^{tot} increases, second indicates a decrease in p^{tot} and the third graph depicts that the model has a tendency towards quintessence era with the increase in model parameter. We find that large χ increases ρ^{tot} and decreases p^{tot} but ω^{tot} does not cross the phantom divide line and always lies in the matter-dominated or quintessence era. The behavior of bulk viscosity with respect to time is decreasing while it decreases with the increase in c_1.

For the intermediate scenario, the Hubble parameter is $H = \lambda\gamma t^{\gamma-1}$ for which Eq. (22) yields

$$\rho(t) = \left[\frac{\tilde{C} - e^{(-3\lambda t^{\gamma}+c_3)D(1+\alpha)}}{D}\right]^{\frac{1}{1+\alpha}}, \tag{28}$$

where c_3 is another integration constant and Eq. (18) gives

$$\xi = \frac{-c_1}{3\lambda\gamma t^{\gamma-1}}. \tag{29}$$

Following the same procedure as above, we obtain the values of total energy density, pressure and EoS parameter. The graphical behavior is shown in Fig. 2. The effect of the model parameter remains the same as in emergent while the behavior of ξ with respect to time is opposite. It increases with the increase in time and decrease in c_1.

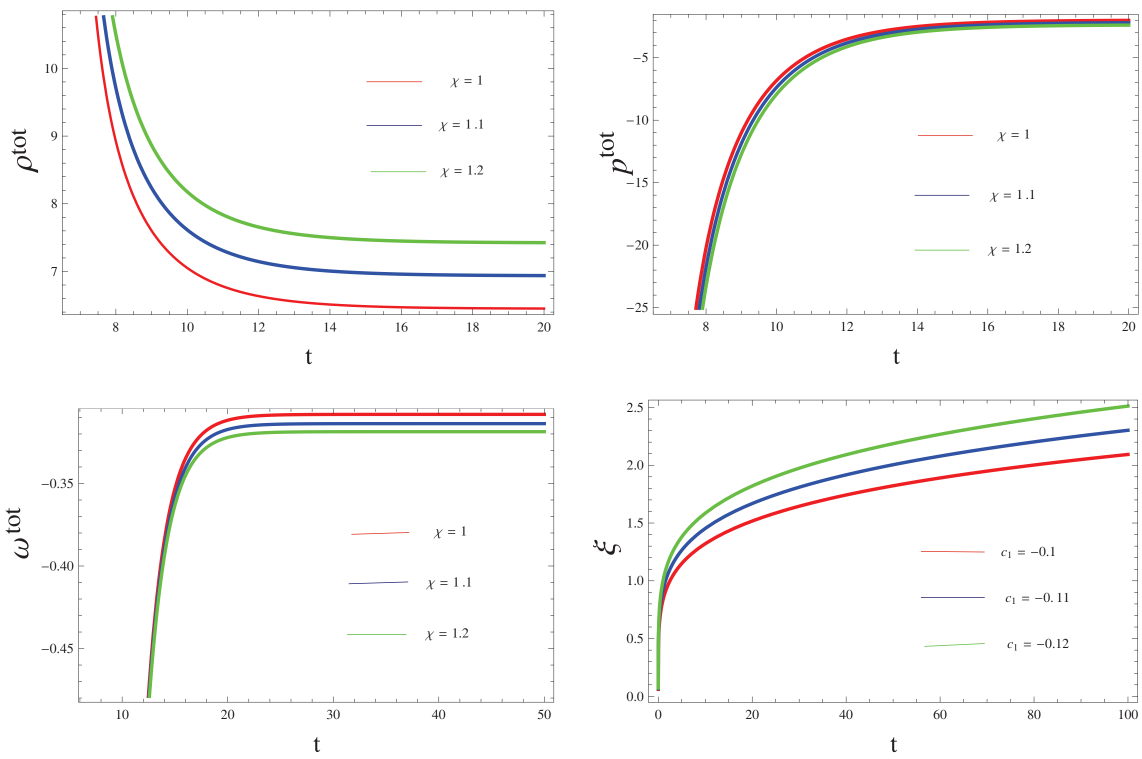

Fig. 2. Plots of ρ^{tot}, p^{tot}, ω^{tot} and ξ vs. time in intermediate universe for $\tilde{B} = 3$, $\tilde{C} = 10$, $\alpha = 0.5$, $b = -1$, $\lambda = 0.05$, $\gamma = 0.8$, $c_1 = -0.1 c_3 = 1$ and $Q = 3Hb\rho$.

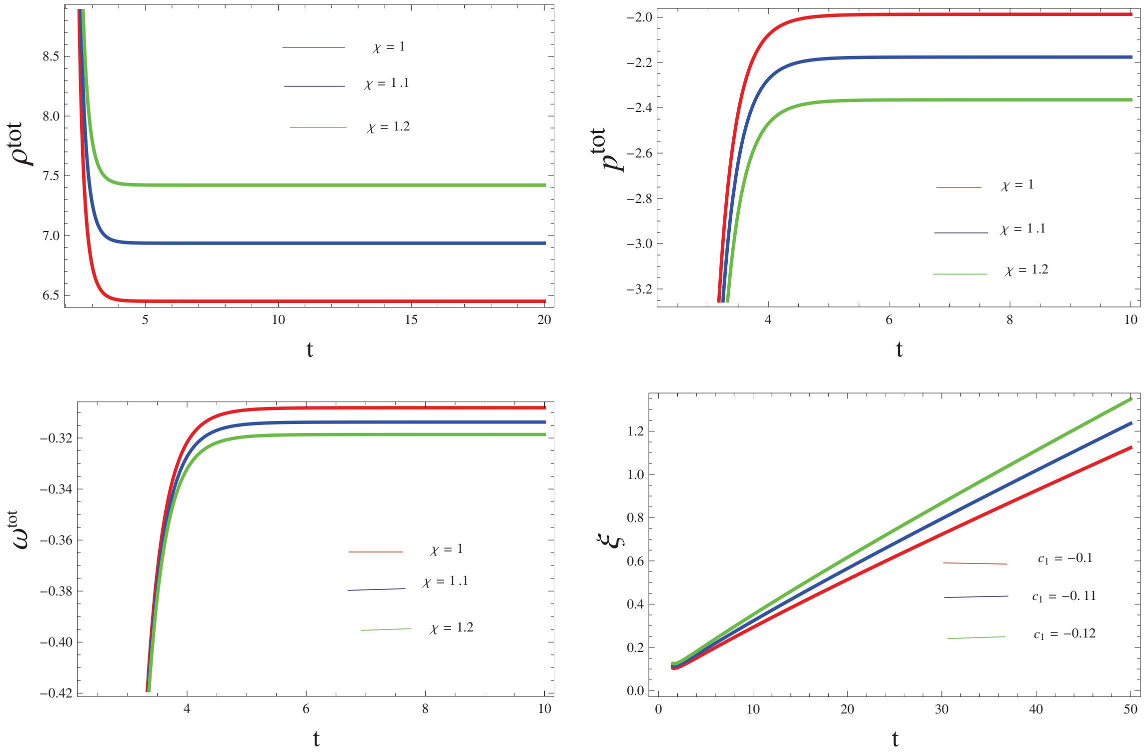

Fig. 3. Plots of ρ^{tot}, p^{tot}, ω^{tot} and ξ vs. time in logamediate universe, for $\tilde{B} = 3$, $\tilde{C} = 10$, $\alpha = 0.5$, $b = -1$, $\nu = 0.3$, $\sigma = 1.5$, $c_1 = -0.1$, $c_4 = 1$ and $Q = 3Hb\rho$.

The Hubble parameter, bulk viscosity and solution of Eq. (22) for the logamediate universe are given by

$$H = \frac{\nu\sigma(\ln t)^{\sigma-1}}{t}, \tag{30}$$

$$\xi = \frac{-c_1 t}{3\nu\sigma(\ln t)^{\sigma-1}}, \tag{31}$$

$$\rho(t) = \left[\frac{\tilde{C} - e^{D(1+\alpha)(c_4 - 3\nu(\ln t)^{\sigma})}}{D}\right]^{\frac{1}{1+\alpha}}, \tag{32}$$

where c_4 is the integration constant. In this case, Fig. 3 indicates the same effect of the model parameter as in the previous cases. The behavior of bulk viscosity is increasing with time as in the intermediate case but with a rapid rate.

3.2. *Interaction $Q = q(\mu\dot{\rho} + 3bH\rho)$*

In this case, we use Eq. (17) in (20) and obtain

$$(1 - q\mu)\dot{\rho} + 3H\left(D\rho - \frac{\tilde{C}}{\rho^{\alpha}}\right) = 0. \tag{33}$$

We obtain the following solutions of Eq. (33) for the emergent as well as intermediate universe, respectively,

$$\rho(t) = \left[\frac{\tilde{C} - e^{\frac{-3De^{kt}m(1+\alpha)}{1+\mu} + \frac{3(1+\alpha)D\sqrt{Am\mu}\arctan\left(\frac{e^{kt}\sqrt{m(1+\mu)}}{\sqrt{A\mu}}\right)}{(1+\mu)^{\frac{3}{2}}} + (1+\alpha)Dc_5}}{D}\right]^{\frac{1}{1+\alpha}}, \qquad (34)$$

$$\rho(t) = \left[\frac{\tilde{C} - e^{\frac{D(1+\alpha)}{\gamma(1+\mu)^2}(\gamma c_6(1+\mu)^2 - 3\gamma\lambda t^{\gamma}(1+\mu) + 3\mu\ln(-(1+\gamma)\mu + t^{\gamma}\gamma\lambda(1+\mu))(\gamma-1))}}{D}\right]^{\frac{1}{1+\alpha}}, \qquad (35)$$

where c_5 and c_6 are constants of integration. For the logamediate scenario, Eq. (33) gives a complicated solution, so we solve it numerically. For this interaction model, the graphical behavior for all cases is shown in Figs. 4–6, respectively. The behavior of ρ^{tot}, p^{tot}, ω^{tot} as well as the effect of model parameter χ is similar to the first interaction model for the emergent and intermediate scenarios. The behavior of pressure and EoS parameter for the logamediate scenario is reversed in this model. Moreover, bulk viscosity also has the same behavior.

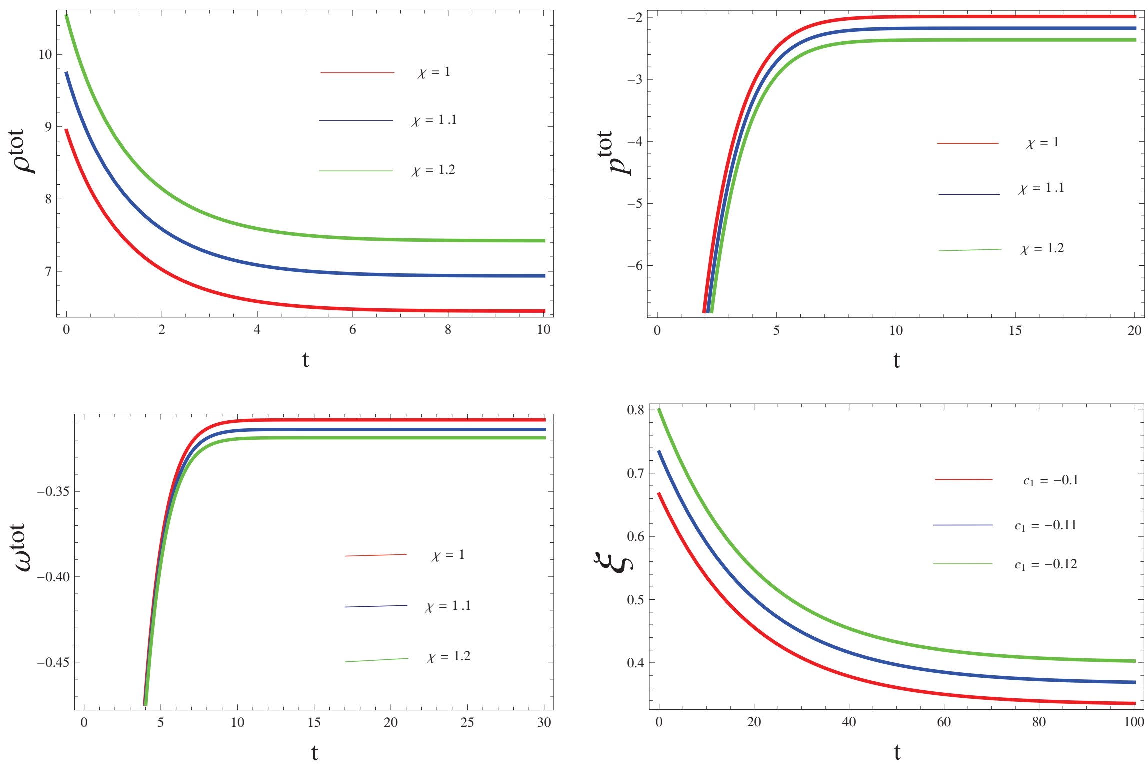

Fig. 4. Plots of ρ^{tot}, p^{tot}, ω^{tot} and ξ vs. time in emergent universe for $\tilde{B} = 3$, $\tilde{C} = 10$, $\alpha = 0.5$, $b = -1$, $A = 1$, $k = 0.05$, $m = 2$, $\mu = 2$, $c_1 = -0.1$, $c_5 = 1$ and $Q = q(\mu\dot{\rho} + 3bH\rho)$.

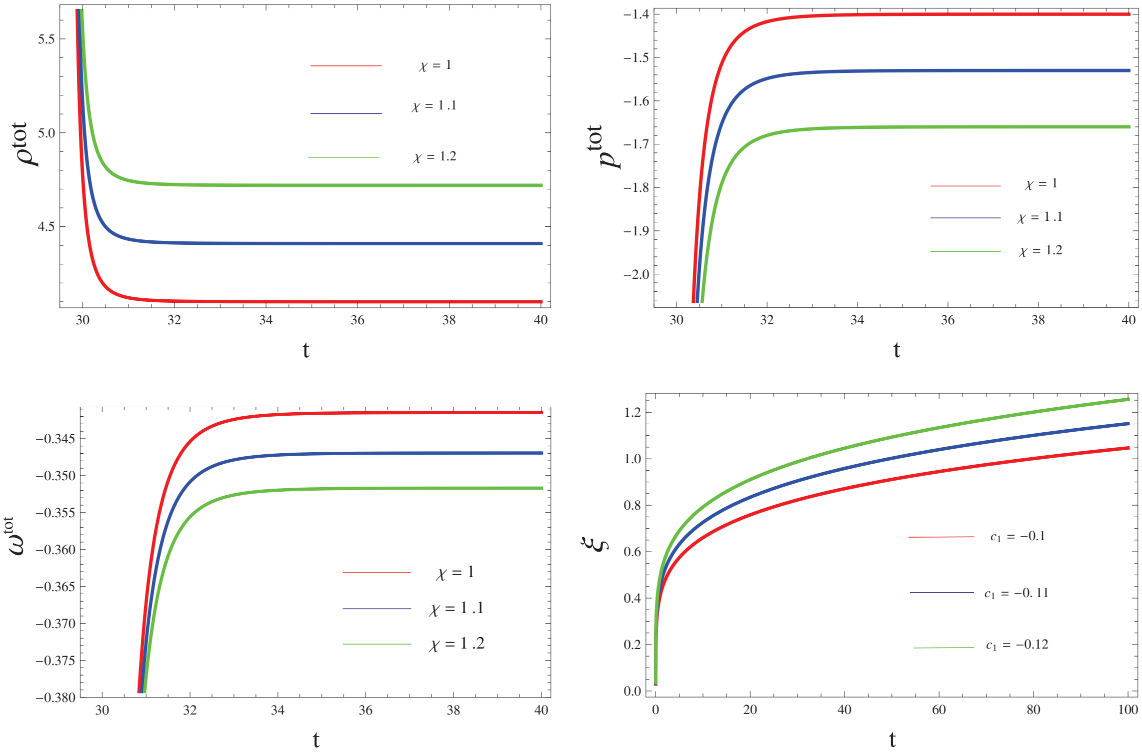

Fig. 5. Plots of $\rho^{\rm tot}$, $p^{\rm tot}$, $\omega^{\rm tot}$ and ξ vs. time in intermediate universe for $\tilde{B} = 8$, $\tilde{C} = 10$, $\alpha = 0.5$, $b = -1$, $\lambda = 0.1$, $\gamma = 0.8$, $\mu = 2$, $c_1 = -0.1$, $c_6 = 1$ and $Q = q(\mu\dot{\rho} + 3bH\rho)$.

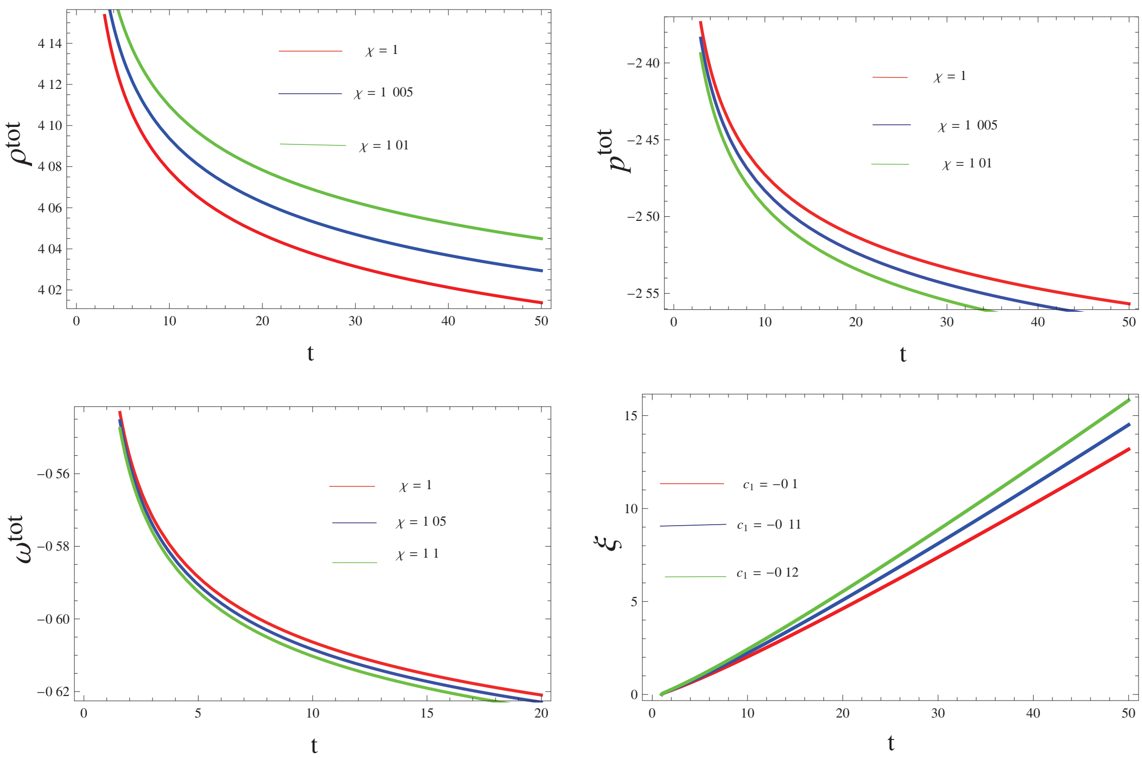

Fig. 6. Plots of $\rho^{\rm tot}$, $p^{\rm tot}$, $\omega^{\rm tot}$ and ξ vs. time in logamediate universe for $\tilde{B} = 0.6$, $\tilde{C} = 1$, $\alpha = 0.5$, $b = -1$, $\nu = 0.5$, $\sigma = 1.5$, $\mu = 2$, $c_1 = -0.1$ and $Q = q(\mu\dot{\rho} + 3bH\rho)$.

4. Concluding Remarks

In this paper, we have investigated the cosmological evolution by considering the interaction between MCG and $f(R,T)$ gravity. We have discussed the evolution in emergent, intermediate as well as logamediate scenarios and the behavior of bulk viscosity for the two interacting models. The range of the model parameter χ is $0 < \chi < \infty$ for all cases. For the first interaction model, we have found that the increase in χ leads to a decrease in total energy density and an increase in total pressure. The total EoS parameter falls in the non-phantom phase for the three considered scenarios. The bulk viscosity decreases for the emergent universe while it increases for the intermediate and logamediate cases.

For the second interaction model, the effect of χ as well as the behavior of ξ is similar to the first for all three scenarios. The behavior of the total EoS parameter and total pressure for the logamediate scenario is reversed in this case. Hence we deduce that emergent and intermediate scenarios lead to the same results for both interaction models, while the logamediate case shows a difference. It is shown[27] that large values of bulk viscosity can produce an expansion of the universe. Thus, we can conclude that for the intermediate and logamediate scenarios bulk viscosity enhances the expansion of the universe. Also, the decreasing value of the integration constant c_1 boosts this expansion. Finally, it is concluded that the interaction of MCG and $f(R,T)$ gravity leads to quintessence phase of dark energy for the three considered scenarios.

Acknowledgment

We would like to thank the Higher Education Commission, Islamabad, Pakistan for its financial support through the *Indigenous Ph.D. 5000 Fellowship Program Phase-II, Batch-III.*

References

1. P. Ratra and L. Peebles, *Phys. Rev. D* **37**, 3406 (1988).
2. R. R. Caldwell, R. Dave and P. J. Steinhardt, *Phys. Rev. Lett.* **80**, 1582 (1998).
3. R. R. Caldwell, *Phys. Lett. B* **545**, 23 (2002).
4. N. Afshordi, D. J. H. Chung and G. Geshnizjani, *Phys. Rev. D* **75**, 083513 (2007).
5. M. R. Setare, *Phys. Lett. B* **648**, 329 (2007); *ibid.* **653**, 116 (2007).
6. S. Chaplygin, *Sci. Mem. Mosc. Univ. Math. Phys.* **21**, 1 (1904).
7. A. Yu Kamenshchik, U. Moschella and V. Pasquier, *Phys. Lett. B* **511**, 265 (2001).
8. M. C. Bento, O. Bertolami and A. A. Sen, *Phys. Rev. D* **66**, 043507 (2002).
9. N. Bilic, G. B. Tupper and R. D. Viollier, *Phys. Lett. B* **535**, 17 (2002).
10. H. B. Benaoum, arXiv:hep-th/0205140.
11. P. F. Gonzalez-Diaz, *Phys. Rev. D* **68**, 021303 (2003).
12. M. Makler, S. G. de Oliveira and I. Waga, *Phys. Lett. B* **555**, 1 (2003).
13. H. Sandvik *et al.*, *Phys. Rev. D* **69**, 123524 (2004).
14. J. Sadeghi and H. Farahani, *Astrophys. Space Sci.* **347**, 209 (2013).
15. J. Naji, B. Pourhassan and A. R. Amani, *Int. J. Mod. Phys. D* **23**, 1450020 (2014).
16. M. Sharif and A. Sarwar, *Mod. Phys. Lett. A* **31**, 1650061 (2016).

17. R. Herrera, M. Olivares and N. Videla, *Eur. Phys. J. C* **73**, 2475 (2013).
18. M. Sharif and R. Saleem, *Eur. Phys. J. C* **74**, 2738 (2014).
19. A. Jawad, S. Butt and S. Rani, *Eur. Phys. J. C* **76**, 274 (2016).
20. T. Harko *et al.*, *Phys. Rev. D* **84**, 024020 (2011).
21. M. Jamil *et al.*, *Eur. Phys. J. C* **72**, 1999 (2012).
22. M. J. S. Houndjo, *Int. J. Mod. Phys. D* **21**, 1250003 (2012).
23. M. Sharif and M. Zubair, *J. Cosmol. Astropart. Phys.* **03**, 28 (2012).
24. M. Sharif and M. Zubair, *Phys. Soc. Jpn.* **82**, 014002 (2013).
25. V. B. Johri and R. Sudharsan, *Phys. Lett. A* **132**, 316 (1988).
26. J. Ren and X. H. Meng, *Phys. Lett. B* **636**, 5 (2006).
27. J. S. Gagnon and J. Lesgourgues, *J. Cosmol. Astropart. Phys.* **09**, 026 (2011).
28. E. H. Baffou, M. J. S. Houndjo and I. G. Salako, *Int. J. Geom. Methods Mod. Phys.* **14**, 1750051 (2017).
29. A. R. Amani and S. L. Dehneshin, *Can. J. Phys.* **93**, 1453 (2015).
30. T. M. Rezaei and A. Amani, doi:10.1139/cjp-2017-0151.
31. R. R. Baruah, *Int. J. Astron.* **5**, 7 (2016).
32. M. Baldi and P. Salucci, *J. Cosmol. Astropart. Phys.* **1202**, 014 (2012).
33. E. Abdalla, L.R. Abramo, L. Sodre and B. Wang, *Phys. Lett. B* **673**, 107 (2009).
34. J. Naji, B. Pourhassan and A. R. Amani, *Int. J. Mod. Phys. D* **23**, 1450020 (2014).
35. D. Bazeia *et al.*, *Phys. Lett. B* **743**, 98 (2015).
36. P. H. R. S. Moraes and J. R. L. Santos, *Eur. Phys. J. C* **76**, 60 (2016).
37. P. H. R. S. Moraes and R. A. C. Correa, arXiv:1606.07045.
38. A. R. Amani and B. Pourhassan, *Int. J. Theor. Phys.* **52**, 1309 (2013).
39. S. Floerchinger, N. Tetradis and U. A. Wiedemann, *Phys. Rev. Lett.* **114**, 091301 (2015).
40. H. Shabani and A. H. Ziaie, *Eur. Phys. J. C* **77**, 31 (2017).
41. H. Wei, *Nucl. Phys. B* **845**, 381 (2011).
42. G. F. R. Ellis and R. Maartens, *Class. Quantum Grav.* **21**, 223 (2004).
43. J. D. Barrow and N. J. Nunes, *Phys. Rev. D* **76**, 043501 (2007).

Communications in Theoretical Physics

PAPER

Viscosity Effects on Anisotropic Universe in Curvature-Matter Coupling Gravity

To cite this article: M. Sharif and Aisha Siddiqa 2018 *Commun. Theor. Phys.* **69** 537

View the article online for updates and enhancements.

Related content

- Effects of Low Anisotropy on Generalized Ghost Dark Energy in Galileon Gravity
  H. Hossienkhani, V. Fayaz, A. Jafari et al.
- Singularities and Entropy in Bulk Viscosity Dark Energy Model
  Meng Xin-He and Dou Xu
- Bianchi type V universe with bulk viscous matter and time varying gravitational and cosmological constants
  Prashant Singh Baghel and Jagdish Prasad Singh

This content was downloaded from IP address 111.68.103.18 on 25/05/2018 at 07:51

Commun. Theor. Phys. **69** (2018) 537–543 Vol. 69, No. 5, May 1, 2018

Viscosity Effects on Anisotropic Universe in Curvature-Matter Coupling Gravity

M. Sharif* and Aisha Siddiqa†

Department of Mathematics, University of the Punjab, Quaid-e-Azam Campus, Lahore-54590, Pakistan

(Received November 1, 2017; revised manuscript received January 23, 2018)

Abstract *In this paper, we study evolution of the universe in the background of $f(R,T)$ gravity using LRS Bianchi type-I model. We discuss scale factors as well as deceleration parameter in dark energy dominated era for different bulk viscosity models. The occurrence of big-rip singularity is also examined. It is concluded that expansion is faster when bulk viscosity is proportional to Hubble parameter as compared to other models.*

PACS numbers: 04.50.Kd, 51.20.+d, 98.80.Jk **DOI:** 10.1088/0253-6102/69/5/537

Key words: $f(R,T)$ gravity, anisotropic universe, bulk viscosity

1 Introduction

The accelerating expansion of the universe is a revolutionary discovery which provides a milestone in cosmology. The reason behind this expansion is assumed to be a hypothetical form of negative pressure named as dark energy. This is the most dominated factor in the energy budget of the universe. There have been many proposals to resolve the puzzling nature of dark energy. One of these proposals is to modify geometric part of the Einstein-Hilbert action leading to modified theories of gravity.

A simple generalization of general relativity is obtained by replacing the Ricci scalar R by $f(R)$ in the Einstein-Hilbert action. Harko *et al.*[1] proposed $f(R,T)$ gravity as a generalized modified theory, where T denotes trace of the energy-momentum tensor. The dependence on T is included due to the considerations of exotic fluids or quantum effects. The coupling of curvature and matter leads to a source term which is expected to yield interesting results. It can produce a matter-dependent deviation from geodesic motion and also worthwhile to discuss dark energy, dark matter interactions as well as late time acceleration.[2]

Jamil *et al.*[3] introduced some cosmic models in this gravity and found that ΛCDM model is reproduced by dust fluid. Houndjo[4] discussed matter dominated and accelerated phases of the universe for the models linear in T while the power of R depends on input parameters. Sharif and Zubair[5] explored thermodynamics of this gravity and concluded that the second law of thermodynamics is valid for phantom as well as non-phantom phases. In Refs. [6]–[8], the higher dimensions are also explored in the framework of $f(R,T)$ gravity. Moraes *et al.*[9] studied hydrostatic equilibrium condition for neutron stars with a specific form of equation of state (EoS) and found that the extreme mass can cross observational limits. Sharif and Nawazish[10] worked on the existence of Noether symmetries interacting with generalized scalar field model in $f(R,T)$ gravity. They found that dust fluid leads to decelerated expansion while perfect fluid yields current cosmic expansion for quintessence model.

Recent experimental data supports anisotropic nature of the universe which tends towards isotropic with the passage of time.[11−13] To study the anisotropic background of cosmos, Bianchi type models have frequently been considered in Refs. [14]–[17]. Bianchi type-I model is the simplest generalization of FRW spacetime. Sharif and Waheed[18] investigated this model in Brans-Dicke theory and concluded that anisotropic fluid tends to become isotropic at later times. Reddy and Kumar[19] examined Bianchi type-III model in $f(R,T)$ theory and observed no initial singularity as well as late time cosmic expansion. Sharif and Saleem[20] studied warm inflation for LRS Bianchi type-I model and showed that this model is consistent with observational data.

Bulk viscosity plays a significant role in cosmology as dissipative processes are thought to be present in any viable theory of cosmic evolution, which may lead to interesting conclusions. Johri and Sudharsan[21] investigated the effects of bulk viscosity on the evolution of FRW universe and found that time independent bulk viscosity can drive a steady state universe. Ren and Meng[22] presented a study on scalar field with bulk viscosity and proposed a model for which ΛCDM is a special case. They concluded that bulk viscosity enhances expansion of the universe. Gagnon and Lesgourgues[23] discussed a bulk viscous model as an alternative to dark energy. Singh and Kumar[24] explored the role of bulk viscosity in $f(R,T)$ gravity for FRW model with perfect fluid and found that bulk viscosity provides a supplement for expansion.

This paper deals with the evolution of viscous fluid in $f(R,T)$ gravity with LRS Bianchi type-I model. The plan of paper is as follows. In the next section, we formulate

*E-mail: msharif.math@pu.edu.pk

†E-mail: aisha.siddiqa17@yahoo.com

© 2018 Chinese Physical Society and IOP Publishing Ltd

the field equations and an evolution equation for H. We discuss the scale factors as well as deceleration parameter and conditions for the occurrence of big-rip singularity for different viscosity models. The last section summarizes the obtained results.

2 Anisotropic Universe with Viscous Fluid

The action for $f(R,T)$ gravity is defined as

$$S=\int \mathrm{d}^4x\sqrt{-g}\Big[\frac{1}{2\kappa^2}f(R,T)+\mathcal{L}_m\Big]\,. \tag{1}$$

Variation of the above action with respect to $g^{\alpha\beta}$ gives the field equations

$$f_R R_{\alpha\beta}-\frac{1}{2}g_{\alpha\beta}f+(g_{\alpha\beta}\Box-\nabla_\alpha\nabla_\beta)f_R \\ =\kappa^2T_{\alpha\beta}-f_T(T_{\alpha\beta}+\Theta_{\alpha\beta})\,, \tag{2}$$

where $f=f(R,T)$, $f_R=\partial f/\partial R$, $f_T=\partial f/\partial T$, and $\Theta_{\alpha\beta}$ is evaluated by

$$\Theta_{\alpha\beta}=g^{\gamma\mu}\frac{\delta T_{\gamma\mu}}{\delta g^{\alpha\beta}}\,,\quad T_{\alpha\beta}=g_{\alpha\beta}\mathcal{L}_m-\frac{\partial\mathcal{L}_m}{\partial g^{\alpha\beta}}\,. \tag{3}$$

Harko *et al.*[1] introduced the model $f(R,T)=R+2f(T)$ while $f(T)=\chi(T)^n$ is taken in Ref. [25], where χ and n are real constants. Thus we can write $f(R,T)=R+2\chi T$,[24] which simplifies the field equations as

$$R_{\alpha\beta}-\frac{1}{2}Rg_{\alpha\beta}=\kappa^2T_{\alpha\beta}-2\chi(T_{\alpha\beta}+\Theta_{\alpha\beta})+\chi g_{\alpha\beta}T\,. \tag{4}$$

The LRS Bianchi type-I universe model is taken as

$$\mathrm{d}s^2=-\mathrm{d}t^2+A^2(t)\mathrm{d}x^2+B^2(t)(\mathrm{d}y^2+\mathrm{d}z^2)\,. \tag{5}$$

We assume that shear and expansion scalars are proportional to each other ($\sigma\propto\Theta$), which gives $A=B^m$ (where $m\neq0$ is a constant).[26] The mean Hubble parameter then becomes

$$H=\frac{1}{3}\Big(\frac{m+2}{m}\Big)\frac{\dot A}{A}\,. \tag{6}$$

The field equations for this metric are

$$\frac{9(2m+1)}{(m+2)^2}H^2=(1+3\chi)\rho-\chi(p-3\xi H)\,, \tag{7}$$

$$\frac{-6\dot H}{(m+2)}-\frac{9(2m+1)(H)^2}{(m+2)^2} \\ =(1+3\chi)(p-3\xi H)-\chi\rho\,, \tag{8}$$

$$-\Big(1+\frac{1}{m}\Big)\frac{3m\dot H}{(m+2)}-\Big(1+\frac{2}{m}\Big)\frac{9m^2H^2}{(m+2)^2} \\ =(1+3\chi)(p-3\xi H)-\chi\rho\,. \tag{9}$$

The anisotropy parameter is given by[18]

$$\mathcal{A}_p=\frac{1}{3}\sum_{i=1}^{3}\Big(\frac{\triangle H_i}{H}\Big)^2\,,\quad \triangle H_i=H-H_i\,, \tag{10}$$

where H_i represent directional Hubble parameters. We evaluate $\mathcal{A}_p$ as

$$\mathcal{A}_p=\frac{2(m-1)^2}{(m+2)^2}\,. \tag{11}$$

The relation between m and $\mathcal{A}_p$ is given in Table 1.

Table 1 Relation of m and $\mathcal{A}_p$.

Range for m	Behavior of $\mathcal{A}_p$
$-\infty<m<-2$	Increasing
$-2<m\leq1$	Decreasing
$1\leq m<\infty$	Increasing

The energy-momentum tensor of viscous fluid is considered as[24]

$$T_{\alpha\beta}=(\rho+p-3\xi H)V_\alpha V_\beta+(p-3\xi H)g_{\alpha\beta}\,, \tag{12}$$

where ρ denotes matter density, p represents pressure, V_α is four velocity and ξ denotes bulk viscosity. The trace of energy-momentum tensor is

$$T=-\rho+3p-9\xi H\,. \tag{13}$$

The first two field equations produce the differential equation in H

$$\frac{6\dot H}{(m+2)}+(\rho+p)(1+2\chi)-3\xi H(1+2\chi)=0\,. \tag{14}$$

To solve this equation for H, we consider the following EoS

$$p=(\gamma-1)\rho\,,\quad 0\leq\gamma\leq2\,, \tag{15}$$

and an expression for bulk viscosity of the form[24]

$$\xi=\xi_0+\xi_1H\,, \tag{16}$$

where ξ_0 and ξ_1 are constants. The matter density is evaluated using Eqs. (15) and (16) in Eq. (7) as

$$\rho=\frac{3H}{(1+4\chi-\gamma\chi)}\Big[\Big(\frac{3(2m+1)}{(m+2)^2}-\chi\xi_1\Big)H-\chi\xi_0\Big]\,. \tag{17}$$

In the following, we consider four different viscosity models and evaluate the expressions for H, A, B, ρ, and q.

2.1 *Fluid with Zero Viscosity* ($\xi=0$)

For a non-viscous fluid, Eq. (14) becomes

$$2(m+2)\dot H+\frac{3\gamma(1+2\chi)(2m+1)}{(1+4\chi-\gamma\chi)}H^2=0\,, \tag{18}$$

where we have used Eqs. (16) and (17). The solution of this equation for $\gamma\neq0$ is given by

$$H=\frac{1}{c_1+(3/2)\gamma(1+2\chi)(1+2m)t/(m+2)(1+4\chi-\gamma\chi)}\,, \tag{19}$$

where c_1 is a constant of integration. The Hubble parameter yields

$$A=\Big(c_2\Big[c_1+\frac{3}{2}\frac{\gamma(1+2\chi)(1+2m)t}{(m+2)(1+4\chi-\gamma\chi)}\Big]^{2(m+2)(1+4\chi-\gamma\chi)/3\gamma(1+2\chi)(1+2m)}\Big)^{3m/(m+2)}\,, \tag{20}$$

here $c_2 > 0$ is another integration constant. This represents a power-law type solution of the scale factor. The scale factor B can be found using $A = B^m \Rightarrow B = A^{1/m}$. The deceleration parameter is obtained as

$$q = -1 - \frac{\dot{H}}{H^2} = -1 + \frac{3}{2}\frac{\gamma(1+2\chi)(1+2m)}{(m+2)(1+4\chi-\gamma\chi)}\,, \tag{21}$$

which is time independent and its value varies with γ, χ and m.

For different values of γ, we have different evolutionary eras. Here, we present a discussion for the dark energy dominated era corresponding to $\gamma = 0$. Solving Eq. (18) for $\gamma = 0$, we have

$$H = c_1'\,,\quad q = -1\,,\quad A = (c_2' e^{c_1' t})^{3m/(m+2)}\,,$$

$$B = (c_2'\, \mathrm{e}^{c_1' t})^{3/(m+2)}\,, \tag{22}$$

$c_1' > 0$ and $c_2' > 0$ are constants of integration. The scale factors are of exponential form. For $m = 1$, the above values correspond to de Sitter universe. The plots for A and B in Eq. (23) are given in Fig. 1. The behavior of both graphs is increasing with time while anisotropy has opposite effects (it increases A and decreases B). Equation (17) yields the expression for density as

$$\rho = \frac{9(2m+1)c_1'^2}{(m+2)^2(1+4\chi)}\,. \tag{23}$$

There is a big-rip singularity when $\rho \to \infty$, i.e., for a non-viscous fluid, big-rip is expected only if $m = -2$ or $\chi = -1/4$. For $m = -2$, the anisotropy parameter $\mathcal{A}_p$ (11) also approaches to infinity.

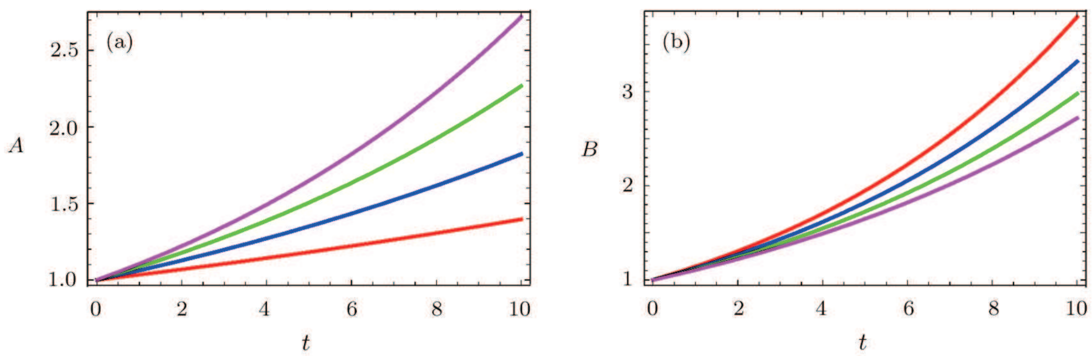

Fig. 1 (Color online) Plots of A and B versus t for $\xi = 0$ and fixing $c_1' = 0.1$, $c_2' = 1$, $m = 0.25$ (red), 0.5 (blue), 0.75 (green) and 1 (purple).

2.2 *Fluid with Constant Viscosity ($\xi = \xi_0$)*

In this case, for $\gamma \neq 0$ Eq. (14) yields the solution

$$H = \frac{\Big(\frac{\xi_0(1+2\chi)(1+4\chi)(m+2)}{2(1+4\chi-\gamma\chi)}\Big)\exp\Big[\frac{\xi_0(1+2\chi)(1+4\chi)(m+2)}{2(1+4\chi-\gamma\chi)}(t+c_3)\Big]}{1+\Big(\frac{3\gamma(1+2\chi)(1+2m)}{2(m+2)(1+4\chi-\gamma\chi)}\Big)\exp\Big[\frac{\xi_0(1+2\chi)(1+4\chi)(m+2)}{2(1+4\chi-\gamma\chi)}(t+c_3)\Big]}\,, \tag{24}$$

where c_3 is an integration constant. Using the above equation, q and A are evaluated as

$$q = -1 - \exp\Big[\frac{-\xi_0(1+2\chi)(1+4\chi)(m+2)}{2(1+4\chi-\gamma\chi)}(t+c_3)\Big]\,, \tag{25}$$

$$A = \Big\{c_4\Big(1 + \frac{3\gamma(1+2\chi)(1+2m)}{2(m+2)(1+4\chi-\gamma\chi)}\exp\Big[\frac{\xi_0(1+2\chi)(1+4\chi)(m+2)(t+c_3)}{2(1+4\chi-\gamma\chi)}\Big]\Big)^{\frac{2(m+2)(1+4\chi-\gamma\chi)}{3\gamma(1+2\chi)(1+2m)}}\Big\}^{3m/(m+2)}\,, \tag{26}$$

$c_4 > 0$ is another integration constant. The scale factors become exponential type. For $\gamma = 0$, we have

$$H = c_3' \exp\Big(\frac{\xi_0(1+2\chi)(m+2)t}{2}\Big)\,, \tag{27}$$

$$q = -1 - \frac{\xi_0(1+2\chi)(m+2)c_3'}{2\,\mathrm{e}^{\xi_0(1+2\chi)(m+2)t/2}}\,, \tag{28}$$

$$A = \Big\{c_4' \exp\Big[\frac{2c_3'}{\xi_0(1+2\chi)(m+2)} \times \exp\Big(\frac{\xi_0(1+2\chi)(m+2)t}{2}\Big)\Big]\Big\}^{3m/(m+2)}\,, \tag{29}$$

here c_3' and $c_4' > 0$ are constants of integration. The graphical behavior of q, A and B are shown in Fig. 2. The decrease in anisotropy has the same effects as for zero viscosity fluid while increase in bulk viscosity shows decrease in both A and B. The deceleration parameter is negative and does not cross the line $q = -1$. The decrease in m as well as increase in ξ_0 decreases the value of q. For a constant viscous fluid, the matter density in dark energy dominated era is obtained as

$$\rho = \frac{3c_3' \exp\left[\xi_0(1+2\chi)(m+2)t/2\right]}{(1+4\chi)} \left\{\frac{3(2m+1)}{(m+2)^2} c_3' \exp\left[\frac{\xi_0(1+2\chi)(m+2)t}{2}\right] - \chi\xi_0\right\}. \tag{30}$$

Again $\rho \to \infty$ or big-rip occurs when $m = -2$ or $\chi = -1/4$. This also holds for the next two cases and we can obtain an expression of time for the big-rip occurrence there.

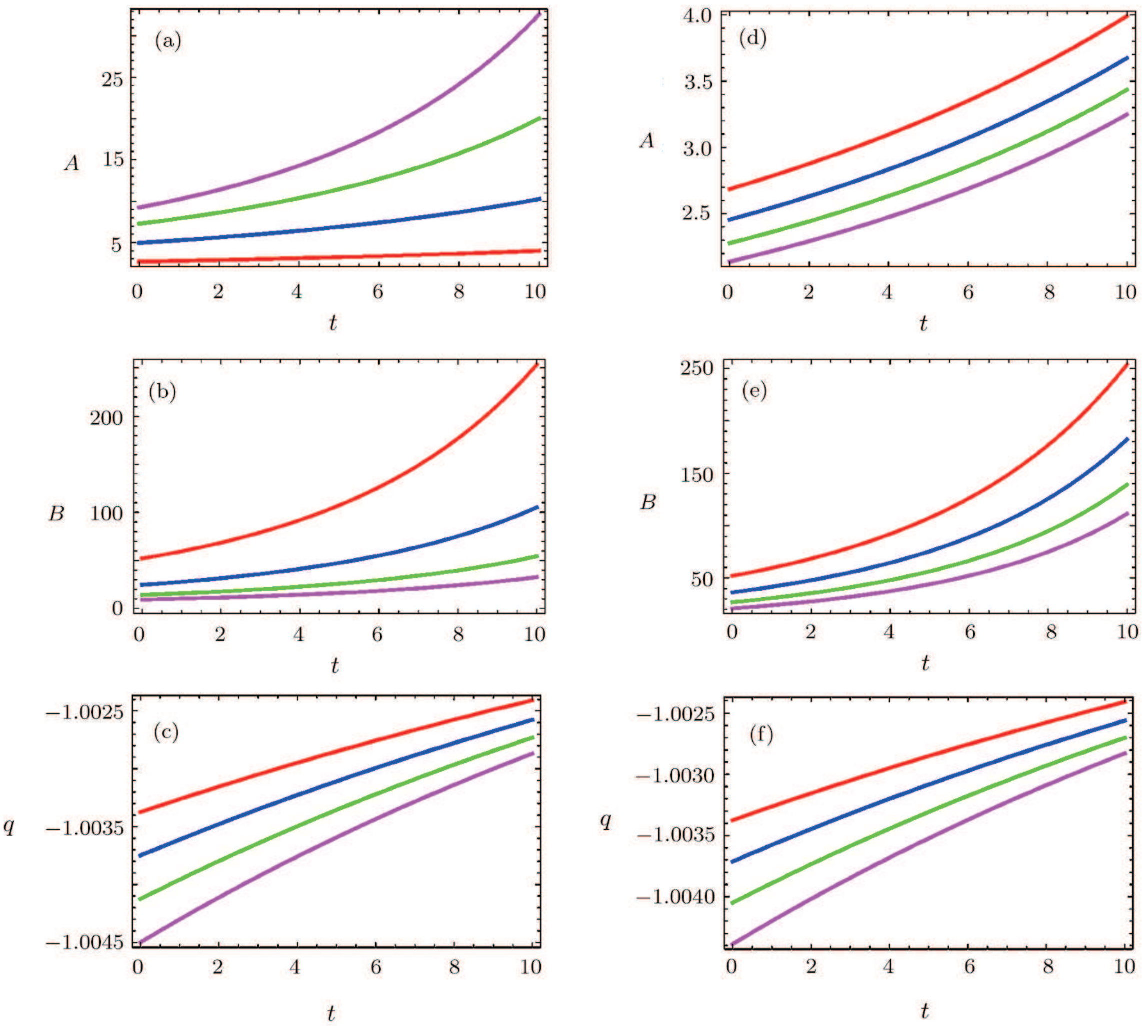

Fig. 2 (Color online) Plots of A, B and q versus t for $\xi = \xi_0$ and fixing $\chi = 1$, $c_3' = 0.1$, $c_4' = 1$, $\xi_0 = 0.01$, $m = 0.25$ (red), 0.5 (blue), 0.75 (green) and 1 (purple) in (a), (b), (c) and fixing $m = 0.25$, $\xi_0 = 0.01$ (red), 0.011 (blue), 0.012 (green) and 0.013 (purple) in (d) (e) (f).

2.3 *Fluid with Viscosity Proportional to H* ($\xi = \xi_1 H$)

In this case, the solution of Eq. (14) for $0 \le \gamma \le 2$ is

$$H = 1\Big/\left\{\frac{(1+2\chi)(m+2)}{2(1+4\chi-\gamma\chi)}\left[\frac{3(2m+1)\gamma}{(m+2)^2} - \xi_1 - 4\chi\xi_1\right]t + c_5\right\}, \tag{31}$$

c_5 represents constant of integration. Similarly, q and A can be obtained as

$$q = -1 + \frac{(1+2\chi)(m+2)}{2(1+4\chi-\gamma\chi)}\left[\frac{3(2m+1)\gamma}{(m+2)^2} - \xi_1 - 4\chi\xi_1\right], \tag{32}$$

$$A = \left\{c_6\left[\frac{(1+2\chi)(m+2)}{2(1+4\chi-\gamma\chi)}\left(\frac{3(2m+1)\gamma}{(m+2)^2} - \xi_1 - 4\chi\xi_1\right)t + c_5\right]^{\frac{2(1+4\chi-\gamma\chi)}{(1+2\chi)(m+2)}\left[\frac{3(2m+1)\gamma}{(m+2)^2} - \xi_1 - 4\chi\xi_1\right]}\right\}^{3m/(m+2)}, \tag{33}$$

$c_6 > 0$ denotes another integration constant. We see that q has a time independent expression as in the first case and A is of power-law type. The scale factor B is obtained in a similar manner. For $\gamma = 0$, the above expressions reduce to

$$H = \frac{1}{c_5 - (1+2\chi)(m+2)\xi_1 t/2}, \tag{34}$$

$$q = -1 - \frac{(1+2\chi)(m+2)\xi_1}{2}\,, \tag{35}$$

$$A = \Big[c_6\Big(c_5 - \frac{(1+2\chi)(m+2)\xi_1 t}{2}\Big)^{-2/(1+2\chi)(m+2)\xi_1}\Big]^{3m/(m+2)}\,. \tag{36}$$

The value of q depends on χ, m as well as ξ_1 and remains less than -1 for positive values of all these constants. The plots of A are shown in Fig. 3. Here the decrease in m and increase in ξ_1 yield an increase in A. We see that the effects of viscosity are same on both A and B while anisotropy has opposite effects on both. So, we only show the graphs of A in this case as well as in next one. For this viscosity model and $\gamma = 0$, ρ becomes

$$\rho = \frac{1}{1+4\chi}\Big[\frac{9(2m+1)}{(m+2)^2} - 3\chi\xi_1\Big]\frac{1}{(c_5 - (1+2\chi)(m+2)\xi_1 t/2)^2}\,. \tag{37}$$

In this case, there is an additional term as compared to the previous cases whose zero value makes density infinite i.e.,

$$\Big(c_5 - \frac{(1+2\chi)(m+2)\xi_1 t}{2}\Big)^2 = 0\,,$$

giving the time of big-rip occurrence

$$t_{\rm br} = \frac{2c_5}{(m+2)(1+2\chi)\xi_1}\,.$$

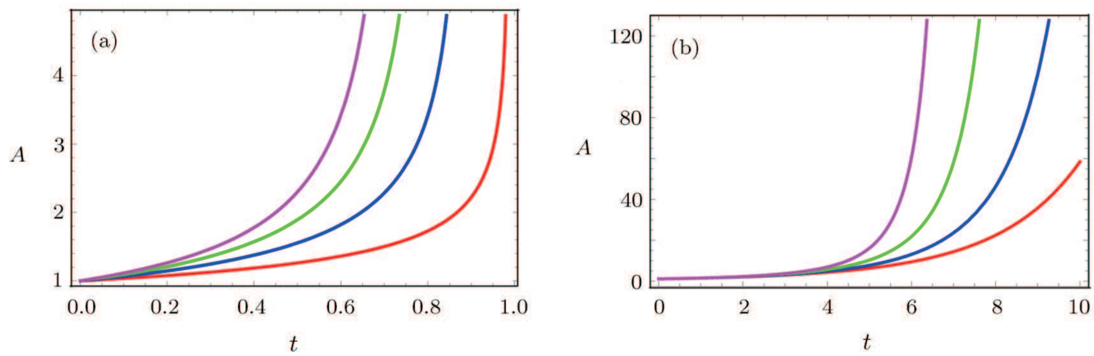

Fig. 3 (Color online) Plots of A versus t for $\xi = \xi_1 H$ and fixing $\chi = 1,\ c_5 = 1,\ c_6 = 1,\ \xi_1 = 0.01,\ m = 0.25$ (red), 0.5 (blue), 0.75 (green) and 1 (purple) in (a) and fixing $m = 0.25,\ \xi_1 = 0.01$ (red), 0.012 (blue), 0.014 (green) and 0.016 (purple) in (b).

2.4 *Fluid with Viscosity of the Form* $\xi = \xi_0 + \xi_1 H$

For this viscosity model and $0 \le \gamma \le 2$, Eq. (14) has the following solution

$$H = \frac{\frac{\xi_0(1+2\chi)(1+4\chi)(m+2)}{2(1+4\chi-\gamma\chi)}\exp\Big[\frac{\xi_0(1+2\chi)(1+4\chi)(m+2)(t+c_7)}{2(1+4\chi-\gamma\chi)}\Big]}{1+\frac{(1+2\chi)(m+2)\big(\frac{3(2m+1)\gamma}{(m+2)^2}-\xi_1-4\chi\xi_1\big)}{2(1+4\chi-\gamma\chi)}\exp\Big[\frac{\xi_0(1+2\chi)(1+4\chi)(m+2)(t+c_7)}{2(1+4\chi-\gamma\chi)}\Big]}\,, \tag{38}$$

leading the expressions of q and A to

$$q = -1 - \exp\Big[\frac{-\xi_0(1+2\chi)(1+4\chi)(m+2)(t+c_7)}{2(1+4\chi-\gamma\chi)}\Big]\,, \tag{39}$$

$$A = \Big\{c_8\Big[1 + \frac{(1+2\chi)(m+2)[3(2m+1)\gamma/(m+2)^2 - \xi_1 - 4\chi\xi_1]}{2(1+4\chi-\gamma\chi)} \times \exp\Big[\frac{\xi_0(1+2\chi)(1+4\chi)(m+2)(t+c_7)}{2(1+4\chi-\gamma\chi)}\Big]\Big]^{\frac{2(1+4\chi-\gamma\chi)}{(1+2\chi)(m+2)(3(2m+1)\gamma/(m+2)^2-\xi_1-4\chi\xi_1)}}\Big\}^{3m/(m+2)}\,, \tag{40}$$

where c_7 and c_8 are integration constants with $c_8 > 0$. Here A has an exponential form and for $\gamma = 0$, we obtain

$$H = \frac{[\xi_0(1+2\chi)(m+2)/2]\exp[\xi_0(1+2\chi)(m+2)(t+c_7)/2]}{[1-(1+2\chi)(m+2)\xi_1/2]\exp[\xi_0(1+2\chi)(m+2)(t+c_7)/2]}\,, \tag{41}$$

$$q = -1 - \exp\Big[\frac{-\xi_0(1+2\chi)(m+2)(t+c_7)}{2}\Big]\,, \tag{42}$$

$$A = \Big\{\Big[c_8\Big[1 - \frac{(1+2\chi)(m+2)\xi_1}{2}\exp\Big[\frac{\xi_0(1+2\chi)(m+2)(t+c_7)}{2}\Big]\Big]\Big]^{\frac{-2}{(1+2\chi)(m+2)\xi_1}}\Big\}^{3m/(m+2)}\,. \tag{43}$$

The behavior of scale factor A is shown in Figs. 4 and 5. The effects of anisotropy and viscosity on scale factors are the same as in the previous case. The plots of deceleration parameter in Fig. 6 indicate that it increases with decrease in anisotropy and increase in viscosity. Also, its value does not cross the line $q = -1$. Similarly, ρ is obtained as

$$\rho = \left\{3\frac{[\xi_0(1+2\chi)(m+2)/2]\exp[\xi_0(1+2\chi)(m+2)(t+c_7)/2]}{1-[(1+2\chi)(m+2)\xi_1]/2\exp[\xi_0(1+2\chi)(m+2)(t+c_7)/2]} \Big/ (1+4\chi-\gamma\chi)\right\}\left\{\left(\frac{3(2m+1)}{(m+2)^2}-\chi\xi_1\right)\right.$$
$$\left.\times\frac{[\xi_0(1+2\chi)(m+2)/2]\exp[\xi_0(1+2\chi)(m+2)(t+c_7)/2]}{1-[(1+2\chi)(m+2)\xi_1/2]\exp[\xi_0(1+2\chi)(m+2)(t+c_7)/2]}-\chi\xi_0\right\}, \tag{44}$$

and the time of big-rip is given by

$$t_{\rm br} = \frac{2}{\xi_0(1+2\chi)(m+2)}\ln\left[\frac{2}{\xi_1(1+2\chi)(m+2)}\right]-c_7. \tag{45}$$

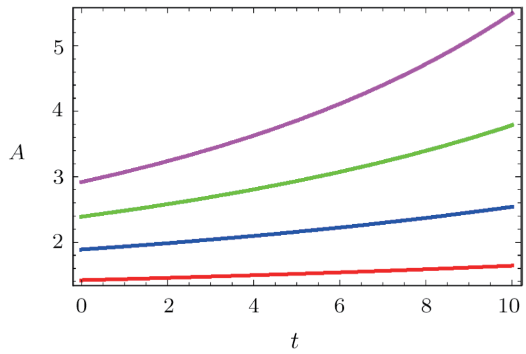

Fig. 4 (Color online) Plot of A versus t for $\xi = \xi_0+\xi_1 H$ and fixing $\chi = 1$, $c_7 = 1$, $c_8 = 1$, $\xi_0 = 0.01$, $\xi_1 = 0.01$, $m = 0.25$ (red), 0.5 (blue), 0.75 (green) and 1 (purple).

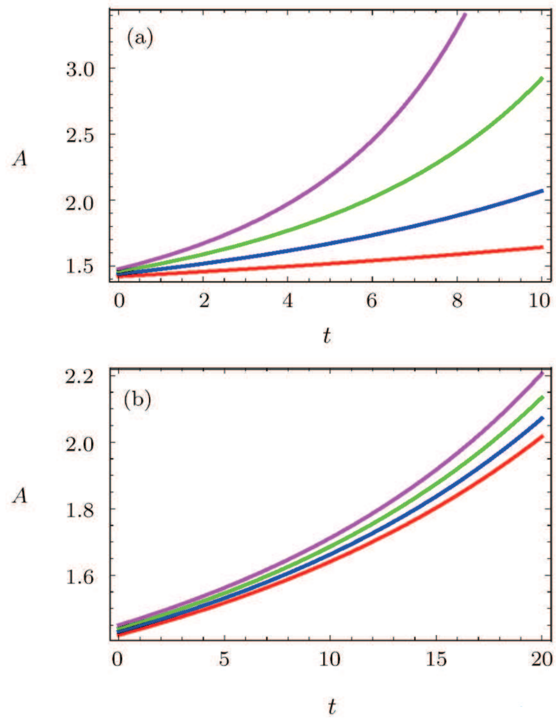

Fig. 5 (Color online) Plots of A versus t for $\xi = \xi_0+\xi_1 H$ and fixing $\chi = 1$, $c_7 = 1$, $c_8 = 1$, $\xi_1 = 0.01$, $m = 0.25$, $\xi_0 = 0.01$ (red), 0.02 (blue), 0.03 (green) and 0.04 (purple) in (a) and fixing $m = 0.25$, $\xi_0 = 0.01$, $\xi_1 = 0.01$ (red), 0.02 (blue), 0.03 (green) and 0.04 (purple) in (b).

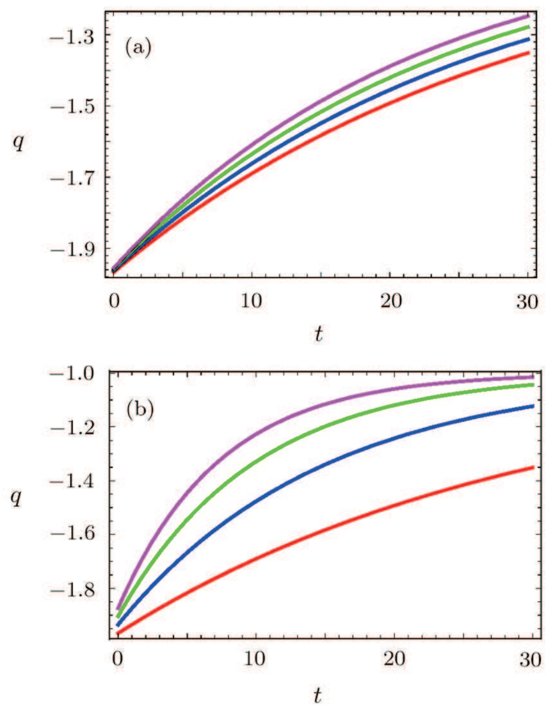

Fig. 6 (Color online) Plots of q versus t for $\xi = \xi_0+\xi_1 H$ and fixing $\chi = 1$, $c_7 = 1$, $c_8 = 1$, $\xi_0 = 0.01$, $m = 0.25$ (red), 0.5 (blue), 0.75 (green) and 1 (purple) in (a) and fixing $m = 0.25$, $\xi_0 = 0.01$ (red), 0.02 (blue), 0.03 (green) and 0.04 (purple) in (b).

3 Concluding Remarks

Our universe is homogeneous and isotropic on large scale but there are anisotropies present on small scales. Also, the bulk viscosity is an important candidate in describing early and late time expansion. Thus it would be worthwhile to explore a deviation from isotropy as well as the effects of bulk viscosity on the evolution of cosmos. In this paper, the evolution of scale factors and deceleration parameter in dark energy dominated era with different forms of viscosity is discussed. The graphical analysis is summarized in Tables 2 and 3. The evolution of scale factors with the decrease in anisotropy remain the same in all cases as shown in Table 2. On the other hand, the increase in viscosity has different effects on scale factors. It produces a decrease in scale factors for $\xi = \xi_0$ while an increase for $\xi = \xi_1 H$ as well as $\xi = \xi_0 + \xi_1 H$. The increase in scale factors with time supports accelerated expansion while an increase in their value with decrease in anisotropy or increase in viscosity show an enhancement in expansion.

It is observed from Table 3 that decrease in anisotropy as well as increase in viscosity decreases q for second and third bulk viscosity models while increases for the last model. The negative value of q indicates an accelerated expansion of the universe and we have $q \leq -1$ for all cases. Hence, the expansion is enhanced due to bulk viscosity for ξ_0 and $\xi = \xi_1 H$. For each case, $m = -2$ and $\chi = -1/4$ are the common conditions for the occurrence of big-rip. For the last two viscosity models, we have also an expression of time at which big-rip could occur. We would like to mention here that for $m = 1$, our results reduce to that of isotropic case.[24] It is concluded that the accelerated expansion is faster for $\xi = \xi_1 H$ as compared to other models.

Table 2 Evolution of scale factors.

Viscosity model	When anisotropy decreases	When bulk viscosity increases
$\xi = 0$	A increases, B decreases	A, B remain the same
$\xi = \xi_0$	A increases, B decreases	A, B decrease
$\xi = \xi_1 H$	A increases, B decreases	A, B increase
$\xi = \xi_0 + \xi_1 H$	A increases, B decreases	A, B increase

Table 3 Evolution of deceleration parameter.

Viscosity model	When anisotropy decreases	When bulk viscosity increases
$\xi = 0$	Constant ($q = -1$)	Constant, ($q = -1$)
$\xi = \xi_0$	Decreases	Decreases
$\xi = \xi_1 H$	Decreases	Decreases
$\xi = \xi_0 + \xi_1 H$	Increases	Increases

Acknowledgments

We would like to thank the Higher Education Commission, Islamabad, Pakistan for its financial support through the Indigenous Ph.D. 5000 Fellowship Program Phase-II, Batch-III.

References

[1] T. Harko, F. S. N. Lobo, S. Nojiri, and S. D. Odintsov, Phys. Rev. D **84** (2011) 024020.

[2] T. Harko and F. S. N. Lobo, Galaxies **2** (2014) 410.

[3] M. Jamil, D. Momeni, M. Raza, and R. Myrzakulov, Eur. Phys. J. C **72** (2012) 1999.

[4] M. J. S. Houndjo, Int. J. Mod. Phys. D **21** (2012) 1250003.

[5] M. Sharif and M. Zubair, J. Cosmol. Astropart. Phys. **03** (2012) 28.

[6] P. H. R. S. Moraes, Eur. Phys. J. C **75** (2015) 168.

[7] P. H. R. S. Moraes and R. A. C. Correa, Astrophys. Space Sci. **361** (2016) 91.

[8] R. A. C. Correa and P. H. R. S. Moraes, Eur. Phys. J. C **76** (2016) 100.

[9] P. H. R. S. Moraes, D. V. A. José, and M. Malheiro, J. Cosmol. Astropart. Phys. **06** (2016) 005.

[10] M. Sharif and I. Nawazish, Eur. Phys. J. C **77** (2017) 198.

[11] C. L. Bennett, *et al.*, Astrophys. J. Suppl. Ser. **148** (2003) 1.

[12] A. de Oliveira-Costa, M. Tegmark, M. Zaldarriaga, and A. Hamilton, Phys. Rev. D **69** (2004) 063516.

[13] D. J. Schwarz, G. D. Starkman, D. Huterer, and C. J. Copi, Phys. Rev. Lett. **93** (2004) 221301.

[14] C. P. Singh, S. Ram, and M. Zeyauddin, Astrophys. Space Sci. **315** (2008) 181.

[15] M. Sharif and M. F. Shamir, Class. Quantum Grav. **26** (2009) 235020.

[16] E. Wilson-Ewing, Phys. Rev. D **82** (2010) 043508.

[17] D. R. K. Reddy, R. Santikumar, and R. L. Naidu, Astrophys. Space Sci. **342** (2012) 249.

[18] M. Sharif and S. Waheed, Eur. Phys. J. C **72** (2012) 1876.

[19] D. R. K. Reddy and R. S. Kumar, Astrophys. Space Sci. **344** (2013) 253.

[20] M. Sharif and R. Saleem, Eur. Phys. J. C **74** (2014) 2738.

[21] V. B. Johri and R. Sudharsan, Phys. Lett. A **132** (1988) 316.

[22] J. Ren and X. H. Meng, Phys. Lett. B **636** (2006) 5.

[23] J. S. Gagnon and J. Lesgourgues, J. Cosmol. Astropart. Phys. **09** (2011) 026.

[24] C. P. Singh and P. Kumar, Eur. Phys. J. C **74** (2014) 3070.

[25] D. Bazeia, A. S. Lobão, and R. Menezes, Phys. Lett. B **743** (2015) 98; P. H. R. S. Moraes and J. R. L. Santos, Eur. Phys. J. C **76** (2016) 60.

[26] M. Sharif and S. Waheed, Phys. Lett. B **726** (2013) 1.